Sensitivity Analysis of Wedge Flows for Newtonian and Non-Newtonian Fluids

CENTRAL LIBRARY

By

Dilawar Hussian

Reg. No. 118-FBAS/PHDMA/F19

Department of Mathematics and Statistics

Faculty of Sciences

International Islamic University, Islamabad

Pakistan

2023

K
TH-27643
PhD
519.4
DIS

Wedge flows
Sensitivity analysis
Numerical analysis

Sensitivity Analysis of Wedge Flows for Newtonian and Non-Newtonian Fluids

By

Dilawar Hussian

Reg. No. 118-FBAS/PHDMA/F19

Supervised by

Dr. Ahmed Zeeshan

Co-Supervised by

Dr. Zaheer Asghar

Department of Mathematics and Statistics

Faculty of Sciences

International Islamic University, Islamabad

Pakistan

2023

Sensitivity Analysis of Wedge Flows for Newtonian and Non-Newtonian Fluids

By

Dilawar Hussain

A Thesis
Submitted in the Partial Fulfillment of the
Requirements for the Degree of

DOCTOR OF PHILOSOPHY

IN

MATHEMATICS

Supervised by

Dr. Ahmed Zeeshan

Co-Supervised by

Dr. Zaheer Asghar

Department of Mathematics and Statistics

Faculty of Sciences

International Islamic University, Islamabad

Pakistan

2023

Author's Declaration

I, **Dilawar Hussain** Reg. No. **118-FBAS/PHDMA/F19** hereby state that my Ph.D. thesis, entitled: **Sensitivity Analysis of Wedge Flows for Newtonian and Non-Newtonian Fluids** is my own work and has not been submitted previously by me for taking any degree from this university, **International Islamic University, Sector H-10, Islamabad, Pakistan** or anywhere else in the country/world.

At any time if my statement is found to be incorrect even after my Graduation, the university has the right to withdraw my Ph.D. degree.

Name of Student: **(Dilawar Hussain)**
Reg. No. **118-FBAS/PHDMA/F19**
Dated: **22/06/2023**

Plagiarism Undertaking

I solemnly declare that research work presented in the thesis, entitled: **Sensitivity Analysis of Wedge Flows for Newtonian and Non-Newtonian Fluids** is solely my research work with no significant contribution from any other person. Small contribution/help wherever taken has been duly acknowledged and that complete thesis has been written by me.

I understand the zero tolerance policy of the HEC and University, **International Islamic University, Sector H-10, Islamabad, Pakistan** towards plagiarism. Therefore, I as an Author of the above titled thesis declare that no portion of my thesis has been plagiarized and any material used as reference is properly referred/cited.

I undertake that if I am found guilty of any formal plagiarism in the above titled thesis even after award of Ph.D. degree, the university reserves the rights to withdraw/revoke my Ph.D. degree and that HEC and the University has the right to publish my name on the HEC/University Website on which names of students are placed who submitted plagiarized thesis.

Student/Author Signature: 

Name: **(Dilawar Hussain)**

Certificate of Approval

This is to certify that the research work presented in this thesis, entitled: **Sensitivity Analysis of Wedge Flows for Newtonian and Non-Newtonian Fluids** was conducted by **Mr. Dilawar Hussain,** Reg. No. **118-FBAS/PHDMA/F19** under the supervision of **Dr. Ahmed Zeeshan.** No part of this thesis has been submitted anywhere else for any other degree. This thesis is submitted to the **Department of Mathematics & Statistics, FoS, IIU, Islamabad** in partial fulfillment of the requirements for the degree of **Doctor of Philosophy in Mathematics, Department of Mathematics & Statistics, Faculty of Sciences, International Islamic University, Sector H-10, Islamabad, Pakistan.**

Student Name: Dilawar Hussain **Signature:** _____

Examination Committee:

a) **External Examiner 1:**
Name/Designation/Office Address **Signature:** Saleem Asghar

Prof. Dr. Saleem Asghar
Professor of Mathematics,
Department of Mathematics,
COMSATS, IIT, Park Road, Chak Shahzad,
Islamabad.

b) **External Examiner 2:**
Name/Designation/Office Address) **Signature:** _____

Prof. Dr. Masood Khan
Professor of Mathematics,
Department of Mathematics,
QAU, Islamabad

c) **Internal Examiner:**
Name/Designation/Office Address) **Signature:** _____

Prof. Dr. Muhammad Sajid T.I
Professor

Supervisor Name:
Dr. Ahmed Zeeshan **Signature:** _____

Co-Supervisor Name:
Dr. Zaheer Asghar **Signature:** _____

Name of HOD:
Prof. Dr. Nasir Ali **Signature:** _____

Name of Dean:
Prof. Dr. Muhammad Irfan Khan **Signature:** _____

Dedication

This thesis is dedicated

to

all those who prayed for me.

Acknowledgements

I am highly grateful to Allah Almighty who encouraged and showed me a way for completing my PhD. Allah Almighty helped me overcome all the hurdles emerging during the whole span of the study. I am also thankful to my Holy Prophet (SAW) who is a source of benediction for all humans. He (SAW) preaching inspires us to inquire and search the universe under the direction of Allah. I offer heartfelt thanks to my supervisor, Dr. Ahmed Zeeshan and co-supervisor Dr. Zaheer Asghar, who facilitated me to commence my research. I found them very generous persons in answering my queries. It's an honor for me to offer deep respect to my teachers Prof. Dr. Nasir Ali, Prof. Dr. Tariq Javed, Prof. Dr. Muhammad Sajid (TI), Prof. Dr. Arshad Zia, Dr. Ahmer Mehmood, Dr. Rahmat Ellahi, Dr. Nayyar Mehmood, Dr. Tahir Mehmood and Dr. Niaz Ahmed who enabled me to achieve the target. Without the contributions of many generous people, the completion of this thesis would never have been possible. My parents' selfless prayers and well wishes have always been a source of my success in all facets of my life. I'm grateful to my brothers for their generous assistance with my doctoral studies. My wife deserves a lot of credit for taking care throughout the completion of the thesis. She has been incredibly sympathetic and supportive of me throughout my doctoral studies, and I appreciate her so much. Many love for little daughter, who is wished well health and the development of a noble character. In addition to all of the above, there are definitely a number of other people who deserve special appreciation but cannot be acknowledged by name. I want to express my gratitude to everyone who helped me during the completion of this thesis, whether it was directly or indirectly. I am also thankful to my friends, relatives, and seniors for their moral support.

Dilawar Hussain

Preface

Sensitivity analysis is an essential problem in engineering and manufacturer process to examine the effect of different input factors on various flow problems. Sensitivity is being used in recent theory and research in engineering and industrial applications of various optimum control systems. The novel idea of sensitivity analysis of physical systems have also pervaded other fields of science and engineering involving manufacturing process in industries, nuclear engineering, environmental science, biological science and socio-economical. In order to perform sensitivity analysis, there is need to develop some empirical relation among each of output and input variables. Researchers and scientists have examined the problems by using a number of empirical methodologies. The best way for determining out how input parameters and output responses relate to one another is the correlation development method. Such an empirical relationship is required to perform sensitivity analysis. Many researchers and Scientists have applied correlation development method in several experimental analysis to develop empirical model.

There is always need to specify a physical or engineering problem in order to perform sensitivity analysis. We are interested to perform sensitivity analysis on the response variables that measure the transport performance in a problem of fluid dynamics. These response variables Cf_x, Nu_x and Sh_x. There are several kinds of the problems of fluid flow. The focus of present study is on flow over a wedge. Because wedge flows have a variety of applications, including designing the wings of airplane, drying systems, crude oil extraction and nuclear engineering etc.

This thesis comprises the sensitivity analysis of wedge flows for Newtonian and some non-Newtonian fluids. Before performing sensitivity analysis, we have first of all transformed the governing PDEs to non-linear ODEs by employing similarity transformations. Matlab's built-in package bvp4c is used to solve these modified ODEs and compare the results to previous work, revealing the best results. Then we adopted RSM to develop empirical relations for transport performance

quantities (Nu_x and Sh_x) by using these numerical values. The ANOVA results generated by using RSM for regression coefficients and output responses are represented in form of table. We have taken 95% confidence interval and prepared Analysis of Variance (ANOVA) table, to see the goodness of fit of the empirical relations among each of response variables i.e Cf_x, Nu_x, $Sn_x$and Sh_x and different input parameters. The residual plots of output responses are depicted in different graphical forms. Then sensitivity analysis is performed for output responses with the effect of various input factors and displayed the graphs in the form of bar chart. This unique mathematical and statistical method is expected to fill the gap in literature and serve as foundation for upcoming problems of fluid dynamics, manufacturing and many industrial problems.

The current thesis has been organized into twelve chapters. Chapter 1 discusses research background, some basic definitions related to current work, literature review, research motivation and objectives, and outline of the thesis. Chapter 2 is comprises methodology, experimental technique, Response Surface Methodology (RSM), Analysis of Variance (ANOVA), Sensitivity analysis and geometry of the problem. Chapter 3 focuses on sensitivity analysis of thermal conductivity, suction parameter and variable viscosity in viscous fluid flowing over a porous wedge. The investigation of this chapter has been published in **International Communications in Heat and Mass Transfer 135(2022), 106104.** Chapter 4 examines sensitivity analysis of Weissenberg number, thermophoresis parameter and Brownian motion parameter on tangent hyperbolic nanofluid flowing over wedge. The findings of this chapter are submitted in **Mathematical Modelling of Natural Phenomenon**. Chapter 5 investigates the sensitivity analysis of Casson fluid parameter, Falkner–Skan exponent and Prandtl number of casson fluid flow over a wedge. The results observed in this chapter are submitted for possible publication in **Thermal Analysis and Calorimeter**. Chapter 6 focuses on sensitivity analysis of magnetic parameter, Schmidt number and chemical reaction parameter of magneto-Carreau fluid over wedge. The findings are submitted in **Research in Mathematical Science.** Chapter 7 investigates the sensitivity analysis of Weissenberg number viscosity ratio parameter and Prandtl number on Carreau fluid flow over a wedge. The results of this chapter are submitted in **Taiba University of science**. Chapter 8 converses the sensitivity analysis of radiation parameter, Dufour number and Prandtl number of Casson fluid

flowing over a wedge. The findings of this chapter are submitted for possible publication in **Thermal Science International Scientific Journal.** Chapter 9 comprises sensitivity analysis of Lewis number, thermophoresis number and Brownian motion parameter of nanofluid flowing over a wedge. The revision investigation of this chapter is submitted in **Propulsion and Power Research** for possible publication. Chapter 10 investigates the sensitivity analysis of thermophoresis parameter, Brownian motion parameter and Prandtl number of nanofluid with activation energy flowing over a wedge. The findings of this chapter are accepted in **Scientific Reports with article DOI 10.1038/s41598-023-28266-z.** Chapter 11 examines the sensitivity analysis of Schmidt number, chemical reaction and Brownian motion parameters of gyrotactic nanofluid with activation energy over a wedge. The investigation observed in this chapter is submitted in **ZAAM** for possible publication. Chapter 12 discusses the sensitivity analysis of Falkner–Skan exponent and Prandtl number of viscous flows with heat transfer over a wedge. The revision of this chapter is submitted in **The European Physical Journal Plus** for possible publication.

Using appropriate similarity transformations, the governing PDEs of chapter 3 to chapter 12 are converted into systems of non-linear ODEs. The numerical solution is then obtained by using Matlab built in routine bvp4c. The numerical values for output responses are computed for different input parameters. The Prime focus of this thesis is to perform sensitivity analysis. In order to meet this objective, we have built expression for output responses. We have used Central Composite Design (CCD) for RSM to construct the function between input factors and output responses. Then performs sensitivity analysis for the output responses by using the numerical values for different input parameters. The graphical results of sensitivity analysis are presented in the form of bar charts.

List of Symbols

	English Symbols	Units
Re	Reynolds Number	-
R_d	Thermal Radiation parameter	-
D_B	Brownian coefficient	-
Pe	Peclet number	-
T_0	Lower plate temperature	(K)
C_0	Concentration at lower plate	-
c_p	Specific heat capacity	$(Jkg^{-1}K^{-1})$
D_T	Thermophoretic coefficient	(m^2s^{-1})
F_A	Magnetic field strength in tangential direction	-
Ec	Eckert number	-
Sh	Sherwood number	-
E	Activation energy parameter	-
We	Weissenberg number	-
q_r	Radiation heat flux	-
t	Time	(s)
S_M	Schmidt Number	-
Nt	Thermophoretic parameter	-
Nb	Brownian motion parameter	-
Q_m	Mass flux	-
Pr	Prandtl number	-
D_B	Brownian Diffusivity	(m^2s^{-1})
K^*	Porosity parameter	-
Nu	Nusselt number	-
p	Pressure	-

Rd	Radiation parameter	-
k	Thermal conductivity	-
D_{mo}	Microorganism diffusion coefficient	-
k	Porosity parameter	-
τ	Stress tensor	-
M_0, N_0	Dimensionless quantities	-

Greek Symbols		Units
$\tilde{\alpha}$	Thermal diffusivity	-
ρ	Fluid Density	$(Kgsm^{-3})$
δ	Electrical conductivity	(Sm^{-1})
μ	Fluid viscosity	(Nsm^{-2})
σ_e	Stefan Boltzmann constant	-
$(\rho c)_p$	Nanoparticle heat capacity	-
$(\rho c)_f$	Nanofluid heat capacity	-
D	Representative length	-
λ	Porosity parameter	-
ϕ	Nanoparticles volume fraction	-
η	Similarity variable	-

Contents

Chapter 1

Preliminary

1.1 Introduction

The research background connected to title of the thesis is described in this chapter. This work will discuss the sensitivity analysis of specific class of flows, i.e wedge flows. The literature review related to wedge flows and sensitivity analysis are presented in subsection 1.2.1 and 1.2.2 respectively. To perform sensitivity analysis by using Response Surface Methodology (RSM), we need to specify the input parameters and output responses. So, in this chapter also include the definitions of selected parameters and output responses which is discussed during this research.

1.2 Research Background

The history of fluid mechanics is rooted in the history of human beings. Each humanoid resolves such a lot of fluids mechanics issues in his life consciously or unconsciously. Wedge flow is one in every of these necessary fluids mechanics issues, it's important in the field of aeromechanics, increased oil recovery, geothermic industries, heat exchangers, plastic films, geothermic systems, metal spinning, metallurgic processes and chemical compound extrusion. Wedge may be a form that's trilateral in segment. In fluid dynamics, once a surface is appointed to associate degree position (wedge) and also the free stream is diverged from the surface, there would be a distinct fluid speed spreading.

William Falkner and Skan initially analyzed the constant streamline flow past a fixed wedge [1] to manifest the presentation of boundary layer theory of Prandtl. Hartman Blasius under the supervision of Ludwigs Prandtl thought-about the two-dimensional boundary-layer flow. Later, Skan and William Falkner extended the two-dimensional Blasius flow to the self-similar wedge flow. Within the previous couple of years, researchers took ample interest within the Falkner-Skan flows by viewing the influences of various parameters. Later, Hartree examined the results and their

parameter effect on the wedge angle [2]. Lin and Lin studied the problem of wedge flows [3] within the existence of magnetic field. Pop and Watanabe [4] bestowed numerical outcomes for MHD free convection flow over a wedge.

Garg and Rajagopal studied the non-Newtonian fluid flow over the wedge during which they extended the work of Beard [5] and studied wedge flow of 2^{nd} grade fluid. Ishak et. al [6] bestowed a paper that mentioned the Falkner-Skan equation for moving wedge with injuction and suction, which is the extended research work of [7]. Liao [8] has developed the analytical solution for the Falkner-Skan equation against wedge parameter β. Abbasbandy and Hayat extended the work of [9] by together with the magnetic effects. Recently, the study of fluid flow over the wedge has shown keen interest among the researchers. Also, there are some offensively revealed papers on this drawback by River [10], Fang [11], and Pal [12]. Other fascinating studies will be viewed in [13–15].

1.2.1 Literature review on wedge flows

These fluids are of great importance and are frequently found in nature for instance, water, air, gases, urine etc. Therefore, lot of attention has been given to these fluids and discussion is made in moving wedge, static wedge, symmetric wedge, moving wedge with suction and injection, stretching wedge, and porous wedge etc.

A massive literature on Skan and William Cuthbert Falkner flows over a wedge is found in the books of Schlichting [16] and loyal [17]. Magnetohydrodynamic laminar boundary-layer flow over a wedge with suction or injection was noted by Kafoussias et al [18]. The fluid was supposed to be electrically conducing, viscous, and incompressible, with a transverse field applied to the flow orientation. Conjointly Yacob et. al [19] mentioned the matter for a stationary and moving wedge in nanofluids. They numerically analyzed the flow of nanofluids past a static or moving wedge in two dimensions. Riley and Weidman thought-about the boundary layer flow over a stagnant or a moving wedge in an exceedingly viscous fluid [20] and Ishak et al. [21], extension of the flow over a static wedge thought-about by Falkner and Skan [1].

Sakiadis [22] projected fluid flows in an extremely motionless fluid medium over a moving wedge with a constant pace. Yacob et al. [23] examined Falkner-Skan

equation for a static/moving wedge in an exceedingly nanofluid. Asaithambi [24] used FDM (finite difference method) to urge numerical results subject to $-0.19884 \leq \beta \leq 2$. Kumari et al. [25] inspected the numerical solution for the case $\beta > 1$. Chang and Yang [26] presented analytical resolution for $\beta = -1$ for a constant plate. Zhang and Fang [27] showed an investigatory resolution for a moving and penetrable wall once $\beta = -1$. Das et. al [28] investigated the thermal radiation consequences on the convective slip flow of a somewhat rarefied fluid that conducts electricity over a wedge.

Unlike the Newtonian fluids there is no any single constituent equation that defines the behaviours of non-Newtonian fluids. This could be due to the numerous natures of non-Newtonian fluids. Navier-Stokes equations are not enough to define the flow behaviour of non- Newtonian fluids. To fill this gap we would like some physical models, just like the Cross and Ellis model, the Casson model, the Carreau model etc. Non-Newtonian fluids unit of measurement is very useful in aerodynamics, paper production, glass process, continuous casting and many others. The use of physical conditions of non-Newtonian fluid flows is tough for scientists and engineers in theoretical and experimental investigations conjointly. The cause behind this could be that these fluids unit of measurement are very difficult in nature and there is no specific constituent equation to represent all flow properties of non-Newtonian fluids. i.e., the flow past a wedge placed symmetrically with relevancy the flow direction. Garg [29] analyzed the passage of a second-grade incompressible fluid past a wedge with surface suction. Chamkha et al. [30] inspected the results of thermal emission on forced convection on non-isothermal wedge. Later, Eraslan and Kim [31] investigated the boundary-layer flow of a power-law fluid over wedges with wall mass injection while maintaining the requirement for the presence of similarity solutions. Hady and Hassanien studied the effect of magnetic flux of nanofluids passing through the porous wedge. Hsu et al. [32] studied how temperature and flow fields past a wedge were affected by viscoelasticity using wall suction/injection. Massoudi [33] recently obtained non-similarity answers for the natural phenomenon and heat transfer equations for non-Newtonian fluid wedge flows. Watanabe [34] and Pop [35] scrutinized forced and free convection boundary layer flows past a wedge, correspondingly. Kumari et al. [36] discussed how a magnetic field affects mixed convection flow across a wedge covered in a highly spongy media.

Several researchers, Hossain et al. [37] Pantokratoras [38] and Pal and Mondal [39], re-examined the wedge flow disadvantage beneath varied thermo-physical circumstances. Kandasamy et al. [40] mentioned the impact of natural process on flow past a wedge inside the existence of injection/ suction.

Riley and Weidman [41] and Ishak et al. [42, 43] extended the natural phenomena flow over a stationary or moving wedge in a very viscous fluid under several physical parameters. They created self-similar equations that were computationally resolved using similarity transformations. Kandasamy et al. [44] described the mutual influence of thermophoresis, variable consistency and associated natural process on combined convection flow over a porous wedge entrenched with an extremely non-Darcy porous medium.

1.2.2 Literature review on sensitivity analysis

After the arrangement of literature review on wedge flows, now we will discuss the literature review on sensitivity analysis. There is sufficient literature on sensitivity analysis we will start from Chan et. al [45], in which they mentioned the sensitivity analysis of a water-based bionanofluid flowing over a wedge surface. They applied Response Surface Methodology (RSM) along with sensitivity analysis to check the dependency of Lewis number, Sherwood number, Nusselt number, Brownian movement parameters and Reynolds number. Darbari et. al [46] examined the entropy and sensitivity analysis for the nanofluid flow passing through a channel by applying RSM. They studied the sensitivity of Reynolds number, solid volume fractions and particle diameter.

Rashidi et al [47] made the sensitivity analysis on heat transfer for different input parameters such as Reynolds number, porous substrate and Darcy number using RSM. They discovered that Nu_x is most sensitive to Darcy number. They also noticed that the sensitivity of Nu_x rises as the thickness of porous substrate increases. In another study Rashidi et al. [48] examined the sensitivity analysis of different responses on triangular obstacle by using RSM. They observed that Nu_x is more sensitive then drag coefficient to wedge angle. Other interesting results of sensitivity analysis for flow through a triangle obstacle can be viewed in [49]. Vahedi et.al [50] mentioned sensitivity analysis and optimization of Cu-water nanofluid flow past a

wedge; they analyzed the results of the wedge angle, the magnetic flux, and also the nanoparticle volume fraction on associate incompressible flow over a wedge. They apprehended that the sensitivity of the common Nusselt range to the wedge angle does not modification with the magnetic parameter. Shafiq et.al [51] discovered the sensitivity analysis of tangent hyperbolic fluids across stretching surface. They discovered that increasing the Lewis and thermophoresis numbers increases the sensitivity of the Nusselt number.

Darbari et al. [52] discussed the sensitivity analysis of nano fluid flow passing through a channel. They used RSM to examine the sensitivity of responses with the effect of different input parameters. They summarized the results as; the Entropy generation is most sensitive to Reynolds number. Another important result concluded by them, the sensitivity of total entropy generation to Reynolds number diminishes as nanoparticle diameter increases. Shirvan et al. [53] examined the sensitivity analysis of different input parameters in solar heat exchanger by using RSM. They concluded that there is positive sensitivity of emissivity and negative sensitivity of Ri-number towards Nu_x. The sensitivity of different input factors of Cu-water nanofluids with the effect of MHD was explored by [54]. They observed that the magnetic effect does not change the sensitivity of Nu_x. Abdelmalek et al. [55] explored the sensitivity of Casson fluid flow by using RSM. The observed results of their investigation were that, for all levels of magnetic parameters there is positive sensitivity to Nu_x towards Stefan blowing parameter. Recently, Hussain et al. [56] discussed the sensitivity analysis of viscous fluid over a wedge with thermal conductivity. They examined how various input parameters affected the dependent output responses using RSM. They concluded that, the sensitivity of Cf_x rises as raising the value of parameter ε. Another conclusion of their observation is that, by increasing the input parameter ξ the sensitivity of Cf_x increases. Nu_x is most sensitive to ξ among other parameters. Some other researchers also applied RSM to investigate the sensitivity of different output responses which may be seen in [57 - 60].

Motivated by the contributions made thus far, the authors intend to investigate sensitivity analysis of wedge flows for Newtonian and non-Newtonian fluids over a wedge. Before performing sensitivity analysis, we have first of all adopted RSM to develop empirical relations for output responses. We have taken 95% confidence interval and prepared Analysis of Variance (ANOVA) table, to see the goodness of fit

of the empirical relations among each of response variables and input parameters. It is clear from the preceding literature that no attempts are made to analyses the sensitivity of wedge flows for Newtonian and non-Newtonian fluids over a wedge. This unique mathematical and statistical method is expected to fill the gap in literature and serve as foundation for upcoming problems of fluid dynamics.

1.3 Research Motivation and Objectives

The present research work is concerned with "Sensitivity analysis of wedge flows for Newtonian and non-Newtonian fluids". The prime focus of this research work is to do the sensitivity analysis of wedge flows. In pursuance to this objective our aim will be to highlight system's sensitivity of some already existing literature. We will also model some new problems and will solve them by providing either analytical or numerical solutions. Then we will utilize this obtained solution to find a list of values for response qualities like Skin friction coefficients, Nusselt, density or Sherwood numbers. Next we will have to develop a correlation among response variables and input variables like, Reynolds number, Prandtl number etc. In order to achieve this objective we will present a detail regarding Response Surface Methodology (RSM) in our research work.

The considered problems will help to obtain following objectives,

- to explore the sensitivity analysis of the different parameters to the wedge angle.
- to explore the impact of sensitivity of different parameters of particles on reaching the thermal boundary layer's edge.
- to combine the two or more different analysis and to develop new theories where it is necessary especially in application point of view.
- we will also examine the advantages and comparative analysis of the established work with existing work and will try to show the reliability and effectiveness of the established work.

1.4 Dimensionless Numbers

Reynolds Number

The physical quantity Reynolds number is the ratio of two quantities (inertial force to viscose force).

Prandtl Number

The Prandtl number, Pr, is a dimensionless parameter that expresses how much momentum is diffused relative to how much heat is diffused in a fluid.

Eckert number

The ratio of the adventive mass transfer to the heat dissipation potential is known as the Eckert number, which has no dimensions. The flow's kinetic energy in relation to enthalpy changes across the thermal boundary layer is measured by the Eckert number.

Weissenberg Number

Weissenberg number actually refers to the ratio of elastic to viscous forces. It is possible to examine the non-Newtonian viscoelastic fluid using this dimensionless number.

Activation Energy

Activation energy is the minimal amount of energy that reactive molecules need to transform into a product.

Thermal Radiation

When a surface is heated, thermal radiation occurs. The process of thermal radiation involves the heated surface emitting energy in all directions, which travels at the speed of light to the site of absorption.

Thermophoresis parameter

Thermophoresis is the transport force caused by the existence of a temperature gradient. This force directs gas-borne particles with sizes smaller than 10 metres in

the direction of the region with lower temperatures.. Thermophoresis is important in high temperature areas, such as the radiant section of a boiler.

Lewis number

The Lewis number is defined as the ratio of heat diffusivity to mass diffusivity. It describes fluid movements that simultaneously transmit heat and mass. As a result, the Lewis number is a measure of the respective thicknesses of the thermal and concentration boundary layers.

Brownian motion

The Brownian motion and porosity parameters exhibit the opposite behaviour when it comes to mass transmission. Both friction factor coefficients rise as the nanoparticle volume fraction increases, whereas the Sherwood number exhibits the opposite effect.

Schmidt number

The dimensionless number known as the Schmidt number is named after the German engineer Ernst Heinrich Wilhelm Schmidt. The ratio of momentum diffusivity to mass diffusivity is known as the Schmidt number.

Skin friction coefficient

The skin friction coefficient is a crucial dimensionless parameter in boundary-layer flows. It describes shear stress as the portion of the local dynamic pressure that is sensed on the surface.

Nusselt number

The ratio of convective to conductive heat transport in a fluid is known as the Nusselt number.

Sherwood number

The Sherwood number was named after Thomas Kilgore Sherwood. The ratio of convective mass transfer to mass diffusivity is described as the Sherwood number.

Chapter 2

Methodology and Geometry of Problems

2.1 Methodology

For every research a method is needed to explain and understand the topic to prove the validity and reliability of the study. This research is exploratory in nature; it will explore the sensitivity analysis of different parameters on the flow of Newtonian and non-Newtonian fluids. The objective of the present work is to develop empirical relation between input parameters and output responses. In order to determine the relationship between the input parameters and the output replies, we employed RSM. The detail of RSM is given in next section 2.2.1 In order to apply RSM we need responses to certain values of governing parameters of problem. The numerical solution is obtained by simulating the modelled problem using symbolic software Matlab. RSM has been used to develop a correlation among response variable(s) to each input variable.

2.2 Experimental Design

It is necessary to establish some sort of actual relationship between output and input variable in order to undertake a sensitivity analysis. Empirical development is a useful approach for obtaining correlations among output/response variables and input variables. It has significance in several experimental analyses like [61-65]. There are different methods to correlate input parameters and output response; some of them are RSM, ANN and time series analysis etc. In this thesis we have used RSM to investigate the empirical development of wedge flows for Newtonian and non-Newtonian fluids. Since RSM is the main subject of the current work, we explain this method briefly in section 2.2.1.

2.2.1 Response Surface Methodology (RSM)

There are different methodologies to obtain empirical models; some of them are time series analysis, machine learning through ANNs and RSM. RSM is a statistical

technique used to model a problem in which responses are analyzed with respect to corresponding input parameters (variables). The RSM is one in every of the foremost wide used experimental styles for optimization. It's an unremarkably used mathematical and applied mathematics for modelling and analysing the results within which completely different variables have an effect on the response of interest and also the purpose of this method is to optimize the response. RSM was developed by Box and Wilson [66] to discuss the sensitivity of model's uncertainty. RSM was also used to examine experimental study and industrial experimental work. In this context Joardar et al. [67] used RSM to discuss the effect of parameters in their experimental work. There are also several works presented in which RSM was used in experimental study [68-74]. The general form of relationships between input parameters and output responses are as follows [75-76].

$$Response = r_o + \sum_{i=1}^{n} r_i a_i + \sum_{i=1}^{n} r_{ii} a_i^2 + \sum \sum_{i<j=2}^{n} r_{ij} a_i a_j. \quad (2.1)$$

n denotes number of input parameters, a_i denotes coded variables, r_o is constant and known as intercept term, r_i , r_{ii} and r_{ij} are coefficients for linear, quadratic, and mixed term respectively. By using Central Composite Design (CCD) we will compute the numerical experimental design whose general expression is $2^n + 2n + P$. Where P is the centre point and n is the number of input parameters. In our work we have choose three input parameters ($n = 3$) namely *Nt, Nb* and *Pr* which are displayed in Table 2 with their symbol and levels. For the case of full quadratic model under RSM, we can express Eqn. (2.1) for output responses in the following forms:

$$Response = r_o + r_1 a_1 + r_2 a_2 + r_3 a_3 + r_{11} a_1 a_2 + r_{12} a_1 a_3 + r_{13} a_2 a_3 + r_{21} {a_1}^2 + r_{22} {a_2}^2 + r_{23} {a_3}^2 , \quad (2.2)$$

The Response Surface Methodology (RSM) is employed for,

- adaptation of a theoretical (empirical) model to the data gathered in accordance with the selected style.
- determining the input (control) parameter circumstances that result in the model's maximum or least amount of responsiveness to a target.

Actually, the ability of the researcher to create a suitable output function approximation is crucial for the use of RSM. Generally, a low-order polynomial in some comparatively little region of the variable area is suitable. In several conditions, either a first-order or a second order model is employed.

2.2.2 Analysis of Variance (ANOVA)

ANOVA is a statistical method by which the model accuracy and validity be checked. ANOVA is also used to explain the model fitness and variability performance. ANOVA will be performed by using statistical software MINITAB-19. By using RSM, ANOVA calculate the R^2,$Adj\ R^2$, F-value, and P-value. The ANOVA table for output response are depicted in tabular form in each chapter, in which all the corresponding F-value and P-value are specified. The regression coefficient for output responses are also shown in tabular form for corresponding problems. With the help of P-value it is decided that which terms should be retained and which one should be neglected. For empirical development the P-value is generally taken to be less than or equal to 0.05.

ANOVA result for different input parameters and output responses are presented in Chapter 3 - 12. By using RSM, regression coefficients for output response are depicted in Tabular form.

2.2.3 Validity of RSM

It is necessary to discuss the residuals, lack of fit, and observation order while utilising RSM. The inconsistency between the dependent variable and the observed input parameters is defined as the residual. Residuals are essential for determining model correctness. If all of the residuals are zero, then the model is perfect. The model's accuracy falls as the residuals go far to zero. The residual plots for the output responses are presented in graphical form in each chapter. When the residuals are compared to the fitted values, a strong relationship is revealed.

Scatter plots, histogram and observation order verses residuals helps to check the validity of developed correlations between the output response and the input parameters. The graphical form of residual plots is displayed to check the validity of empirical models in each chapter. Scatter plot shows the connection between the output response and the input parameters. The histogram which has the symmetrical scattering and less skewed which demonstrates the good relationship of output responses with input parameters. The observation order verses residuals demonstrate that if observation order is increased, the residual of the output responses drops,

demonstrating good agreement between the probabilities plots. The residuals graph with largest fluctuation for responses indicates the strong correlations between input parameters and output variables.

2.3 Sensitivity Analysis

It is the study of abstruseness criteria generated within the output of the model, dealt out by the input factors that end up in the assessment of the lustiness of the model. Sensitivity analysis is applied in engineering issues to see in what ways different values of variable completely have an effect on a desired output. This system is incredibly helpful once trying to see the effect of many influence parameters on outputs of a problem. Sensitivity analysis can even facilitate the scientists and engineers to see that parameters are the key drivers of a model's results. This method is used to determine how a different value for an independent parameter will affect a particular dependent parameter under a particular set of assumptions.

Establishing our analysis's objective and, in turn, defining the output function's shape, are general procedures to be taken before conducting a sensitivity analysis. Then decide the input factors that are the parameter such as, Reynolds number, Prandtl number, Hartman number, Brinkman number, Soret number and many others. In order to develop correlation among output variable(s) and input variables we take data for output variables. Then we fit nonlinear regression model on the data. Then we evaluate the model and produce the output. Finally, we will analyze the model outputs and will draw our conclusions.

2.4 Geometry of the Problems

The two-dimensional incompressible fluid flow across a wedge is considered in this thesis. Figure 2.1 depicts the geometry of the flow problem of this thesis. The tip of the wedge is considered as origin. Consider the x-axis parallel to the flow direction and the y-axis perpendicular to the wedge. The velocity of fluid at the wedge's wall is $U_w(x)$, and the wedge's free stream velocity as $U_e(x) = U_0 x^m$ where, U_∞ and U_0 are constant and m is known as Falkner- Skan constant with $0 \leq m < 1$. The wedge angle is equal to $\Omega = \beta\pi$ where $\beta = \frac{2m}{m+1}$ is the Hartree pressure gradient parameter.

Also, we considered the temperature at the wedge surface is T_w and the ambient temperature is taken as T_∞.

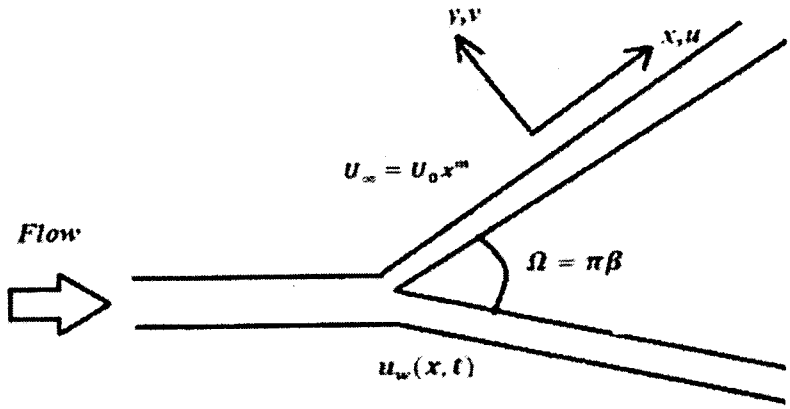

Figure 2.1 Geometry of the problem

Chapter 3

Viscous Fluid Flowing over a Porous Wedge

In this chapter, the sensitivity of pertained parameter thermal conductivity, suction parameter and variable viscosity for a viscous fluid flowing over a wedge is evaluated by using Response Surface Methodology (RSM). Using the proper similarity transformation, the governing PDEs are converted into a collection of non-linear ODEs. The numerical values of transformed ODEs are calculated by using a numerical technique bvp4c. The obtained results are then compared by previous work and found good results which are shown in tabular form. This shows the validity of our numerical results. The data extracted from numerical simulation helps to calculate the data as responses for all combination of parameters in experimental design. The correlated equations for input and output responses are developed by using RSM. Also, the residuals for output responses are plotted by using ANOVA. After developing a correlation for each response variables, sensitivity analysis is performed and results are shown using tables and graphs.

3.1 Mathematical Formulation

In this chapter the problem of viscous fluid flowing over a porous wedge is considered. The simplified form of governing equations is those formulated in [37]. The governing boundary layer equations for the problem are [37],

$$\frac{\partial u}{\partial x}+\frac{\partial u}{\partial y}=0, \tag{3.1}$$

$$u\frac{\partial u}{\partial x}+v\frac{\partial u}{\partial y}=U_e\frac{dU_e}{dx}+\frac{1}{\rho}\frac{\partial}{\partial y}\left(\mu\frac{\partial u}{\partial y}\right), \tag{3.2}$$

$$u\frac{\partial T}{\partial x}+v\frac{\partial T}{\partial x}=\frac{1}{\rho c_p}\frac{\partial}{\partial y}\left(\kappa\frac{\partial T}{\partial x}\right). \tag{3.3}$$

Here u and v are horizontal and vertical components of velocity respectively, T is the temperature, $U_e(x)$ is the free stream velocity, μ is the dynamic viscosity and κ the thermal conductivity. Here thermal conductivity and dynamic viscosity varies with temperature and are defined by [37],

$$\mu = \mu_\infty \left[1 + \alpha_1 \frac{T-T_\infty}{T_0-T_\infty}\right], \kappa = \kappa_\infty \left[1 + \alpha_2 \frac{T-T_\infty}{T_0-T_\infty}\right]. \tag{3.4}$$

Where μ_∞ is scalar viscosity and κ_∞ is the scalar thermal conductivity of the ambient fluid, α_1 and α_2 are constants. T_0 is some reference temperature and T_∞ is the temperature of the ambient fluid. The associated boundary conditions of the problem are [37],

$$\begin{aligned} &u=0, \quad v = -V_w, \quad -\kappa_\infty \left(\frac{\partial T}{\partial y}\right)_{y=0} = q_w, \, at \, y = 0, \\ &u \to U_\infty = U_0 x^m, \; T \to T_\infty \quad as \; y \to \infty. \end{aligned} \tag{3.5}$$

The simplified form of Eqns. (1) – (3) governing the flow and heat transport subject to transformation [37],

$$\begin{aligned} &\psi = v_\infty \sqrt{\frac{2}{1+m}} Re_x^{1/2} [f(\xi,\eta) + \frac{1+m}{2}\xi], \\ &T - T_\infty = \sqrt{\frac{2}{1+m}} \frac{q_w x}{k_\infty} Re_x^{-1/2} \theta(\xi,\eta), \\ &\eta = \sqrt{\frac{m+1}{2}} \frac{y}{x} Re_x^{1/2}, \\ &\xi = \sqrt{\frac{2}{1+m}} \frac{V_w x}{v_\infty} Re_x^{-1/2}, \end{aligned} \tag{3.6}$$

where ψ is the stream function, $f(\xi,\eta)$ is the dimensionless stream function, η is similarity variable, $\theta(\xi,\eta)$ is the dimensionless temperature of the fluid, $v_\infty = \mu_\infty/\rho$ is the free stream kinematic viscosity, $Re_x = U_e x/v_\infty$ is the local Reynolds number and ξ is termed as the local transpiration parameter, which varies in value (positive and negative) when injected and suctioned via the surface, are

$$(1 + \varepsilon\xi\theta)f''' + \varepsilon\xi\theta' f'' + ff'' + \frac{2m}{1+m}(1 - f'^2) + \xi f'' = \frac{1-m}{1+m}\xi \left(f' \frac{\partial f'}{\partial \xi} - f''' \frac{\partial f}{\partial \xi}\right), \tag{3.7}$$

$$\frac{1}{Pr}(1 + \gamma\xi\theta)\theta'' + \gamma\xi\theta'^2 + f\theta' - \frac{1-m}{1+m}\theta f' + \xi\theta' = \frac{1-m}{1+m}\xi \left(f' \frac{\partial \theta}{\partial \xi} - \theta' \frac{\partial f}{\partial \xi}\right). \tag{3.8}$$

The boundary conditions (3.5) in view of transformation (3.6) yield,

$$f(\xi,0) = f'(\xi,0) = 0, \qquad \theta'(\xi,0) = -1,$$

$$f'(\xi,\infty) \to 1\,, \quad \theta(\xi,\eta) \to 0 \; as \; \eta \to \infty. \tag{3.9}$$

Important flow quantities that describe the hydrodynamics and thermal performance are Cf_x and Nu_x respectively and are defined by

$$C_{fx} = \frac{\tau_w x}{(1/2)\rho U_\infty^2} \;\; and \;\; Nu_x = \frac{q_w x}{\kappa_\infty (T_0 - T_\infty)}. \tag{3.10}$$

Where τ_w is the shear stress at the surface defined by

$$\tau_w = \mu_\infty \left(\frac{\partial u}{\partial y}\right)_{y=0} \tag{3.11}$$

In view of transformation (3.6), the Cf_x and Nu_x from Eq. (3.10) now become in the following form,

$$\frac{1}{\sqrt{2}(1+m)} C_{fx} Re_x^{1/2} = f''(\xi,0) \tag{3.12}$$

and

$$\sqrt{\frac{2}{1+m}} \frac{Nu_x}{Re_x^{1/2}} = \frac{1}{\theta(\xi,0)} \tag{3.13}$$

The perturbation approach is used to identify the problem's several solutions. (Eqns. (3.7) – (3.9)) in terms of small parameter ξ.

Solution for $0 < \xi < 1$

In this context, expand the functions f(ξ, η)and θ(ξ, η) as power series of ξ [37],

$$f(\xi,\eta) = \sum_{i=0}^{\infty} \xi^i f_i(\eta)\,, \;\; \theta(\xi,\eta) = \sum_{i=0}^{\infty} \xi^i \theta_i(\eta)\,, \tag{3.14}$$

On invoking Eq. (3.14) into Eqns. (3.7) – (3.10), the following systems of non-linear ODE's are formed:

Zeroth order system ($O(\xi^0)$)

$$f_0''' + f_0 f_0'' + \frac{2m}{1+m}(1 - f_0'^2) = 0, \tag{3.15}$$

$$\frac{1}{Pr}\theta_0'' + f_0\theta_0' - \frac{1-m}{1+m}\theta_0 f_0' = 0, \tag{3.16}$$

$$f_0(0) = f_0'(0) = 0, \theta_0'(0) = -1, f_0'(\infty) \to 1, \theta_0(\infty) \to 0. \tag{3.17}$$

First order system ($O(\xi^1)$):

$$f_1''' + \varepsilon(\theta_0 f_0''' + \theta_0' f_0'') + f_0 f_1'' + \frac{1}{1+m} f_1 f_0'' + f_0'' - \frac{1+3m}{1+m} f_1' f_0' = 0, \tag{3.18}$$

$$\frac{1}{Pr}\theta_1'' + \frac{1}{Pr}\gamma(\theta_0\theta_0'' + \theta_0'^2) + f_0\theta_1' + \frac{2}{1+m} f_1\theta_0' - \frac{1-m}{1+m}\theta_0 f_1' - \frac{2(1-m)}{1+m}\theta_1 f_0^1 + \theta_0' = 0, \tag{3.19}$$

$$f_1(0) = f_1'(0) = \theta_1'(0) = 0,$$

$$f_1'(\infty) = \theta_1(\infty) = f_0'(\infty) \to 1, \tag{3.20}$$

$$\theta_0(\infty) \to 0.$$

Second order system ($O(\xi^2)$):

$$f_2''' = \varepsilon(\theta_0 f_1''' + \theta_1 f_0''' + \theta_0' f_1'' + \theta_1' f_0'') + f_0 f_2'' + \frac{2}{1+m} f_1\theta_1' + \frac{3-m}{1+m} f_2\theta_0' + \theta_1' - \frac{1-m}{1+m}\theta_0 f_2' = 0, \tag{3.21}$$

$$\frac{1}{Pr}\theta_2'' + \gamma(\theta_0\theta_1'' + \theta_1\theta_0'' + 2\theta_1'\theta_0') + f_0\theta_2' - \frac{2(1-m)}{1+m}\theta_1 f_1' - \frac{3(1-m)}{1+m}\theta_2 f_0' = 0, \tag{3.22}$$

$$f_2(0) = f_2'(0) = \theta_2'(0) = 0,$$

$$f_2'(\infty) = \theta_2(\infty) \to 0. \tag{3.23}$$

Now by using the perturbation expansion Eq. (3.14) into skin friction coefficient and Nusselt number in Eq. (3.12) and Eq. (3.13) respectively, have the following forms,

$$\frac{1}{\sqrt{2}(1+m)} C_{fx} Re_x^{1/2} = f_0''(0) + \xi f_1''(0) + O(\xi^2), \tag{3.24}$$

$$\sqrt{\frac{2}{1+m}} \frac{Nu_x}{Re_x^{1/2}} = \frac{1}{\theta_0(0) + \xi\theta_1(0) + O(\xi^2)}. \tag{3.25}$$

Solution for $\xi > 1$:

Given the fact that $\theta = O(\xi^{-1})$ as $\xi \to \infty$, it is important to determine the proper scaling for f and η. As a result, the dependent and independent variables are substituted as follows:

$$f = \xi^{-1}\hat{f} = 0, \quad \theta = \xi^{-1}\hat{\theta}, \quad \hat{\eta} = \xi\eta. \tag{3.26}$$

Substituting these transformations into Eqns. (3.7) – (3.9) and removing the hats for simplicity, we have

$$(1+\epsilon\theta)f''' + \epsilon\theta' f'' + \frac{2m}{1+m}\xi^{-2}[ff'' + 1 - f'^2] + (1+\varepsilon\theta)^2 f'' = \frac{1-m}{1+m}\xi^{-1}\left(f'\frac{\partial f'}{\partial \xi} - f'''\frac{\partial f}{\partial \xi}\right), \tag{3.27}$$

$$\frac{1}{Pr}(1+\gamma\theta)\theta'' + \frac{1}{Pr}\gamma\theta'^2 + \theta' + \frac{2m}{1+m}\xi^{-2}f\theta' = \frac{1-m}{1+m}\xi^{-1}\left(f'\frac{\partial \theta}{\partial \xi} - \theta'\frac{\partial f}{\partial \xi}\right). \tag{3.28}$$

The corresponding boundary conditions are

$$f(\xi,0) = f'(\xi,0) = 0, \theta'(\xi,0) = -1,\ f'(\xi,\infty) \to 1, \theta(\xi,\infty) \to 0. \tag{3.29}$$

Now by using regular perturbation method and expand the functions f(ξ, η)and θ (ξ, η) in powers of ξ^{-2} as shown below.

$$f(\xi,n) = \sum_{i=0}^{\infty}\xi^{-i} f_i(\eta),\ \theta(\xi,n) = \sum_{i=0}^{\infty}\xi^{-i}\theta_i(\eta). \tag{3.30}$$

When we plug the following expansions into Eq. (3.27) and Eq. (3.28) and take terms up to O (ξ^{-2}), we obtain

Zeroth order system ($O(\xi^0)$):

$$(1+\varepsilon\theta_0)f_0''' + \varepsilon\theta_0' f_0'' + f_0'' = 0, \tag{3.31}$$

$$\frac{1}{Pr}(1+\gamma\theta_0)\theta_0'' + \frac{1}{Pr}\gamma\theta_0'^2 + \theta_0' = 0, \tag{3.32}$$

$$f_0(0) = f_0'(0) = 0, \theta_0'(0) = -1, \qquad f_0'(\infty) \to 1, \theta_0(\infty) \to 0. \tag{3.33}$$

First order system ($O(\xi^{-1})$):

$$(1+\varepsilon\theta_0)f_1''' + \epsilon(\theta_1' f_0''' + f_1''\theta_0' + f_0''\theta_1') + \left(\frac{2m}{1+m}f_0 f_0'' + \frac{2m}{1+m}(1-f_0'^2) + f_1''\right) = 0. \tag{3.34}$$

$$\frac{1}{Pr}(1+\gamma\theta_0) + \frac{1}{Pr}\gamma(\theta_1\theta_0'' + 2\theta_1'\theta_0') + \theta_1' + \frac{2m}{1+m}f_0\theta_0' = 0, \tag{3.35}$$

$$f_1(0) = f_1'(0) = \theta_1'(0) = 0,\ f_1'(\infty) = \theta_1(\infty) \to 0. \tag{3.36}$$

Second order system ($O(\xi^{-2})$):

$$(1+\varepsilon\theta_0)f_2''' + \epsilon(\theta_1 f_1''' + \theta_2 f_0''' + \theta_2' f_0'' + \theta_1' f_1'' + \theta_0 f_2'') + f_2'' + \frac{2m}{1+m} f_0 f_1'' + \frac{2(2m-1)}{1+m} f_1 f_0'' + \frac{2(3m-1)}{1+m} f_1' f_0' = 0, \tag{3.37}$$

$$\frac{1}{Pr}(1+\gamma\theta_0)\theta_2'' + \frac{1}{Pr}\gamma(\theta_1\theta_1'' + \theta_2\theta_0'' + \theta_1'^2 + 2\theta_2'\theta_0') + \theta_2' + \frac{2m}{1+m} f_0\theta_1' - \frac{2(1-m)}{1+m} f_0'\theta_1 + f_1\theta_0' = 0, \tag{3.38}$$

$$f_2(0) = f_2'(0) = \theta_2'(0) = 0,\ f_2'(\infty) = \theta_2(\infty) \to 0. \tag{3.39}$$

The asymptotic values of the local skin-friction (Cf_x) and the local Nusselt number (Nu_x) may be determined using the following relationships:

$$\frac{1}{\sqrt{2}(1+m)} C_{fx} Re_x^{1/2} = \xi[f_0''(\xi,0) + \xi^{-2} f_1''(\xi,0) + \ldots], \tag{3.40}$$

$$\sqrt{\frac{2}{1+m}} \frac{Nu_x}{Re_x^{1/2}} = \frac{\xi}{\theta_0(\xi,0) + \xi^{-2}\theta_1(\xi,0) + \ldots}. \tag{3.41}$$

The non-linear system of perturbed equations are simulate numerically for different ordered systems by using Matlab built in routine bvp4c. The simulated results for Cf_x and Nu_x are presented in Table 3.1 and Table 3.2 and compared them with [37] and find close agreement.

Table 3.1: Comparison for the local skin friction coefficient

ξ	$\varepsilon = 0.0$				$\varepsilon = 0.5$			
	$\gamma = 0$		$\gamma = 0.5$		$\gamma = 0$		$\gamma = 0.5$	
	[37]	Present	[37]	Present	[37]	Present	[37]	Present
0.0	1.0389	1.0389	1.0389	1.0389	1.0389	1.0389	1.0389	1.0389
0.2	1.1540	1.1501	1.1540	1.1501	1.0378	1.0377	1.0378	1.0377
0.4	1.2692	1.2612	1.2692	1.2612	1.0368	1.0365	1.0368	1.0365
0.8	1.4995	1.4836	1.4995	1.4836	1.0348	1.0342	1.0348	1.0342
1.0	1.6146	1.5947	1.6146	1.5947	1.0338	1.0330	1.0338	1.0330

Table 3.2: Comparison for the local Nu_x

ξ	$\varepsilon = 0.0$				$\varepsilon = 0.5$			
	$\gamma = 0$		$\gamma = 0.5$		$\gamma = 0$		$\gamma = 0.5$	
	[37]	Present	[37]	Present	[37]	Present	[37]	Present
0.0	0.5604	0.5605	0.5604	0.5604	0.5604	0.5605	0.5604	0.5605
0.2	0.6503	0.6411	0.5875	0.5822	0.6357	0.6352	0.5756	0.5754
0.4	0.7744	0.7488	0.6174	0.6056	0.7344	0.7330	0.5917	0.5911
0.8	1.2524	1.1280	0.6872	0.6587	1.0648	1.0589	0.6266	0.6253
1.0	1.8116	1.5104	0.7284	0.6889	1.3739	1.3616	0.6457	0.6439

3.2 Experimental Design

3.2.1 Response Surface Methodology (RSM)

The selected input parameters along with their levels according to CCD are presented in Table 3.3.

Table 3.3: Design input factor and their level.

Type	Factor	Symbol	Levels		
			-1	0	1
Input Factors	ξ	A	0	5	10
	ε	B	0	0.25	0.5
	γ	C	0	0.25	0.5

Table 3.4: Experimental design and measured responses.

Experiment number	Point type	Coded values			Real values			Responses	
		A	B	C	ξ	ε	Γ	Cf_x	Nu_x
1	Factorial	-1	-1	-1	0	0.00	0.00	1.0389	0.5605
2		1	-1	-1	10	0.00	0.00	10.1333	7.0400
3		-1	1	-1	0	0.50	0.00	1.0389	0.5605
4		1	1	-1	10	0.50	0.00	5.9463	7.0338
5		-1	-1	1	0	0.00	0.50	1.0389	0.5605
6		1	-1	1	10	0.00	0.50	10.1333	2.1204
7		-1	1	1	0	0.50	0.50	1.0389	0.5605
8		1	1	1	10	0.50	0.50	3.0195	2.0817
9	Axial	-1	0	0	0	0.25	0.25	1.0389	0.5605
10		1	0	0	10	0.25	0.25	7.5405	4.5484
11		0	-1	0	5	0.00	0.25	5.2681	2.3682
12		0	1	0	5	0.50	0.25	2.6457	2.3447
13		0	0	-1	5	0.25	0.00	3.9457	3.5770

14		0	0	1	5	0.25	0.50	2.8093	1.2508
15-20	Centre	0	0	0	5	0.25	0.25	3.5164	2.3547

3.2.2 Analysis of variance (ANOVA):

ANOVA specifies which terms of the equation in correlations should be preserved. All the statistics for Cf_x and the Nu_x are determined using ANOVA, which are reported in Table 3.5 and Table 3.7 respectively. Each term of Eqn. (2.2) has a specific P-value and F-value. All the P-value and F-value are depicted in Table 3.5 and Table 3.7. In case of skin friction coefficient the coefficient of determination (R^2) and adjusted coefficient of determination ($Adj\ R^2$) of the RSM model were found as 99.12% and 98.33% respectively. The F-test result is 125.39 indicating that the model is significant. However, in case of coefficient of determination(R^2) and adjusted coefficient of determination ($Adj\ R^2$) of the RSM model are 99.99 % and 99.97% respectively.

Table 3.5: ANOVA for (a) Cf_x (b) Nu_x

Source	DF	Adj SS	Adj MS	F-Value	P-Value	
(a)						
Model	9	141.119	15.6799	125.39	0.000	Significant
Linear	3	120.756	40.2520	321.89	0.000	-
Square	3	2.258	0.7526	6.02	0.013	-
Interaction	3	18.105	6.0350	48.26	0.000	-
Error	10	1.251	0.1251			
Lack-of-Fit	5	1.251	0.2501	*	*	Significant
Pure Error	5	0.000	0.0000			-
Total	19					-

(b)

Model	9	67.3445	7.4827	7863.28	0.000	Significant
Linear	3	54.9666	18.3222	19254.03	0.000	-
Square	3	0.1962	0.0654	68.74	0.000	-
Interaction	3	12.1817	4.0606	4267.08	0.000	-
Error	10	0.0095	0.0010			-
Lack-of-Fit	5	0.0095	0.0019	*	*	Significant
Pure Error	5	0.0000	0.0000			-
Total	19	67.3540				-

Table 3.6: Estimated Regression coefficients for (a) Cf_x (b) Nu_x

Terms	Coefficient	Significant
(a)		
Constants	3.577	Yes
A	3.158	Yes
B	-1.392	Yes
C	-0.406	Yes
A^2	0.621	Yes
B^2	0.289	No
C^2	-0.291	No
AB	-1.413	Yes
AC	-0.366	Yes
BC	-0.366	Yes
	$R^2 = 99.12\%$	$Adj\ R^2 = 98.33\%$

(b)		
Constants	2.3621	Yes
A	2.00218	Yes
B	-0.00684	No
C	-1.21979	Yes
A^2	0.1813	Yes
B^2	-0.0167	No
C^2	0.0408	No
AB	-0.0056	No
AC	-1.2340	Yes
BC	-0.0041	No
	$R^2 = 99.99\%$	$Adj\ R^2 = 99.97\%$

3.3 Sensitivity Analysis

The significant factors for Cf_x are A, B, C, A^2, AB, AC and BC while $A, C,\ A^2$ and AC are important terms for Nu_x. Hence, mathematical Eq. (2.2) for Cf_x and Nu_x can be written as,

$$Cf_x = 3.577 + 3.158A - 1.392B - 0.406C - 1.413AB - 0.366AC - 0.366BC + 0.612A^2, \quad (3.42)$$

$$Nu_x = 2.3621 + 2.00218A - 1.21979C - 1.2340AC + 0.1813A^2. \quad (3.43)$$

The sensitivity of the response variables (Cf_x) and (Nu_x) to the input factors A, B and C can be derived from Eqn. (3.42) and Eqn. (3.43) as a first rate of change and is given by,

$$\frac{\partial}{\partial A}(Cf_x) = 3.158 + 1.242A - 1.413B - 0.366C, \quad (3.44)$$

$$\frac{\partial}{\partial B}(Cf_x) = -1.392 - 1.413A - 0.366C, \quad (3.45)$$

$$\frac{\partial}{\partial C}(Cf_x) = -0.406 - 0.366A - 0.366B, \tag{3.46}$$

$$\frac{\partial}{\partial A}(Nu_x) = 2.00218 + 0.3626A - 1.2340C, \tag{3.47}$$

$$\frac{\partial}{\partial B}(Nu_x) = 0, \tag{3.48}$$

$$\frac{\partial}{\partial C}(Nu_x) = -1.21979 - 1.2340A. \tag{3.49}$$

The Cf_x and Nu_x for variations in ξ, ε and γ are given in Table 3.7 and Table 3.8. Fig. 3.1 and Fig. 3.2 present the sensitivity of output responses. The positive bar chart indicates that the responses are increasing by increasing the input parameters.

Table 3.7: Sensitivity analysis of Cf_x when $A=0$.

B	C	$\partial Cf_x/\partial A$	$\partial Cf_x/\partial B$	$\partial Cf_x/\partial C$
-1	-1	4.937	-1.026	-0.04
	0	4.571	-1.392	-0.04
	1	4.205	-1.758	-0.04
0	-1	3.524	-1.026	-0.406
	0	3.158	-1.392	-0.406
	1	2.792	1.758	-0.406
1	-1	2.111	-1.026	-0.772
	0	1.745	-1.392	-0.772
	1	1.379	1.758	-0.772

Table 3.8: Sensitivity analysis of Nu_x when $B=0$.

A	C	$\partial Nu_x/\partial A$	$\partial Nu_x/\partial B$	$\partial Nu_x/\partial C$
-1	-1	2.87358	0	0.01412
	0	1.63958	0	0.01412
	1	0.40558	0	0.01412
0	-1	3.23618	0	-1.21979
	0	2.00218	0	-1.21979
	1	0.76818	0	-1.21979
1	-1	3.59879	0	-2.45379
	0	2.36478	0	-2.45379
	1	1.13078	0	-2.45379

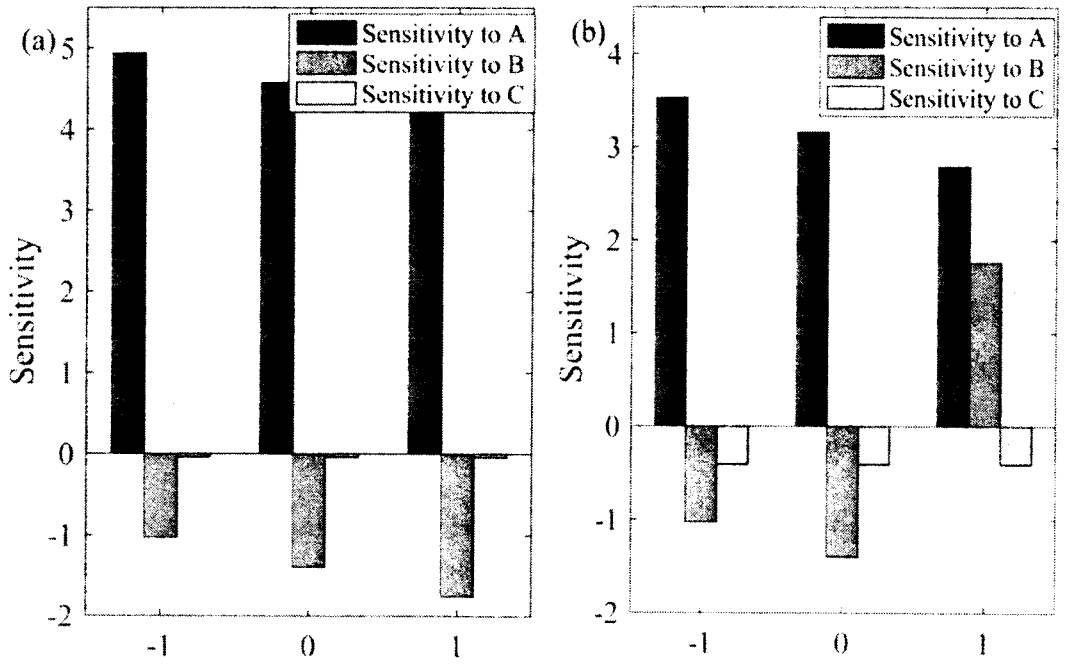

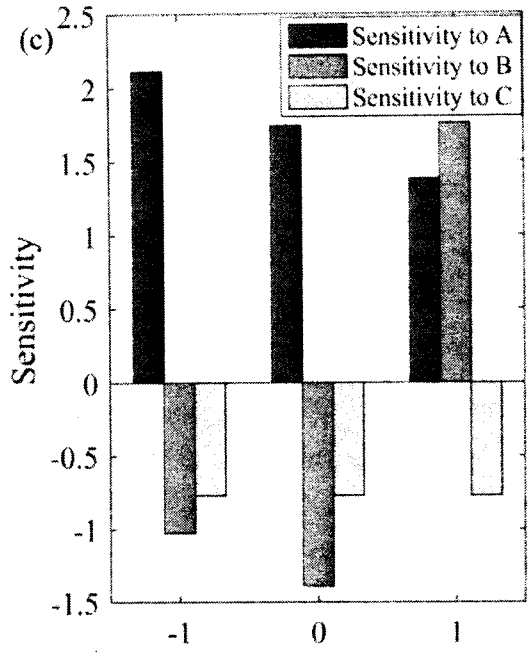

Figure 3.1: Sensitivity plot for Cf_x with $A=0$ (a) $B=-1$ (b), $B=0$ (c) $B=1$

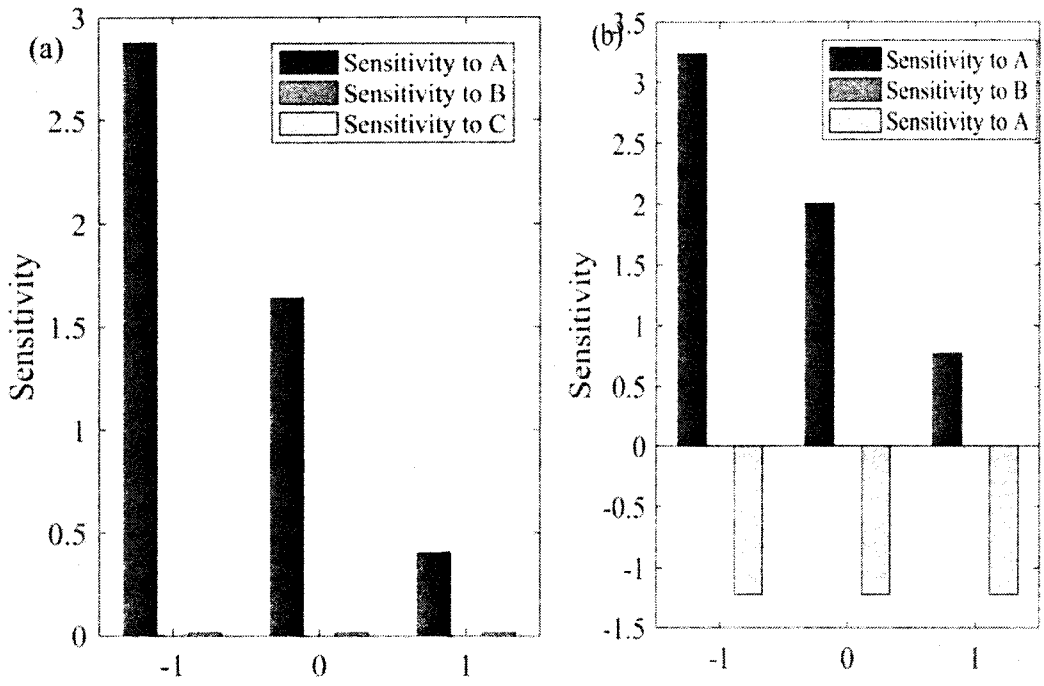

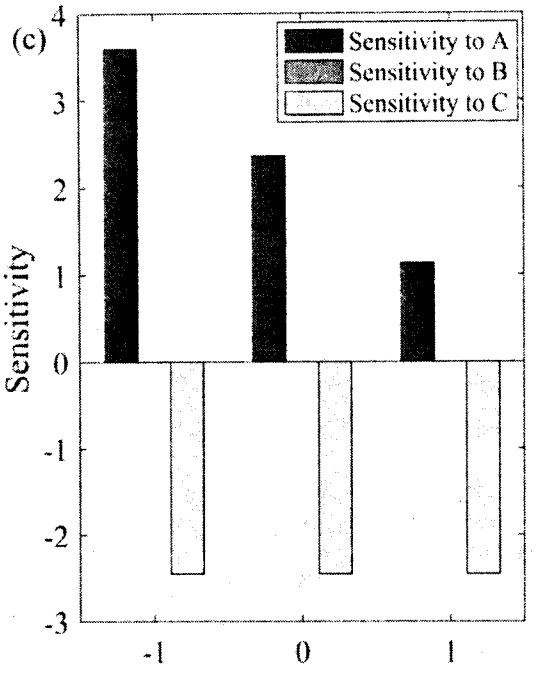

Figure 3.2: Sensitivity plot for Nu_x with $A=0$ (a) $B=-1$ (b) $B=0$ (c) $B=1$

3.4 Discussion of the Results

The findings of the sensitivity analysis of viscous fluids flowing over a porous wedge are discussed in this section. The governing equations [37] are transformed into boundary layer equations by using similarity transformation. These obtained equations are non-linear ODEs. Then we have solved these non-linear equations by using regular perturbation method for small as well as ξ and solved numerically by using bvp4c. The numerical results are compared with those presented in [37] and arranged this comparison in Table 3.1 and Table 3.2 and found well agreement.

While discussing the sensitivity it is also important to consider the residuals and lack of fit. ANOVA and data entry into analytical tools are used to generate residual plots. These plots are showed in Fig. 3.3 and Fig. 3.4. These figure shows that the histograms are less skewed and more comparable to a symmetrical distribution. When the residual diagrams are compared to the fitted values, the observed and fitted values show a strong connection. The highest residuals among all responses are observed to be in the proximity of 0.25 and 0.075 for the Cf_x and Nu_x respectively. As it is clear from the figures as by increasing the observation order, residual of both Cf_x and Nu_x

decreases it shows that probability plots are in good agreement. It also shows the best correlation between fitted values and observed values. The plots between residual and fitted values show the maximum deviation for both Cf_x and Nu_x which implies the accuracy of the model.

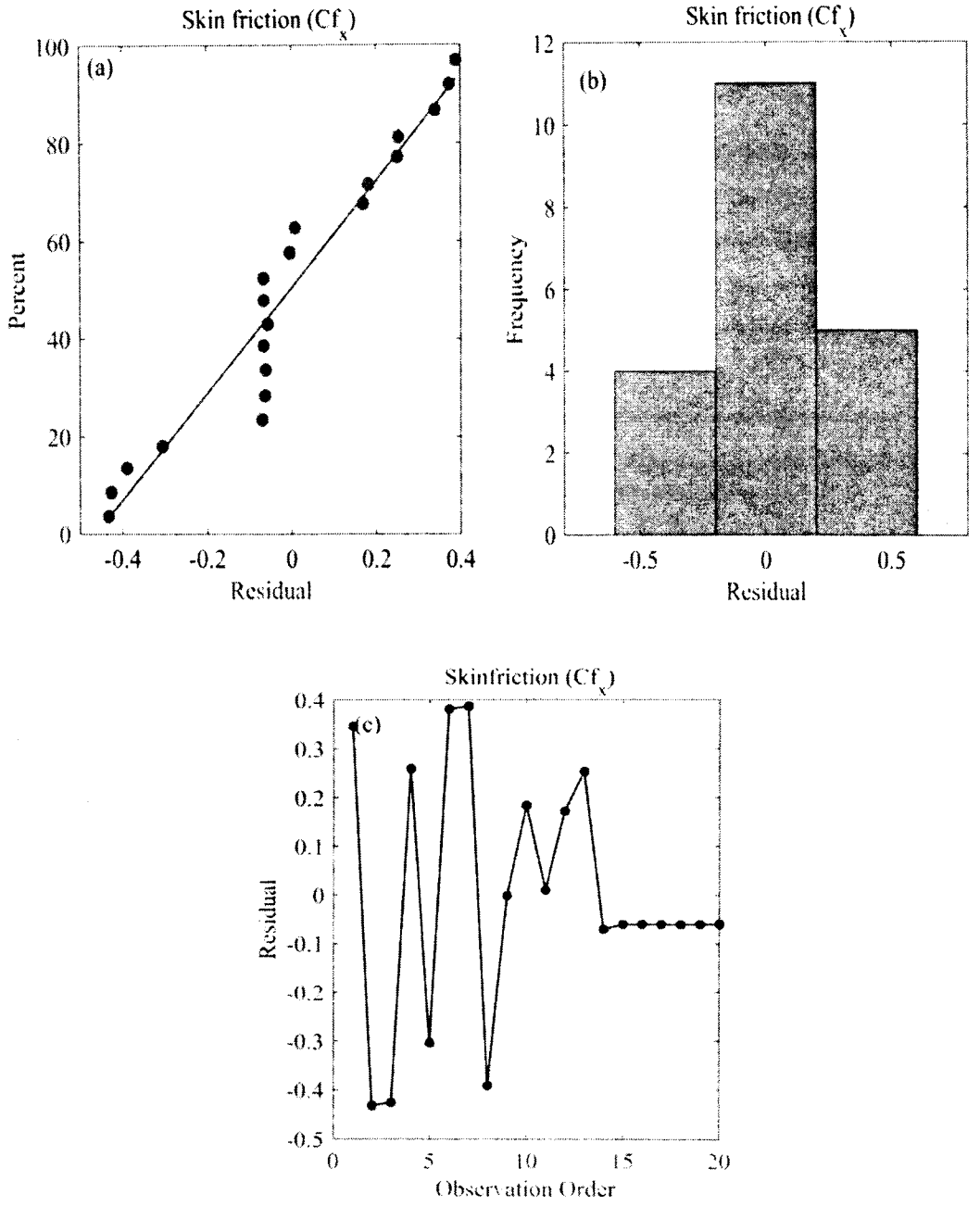

Figure 3.3: Normal probability plot, histogram and order residuals for Cf_x

TH-27643

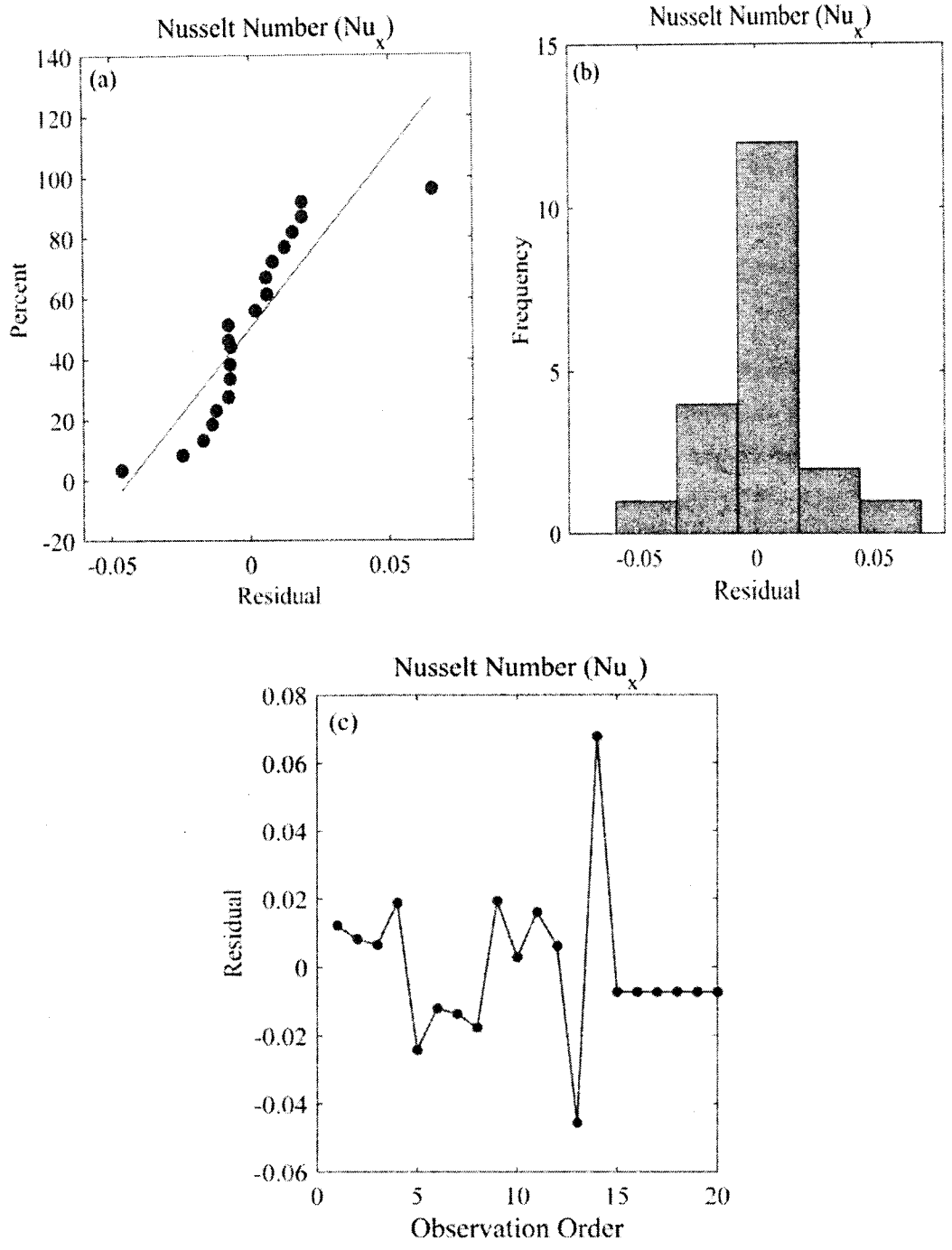

Figure 3.4: Normal probability plot, histogram and residuals for Nu_x

R-squared (R^2) and adjusted R-squared ($Adj\ R^2$) for both responses, such as Cf_x and Nu_x which are presented in Table 3.5 and Table 3.6. R^2 and $Adj\ R^2$ provide information on the goodness of fit Response Surface Methodology. It is clear from Table 3.5 and Table 3.6 that R^2 and $Adj\ R^2$ have large values, indicating that the independent output responses and input parameters are perfectly correlated.

As perceived in Figs. 3.1(a) – 3.2(c), sensitivity of Cf_x to the suction parameter is positive for all values of the thermal conductivity. This means that skin friction coefficient will increase by increasing the thermal conductivity. From Fig. 3.1(a) it can be observed that the sensitivity of Cf_x to the thermal conductivity radiation and viscosity variation parameter is negative for all values of thermal conductivity radiation. This will result in decrease of skin friction coefficient with an increase of these parameters.

Fig. 3.1(b) shows that the sensitivity of Cf_x to suction parameter is positive whereas it is negative both for thermal conductivity radiation and viscosity variation parameter for the entire central composite design. Figure 3.1(c) displays similar behaviour both for suction parameter and thermal conductivity radiation for the entire design whereas a mixed behaviour is observed for viscosity variation parameter. Here we can conclude that skin friction coefficient will rise by increasing variation of both suction parameter and thermal conductivity radiation. Whereas skin friction coefficient will increase and then decrease with viscosity variation parameter.

The sensitivity of the Nu_x in details that is represented in Fig. 3.2(a) – (c). It is perceived from Figs. 3.2(a) to 3(c) that sensitivity of Nu_x to the suction parameter is positive for all values of suction parameter. This means that Nu_x will increase by increasing the suction parameter. Figure 3.2(a) displays positive sensitivity for suction parameter for the entire design whereas a mixed behaviour is observed for thermal conductivity radiation. From Fig. 3.2(b) it can be observed that the sensitivity of Nu_x is positive to the suction parameter and negative to the thermal conductivity radiation for all values of suction parameter. This will result in increase of Nu_x with an increase of suction parameter and decrease in Nu_x by increasing the thermal conductivity radiation. Fig. 3.2(c) shows the same positive sensitivity of the Nu_x towards the suction parameters for all values of viscosity variation parameter and vice versa for thermal conductivity radiation. Since Nu_x is independent of viscosity therefore we do not discuss sensitivity of Nu_x to viscosity variation parameter.

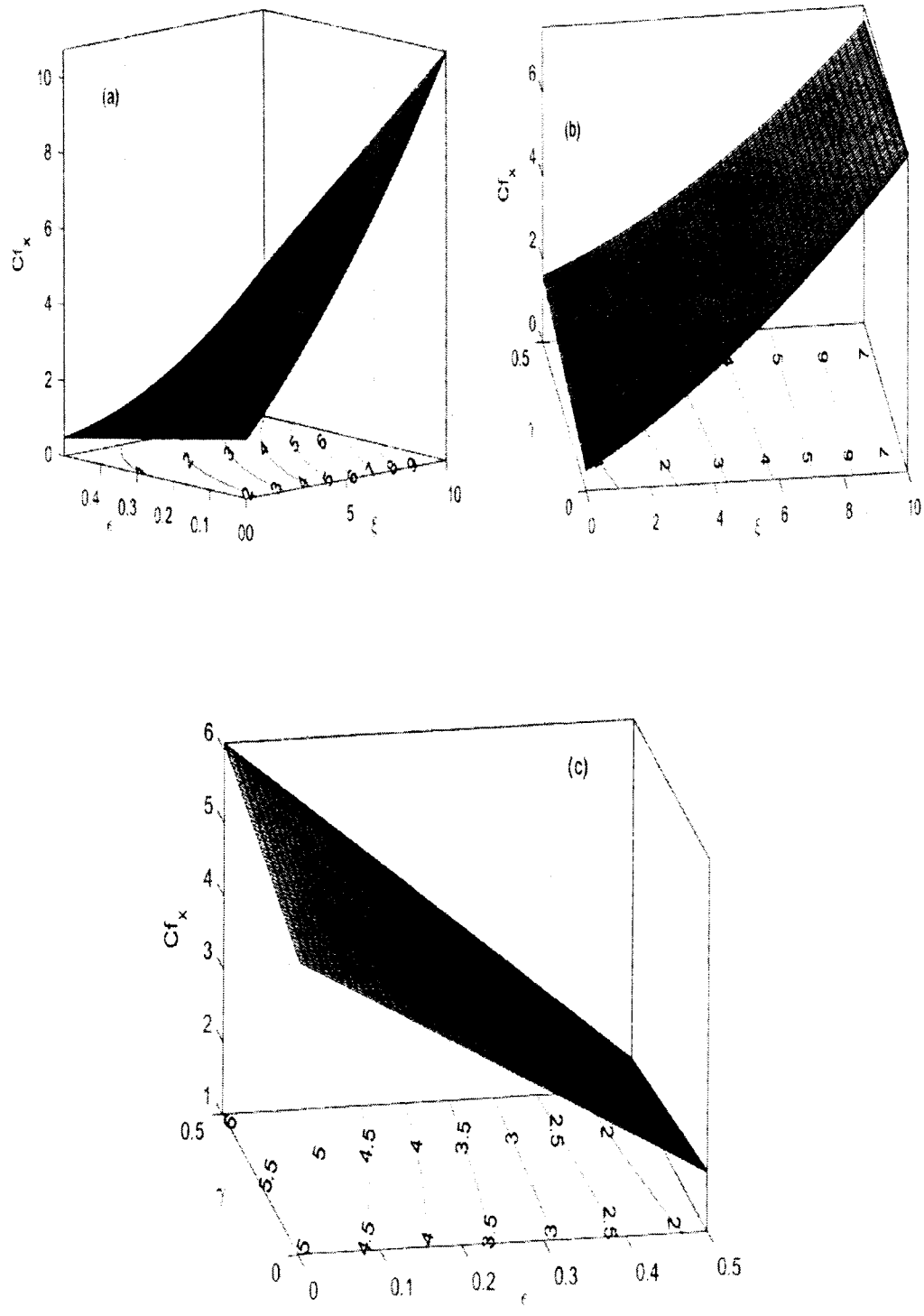

Figure 3.5: Contour plot of Cf_x when (a) C=0 (b) B=0 (c) A=0

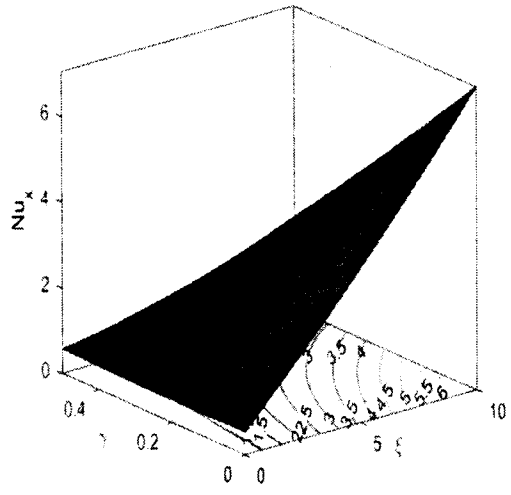

Figure 3.6: Contour plot of Cf_x when $B=0$.

The 3D combined surface contour plots of Cf_x and Nu_x are depicted in Fig. 3.5 and Fig. 3.6 respectively. The effects of ξ and the ε on the Cf_x for $C=0$ are displayed in Fig. 3.5(a). It is found that, minimum Cf_x occurs for the lower level of ξ and higher level for ε. The effects of ξ and γ for $B=0$ are examined in Fig. 3.5(b). It can be observed that minimum Cf_x occurs for lower level of ξ and higher level of γ whereas maximum value is achieved for higher level of ξ and lower level of γ. Fig. 3.5(c) shows the effects of the ε and γ for $A=0$. It is indicated that Cf_x is minimum for high level of both ε and γ however Cf_x is maximum near lower level of ε and higher level of γ.

As Nu_x is independent of viscosity variation parameter (ε) so we will only discuss the variation of ξ and γ. It is clear from Fig. 3.6 that maximum Nu_x occurs for higher level of ξ and lower level of γ and minimum Nu_x occurs near lower level of ξ and higher level of γ.

Chapter 4

Tangent Hyperbolic Nanofluid Flowing over a Wedge

The transport performance for a convective nanofluid with mass and heat transfer can be measured through Nu_x, Sh_x, and Cf_x. The purpose of the present chapter is to explore the sensitivity analysis of such performances for magneto-hydrodynamics (MHD) non-Newtonian nanofluid flow using Tangent hyperbolic fluid model. The equations governing the flow problem are coupled nonlinear PDEs. By using suitable similarity transformation the non-linear PDEs are converted into system of ODEs and then solved theses ODEs by using numerical technique bvp4c. The results give good agreement with [77]. In order to make the sensitivity analysis of Nu_x, Sh_x, and Cf_x, first of all derive empirical relations for these quantities using response surface methodology. The goodness of fit for empirical relations is decided on the basis of coefficient of determination ANOVA table. The comprehensive discussion based graphs and table are made and empirical relation is developed on this based.

4.1 Mathematical Formulation

In this chapter the problem of non-Newtonian tangent hyperbolic nanofluid flowing over a wedge is considered. The simplified form of governing equations is those formulated in [77]. The governing PDEs for non-Newtonian tangent hyperbolic nanofluids are considered due to [77] are follows,

$$\frac{\partial u}{\partial x}+\frac{\partial u}{\partial y}=0, \tag{4.1}$$

$$\frac{\partial u}{\partial t}+u\frac{\partial u}{\partial x}+u\frac{\partial v}{\partial y}=\frac{\partial U_e}{\partial t}+U_e\frac{\partial u}{\partial x}+\nu_f\left((1-n)+\sqrt{2}n\gamma\frac{\partial u}{\partial y}\right)\frac{\partial^2 u}{\partial y^2}+\left(\frac{\sigma B_0^2}{\rho_f}+\frac{\mu_f}{K}\right)(U_e-u), \tag{4.2}$$

$$\frac{\partial T}{\partial t}+u\frac{\partial T}{\partial x}+v\frac{\partial T}{\partial y}=\alpha_f\frac{\partial^2 T}{\partial y^2}+\left(D\frac{\partial T}{\partial y}\frac{\partial C}{\partial y}+\frac{D}{T_\infty}\left(\frac{\partial T}{\partial y}\right)^2\right), \tag{4.3}$$

$$\frac{\partial C}{\partial t}+u\frac{\partial C}{\partial x}+v\frac{\partial C}{\partial y}=D\frac{\partial^2 C}{\partial y^2}+\frac{D}{T_\infty}\frac{\partial^2 T}{\partial y^2} \tag{4.4}$$

The associated boundary conditions are as follows,

$$u(x,0,t) = u_w(x,t),\ v(x,0,t) = 0,\ T(x,0,t) = T_w(x,t),\ \left(D\frac{\partial C}{\partial y} + \frac{D}{T_\infty}\frac{\partial T}{\partial y}\right)_{(x,0,t)} = 0, \tag{4.5}$$

$$u(x,\infty,t) \to U_e(x,t),\ T(x,\infty,t) \to T_\infty,\ C(x,\infty,t) \to C_\infty. \tag{4.6}$$

B_0 denotes the magnetic fields, σ refers to electrical conductivity, ν_f denotes the fluid kinematic viscosity and α_f refers to fluid diffusivity. We consider the stream function $\psi(x, y)$ which satisfies $u = \frac{\partial \psi}{\partial y}$ and $v = -\frac{\partial \psi}{\partial x}$. To convert Eqns. (4.1) to (4.4) into sets of ODEs the following similarity transformations are considered as,

$$\eta = y\sqrt{\frac{U_e(1+m)}{2x\nu_f}},\ \psi = \sqrt{\frac{2x\nu_f U_e}{1+m}}F(\eta),\ \theta(\eta) = \frac{T-T_\infty}{T_w-T_\infty},\ \phi(\eta) = \frac{C-C_\infty}{C_0-C_\infty}. \tag{4.7}$$

By using the similarity transformations in Eqn. (4.7) the Eqns. (4.2) to (4.4) are transformed into set of non-linear ODEs as follows,

$$\left((1-n) + nWe\sqrt{1+m}f''\right)f''' + ff'' + \frac{2m}{1+m}(1-f'^2) + \frac{A}{1+m}\left(2 - 2f' - \eta f''\right) + \frac{2(M_g + Da^{-1})}{1+m}(1-f') = 0, \tag{4.8}$$

$$\frac{1}{Pr}\theta'' + Nb\theta'\phi' + Nt\theta'^2 + f\theta' - \frac{2m}{1+m}f'\theta - \frac{A}{1+m}\left(2\theta + \eta\theta'\right) = 0, \tag{4.9}$$

$$\phi'' + \frac{Nt}{Nb}\theta'' + PrLe\left(f\phi' - \frac{2m}{1+m}f'\phi\right) - \frac{A}{1+m}PrLe\left(2\phi + \eta\phi'\right) = 0. \tag{4.10}$$

The associated dimensionless boundary conditions are,

$$f(0) = 0,\ f'(0) = \gamma,\ \theta(0) = 1,\ Nb\phi'(0) + Nt\theta'(0) = 0, \tag{4.11}$$

$$f'(\infty) \to 1,\ \theta(\infty) \to 0,\ \phi(\infty) \to 0. \tag{4.12}$$

Where, m designate the Falkner-Skan exponent, $We = \frac{\gamma U^{3/2}}{\sqrt{\nu_f x}}$ is Weissenberg number, Prandtl number denotes by $Pr = \frac{\nu_f}{\alpha_f}$, Lewis number $Le = \frac{\alpha_f}{D}$, the unsteady parameter $A = \frac{\lambda}{bx^{m-1}}$, $M_g = \frac{\sigma_f B_0^2}{\rho_f U}$ represents magnetic field parameter, $Nt = \frac{D(T_w - T_\infty)}{T_\infty \nu_f}$ indicates the thermophoresis parameter, $Nb = \frac{D(C_0 - C_\infty)}{\nu_f}$ shows the Brownian motion parameter, $\gamma = \frac{b}{a}$ represents the velocity ratio parameter and $Da^{-1} = \frac{\nu_f x}{KU_e}$ mentions to Darcy number.

Now, Cf_x, Nu_x and Sh_x are expressed as,

$$Cf_x = \frac{\tau_w x}{(1/2)\rho_f U^2},\ Nu_x = \frac{q_w x}{\kappa_f(T_w - T_\infty)}\ and\ Sh_x = \frac{q_m x}{D(C_0 - C_\infty)}. \tag{4.13}$$

In the above Eqn. (4.13), τ_w shows surface shear stress, q_w represents heat transfer and q_m denotes the mass transfer.

In non-dimensionless form the Cf_x, Nu_x and Sh_x are formulated as,

$$Re^{\frac{1}{2}}Cf_x = \left(\sqrt{1+m}(1-n)f''(0) + \frac{1+m}{2}nWef''(0)^2\right), \tag{4.14}$$

$$Re^{\frac{1}{2}}Nu_x = -\sqrt{1+m}\theta'(0), \tag{4.15}$$

$$Re^{\frac{1}{2}}Sh_x = -\sqrt{1+m}\phi'(0), \tag{4.16}$$

where, $Re = \frac{U_e x}{2Lv_f}$ represents Reynolds number.

4.2 Experimental Design

4.2.1 Response Surface Methodology (RSM)

In this chapter the selected input parameters are the Weissenberg number (We), the thermophoresis parameter (Nt), and the Brownian motion parameter (Nb). The symbol and their ranges and represented in Table 4.1.

Table 4.1: Design input factor and their level.

Type	Factor	Symbol	Levels		
			-1	0	1
Input Factors	We	A	0	2.5	5
	Nt	B	0.1	0.5	1
	Nb	C	0.1	0.5	1

The goodness of fit for the response surfaces Cf_x, Nu_x and Sh_x is decided on the basis of ANOVA. The detail of ANOVA is given in next section.

Table 4.2: Experimental design and measured responses.

Experiment number	Point type	Coded values			Real values			Responses		
		A	B	C	We	Nt	Nb	Cf_x	Nu_x	Sh_x
1	Factorial	-1	-1	-1	0	0.00	0.00	2.2384	6.5074	-6.5074
2		1	-1	-1	10	0.00	0.00	9.0856	6.3138	-6.3138
3		-1	1	-1	0	0.50	0.00	2.2384	3.1318	-31.318
4		1	1	-1	10	0.50	0.00	9.0737	3.0853	-30.8532
5		-1	-1	1	0	0.00	0.50	2.2384	6.6296	-0.6630
6		1	-1	1	10	0.00	0.50	9.0739	6.3921	-0.6392
7		-1	1	1	0	0.50	0.50	2.2384	3.1423	-3.1423
8		1	1	1	10	0.50	0.50	9.0738	3.0928	-3.0928
9	Axial	-1	0	0	0	0.25	0.25	2.2384	4.0536	-4.0536
10		1	0	0	10	0.25	0.25	9.0745	3.9735	-3.9735
11		0	-1	0	5	0.00	0.25	7.2997	6.3740	-1.1589
12		0	1	0	5	0.50	0.25	7.2997	3.0929	-5.6234
13		0	0	-1	5	0.25	0.00	7.2997	3.9712	-21.8416
14		0	0	1	5	0.25	0.50	7.2997	3.9896	-2.1943
15-20	Centre	0	0	0	5	0.25	0.25	7.2997	3.9804	-3.9804

4.2.2 Analysis of Variance (ANOVA)

For Cf_x the following factors are significant A, B, C, A^2, AB, AC and C . For Nu_x the following terms A, B, C, A^2, B^2, BA and BC are important and for Sh_x the following factors B, C, C^2 and BC are significant. Hence, mathematical Eqns. (2.2) can be rewritten as,

$$Cf_x = 7.29954 + 3.41895\,A - 0.001200\,B - 0.001160\,C - 0.001500\,AB - 0.001450\,AC + 0.001475\,BC - 1.64284\,A^2\,, \quad (4.17)$$

$$Nu_x = 3.97745 - 0.06072A - 1.66718B + 0.02369\,C + 0.04189AB - 0.02281\,BC + 0.0405A^2 + 0.7604B^2, \quad (4.18)$$

$$Sh_x = -4.147 - 5.875\,B + 8.710\,C + 5.552\,BC - 7.62\,C^2\,. \quad (4.19)$$

Table 4.3 shows the statistical estimators for the simplified models of Cf_x, Nu_x and Sh_x. It is clear that all of the simplified models have goodness of fit because coefficient of determination for the models for Cf_x, Nu_x and Sh_x are 100%, 99.99% and 97.73% respectively as given in Table 4.4. After having best fitted model for the response surface Cf_x, Nu_x and Sh_x we focus on our next objective of the sensitivity analysis which is described in next section.

Table 4.3: ANOVA for (a) Cf_x (b) Nu_x (c) Sh_x

Source	DF	Adj SS	Adj MS	F-Value	P-Value	
(a)						
Model	9	130.379	14.487	5376082.3	0.0001	Significant
Linear	3	116.892	38.964	14459911.90	0.0001	-
Square	3	13.487	4.496	1668328.83	0.0001	-
Interaction	3	0.000	0.000	6.46	0.010	
Error	10	0.000	0.000			
Lack-of-Fit	5	0.000	0.000	*	*	Significant
Pure Error	5	0.000	0.000			-
Total	19	130.379				-

(b)

Model	9	30.9759	3.4418	9166.77	0.000	Significant
Linear	3	27.8374	9.2791	24713.91	0.000	-
Square	3	3.1201	1.0400	2770.01	0.000	-
2-Way Interaction	3	0.0185	0.0062	16.40	0.000	-
Error	10	0.0038	0.0004			-
Lack-of-Fit	5	0.0038	0.0008	*	*	Significant
Pure Error	5	0.0000	0.0000			-
Total	19	30.9797				-
(c)						
Model	9	1585.51	176.168	47.80	0.000	Significant
Linear	3	1103.87	367.168	99.84	0.000	-
Square	3	234.98	78.325	21.25	0.000	-
2-Way Interaction	3	246.66	82.221	22.31	0.000	-
Error	10	36.85	3.685			-
Lack-of-Fit	5	36.85	7.371	*	*	Significant
Pure Error	5	0.00	0.000			-
Total	19	1622.37				-

Table 4.4: Regression numbers for output responses (a) Cf_x (b) Nu_x (c) Sh_x

Terms	Coefficient	P-value	Significant
(a)			
Constants	7.29954	0.000	Significant
A	3.41895	0.000	Significant
B	-0.001200	0.043	Significant
C	-0.001160	0.049	Significant
A^2	-1.64284	0.000	Significant
B^2	0.000409	0.688	Not Significant
C^2	0.000409	0.688	Not Significant
AB	-0.001500	0.027	Significant
AC	-0.001450	0.032	Significant
BC	0.001475	0.029	Significant
	$R^2 = 100.00\%$		$Adj\ R^2 = 100.00\%$
(b)			
Constants	3.97745	0.000	Significant
A	-0.06072	0.000	Significant
B	-1.66718	0.000	Significant
C	0.02369	0.003	Significant
A^2	0.0405	0.006	Significant
B^2	0.7604	0.000	Significant
C^2	0.0074	0.542	Not Significant
AB	0.04189	0.000	Significant
AC	-0.00586	0.421	Not Significant
BC	-0.02281	0.008	Significant

	R^2 = 99.99%		Adj R^2 = 99.98%
(c)			
Constants	-4.147	0.000	Significant
A	0.081	0.896	Not Significant
B	-5.875	0.000	Significant
C	8.710	0.000	Significant
A^2	0.38	0.747	Not Significant
B^2	1.01	0.405	Not Significant
C^2	-7.62	0.000	Significant
AB	0.037	0.957	Not Significant
AC	-0.037	0.916	Not Significant
BC	5.552	0.000	Significant
	R^2 = 97.73%		Adj R^2 = 95.68%

4.3 Sensitivity analysis

This section is to examine the sensitivity of output responses/variables(Cf_x, Nu_x and Sh_x) to input independent parameters (*We*, *Nt* and *Nb*). Table 4.4 shows the regression coefficients for Cf_x, Nu_x and Sh_x respectively. The sensitivity functions developed below can be used to analyze the sensitivity of output responses with regard to input factors *A*, *B*, and *C*.

$$\frac{\partial}{\partial A}(Cf_x) = 3.41895 - 0.001500\,AB - 0.001450\,C - 3.28568\,A, \tag{4.20}$$

$$\frac{\partial}{\partial B}(Cf_x) = -0.001200 - 0.001500\,A + 0.001475\,C, \tag{4.21}$$

$$\frac{\partial}{\partial C}(Cf_x) = -0.001160 - 0.001450\,A + 0.001475\,B, \tag{4.22}$$

$$\frac{\partial}{\partial A}(Nu_x) = -0.06072 + 0.04189B + 0.081A, \tag{4.23}$$

$$\frac{\partial}{\partial B}(Nu_x) = -1.66718 + 0.04189A - 0.02281\,C + 1.5280\,B, \tag{4.24}$$

$$\frac{\partial}{\partial C}(Nu_x) = 0.02369\ - 0.02281\,B, \tag{4.25}$$

$$\frac{\partial}{\partial A}(Sh_x) = 0, \tag{4.26}$$

$$\frac{\partial}{\partial B}(Sh_x) = -5.875\ + 5.552\,C, \tag{4.27}$$

$$\frac{\partial}{\partial C}(Sh_x) = 8.710\ + 5.552\,B - 15.24\,C. \tag{4.28}$$

The sensitivity of Cf_x, Nu_x and Sh_x against variations of We, Nt and Nb are enlisted in Table 4.5, Table 4.6 and Table 4.7 respectively.

Table 4.5: Analysis of sensitivity for output responses Cf_x when $A = 0$.

B	C	$\partial Cf_x/\partial A$	$\partial Cf_x/\partial B$	$\partial Cf_x/\partial C$
-1	-1	3.4204	-0.002675	-0.002635
	0	3.41895	-0.0012	-0.002635
	1	3.4175	0.000275	-0.002635
0	-1	3.4204	-0.002675	-0.001160
	0	3.41895	-0.0012	-0.001160
	1	3.4175	0.000275	-0.001160
1	-1	3.4204	-0.002675	0.000315
	0	3.41895	-0.0012	0.000315
	1	3.4175	0.000275	0.000315

Table 4.6: Analysis of sensitivity for output responses Nu_x when $A= 0$.

B	C	$\partial Nu_x/\partial A$	$\partial Nu_x/\partial B$	$\partial Nu_x/\partial C$
-1	-1	-0.10261	-3.17237	0.0465
	0	-0.10261	-3.19518	0.0465
	1	-0.10261	-3.21799	0.0465
0	-1	-0.06072	-1.64437	0.02369
	0	-0.06072	-1.66718	0.02369
	1	-0.06072	-1.68999	0.02369
1	-1	-0.01883	-0.11637	0.00088
	0	-0.01883	-0.13918	0.00088
	1	-0.01883	-0.16199	0.00088

Table 4.7: Analysis of sensitivity for output responses Sh_x when $A= 0$.

B	C	$\partial Sh_x/\partial A$	$\partial Sh_x/\partial B$	$\partial Sh_x/\partial C$
-1	-1	0	-11.427	18.398
	0	0	-5.875	3.158
	1	0	-0.323	-12.082
0	-1	0	-11.427	23.95
	0	0	-5.875	8.710
	1	0	-0.323	-6.53
1	-1	0	-11.427	29.502
	0	0	-5.875	14.262
	1	0	-0.323	-0.978

The obtained results are also portrayed graphically as Fig. 1 to Fig. 3. The discussion of the obtained results is made in section 5.

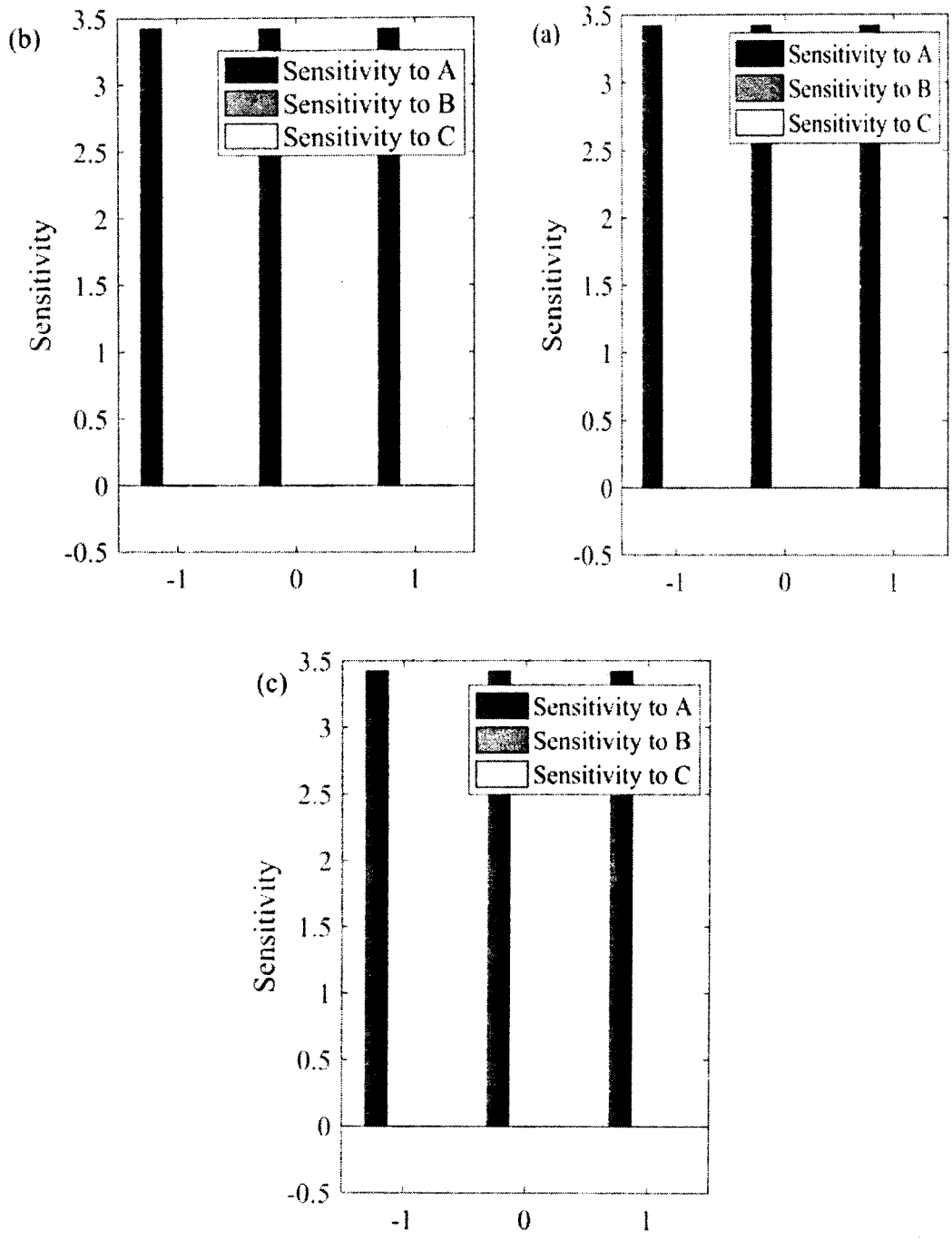

Fig.4.1: Sensitivity plot for output response (Cf_x) with B = 0 (a) $A = -1$ (b) $A = 0$ (c) $A = 1$.

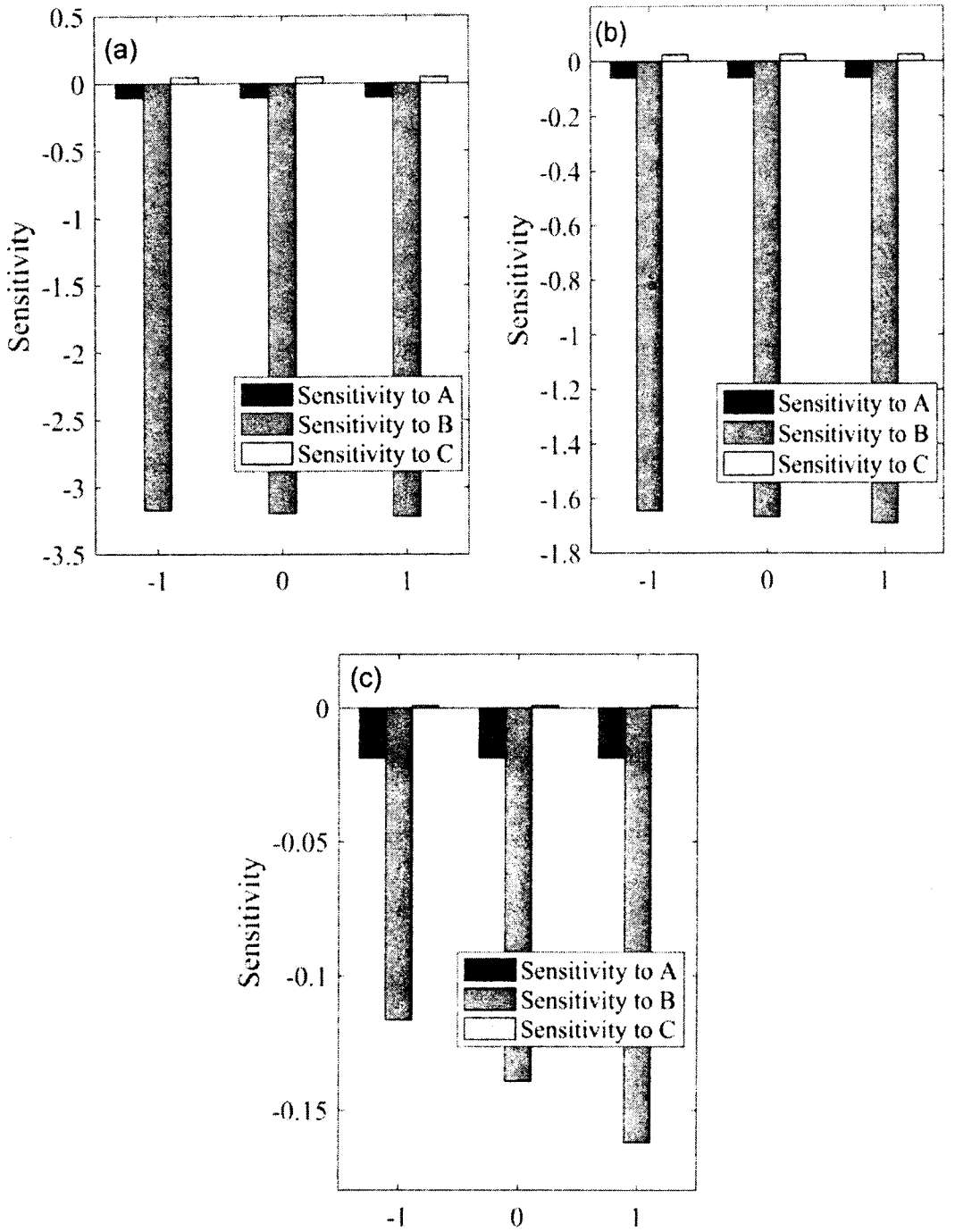

Fig. 4.2: Sensitivity plot for output response (Nu_x) with $A = 0$ (a) $B = -1$ (b) $B = 0$ (c) $B = 1$.

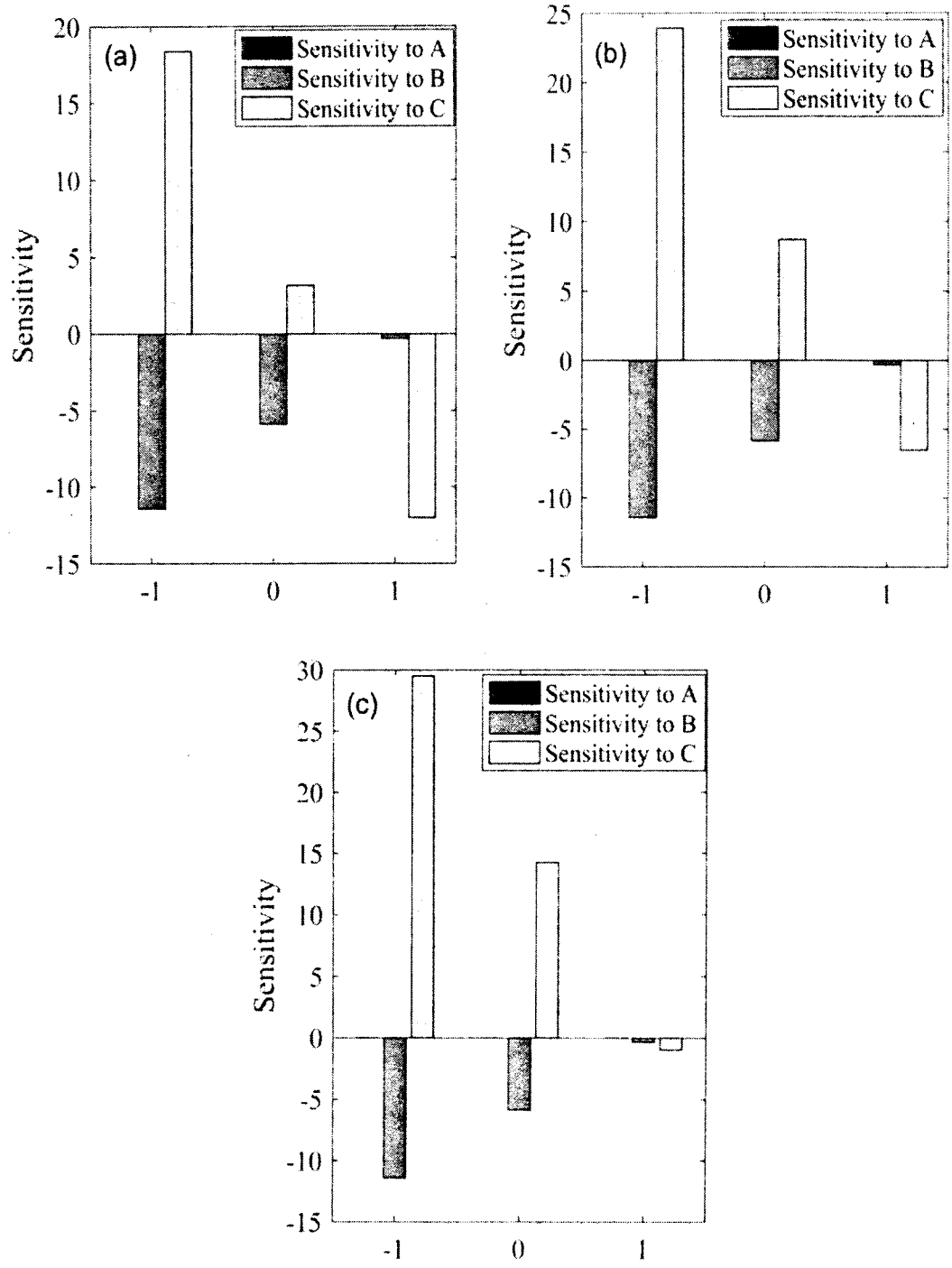

Fig. 4.3: Sensitivity plot for output response (Sh_x) with $A = 0$ (a) $B = -1$ (b) $B = 0$ (c) $B = 1$.

4.4 Discussion of the Results

This section is meant for discussion of the results obtained for sensitivity analysis and empirical development of transport performance quantities for tangent hyperbolic nanofluid flowing over a wedge. The numerical solution of the problem are calculated by Matlab built in routine bvp4c. The prime focus of this study is the sensitivity analysis. In order to meet this objective, we have built expression for Cf_x, Nu_x and Sh_x. CCD are used for RSM to construct the function between input factors and output responses which are described in Eqns. (4.18) – (4.20) respectively.

The sensitivity of the regression models to We, Nt and Nb is calculated and shown in Figs. (4.1– 4.3). The sensitivity functions, Eqns. (4.21 – 4.29) may be used to compute increasing or decreasing trend of the responses with regard to input parameters A, B and C. At $A = 0$, the sensitivity of Cf_x for a factor is positive as the height of the bar increases. The sensitivities of the Cf_x for parametric variation are illustrated in Fig. 4.1. Fig. 4.1(a) reflects that sensitivity of Cf_x for We, Nt and Nb is positive for all levels. Also it is cleared that the sensitivity of Cf_x against We is the highest for all levels such as low (-1), medium (0) and high (+1). However Nt and Nb has little influence on Cf_x. The effect of Nt for low level (-1) on Cf_x is negligible in the case $B = 0$ and $A = -1$. Both the Figs. 4.1(b) and 4.1(c) showed the positive sensitivity of We for all levels but negative sensitivity for Nt and Nb. Also it is cleared that We is more sensitive as compared to Nt and Nb. Now we will discuss sensitivity of Nu_x to We, Nt and Nb. It can be noted that sensitivity of Nu_x for We and Nt comes out to be negative this means that they have a decreasing impact on Nu_x. This means that Nu_x decreases by increasing We and Nt. The sharp changes in sensitivity of Nu_x are observed against Nt whereas Nb and We do not have major effects on Nu_x. Finally, we will discuss the sensitivity of Sherwood number to We, Nt and Nb. It is cleared from Fig. 4.3 that the sensitivity of Nt is always negative for all level and each case which is depicted in Fig. 4.3 (a) to (c). Which means that by increasing the input parameter Nt the Sh_x decreases. Also it can be seen that the sensitivity of Sh_x to Nt is greatest at low levels and its sensitivity decreases as approaching to high level. This means that by increasing Nt the Sh_x decreases. Also it is clear that the sensitivity of Sh_x to Nb have a mixed behavior. The sensitivity of Sh_x to Nb increases at low level (-1) and middle level (0) but it decreases at high

level (+1). The sensitivity of Nb is always greater for all case for low level (-1). There is no any effect of We on Sh_x because it is independent of We. So finally it is concluded that by increasing Nb the sensitivity of Sh_x also increases at low (-1) and medium (0) levels but decreases at high (+1) level.

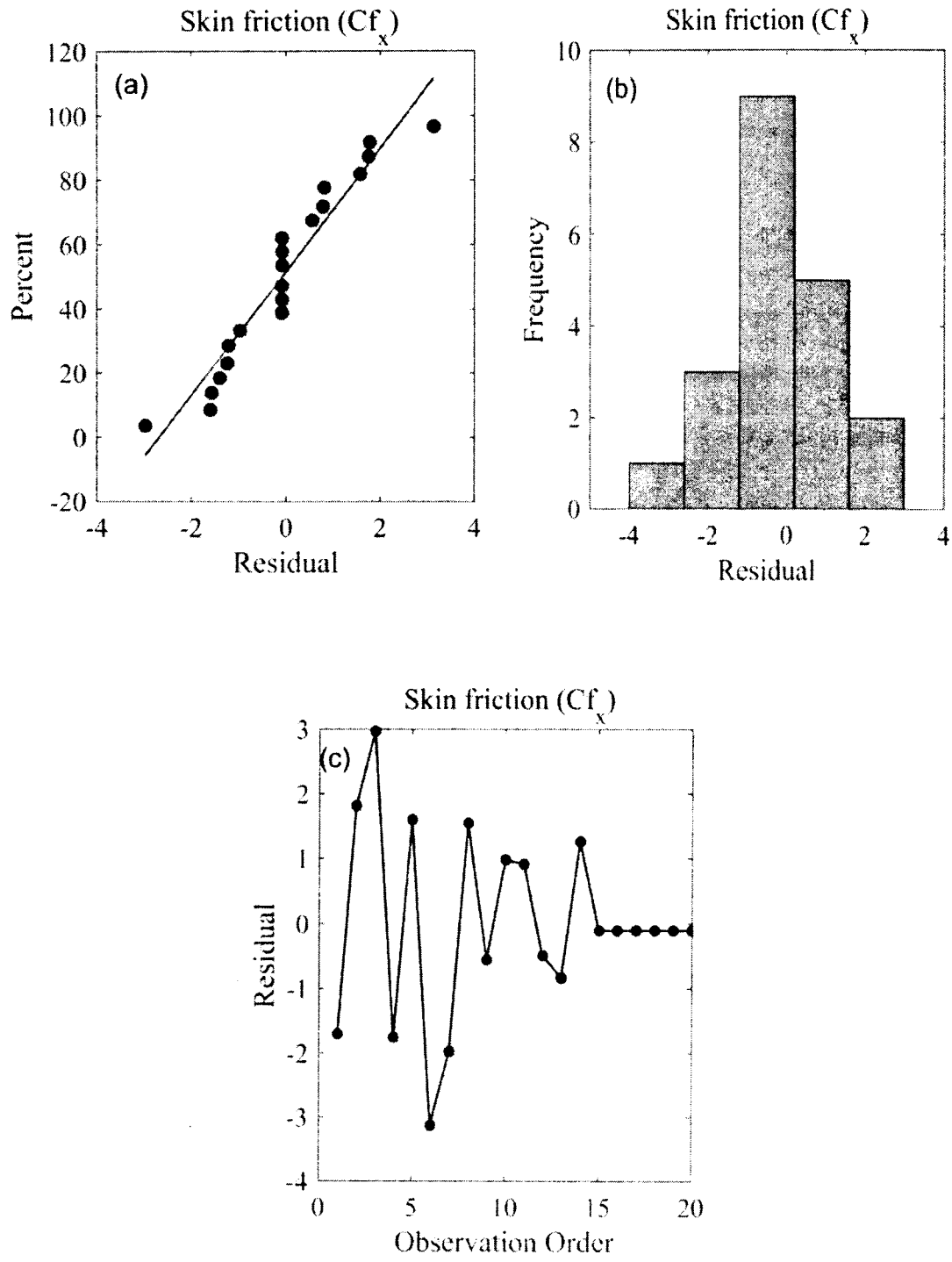

Fig. 4.4: Residual plots for output response (Cf_x) (a) normal probability plot (b) histogram (c) residual plot

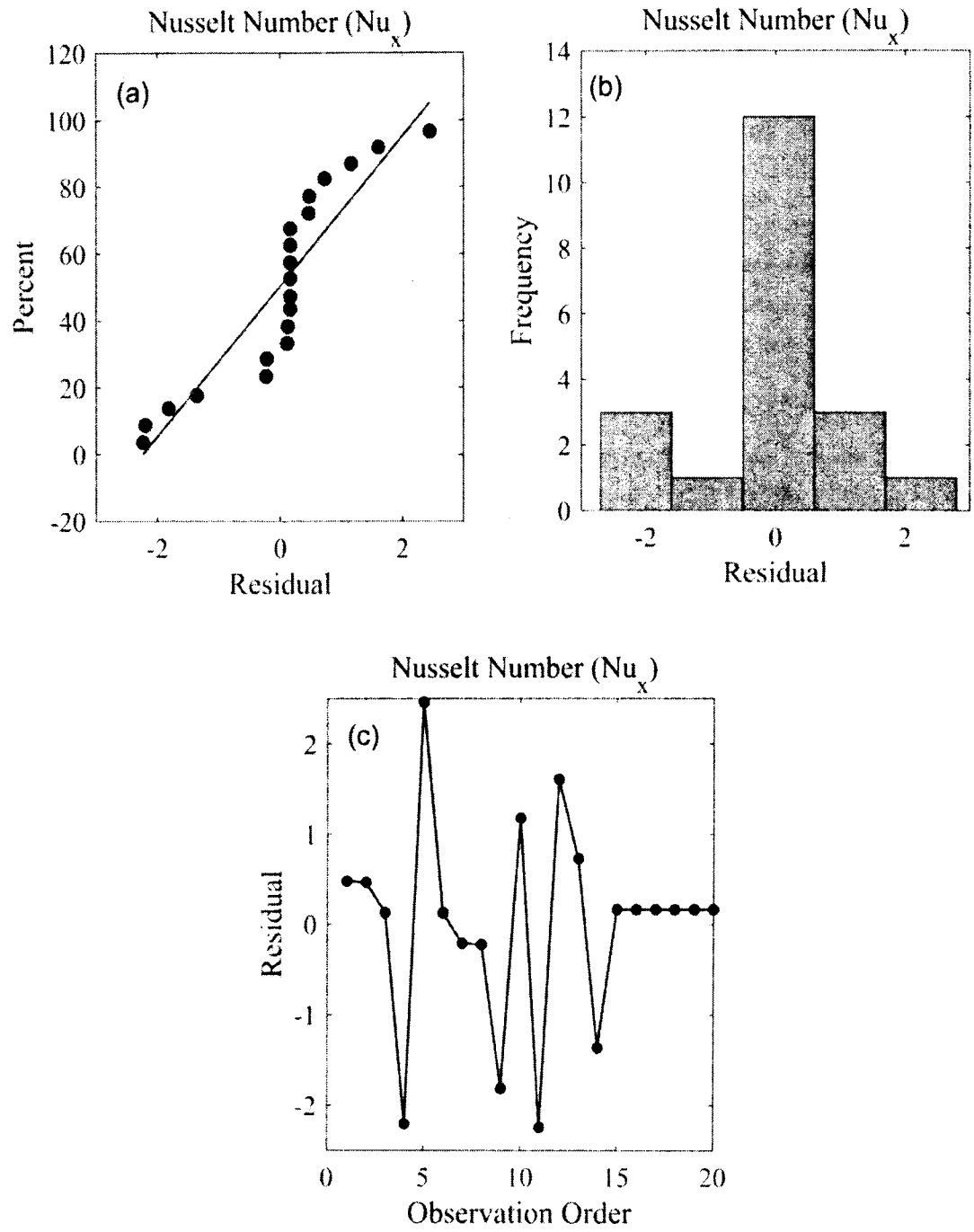

Fig. 4.5: Residual plots for output response (Nu_x) (a) normal probability plot (b) histogram (c) residual plot

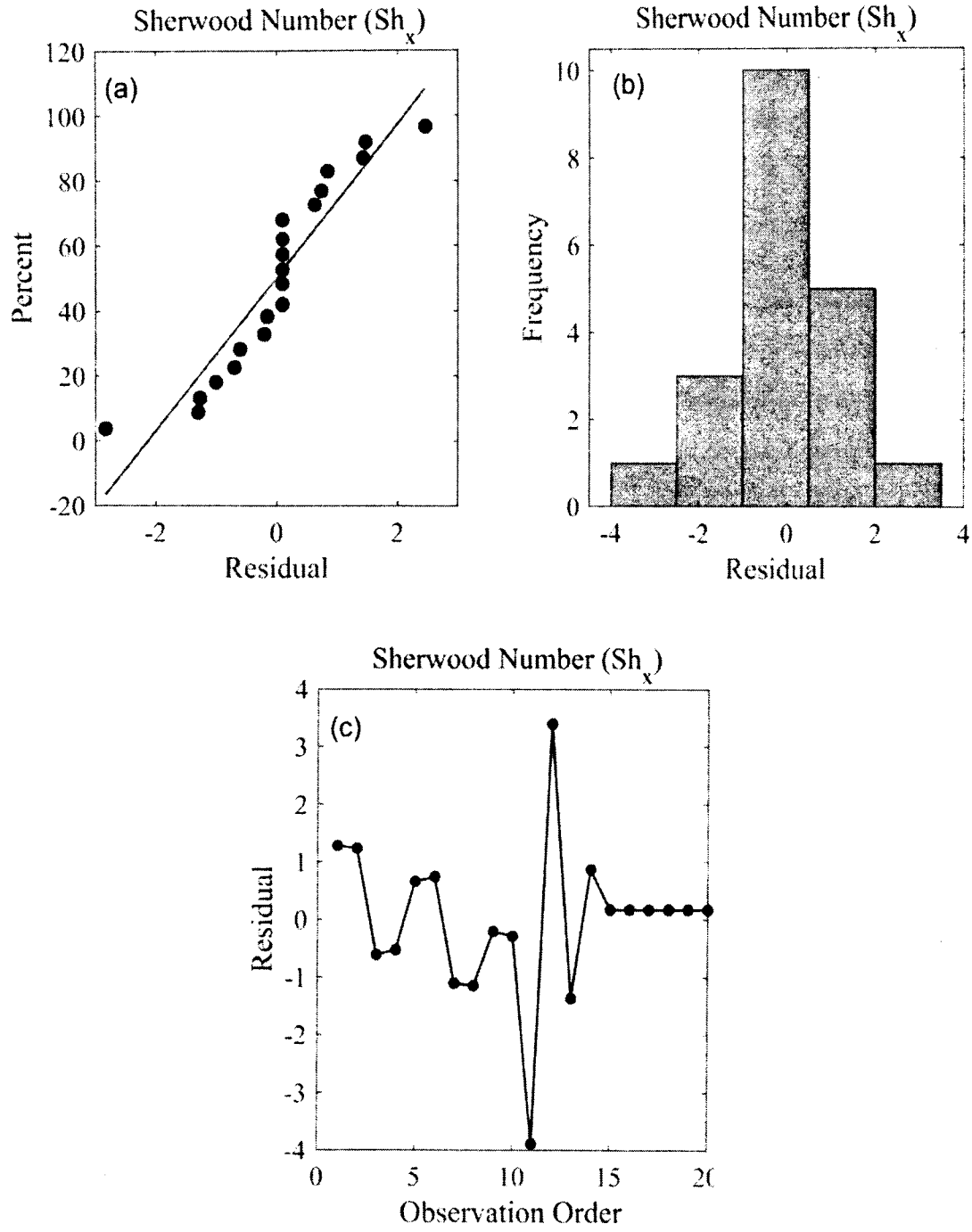

Fig.4.6: Residual plots for output response (Nu_x) (a) normal probability plot (b) histogram (c) residual plot

To determine the accuracy between two variables it is necessary to deliberate the residual graphical representations. ANOVA are used to describe these residual graphs which are depicted in Fig. 4.4 to Fig. 4.6. The positive linear relationship in Fig. 4.4(a), Fig. 4.5(a) and Fig. 4.6(a) shows strongest relationship between input factors and output responses. Fig. 4.4(b), Fig. 4.5(b) and Fig. 4.6(b) depicts the histograms of

residuals. The histograms are more comparable to normal curve and also less skewed. This also shows the validation of the models while using ANOVA. Finally, Fig. 4.4(c), Fig. 4.5(c) and Fig. 4.6(c) displayed the graph of residuals verses observation order for output responses. These graphs showed the strong relationship between observed and fitted values. It also can be seen from figures that residuals are reduces when observation order rises which follows that the probability plots are in good relationship.

For a linear regression model, R-squared determines the proportion of the variance in dependent variable explained by independent variables. The large value of R^2 and $Adj\ R^2$ shows the perfect correlation between input factors and output responses which can be seen Table 4.3 and Table 4.4.

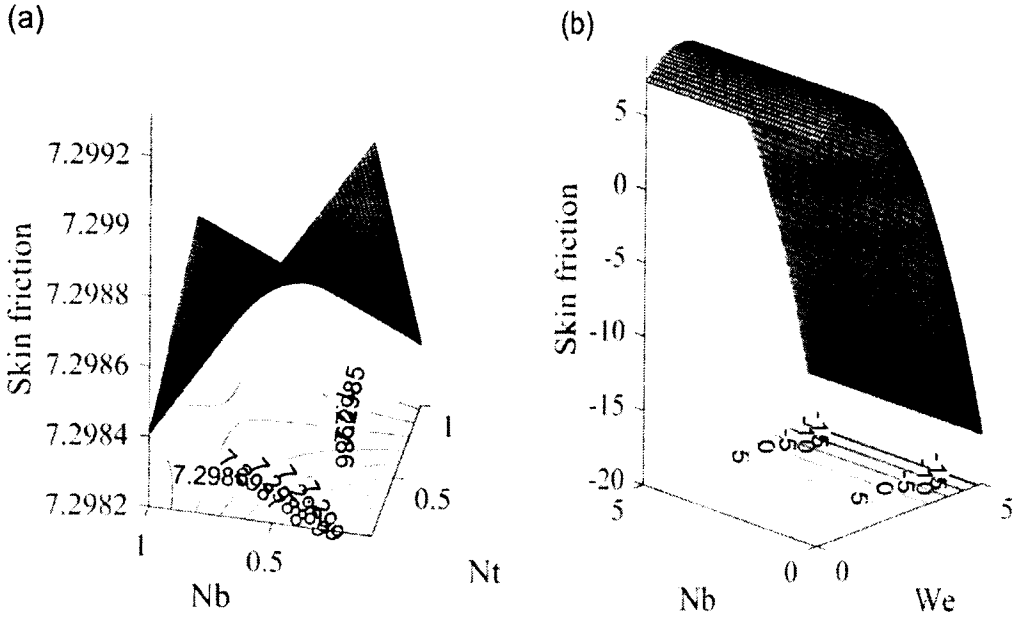

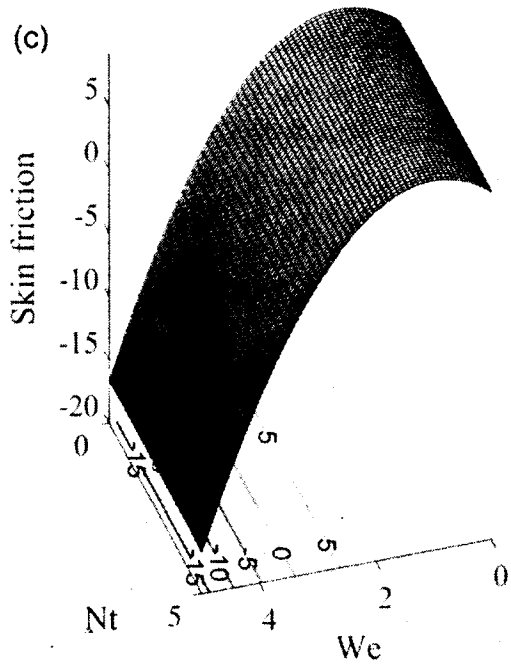

Fig.4.7: Contour plot of output response (Cf_x) when (a) $A = 0$ (b) $B = 0$ (c) $C = 0$.

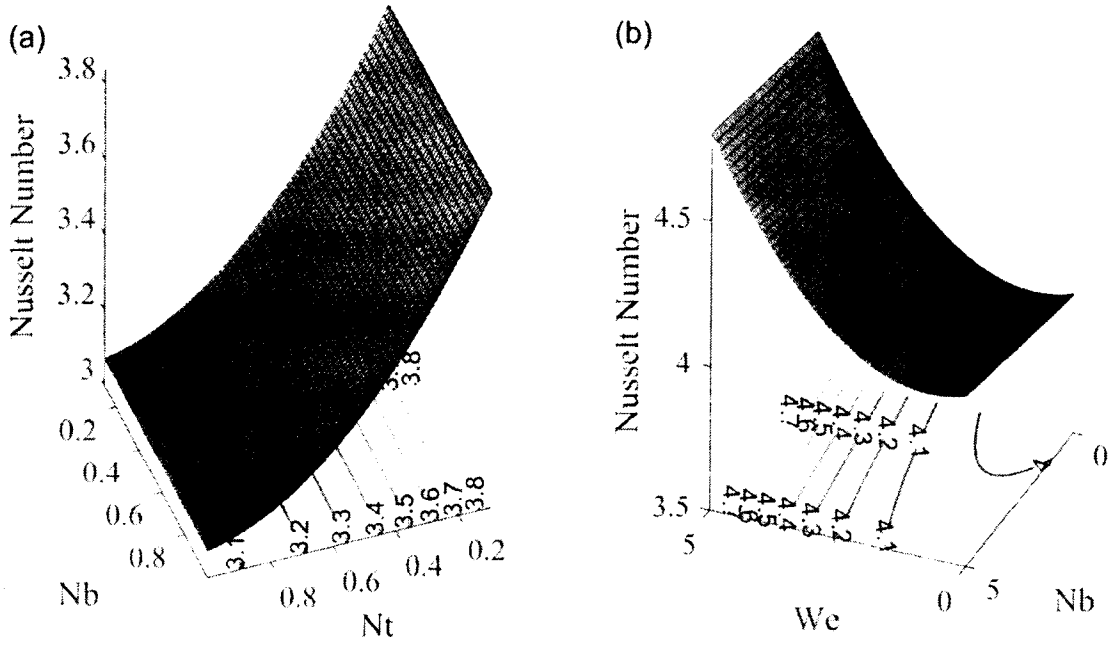

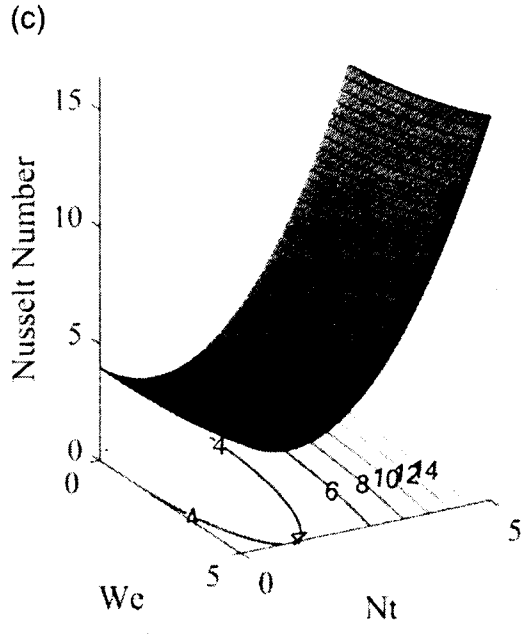

Fig.4.8: Contour plot of output response (Nu_x) when (a) $A = 0$ (b) $B = 0$ (c) $C = 0$.

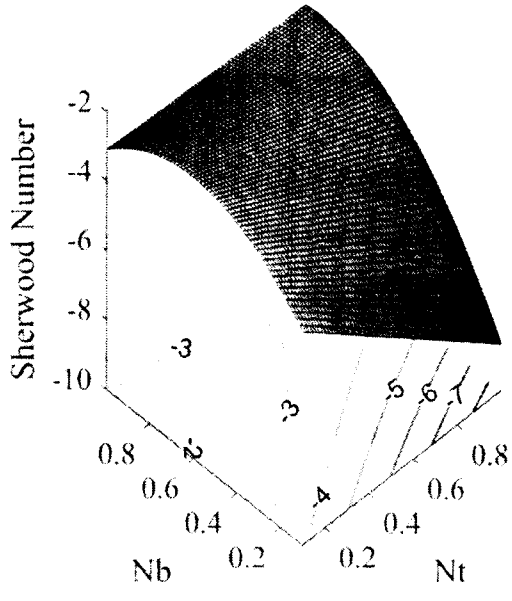

Fig.4.9: Contour plot of output response (Sh_x) when $A = 0$.

The contour plots of Cf_x, Nu_x and Sh_x are represented in Fig. 4.7 to Fig. 4.9 respectively. The influence of input parameters Nt and Nb on response Cf_x are displayed in Fig. 4.7(a). It can be perceived that the maximum Cf_x occurs near the

low level of *Nt* and *Nb*. Also the effect of *We* and *Nb* on Cf_x are depicted in Fig. 4.7(b). It is comprehended that minimum Cf_x occurs for both *We* and *Nb* at the low level and also by increasing the We the Cf_x increases from low to high level. The level curves of Cf_x show that Cf_x increases by increasing *We*. Further notice that there is negligible effect of *Nb* on Cf_x. The effect of *We* and *Nt* on Cf_x are shown in Fig. 4.7(c). The effects of these input parameters are nearly same as previously described in Fig. 4.7(b).

The effect of *Nt* and *Nb* are displayed in Fig. 4.8 (a). It is observed that the maximum Nu_x arises near the low level for *Nt* and high level of *Nb*. As from Fig. 4.8(b) it is observed that maximum Nu_x occurs at low level of *We* and *Nb*. From Fig. 4.8(c) it is observed that Nu_x decreases and also it is clear from the figure that maximum Nu_x occurs for high level of *We* and low level of *Nt*. The level curves of Nu_x show a decreasing trend.

As from Table. 4.7 it is cleared that Sherwood number is independent from the parameter *We*, which means that there is no effect of *We* on Sh_x. So we will only have one figure for Sh_x which is presented in Fig. 4.9. It is cleared from Fig. 4.9 that Sh_x is maximum for high level of *Nb* and increases with *Nb* and *Nt*.

Chapter 5

Casson Fluid Flowing over a Wedge

The sensitivity of Casson fluid flowing over a wedge is investigated in this chapter. To perform sensitivity analysis a third order non-linear PDEs along with boundary conditions are adopted from [78]. The governing PDEs are converted into ODEs by using similarity transformation. These equations are simulated using numerical technique bvp4c and then compared the values of Cf_x and Nu_x with [78] and found excellent agreement. In order to make sensitivity analysis we need to derive the empirical relations of these responses. RSM is used to obtain these responses. The ANOVA for these correlations of Cf_x and Nu_x are performed. Finally, sensitivity analysis is performed and tables and graphs are made to express the empirical development of parameters and their effect.

5.1 Mathematical Formulation

In this chapter the problem of steady, two-dimensional, laminar boundary layer of a non-Newtonian Casson fluid flowing over a wedge is considered. The simplified form of governing equations is those formulated in [78].

$$\frac{\partial u}{\partial x}+\frac{\partial u}{\partial y}=0, \tag{5.1}$$

$$u\frac{\partial u}{\partial x}+v\frac{\partial u}{\partial y}=U_e\frac{\partial U_e}{\partial x}+\nu_f\left(1+\frac{1}{\beta}\right)\frac{\partial^2 u}{\partial y^2}, \tag{5.2}$$

$$u\frac{\partial T}{\partial x}+v\frac{\partial T}{\partial y}=\kappa\frac{\partial^2 T}{\partial y^2}. \tag{5.3}$$

The associated boundary conditions for aforementioned problem are follows by [78],

$$u=0,\ v=0,\ T=T_w,\ at\ y=0, \tag{5.4}$$

$$u=u(x)=x^m, T\to T_\infty as\ y\to\infty. \tag{5.5}$$

where T_w denotes the temperature at wall and T_∞ is the ambient temperature.

Now by using the similarity transformation, Eq. (4.7), the above PDEs are converted into set of non-linear ODEs as follows by [78].

$$(1+\frac{1}{\beta})f''' + ff'' + \frac{2m}{m+1}(1-f'^2)=0, \tag{5.6}$$

$$\frac{1}{Pr}\theta'' + f\theta' = 0, \tag{5.7}$$

where $Pr = {}^{\nu}/_{\kappa}$ and β is the Casson fluid parameter. The associated boundary conditions are as follows [78],

$$f'(\eta) = 0, f(\eta) = 0, \theta = 1 \; at \; \eta = 0, \tag{5.8}$$

$$f'(\eta) = 1, \theta = 0 \; at \; \eta \to \infty. \tag{5.9}$$

The numerical solution for the simplified governing equations with boundary conditions is solved by bvp4c.

Table 5.1: Comparision of Cf_x with literature [78 - 80].

m	[78]	[79]	[80]	Present results
-0.05	0.213802	0.213802	0.213484	0.2135
0	0.332206	0.332206	0.332206	0.3321
0.33	0.75744	0.75758	0.75758	0.7543
1	1.232710	1.232710	1.232710	1.2326

Table 5.2: Comparison of Nusselt number (Nu_x) with literature [78], [80 - 81].

Pr	[78]	[81]	[80]	Present results
0.01	0.051589	0.051590	0.051589	0.0515
1	0.332057	0.332057	0.332057	0.3321
10	0.728141	0.728148	0.728141	0.7281
100	*	1.571860	1.571832	1.5718
1000	*	3.387100	3.387085	3.3871
10000	*	7.297400	7.297400	7.2975

5.2 Experimental Design

5.2.1 Response Surface Methodology (RSM)

In this chapter, the experimentation parameters are the Casson fluid parameter (β), Falkner–Skan exponent (m) and the Prandtl number (Pr). Table 5.3 shows these factors and their values as low (1), central (0), and high (+1). The correlations of Cf_x and Nu_x can be stated in the following general manner in terms of input parameters.

$$Cf_x = \alpha_0 + \alpha_1 A + \alpha_2 B + \alpha_3 C + \alpha_{11} AB + \alpha_{12} AC + \alpha_{13} BC + \alpha_{21} A^2 + \alpha_{22} B^2 + \alpha_{23} C^2, \tag{5.10}$$

$$Sh_x = \gamma_0 + \gamma_1 A + \gamma_2 B + \gamma_3 C + \gamma_{11} AB + \gamma_{12} AC + \gamma_{13} BC + \gamma_{21} A^2 + \gamma_{22} B^2 + \gamma_{23} C^2. \tag{5.11}$$

The regression coefficients for output responses with coded and real values are shown in Table 5.4.

Table 5.3: Input design factors and their levels.

Type	Factor	Symbol	Levels		
			-1	0	+1
Input Factors	β	A	0.2	2.6	5
	m	B	-0.05	0.475	1
	Pr	C	0.001	5.0005	10

Table 5.4: Experimental design and measured responses.

Experiment number	Point type	Coded values			Uncoded values			Responses	
		A	B	C	β	m	Pr	Cf_x	Nu_x
1	Factorial	-1	-1	-1	0	0.00	0.00	0.13878	0.12541
2		1	-1	-1	10	0.00	0.00	-0.24335	0.12462
3		-1	1	-1	0	0.50	0.00	0.50323	0.12577
4		1	1	-1	10	0.50	0.00	1.12520	0.12603
5		-1	-1	1	0	0.00	0.50	0.13878	0.69859
6		1	-1	1	10	0.00	0.50	-0.24335	0.00000
7		-1	1	1	0	0.50	0.50	0.50323	1.02290
8		1	1	1	10	0.50	0.50	1.12520	1.30400
9	Axial	-1	0	0	0	0.25	0.25	0.41838	0.76250
10		1	0	0	10	0.25	0.25	0.93524	0.97017
11		0	-1	0	5	0.00	0.25	-0.22581	0.00000
12		0	1	0	5	0.50	0.25	1.04750	0.99782
13		0	0	-1	5	0.25	0.00	0.87066	0.12597
14		0	0	1	5	0.25	0.50	0.87066	1.21280
15-20	Centre	0	0	0	5	0.25	0.25	0.87066	0.95004

5.2.2 Analysis of Variance (ANOVA)

To get the optimal polynomial correlations for the responses (Cf_x and Nu_x), multiple regressions are utilised. ANOVA is used to assess the regression model's fit with thirteen runs which is displayed in Table 5.4. Table 5.5 and Table 5.6 displays all of

the statistical estimators generated using the ANOVA method. Each of the Eqn.(5.10) and Eqn. (5.11) has its own F-value and P-value. The variance of the data is calculated using the F-value. If the F-value is greater the 1 then the input data is accurate. Table 12.6 shows the statistical estimated regression coefficients for the simplified models of Cf_x and Nu_x. The ANOVA shows the results of $R^2 = 96.50\,\%$ and $Adj\ R^2 = 93.35\,\%$ for Cf_x and $R^2 = 99.51\,\%$ and $Adj\ R^2 = 99.07\,\%$ for Nu_x.

Table 5.5: ANOVA for (a) $\boldsymbol{Cf_x}$ (b) $\boldsymbol{Nu_x}$

Source	DF	Adj SS	Adj MS	F-Value	P-Value	
(a)						
Model	9	3.88924	0.43214	30.66	0.000	Significant
Linear	3	2.34542	0.78181	55.47	0.000	Significant
Square	3	1.03972	0.34657	24.59	0.000	Significant
Interaction	3	0.50411	0.16804	11.92	0.001	
Error	10	0.14095	0.01410			
Lack-of-Fit	5	0.14095	0.02819	*	*	Significant
Pure Error	5	0.00000	0.00000			-
Total	19	4.03020				-
(b)						
Model	9	0.599759	0.066640	225.09	0.000	Significant
Linear	3	0.415415	0.138472	467.71	0.000	Significant
Square	3	0.177889	0.059296	200.28	0.000	Significant
Interaction	3	0.006454	0.002151	7.27	0.007	Significant
Error	10	0.002961	0.000296			-
Lack-of-Fit	5	0.002961	0.000592	*	*	Significant
Pure Error	5	0.00000	0.000000			-
Total	19	0.602719				-

Table 5.6: Regression coefficients for (a) Cf_x (b) Nusselt number (Nu_x).

Terms	Coefficient	P-value	Significant
(a)			
Constants	0.8468	0.000	Yes
A	0.0997	0.024	Yes
B	0.4739	0.000	Yes
C	0.0000	1.000	No
A^2	-0.1342	0.090	No
B^2	-0.4002	0.000	Yes
C^2	0.0596	0.424	No
AB	0.2510	0.000	Yes
AC	0.0000	1.000	No
BC	0.0000	1.000	No
$R^2 = 96.50\%$			$Adj\ R^2 = 93.35\%$
(b)			
Constants	0.98986	0.000	Yes
A	0.01654	0.012	Yes
B	0.02070	0.003	Yes
C	0.20209	0.000	Yes
A^2	-0.0303	0.015	Yes
B^2	0.0036	0.734	No
C^2	-0.1712	0.000	Yes
AB	0.00239	0.703	No
AC	0.01358	0.050	No
BC	0.02483	0.002	Yes

$R^2 = 99.51\%$	$Adj\ R^2 = 99.07\%$

5.3 Sensitivity analysis

The sensitivity of output responses Cf_x and Nu_x to input parameters wedge angle (β), Falkner-Skan exponent (m), and Prandtl number (Pr) is investigated in this section. The regression coefficient of Cf_x and Nu_x are displayed in Table 5.6. The P-value less than 0.05 is statistically important and must be retained if not it will be overlooked. Consequently, the skin friction coefficient is affected by A, B, B^2 and AB, while the Nusselt number is affected by A, B, C, BC, A^2 and C^2. As a result, mathematical Eqn. (2.2) may be rewritten as follows:

$$Cf_x = 0.8468 + 0.0997\,A + 0.4793\,B - 0.4002B^2 + 0.2510\,AB, \tag{5.12}$$

$$Nu_x = 0.98986 + 0.01654A + 0.0207B + 0.20209\,C + 0.02483\,BC - 0.0303A^2 - 0.1712C^2\,. \tag{5.13}$$

The sensitivity functions developed below can be used to calculate the growing or falling tendency of the responses (Cf_x and Nu_x) with regard to the input parameters A, B, and C.

$$\frac{\partial}{\partial A}(Cf_x) = 0.0997 + 0.2510B, \tag{5.14}$$

$$\frac{\partial}{\partial B}(Cf_x) = 0.4739 - 0.8004B + 0.2510A, \tag{5.15}$$

$$\frac{\partial}{\partial C}(Cf_x) = 0, \tag{5.16}$$

$$\frac{\partial}{\partial A}(Nu_x) = 0.01654 - 0.0606A, \tag{5.17}$$

$$\frac{\partial}{\partial B}(Nu_x) = 0.02078 + 0.02483C, \tag{5.18}$$

$$\frac{\partial}{\partial C}(Nu_x) = 0.20209 + 0.02483B - 0.3424C. \tag{5.19}$$

The sensitivity of various values of input parameters β, m and Pr is calculated. The sensitivity variation of output responses such as Cf_x and Nu_x are depicted in Table 5.7. The rising of bar chart in positive direction means the responses increase as by increasing the input parameters and vice versa. As well as the height of the bar chart increases the response becomes more sensitive to the input parameter. The sensitivity

plots of different input parameters for output responses are shown in Fig. 5.1 and Fig. 5.2

Table 5.7: Sensitivity analysis of Cf_x and Nu_x when $A=0$.

B	C	$\partial Cf_x/\partial A$	$\partial Cf_x/\partial B$	$\partial Cf_x/\partial C$	$\partial Nu_x/\partial A$	$\partial Nu_x/\partial B$	$\partial Nu_x/\partial C$
-1	-1	-0.1513	1.2743	0	0.01654	-0.00405	0.51966
	0	-0.1513	1.2743	0	0.01654	0.02078	0.17726
	1	-0.1513	1.2743	0	0.01654	0.04561	-0.16514
0	-1	0.0997	0.4739	0	0.01654	-0.00405	0.54449
	0	0.0997	0.4739	0	0.01654	0.02078	0.20209
	1	0.0997	0.4739	0	0.01654	0.04561	-0.14031
1	-1	0.3507	-0.3265	0	0.01654	-0.00405	0.56932
	0	0.3507	-0.3265	0	0.01654	0.02078	0.22692
	1	0.3507	-0.3265	0	0.01654	0.04561	-0.11548

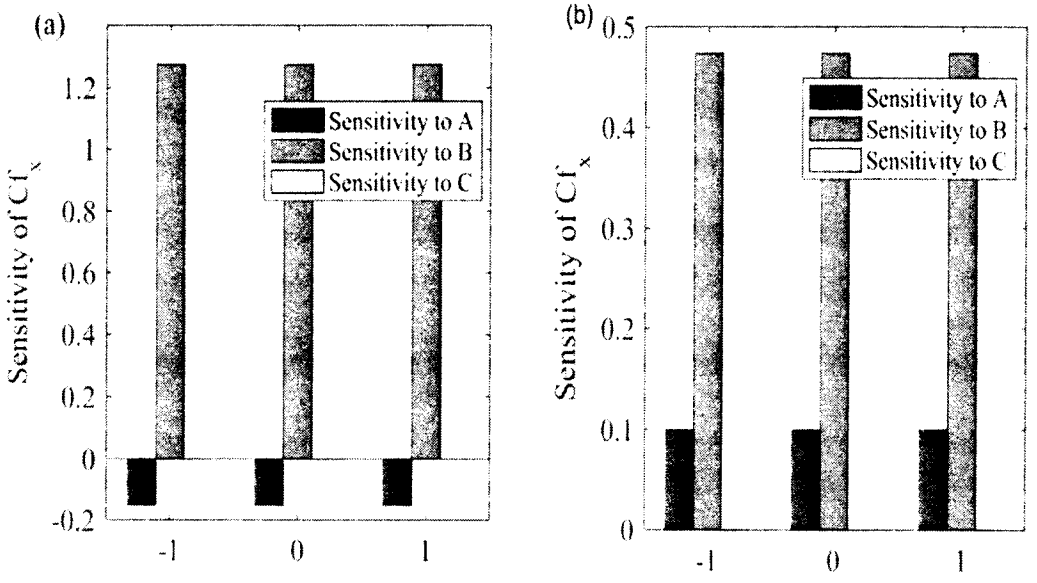

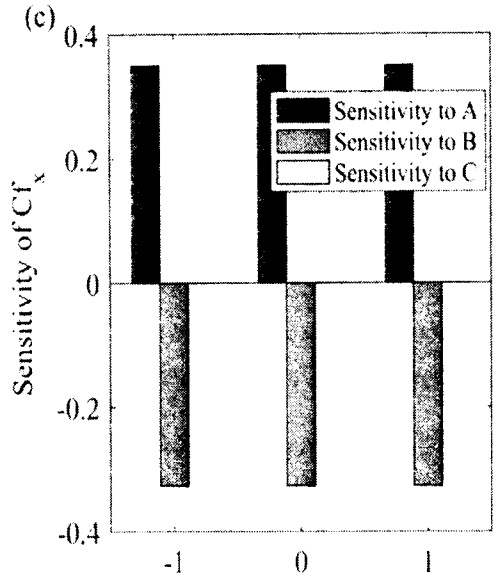

Figure 5.1: Sensitivity plots for Cf_x with $A=0$, (a) $B=-1$ (b) $B=0$ (c) $B=1$.

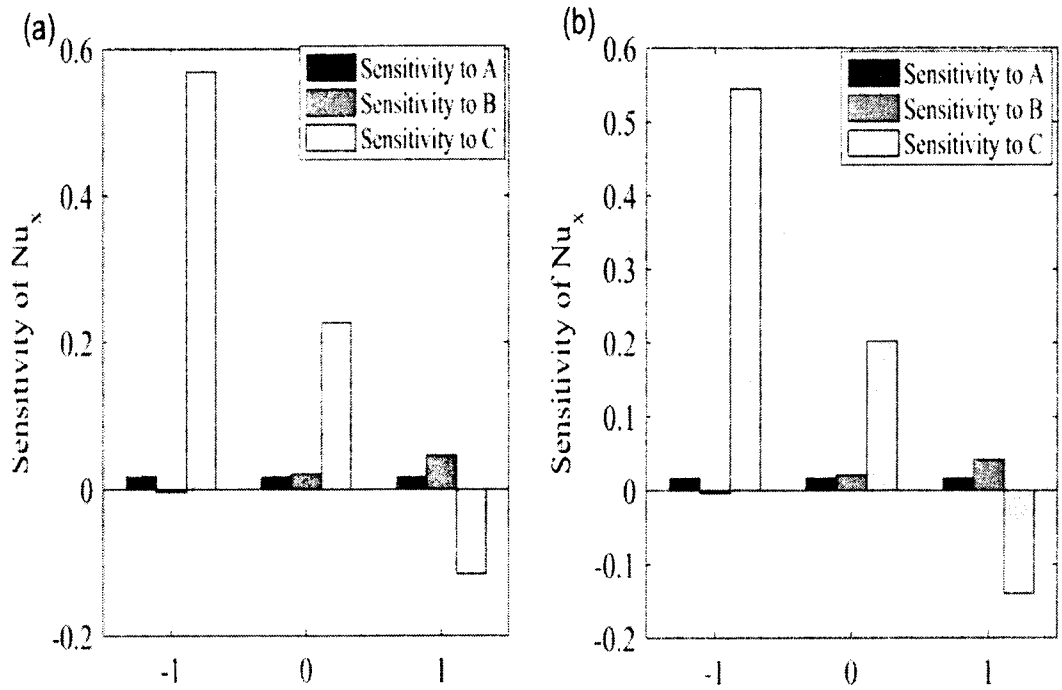

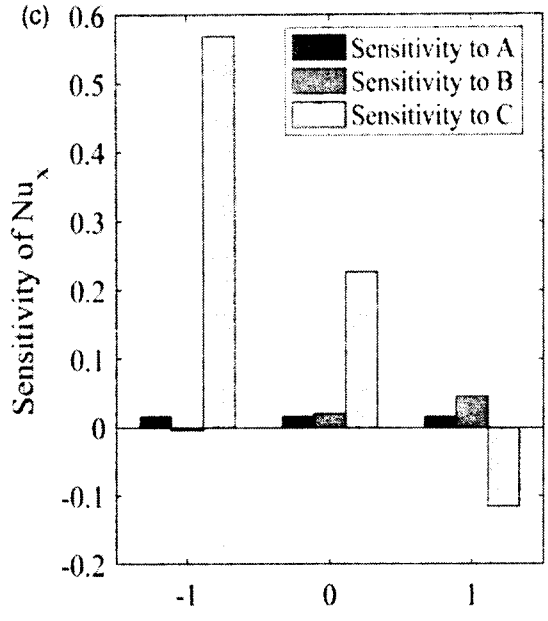

Figure 5.2: Sensitivity plots for Nu_x with $A=0$(a) $B=-1$ (b) $B=0$ (c) $B=1$.

5.4 Discussion of the Results

This section is meant for the discussion of the results for the sensitivity analysis of Casson fluid flowing over a wedge by using RSM. The governing non-linear differential equations [78] associated with its boundary conditions are solved numerically by using bvp4c. Then compare the obtained results of $Cf_x$and $Nu_x$with already existing work and found excellent agreement which can be seen in Table. 5.1 and Table. 5.2 respectively. Another Prime focus of this study is the sensitivity analysis of Cf_x and Nu_x for the parameters β, m and Pr governing to the problem. In order to meet this objective, we have used RSM to built expression for Cf_x and Nu_x as functions of β, m and Pr which can be seen in Eqn. (5.12) and Eqn. (5.13) respectively.

In order to perform sensitivity analysis, there is need to develop some empirical relation among each of output variables and input factors. Empirical development is a useful approach for obtaining correlations among output/response variables and input variables. It has significance in several experimental analyses to develop empirical model for viscosity and thermal conductivity ratio of nanomaterials. By using RSM we have calculated the values of responses by regression models fit to twenty runs which can be seen in Table 5.4. Both the coded and uncoded values may also by see

in Table 5.4. The ANOVA table for both Cf_x and Nu_x are depicted in Table 5.5 in which all the corresponding F-value and P-value are specified. The regression coefficient for Cf_x and Nu_x is shown in Table 5.6.

Fig. 5.1 displayed the sensitivity analysis of Cf_x for different parameters such as β, m and Pr. Fig. 5.1(a) shows the positive sensitivity of Cf_x to m and negative sensitivity of $Cf_x$to β. Which means that the sensitivity of Cf_x increases by increasing m and the Cf_x decreases as increasing β. The large magnitude of sensitivity of Cf_x relative to m shows that Cf_x is more sensitive to m whereas Cf_x is less sensitive to β. The sensitivity of Cf_x for the case $A = 0$ and $B = 0$ is shown in Fig. 5.1(b). The sensitivity of Cf_x to both β and m are positive for all values of β and m. It means that Cf_x will increase as by increasing both the parameters β and m. It is cleared from the figure that Cf_x is more sensitive in comparison to β. Also in this case there is no effect of Pr. Fig. 5.1(c) shows the sensitivity analysis of Cf_x for $A = 0$ and $B = 1$. β has positive sensitivity and m has a negative sensitivity which means that Cf_x will be increase by increasing β and decreases as increasing the value of m.

Now, the sensitivity analysis of Nu_x for the parameters β, m and Pr are examine. Fig. 5.2 displayed mixed behaviour of sensitivity of Nu_x to β, m and Pr. From figure, it can be observe that there is a positive sensitivity of β on Nusselt number for all levels which means that by increasing the value of β, Nu_x also increases. The small magnitude of sensitivity function shows that Nu_x is not much sensitive to β. Pr has positive sensitivity for low (-1) and middle (0) levels and it has negative sensitivity for high levels (+1) of Nusselt number. We can also conclude that Nu_x is most sensitive to Prandtl number (Pr) which means that the effect of Pr is much greater to Nusselt number than others. Another interesting thing is that sensitivity function shows a mixed behaviour with variation of Pr. This trend shows that optimization to Nu_x is affected greatly by Pr in comparison to parameters β and m.

RSM demands the discussion of residuals, lack of fit and level of residual with observation order. Residual is the difference between fitted values and actual values. Residuals are very important to check the accuracy of models. The residual plots are shown for output responses Cf_x and Nu_x in Fig. 5.3 and Fig. 5.4 respectively. The comparison of fitted values and residuals shows a good relation which assure the perfect correlation between input parameters β, m and Pr and output responses Cf_x

and Nu_x. Lack of fit describes the unexplained records points within the regression line when the models not succeed to express the relation between input variables and out responses.

The residual plots are shown in Fig.5.3 and Fig. 5.4. The scatter plots for output responses are shown in Fig. 5.3(a) and Fig. 5.4(a). The scatter plot depicts the relationship between the input factors and the output responses. The strength of the correlation between the two variables is important for scatter plots. When the slope is 1, the greatest linear connection arises. This indicates that as the input variables are increased, the output responses grow at the same rate. As a result, Fig. 5.3(a) and Fig. 5.4(a) show a significant relationship between the input factors and the output responses. The histograms in Fig. 5.3(b) and Fig. 5.4(b) have symmetrical scattering and are less skewed, indicating that Cf_x and Nu_x have a good connection with the input parameters. The observation order verses residuals of Cf_x and Nu_x are represented in Figs. 5.3(c) and 5.4(c), respectively. The results also show that increasing the observation order decreases the residual of the Cf_x and Nu_x, exhibiting strong relationship between the probability plots. The residuals graph demonstrates the greatest volatility for both Cf_x and Nu_x, indicating that the model is valid.

While discussing ANOVA and perfect correlation of input parameters and output variables/response(s) it is important to describe R-squared (R^2) and adjusted R-squared $(Adj\ R^2)$. R^2 and $Adj\ R^2$ validates the goodness of fit for RSM. $R^2 = 96.50\%$ and $Adj\ R^2 = 93.35\ \%$ for Cf_x and $R^2 = 99.51\ \%$ and $Adj\ R^2 = 99.07\ \%$ for Nu_x show the best correlation between input parameters and output responses which can be seen Table 5.6.

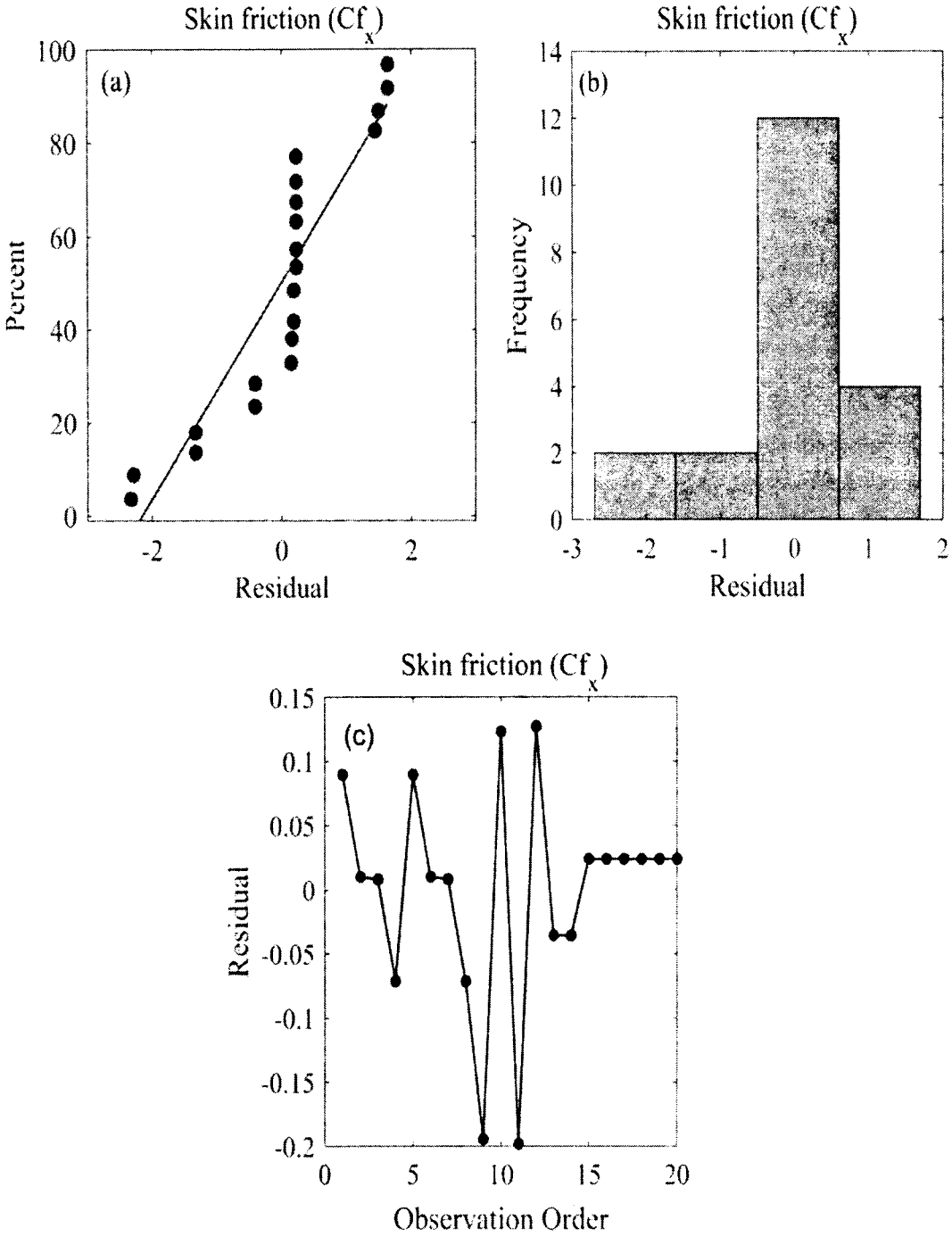

Figure 5.3: Residual plots for Cf_x (a) Normal probability plot (b) histogram (c) residual plot.

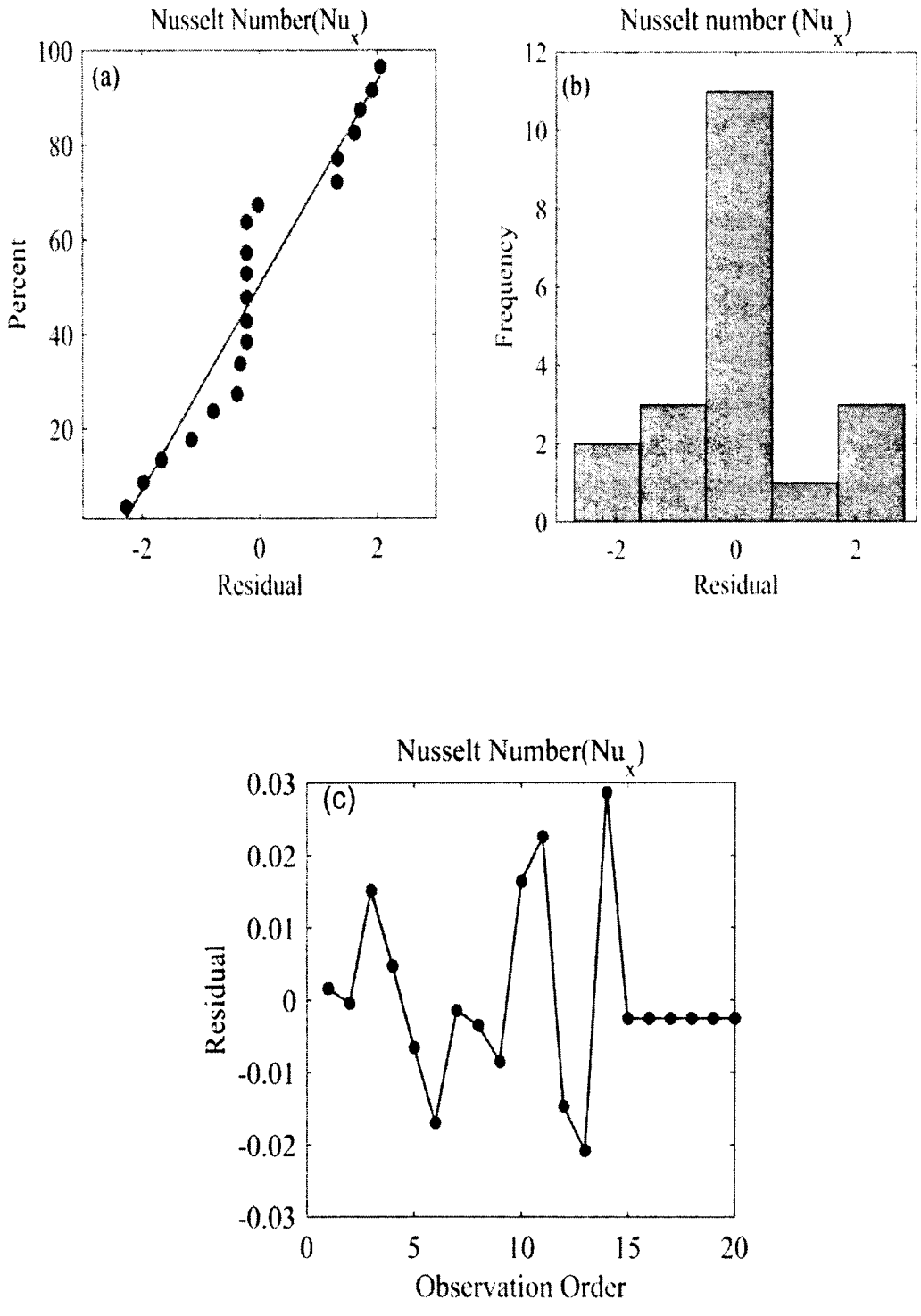

Figure 5.4: Residual plots for Nu_x (a) Normal probability plot (b) histogram (c) residual plot.

Fig. 5.5 and Fig. 5.6 display the surface contour plot of predicted responses. The effect of wedge angle (β), Falkner-Skan exponent (m), and Prandtl number (Pr) on output responses Cf_x will discuss first. Table 5.7 clears that Cf_x only depends on wedge angle (β) and Falkner-Skan exponent (m). Cf_x is independent from Prandtl

number (Pr) as $\frac{\partial Cf_x}{\partial C} = 0$. So, we have only one surface-contour graph for Cf_x which is shown in Fig. 5.5. Fig. 5.5 shows the effect of β and m on Cf_x. It is observed that maximum value of Cf_x occurs near high level of both β and m. And also the Cf_x decreases as approaching from lower level of β and higher level of m.

Fig. 5.6(a) displays the effect of Falkner- Skan exponent (m) and Pr. It is perceived that minimum Nusselt number arises near low level of m and high level of Pr. Fig. 5.6(b) depicted the effect of β and Pr on Nusselt number. As shown from the figure that minimum Nu_x occurs near the high levels of β and Pr and maximum Nu_x arises near the low level of both β and Pr. Finally, we will explain the effects of input parameters m and β on Nu_x. Fig. 5.6(c) shows the effect of m and β on Nu_x. It is observed that least value of Nu_x take place near the low levels of m and β. This means that thermal properties are greatly affected by the variation of Pr, β and m.

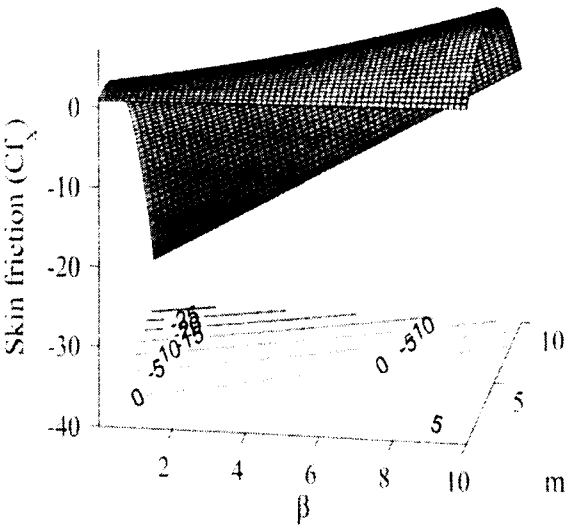

Figure 5.5: Surface-contour plot of Cf_x

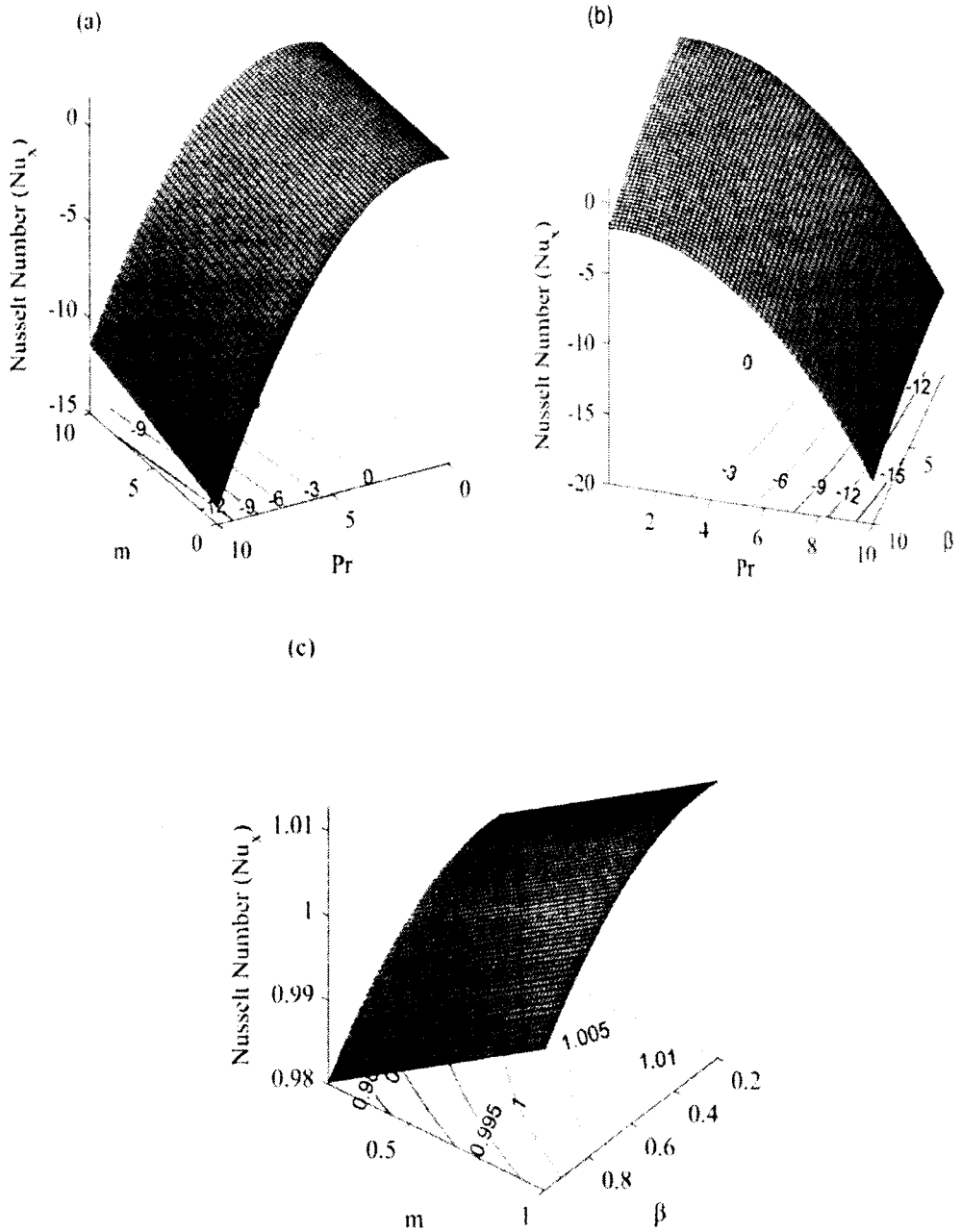

Figure 5.6: Contour plot of Nu_x when (a) $A=0$ (b) $B=0$ (c) $C=0$

Chapter 6

Magneto-Carreau Fluid over a Wedge

In this chapter, the sensitivity analysis and empirical modelling of magneto-Carreau fluid flowing over a wedge by RSM is studied. The non-linear PDEs are adopted from [82]. The transformed PDEs are solved with MATLAB built in software bvp4c and compared with [82-86] and found good agreement. These numerical values are then used to design experimental models between input variables and output responses with the help of statistical software MINITAB-19. RSM is used to develop an empirical modelling for skin friction coefficient and Sherwood number. By using RSM, ANOVA tables are generated for input parameters We, Ha and β for skinfriction coefficient and Ha, Sc and γ for Sherwood number. Sensitivity analysis is performed for different output responses against their respective input parameters and results are depicted in the form of tables and graph.

6.1 Mathematical Formulation

Consider the problem of non-Newtonian magneto-Carreau fluid flowing over a wedge. The governing boundary layer equations for continuity, momentum and energy equation are follows as [82],

$$\frac{\partial u}{\partial x}+\frac{\partial v}{\partial y}=0, \tag{6.1}$$

$$u\frac{\partial u}{\partial x}+v\frac{\partial u}{\partial y}=U_e\frac{dU_e}{dx}-\frac{\sigma B_e^2}{\rho}(u-U_e)+v\frac{\partial^2 u}{\partial y^2}\left[1+\Gamma^2\left(\frac{\partial u}{\partial y}\right)^2\right]^{\frac{n-1}{2}} v(n-1)\Gamma^2\frac{\partial^2 u}{\partial y^2}\left(\frac{\partial u}{\partial y}\right)^2\left[1+\Gamma^2\left(\frac{\partial u}{\partial y}\right)^2\right]^{\frac{n-3}{2}}, \tag{6.2}$$

$$u\frac{\partial T}{\partial x}+v\frac{\partial T}{\partial y}=\frac{1}{\rho c_p}\frac{\partial}{\partial y}[k(T)\frac{\partial T}{\partial y}], \tag{6.3}$$

$$u\frac{\partial C}{\partial x}+v\frac{\partial C}{\partial y}=D\frac{\partial^2 C}{\partial y^2}-R(C-C_\infty). \tag{6.4}$$

The temperature dependent thermal conductivity are expressed as,

$$k(T) = k_\infty(1+\epsilon \frac{T-T_\infty}{T_w-T_\infty}). \tag{6.5}$$

The boundary conditions for stated problem is follows by [82],

$$u = u_{slip}, \quad v = 0, \quad T = T_w + T_{slip}, \quad C = C_w + C_{slip}, \quad at\ y = 0, \tag{6.6}$$

$$u = U_e(x) = U_\circ x^m, \quad T \to T_\infty, \quad C \to C_\infty, \quad as\ y \to \infty. \tag{6.7}$$

Where, u and v represents the velocity along x-axis and y-axis respectively. The electrical conductivity is denoted by σ, ρ denotes the fluid density, B_o represents the magnetic field, Γ denotes relaxation time, T denotes fluid temperature, n is the power law index, D denotes solutal and R is the chemical reaction parameter. Also, $u_{slip} = L\frac{\partial u}{\partial y}\left[1 + \Gamma^2\left(\frac{\partial u}{\partial y}\right)^2\right]^{\frac{n-1}{2}}$ represents the wall slip velocity, $T_{slip} = M\frac{\partial T}{\partial y}$, denotes thermal slip and $C_{slip} = N\frac{\partial C}{\partial y}$ is the concentration slip. L, M and N are the velocity, temperature and concentration slip factors.

The similarity transformations are followed by [82],

$$\psi(x,y) = \sqrt{\frac{2\nu U_e}{1+m}}x^{\frac{m+1}{2}}f(\eta), \quad \eta = y\sqrt{\frac{U_e(1+m)}{2\nu_f}}x^{\frac{m-1}{2}},$$
$$\theta(\eta) = \frac{T-T_\infty}{T_w-T_\infty}, \qquad C(\eta) = \frac{C-C_\infty}{C_w-C_\infty}. \tag{6.8}$$

The stream function ψ is defined as $u = \frac{\partial \psi}{\partial y}$ and $v = -\frac{\partial \psi}{\partial x}$ and the dimensionless velocity components expressed by [82] are as follows,

$$u = U_e x^m f'(\eta),\ v = -\sqrt{\frac{U_e(1+m)\nu}{2}}x^{\frac{m-1}{2}}[f(\eta) + \eta(\frac{m-1}{m+1})f'(\eta)]. \tag{6.9}$$

By using the expressions in Eqn. 6.8 and Eqn. 6.9, the transformed non-linear linear ODEs are [82],

$$\{1 + nWe^2(f'')^2\}\{1 + We^2(f'')^2\}^{\frac{n-3}{2}}f''' + ff'' + \beta(1-(f')^2) + Ha^2(1-f') = 0, \tag{6.10}$$

$$(1+\epsilon\,\theta)\theta'' + \varepsilon(\theta')^2 + Prf\theta' = 0, \tag{6.11}$$

$$\theta'' + Sc(f\theta' - \gamma\phi) = 0. \tag{6.12}$$

The transformed boundary conditions are followed by [82],

$$f(0) = 0, \quad f'(\infty) = \frac{S_1}{\sqrt{2-\beta}}, \; f''(0)\left[1 + We^2\left(f''(0)\right)^2\right]^{\frac{n-1}{2}}, \tag{6.13}$$

$$\theta(0) = 1 + \frac{S_2}{\sqrt{2-\beta}}\theta'(0),$$

$$\phi(0) = 1 + \frac{S_3}{\sqrt{2-\beta}}\phi'(0), \; f'(\infty) \to 1, \; \theta(\infty) \to 0, \; \phi(\infty) \to 0. \tag{6.14}$$

The Cf_x, Nu_x and Sh_x can be measured with the help of following relations,

$$C_{fx} = \frac{\tau_w}{\rho u_w^2/_2}, \; Nu_x = \frac{xq_w}{k(T_w - T_\infty)}, \; Sh_x = \frac{xq_m}{D_B(C_w - C_\infty)}. \tag{6.15}$$

τ_w, q_w and q_m are wall shear stress, heat and mass flux respectively and given as,

$$\tau_w = \mu_\circ \frac{\partial u}{\partial y}\left[1 + \Gamma^2\left(\frac{\partial u}{\partial y}\right)^2\right]^{\frac{n-1}{2}}\Bigg|_{y=0}, \; q_w = -k\left(\frac{\partial T}{\partial y}\right)\Big|_{y=0}, \; q_m = -D\left(\frac{\partial C}{\partial y}\right)\Big|_{y=0}. \tag{6.16}$$

By using the dimensionless parameters Cf_x, Nu_x and Sh_xcan be expressed as, $Re^{\frac{1}{2}}C_{fx} = \frac{2}{\sqrt{2-\beta}}f''(0)\left[1 + We^2\left(f''(0)\right)^2\right]^{\frac{n-1}{2}}$, $Re^{-\frac{1}{2}}Nu_x = -\frac{2}{\sqrt{2-\beta}}\theta'(0)$ *and* $Re^{-\frac{1}{2}}Su_x = -\frac{2}{\sqrt{2-\beta}}\phi'(0)$. (6.17)

Table 6.1: Comparision of $Cf_x$with literature [82–85].

m	[82]	[83]	[84]	[85]	Present
0.0	0.4696	0.4699	0.4696	0.4696	0.4696
1/11	0.6549	0.6574	0.6549	0.6550	0.6548
1/5	0.8021	0.8045	0.8021	0.8021	0.8021
1/3	0.9276	0.9298	0.9276	0.9277	0.9278
1.0	1.2325	1.2358	1.2325	1.2326	1.2326

Table 6.2: Comparision of Nu_x with literature [82] and [86].

m	[86]	[82]	Present
1/11	0.4473	0.4473	0.4473
1/7	0.4569	0.4569	0.4569
1/5	0.4650	0.4650	0.4650
1/3	0.4781	0.4781	0.4781

6.2 Experimental Design

6.2.1 Response Surface Methodology (RSM)

RSM will design the model within a specific range, so it is necessary to define the levels. The levels of input parameters and their symbol are displayed in Table 6.3 and Table 6.4

Table 6.3: Design input factor and their levels for Cf_x.

Type	Factor	Symbol	Levels		
			Low (-1)	Middle (0)	High (1)
Input Factors	We	A	1	3	5
	Ha	B	0.1	0.55	1
	β	C	0.1	0.3	0.5

Table 6.4: Design input factor and their levels for Sh_x.

Type	Factor	Symbol	Levels		
			Low (-1)	Middle (0)	High (1)
Input Factors	Ha	D	0.1	0.55	1
	Sc	E	0.5	0.75	1
	γ	F	0.2	0.4	0.6

The experimental design for output response Cf_x and Sh_x are displayed in Table 6.5 and Table 6.6 respectively.

Table 6.5: Experimental design and measured responses for Cf_x.

Experiment number	Point type	Coded values			Real values			Response
		A	B	C	We	Ha	β	Cf_x
1	Factorial	-1	-1	-1	1	0.10	0.1	0.6635
2		1	-1	-1	5	0.10	0.1	0.4630
3		-1	1	-1	1	1.00	0.1	0.9030
4		1	1	-1	5	1.00	0.1	0.5916
5		-1	-1	1	1	0.10	0.5	0.9100
6		1	-1	1	5	0.10	0.5	0.6102
7		-1	1	1	1	1.00	0.5	1.0532
8		1	1	1	5	1.00	0.5	0.6898
9	Axial	-1	0	0	1	0.55	0.3	0.8683
10		1	0	0	5	0.55	0.3	0.5794
11		0	-1	0	3	0.10	0.3	0.6426
12		0	1	0	3	1.00	0.3	0.7599
13		0	0	-1	3	0.55	0.1	0.6115
14		0	0	1	3	0.55	0.5	0.7580
15-20	Centre	0	0	0	3	0.55	0.3	0.6876

Table 6.6: Experimental design and measured responses for Sh_x.

Experiment number	Point type	Coded values			Real values			Responses
		D	E	F	Ha	Sc	γ	Sh_x
1	Factorial	-1	-1	-1	0.10	0.50	0.2	0.5810
2		1	-1	-1	1.00	0.50	0.2	0.6013
3		-1	1	-1	0.10	1.00	0.2	0.7193
4		1	1	-1	1.00	1.00	0.2	0.7454
5		-1	-1	1	0.10	0.50	0.6	0.6818
6		1	-1	1	1.00	0.50	0.6	0.6963
7		-1	1	1	0.10	1.00	0.6	0.8363
8		1	1	1	1.00	1.00	0.6	0.8537
9	Axial	-1	0	0	0.10	0.75	0.4	0.7202
10		1	0	0	1.00	0.75	0.4	0.7396
11		0	-1	0	0.55	0.50	0.4	0.6425
12		0	1	0	0.55	1.00	0.4	0.7920
13		0	0	-1	0.55	0.75	0.2	0.6699
14		0	0	1	0.55	0.75	0.6	0.7773
15-20	Centre	0	0	0	0.55	0.75	0.4	0.7282

Eqn. (2.2) can be expressed as,

$$Cf_x = \alpha_0 + \alpha_1 A + \alpha_2 B + \alpha_3 C + \alpha_{11} AB + \alpha_{12} AC + \alpha_{13} BC + \alpha_{21} A^2 + \alpha_{22} B^2 + \alpha_{23} C^2. \quad (6.18)$$

$$Sh_x = \gamma_0 + \gamma_1 A + \gamma_2 B + \gamma_3 C + \gamma_{11} AB + \gamma_{12} AC + \gamma_{13} BC + \gamma_{21} A^2 + \gamma_{22} B^2 + \gamma_{23} C^2. \quad (6.19)$$

where α_i ,α_{ij}, γ_i and γ_{ij} are unknown constants. These unknown coefficients can be found by using RSM.

6.2.2 Analysis of Variance (ANOVA)

ANOVA will be performed with the help of statistical software MINITAB-19. By using RSM, ANOVA calculate the R^2, $Adj\ R^2$, F-value, and P-value. Table 6.7 displayed the ANOVA result for different input factors and output variables. With the help of Table 6.8, we will design a model for output response. We will only accept the coefficient in Table 6.8 whose p-value is less than 0.05. The coefficients whose p-value is greater than 0.05 is not statistically significant therefore will not consider. As a result, mathematical Eqn. (6.18) and Eqn. (6.19) may be rewritten as follows:

$$Cf_x = (0.68747) - (0.1464)A + (0.07082)B + (0.07886)C + (0.03657)A^2 + (0.01397)B^2 - (0.02181)AB - (0.01891)AC - 0.01816BC. \quad (6.20)$$

$$Sh_x = (0.728195) + (0.00977)A + (0.074380)B + (0.052850)C + (0.001714)A^2 - (0.010936)B^2 - (0.004586)C^2 + (0.001087)AB - (0.001812)AC + (0.003687)BC. \quad (6.21)$$

Table 6.7: ANOVA for (a) Cf_x (b) Nu_x

Source	DF	Adj SS	Adj MS	F-Value	P-Value	Significant
(a)						
Model	9	0.345976	0.038442	520.56	0.000	Yes
Linear	3	0.326673	0.108891	1474.56	0.000	Yes
Square	3	0.009996	0.003332	45.12	0.000	Yes
Interaction	3	0.009307	0.003102	42.01	0.000	Yes
Error	10	0.000738	0.000074			
Lack-of-Fit	5	0.000738	0.000148			
Pure Error	5	0.000000	0.000000			

Total	19	0.346714				
(b)						
Model	9	0.085213	0.009468	29471.80	0.000	Yes
Linear	3	0.084210	0.028070	87373.92	0.000	Yes
Square	3	0.000859	0.000286	891.51	0.000	Yes
Interaction	3	0.000145	0.000048	149.95	0.000	Yes
Error	10	0.000003	0.000000			
Lack-of-Fit	5	0.000003	0.000001			
Pure Error	5	0.000000	0.000000			
Total	19	0.085217				

Table 6.8: Regression coefficients for (a) Cf_x (b) Nu_x

Terms	Coefficient	P-value	Significant
(a)			
Constants	0.68747	0.000	Yes
A	-0.14640	0.000	Yes
B	0.07082	0.000	Yes
C	0.07886	0.000	Yes
A^2	0.03657	0.000	Yes
B^2	0.01397	0.022	Yes
C^2	-0.00253	0.636	No
AB	-0.02181	0.000	Yes
AC	-0.01891	0.000	Yes

BC	-0.01816	0.000	Yes
	$R^2 = 99.79\%$		$Adj\ R^2 = 99.60\%$
(b)			
Constants	0.728195	0.000	Yes
D	0.009770	0.000	Yes
E	0.074380	0.000	Yes
F	0.052850	0.000	Yes
D^2	0.001714	0.001	Yes
E^2	-0.010936	0.000	Yes
F^2	-0.004586	0.000	Yes
DE	0.001087	0.000	Yes
DF	-0.001812	0.000	Yes
EF	0.003687	0.000	Yes
	$R^2 = 100.00\%$		$Adj\ R^2 = 99.99\ \%$

6.3 Sensitivity analysis

By using Eqn. (6.20) and Eqn. (6.21) the sensitivity function of output responses (Cf_x and Sh_x) are developed in Eqns. (6.22- 6.27).

$$\frac{\partial}{\partial A}(Cf_x) = -(0.1464) + 2(0.03657)A - (0.02181)B - (0.01891)C, \quad (6.22)$$

$$\frac{\partial}{\partial B}(Cf_x) = (0.07082) + 2(0.01397)B - (0.02181)A - (0.01816)C, \quad (6.23)$$

$$\frac{\partial}{\partial C}(Cf_x) = (0.07886) - (0.01891)A - (0.01816)B, \quad (6.24)$$

$$\frac{\partial}{\partial D}(Sh_x) = (0.009770) + 2(0.001714)D + (0.001087)E - (0.001812)F, \quad (6.25)$$

$$\frac{\partial}{\partial E}(Sh_x) = (0.074380) - 2(0.010936)E + (0.001087)D + (0.003687)F, \quad (6.26)$$

$$\frac{\partial}{\partial F}(Sh_x) = (0.052850) - 2(0.004586)F - (0.001812)D + (0.003687)E. \quad (6.27)$$

By using Eqns. (6.22 - 6.27) the sensitivity of various values of input parameter is performed. Table 6.9 and Table 6.10 shows the sensitivity of Cf_x and Sh_x respectively. These tables are utilized to plot bar graph of output response Cf_x and Sh_x against various input parameters. The responses are more sensitive to the input factors as the bar chart's height increases. The sensitivity graphs are shown in Fig. 6.1 and Fig. 6.2 for Cf_x and Sh_x respectively.

Table 6.9: Sensitivity analysis of skin friction coefficient when $A=0$.

B	C	$\partial Cf_x/\partial A$	$\partial Cf_x/\partial B$	$\partial Cf_x/\partial C$
-1	-1	-0.1057	0.0610	0.0970
	0	-0.1246	0.0429	0.0970
	1	-0.1435	0.0247	0.0970
0	-1	-0.1275	0.0890	0.0789
	0	-0.1464	0.0708	0.0789
	1	-0.1653	0.0527	0.0789
1	-1	-0.1493	0.1169	0.0607
	0	-0.1682	0.0988	0.0607
	1	-0.1871	0.0806	0.0607

Table 6.10: Sensitivity analysis of Sh_x number when $D=0$.

E	F	$\partial Sh_x/\partial D$	$\partial Sh_x/\partial E$	$\partial Sh_x/\partial F$
-1	-1	0.0105	0.0926	0.0583
	0	0.0087	0.0963	0.0492
	1	0.0069	0.0999	0.0400
0	-1	0.0116	0.0707	0.0620
	0	0.0098	0.0744	0.0529
	1	0.0080	0.0781	0.0437
1	-1	0.0127	0.0488	0.0657
	0	0.0109	0.0525	0.0565
	1	0.0090	0.0562	0.0474

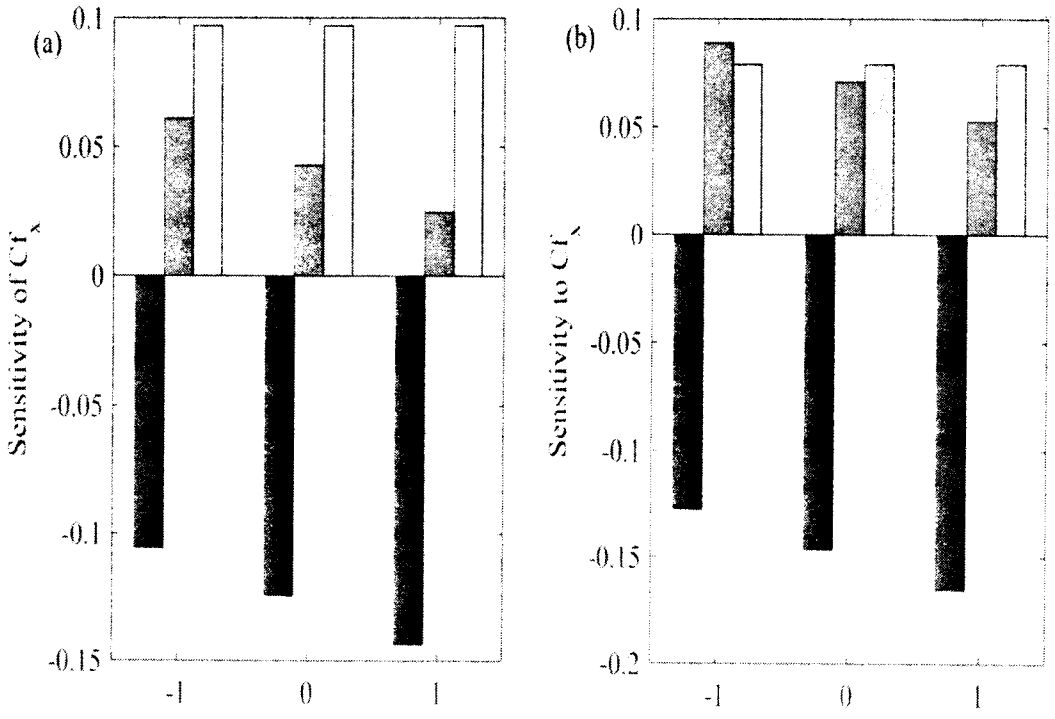

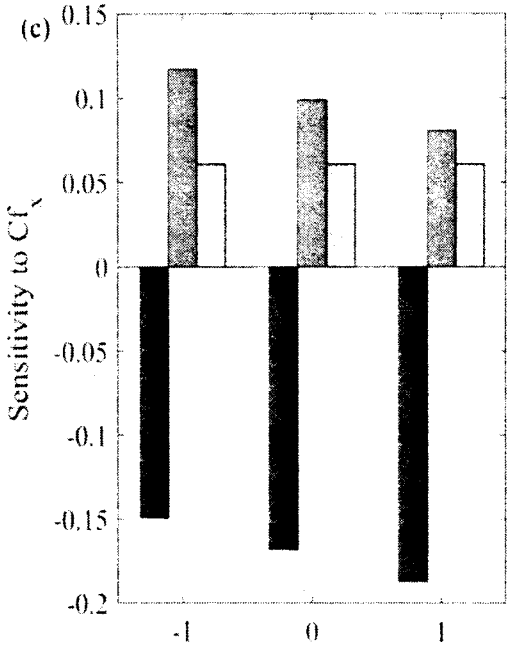

Figure 6.1: Sensitivity plots for output Sh_x for $A=0$ (a) $B=-1$ (b) $B=0$

(c) $B=1$

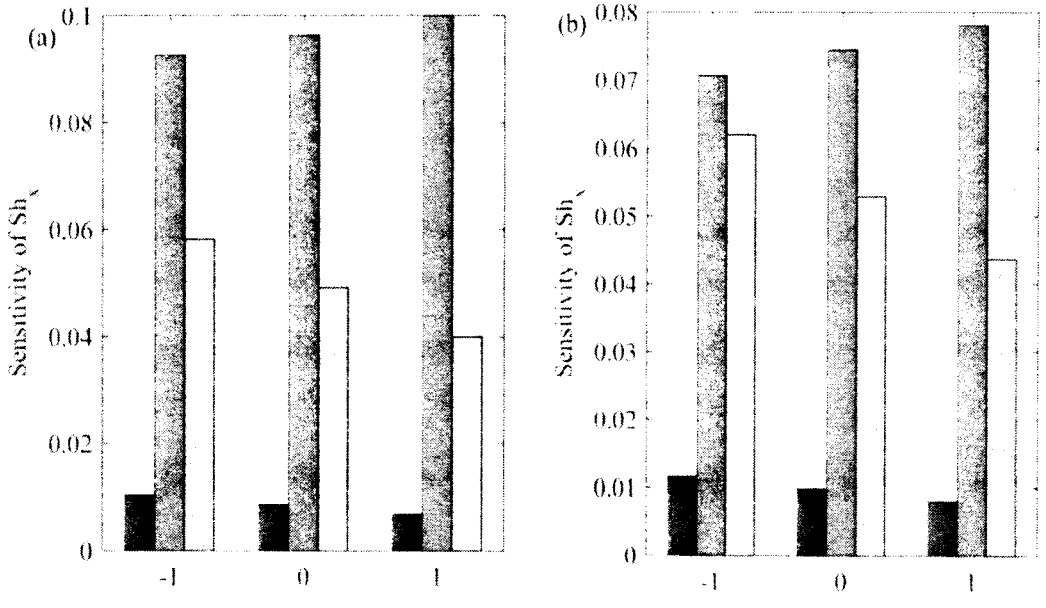

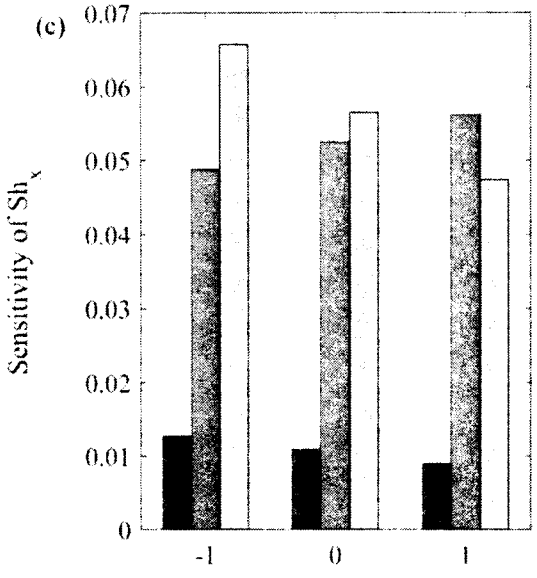

Figure 6.2: Sensitivity plots for output Sh_x for $A=0$ (a) $B=-1$(b) $B=0$

(c) $B=1$

6.4 Discussion of the results

This section is arranged to describe the sensitivity analysis and empirical development of magneto-Carreau fluid flow over a wedge by using RSM. The prime objective of this chapter is to carry out sensitivity analysis of output responses for different input factors. To achieve this purpose we have calculated numerical results of the problem using Matlab's built-in package bvp4c and compared these results with [82 - 86], which shows excellent agreement. We have created a correlation for output responses (Cf_x and Nu_x) against input parameters by using RSM which is described in Eqn. (6.20) and Eqn. (6.21). By using CCD with the help of RSM we have design an ANOVA table and regression of coefficients for different input parameters which is depicted in Table (6.5) to Table (6.8). To check the validity of designed experimental scheme we have plotted the different forms of residuals graphically. The residuals are plotted in form of normal probability, histograms and verses order which are portrayed in Fig. 6.3 and Fig. 6.4. The scatter plots are closer to a straight line in Fig. 6.3(a) and Fig. 6.4(a), which demonstrates that, the experimental models are perfectly correlated. The histograms in Fig. 6.3(b) and Fig. 6.4(b) are symmetrical and continuous which shows the validity of experimental models. The observation verses order in Fig. 6.3(c) and Fig. 6.4(c) illustrates that residuals are reduces when

observation order rises. These residual plots show the strong correlations between input factors and output responses.

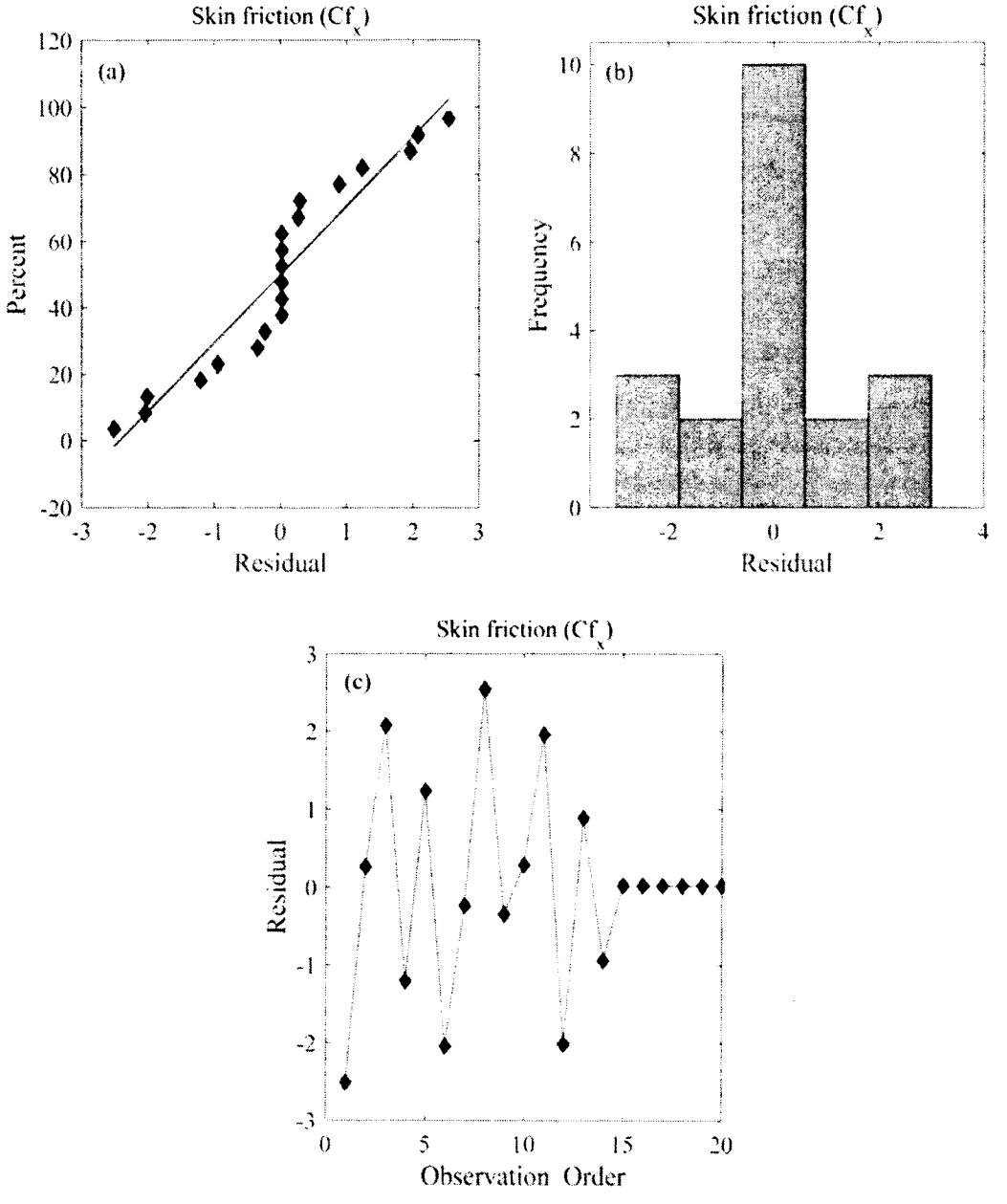

Figure 6.3: Residuals of output response Cf_x (a) Normal probability (b) Histogram (c) Residual plot

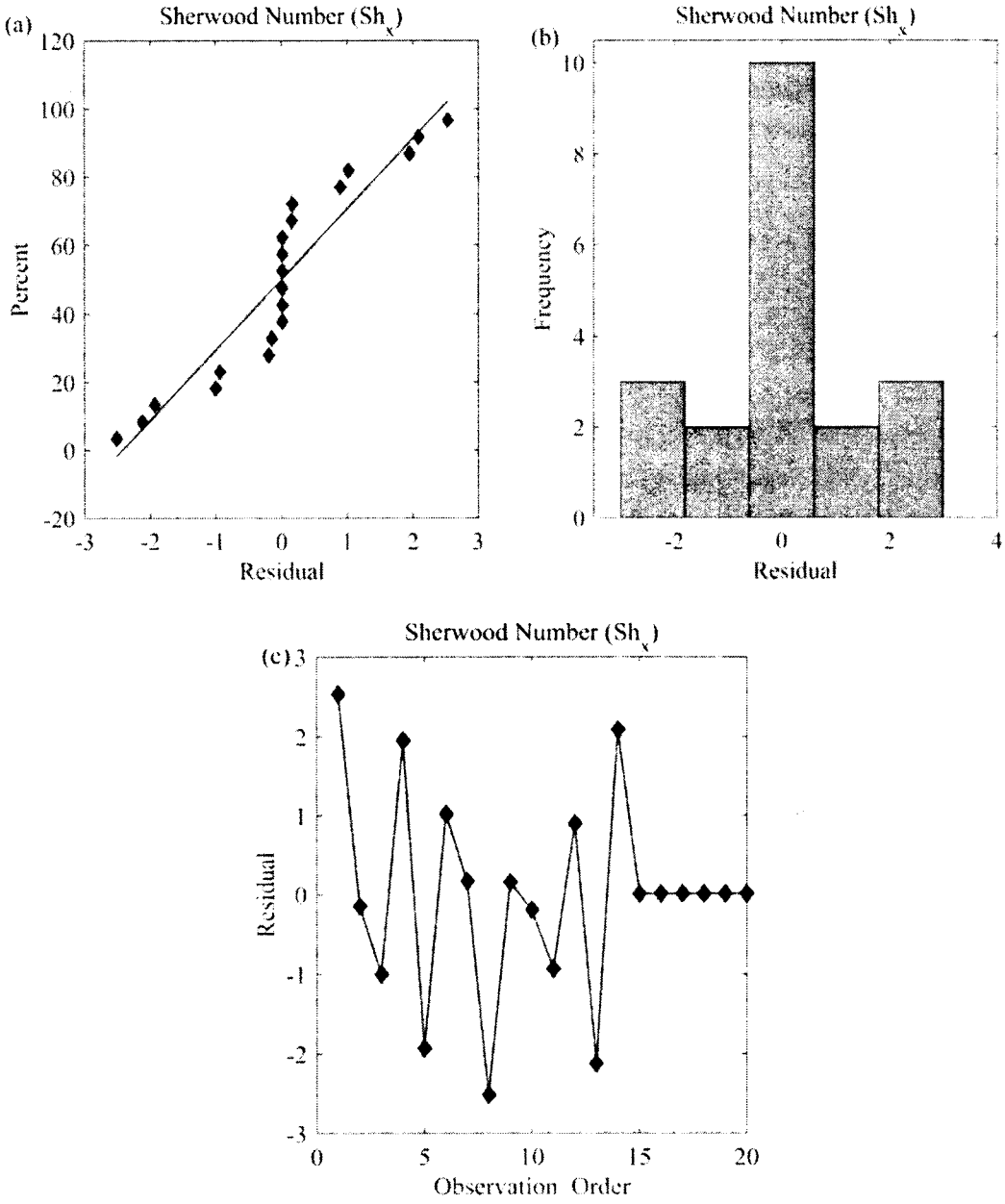

Figure 6.4: Residuals of output response Sh_x (a) Normal probability (b) Histogram (c) Residual plot.

The sensitivity plots of Cf_x and Sh_x is displayed in Fig. 6.1 and Fig. 6.2 respectively. The height of the bar graph displayed the sensitivity of the input parameter. The most sensitive parameter shows the highest bar graph. The bar graph in upward direction shows positive sensitivity, and the bar graph in the downward direction denotes negative sensitivity. Positive sensitivity means that, by increasing the input parameter, the output response also increases. And in negative sensitivity, the output response declines by raising the input parameter. Fig. 6.1 displays the sensitivity analysis of

Cf_x for We, Ha and β. Fig. 6.1(a) to Fig. 6.1(c) displays the positive sensitivity of Cf_x to Ha and β and negative sensitivity to We. This demonstrates that by increasing Ha and β the output response increases and by increasing the parameter We, the response decreases. It is also concluded that Cf_x is most sensitive to We.

Fig. 6.2 shows the sensitivity plots of Sh_x for input parameters Ha, Sc and γ. From Fig. 6.2(a) to Fig. 6.2(c), it is clear that all input parameters have a positive sensitivity at all levels. We can also observe that Sc is most sensitive to Sh_x to the case $D = 0, E = -1$ and $D = 0, E = 0$. In the case of $D = 0, E = 1$, γ is most sensitive among others at low and middle level and the Sc is most sensitive for high level.

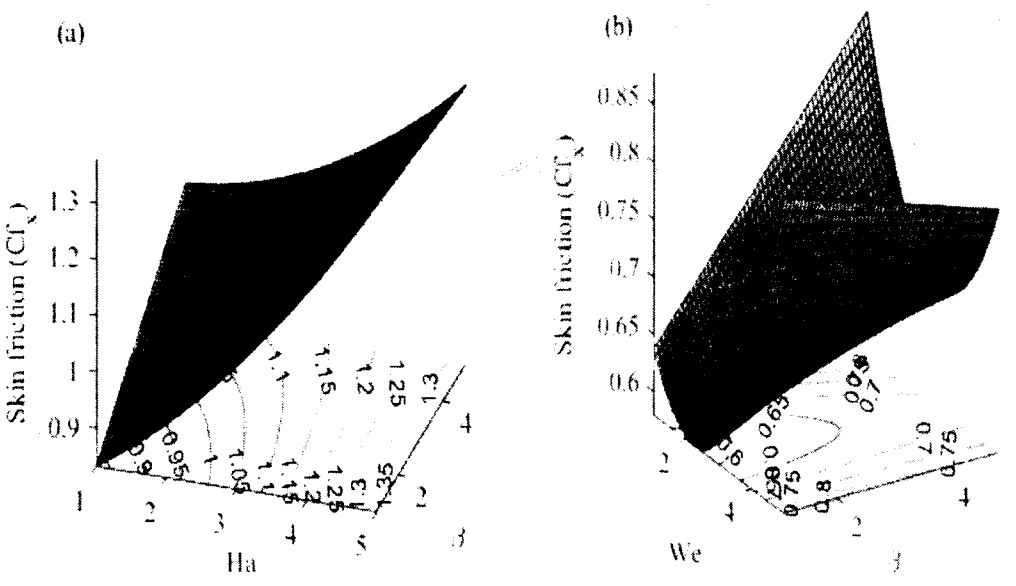

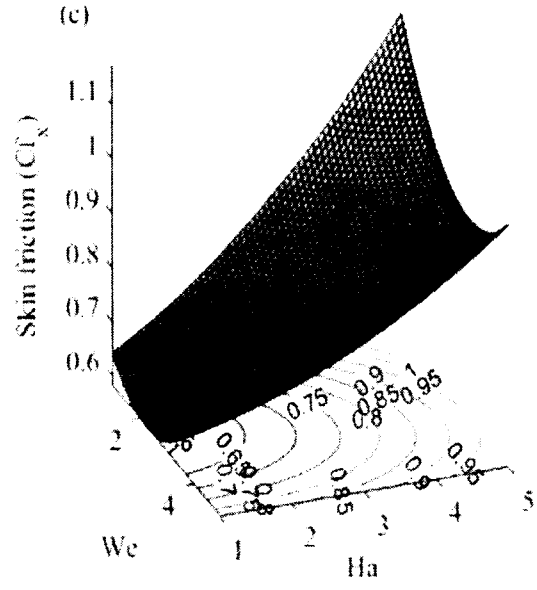

Figure 6.5: Contour plot for Cf_x (a) A=0 (b) *B=0*

(c) *C=0.*

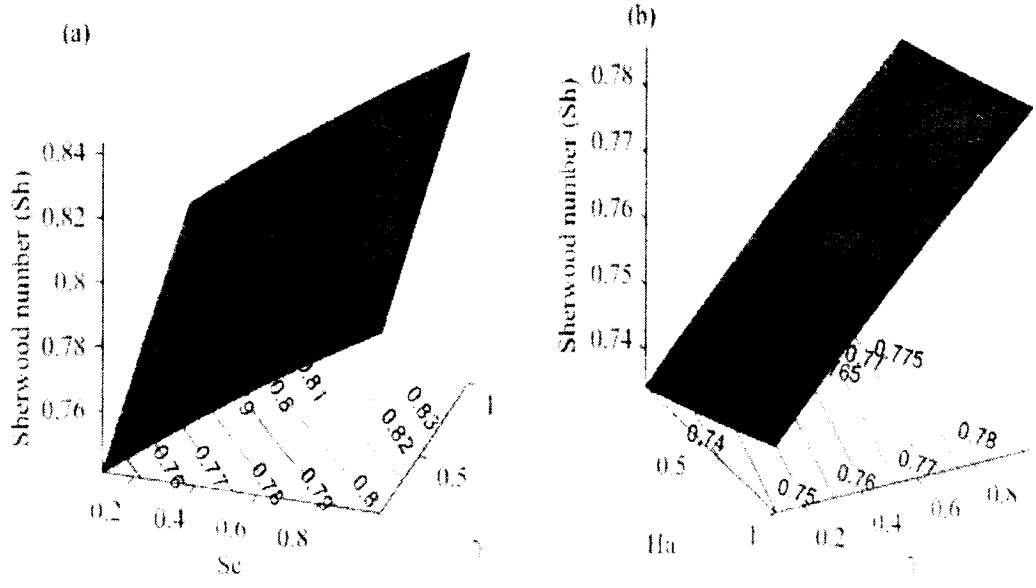

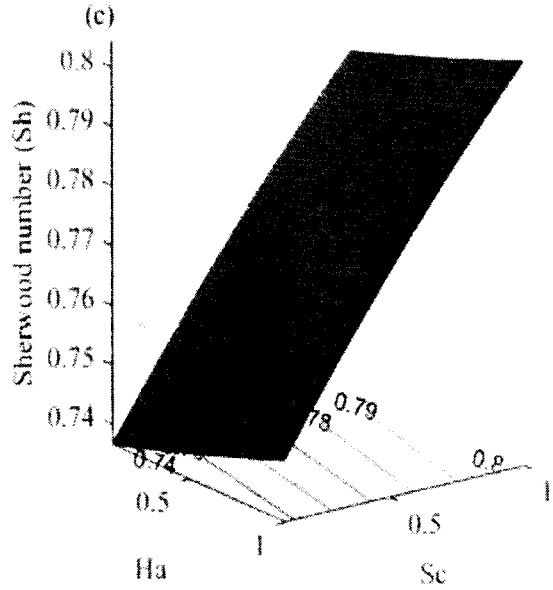

Figure 6.6: Contour plot for Sh_x (a) $D=0$ (b) $E=0$ (c) $F=0$.

Fig. 6.5 and Fig. 6.6 display the contour plot of predicted responses. The influence of Ha and β on Cf_x is depicted in Fig. 6.5(a). From the figure, it is observed that Cf_x is maximum for high level of Ha and β and minimum for low level of said parameters. Fig. 6.5(b) depicts the effect of We and β on Cf_x. It has been discovered that maximum Cf_x occurs at higher level of We and lower level of β. It's worth noting that in this case, the maximum Cf_x occurs at lower level of We and higher level of β.The minimum Cf_x occurs at middle level of We and β. Fig. 6.5(c) depicts the effect of We and Ha on Cf_x. The maximumCf_x occurs at low level of We and high level of Ha and the minimum Cf_x occurs at middle level of We and low level of Ha.

The effects of input parameters Ha, Sc and γ on Sh_x are displayed in Fig. 6.6. As shown in Fig. 6.6(a) maximum Sh_x occurs at a high level of Sc and γ Figures 6.6(b) and 6.6(c) show the same effect as Fig. 6.6(a). Maximum Sh_x occurs at a high level of Ha and γ, as illustrated in Fig. 6.6(b). Finally, Fig. 6.6(c) depicts the consequences of Ha and Sc on Sh_x and it is observed that maximum Sh_x occurs at high level of Ha and Sc.

Chapter 7

Carreau Fluid Flowing over a Wedge

This chapter investigates the numerical and statistical analysis of Carreau fluid flow across a wedge in the presence of shear rate viscosity. To obtain this objective, first of all by using similarity transformations the PDEs are converted into non-linear ODEs and these non-linear ODEs are solved with the help of Matlab built-in algorithm bvp4c. The numerical findings are matched with previous work and verified to be correct. Then, using RSM, a relationship between the independent input parameters and the dependent output responses are established. By using RSM, we have obtained the ANOVA results for coefficients of determination for Cf_x and Nu_x. Sensitivity analysis is performed and the results are shown using graph and tables.

7.1 Mathematical Formulation

In this chapter, steady two-dimensional, laminar incompressible Carreau fluid flowing over a wedge is considered. The convective transport model for Carreau fluid is adopted from [87]. The simplified form of mass, momentum and energy equation is follows by [87].

$$\frac{\partial u}{\partial x}+\frac{\partial v}{\partial y}=0. \tag{7.1}$$

$$u\frac{\partial u}{\partial x}+v\frac{\partial u}{\partial y}=U_e\frac{dU_e}{dx}+\upsilon\frac{\partial^2 u}{\partial y^2}\left[\gamma+(1-\gamma)\{1+\Gamma^2\left(\frac{\partial u}{\partial y}\right)^2\}\right]^{\frac{n-1}{2}}+ \tag{7.2}$$
$$v(n-1)(1-\gamma)\Gamma^2\frac{\partial^2 u}{\partial y^2}\left(\frac{\partial u}{\partial y}\right)^2\left[1+\Gamma^2\left(\frac{\partial u}{\partial y}\right)^2\right]^{\frac{n-3}{2}},$$

$$u\frac{\partial T}{\partial x}+v\frac{\partial T}{\partial y}=\alpha\frac{\partial^2 T}{\partial y^2}. \tag{7.3}$$

The boundary conditions for stated problem is follows by [87],

$$u=0,\quad v=0,\quad T=T_w,\qquad at\ y=0, \tag{7.4}$$

$$u=U_e(x)=cx^m,\quad T\to T_\infty,\qquad as\ y\to\infty. \tag{7.5}$$

The transformed non-linear systems of ODEs which are due to [87] are as follows,

$$[\gamma + (1-\gamma(1+We^2(f'')^2)^{\frac{n-3}{2}})(1+nWe^2(f'')^2)]f''' + ff'' + \beta(1 - f'^2) = 0, \tag{7.6}$$

$$\frac{1}{Pr}\theta'' + f\theta' = 0. \tag{7.7}$$

Where $\gamma = \frac{\mu_\infty}{\mu_0}$ represent the viscosity ratio parameter, $Pr = \frac{\mu C_p}{\kappa}$ denotes Prandtl number and $We = (\frac{c^3\Gamma^2 x^{3m-1}}{2\nu})^{\frac{1}{2}}$ represents the Weissenberg number. The associated boundary conditions are as follows [87],

$$f'(\eta) = \lambda, \quad f(\eta) = 0, \quad \theta(\eta) = 1 \; at \; \eta = 0, \tag{7.8}$$

$$f'(\eta) \to 1, \quad \theta(\eta) \to 0 \quad at \; \eta \to \infty, \tag{7.9}$$

where $\lambda = \frac{b}{c}$ is the velocity ratio parameter. These non-linear systems of ODE's along with boundary conditions are solved numerically with the help of MATLAB built in package bvp4c and compared with [87] and found excellent agreement. The comparison table of Cf_x and Nu_x are shown in Table 7.1 and Table 7.2 respectively.

Table 7.1: Comparison table for numerical values of Cf_x for different values of γ, β and λ when $Pr = 1$ and $We = 3$.

γ	β	λ	$n = 0.75$		$n = 1.75$	
			[87]	Present	[87]	Present
0	0.3	0.2	0.9610	0.9610	1.2298	1.2298
0.2			0.9793	0.9793	1.2010	1.2010
0.4			0.9962	0.9962	1.1692	1.1692
0.8			1.0269	1.0269	1.0917	1.0917
0.001	0	0.2	0.5944	0.5944	0.7064	0.7065
	0.3		0.9611	0.9611	1.2296	1.2296
	0.6		1.3106	1.3107	1.7714	1.7714
	1.2		2.2330	2.2330	3.2638	3.2638
0.001	0.3	-0.3	1.1705	1.1705	1.5632	1.5634
		-0.2	1.1570	1.1570	1.5476	1.5478
		0	1.0846	1.0846	1.4323	1.4323
		0.2	0.9611	0.9611	1.2296	1.2296

Table 7.2: Comparison table for numerical values of Nu_x for different values of γ, β and λ when $Pr = 1$ and $We = 3$.

γ	β	λ	$n = 0.75$		$n = 1.75$	
			[87]	Present	[87]	Present
0	0.3	0.2	0.9166	0.9166	0.8607	0.8607
0.2			0.9121	0.9121	0.8656	0.8656
0.4			0.9080	0.9080	0.8713	0.8714
0.8			0.9009	0.9009	0.8866	0.8866
0.001	0	0.2	0.7951	0.7952	0.7588	0.7589
	0.3		0.9166	0.9166	0.8607	0.8607
	0.6		1.0458	1.0458	0.9736	0.9736
	1.2		1.4420	1.4420	1.3302	1.3303
0.001	0.3	-0.3	0.6644	0.6645	0.5297	0.5300
		-0.2	0.7228	0.7229	0.6052	0.6053
		0	0.8259	0.8259	0.7409	0.7409
		0.2	0.9166	0.9166	0.8607	0.8607

7.2 Experimental Design

7.2.1 Response Surface Methodology (RSM)

RSM requires twenty runs and nineteen degrees of freedom corresponding to three different parameters namely γ, We and Pr. The levels of these factors high (+1), central (0), and low (-1) are displayed in table 7.3.

Table 7.3: The levels and design of input factors.

Type	Factor	Symbol	Levels		
			Low (-1)	Middle (0)	High (1)
Input Factors	γ	A	0.1	0.55	1
	We	B	0.1	50	100
	Pr	C	1	5.5	10

Table 7.4: Experimental design and measured responses.

Experiment number	Point type	Coded values			Real values			Responses	
		A	B	C	γ	We	Pr	Cf_x	Nu_x
1	Factorial	-1	-1	-1	0.10	0.10	1.0	1.0415	0.8978
2		1	-1	-1	1.00	0.10	1.0	1.0410	0.7418
3		-1	1	-1	0.10	100.00	1.0	3.0953	0.8978
4		1	1	-1	1.00	100.00	1.0	1.0410	2.3210
5		-1	-1	1	0.10	0.10	10.0	1.0414	2.3213
6		1	-1	1	1.00	0.10	10.0	1.0410	1.9981
7		-1	1	1	0.10	100.00	10.0	3.0953	2.3213
8		1	1	1	1.00	100.00	10.0	1.0410	1.5614
9	Axial	-1	0	0	0.10	50.05	5.5	2.3936	1.8097
10		1	0	0	1.00	50.05	5.5	1.0410	1.8096
11		0	-1	0	0.55	0.10	5.5	1.0412	1.5684
12		0	1	0	0.55	100.00	5.5	2.3222	0.7864

13		0	0	-1	0.55	50.05	1.0	1.9401	2.0791
14		0	0	1	0.55	50.05	10.0	1.9401	1.6047
15-20	Centre	0	0	0	0.55	50.05	5.5	1.9401	0.8978

7.3.2 Analysis of Variance (ANOVA)

ANOVA is used to determine which equation terms in the correlations should be retained and which should be removed. Table 7.5 and Table 7.6 illustrate all of the statistical estimators generated using the ANOVA method. Eqn. (7.10) and Eqn. (7.11) each have their own F-value and P-value. Table 7.6 shows the statistically calculated coefficient of determination for the simplified models of output responses Cf_x and Nu_x. The mathematical Eqn. (2.2) may be rewritten as follows:

$$Cf_x = 1.9262 - 0.5462A + 0.5389B - 0.1880A^2 - 0.2236B^2 - 0.5135AB, \quad (7.10)$$

$$Nu_x = 1.6117 + 0.0728A - 0.0720B + 0.6819C + 0.0633A^2 + 0.0667B^2 - 0.1895C^2 + 0.0599AB. \quad (7.11)$$

It is clear that all of the simplified models have goodness of fit because coefficient of determination for the models for Cf_x and Nu_x are 99.17 % and 99.59 % respectively as given in Table 7.6. After having best fitted model for the response surface Cf_x and Nu_x we focus on our next objective of the sensitivity analysis which is described in next section.

Table 7.5: ANOVA for output responses (a) Cf_x (b) Nu_x.

Source	DF	Adj SS	Adj MS	*F*-Value	*P*-Value	
(a)						
Model	9	8.59519	0.95502	132.40	0.000	Significant
Linear	3	5.88726	1.96242	272.05	0.000	Significant
Square	3	0.59877	0.19959	27.67	0.000	Significant
Interaction	3	2.10915	0.70305	97.46	0.000	Significant
Error	10	0.07213	0.00721			
Lack-of-Fit	5	0.07213	0.01443	*	*	Significant
Pure Error	5	0.00000	0.00000			-
Total	19	8.66732				-
(b)						
Model	9	4.89012	0.54335	269.40	0.000	Significant
Linear	3	4.75511	1.58504	785.90	0.000	Significant
Square	3	0.09937	0.03312	16.42	0.000	Significant
Interaction	3	0.03565	0.01188	5.89	0.014	Significant
Error	10	0.02017	0.00202			-
Lack-of-Fit	5	0.02017	0.00403	*	*	Significant
Pure Error	5	0.00000	0.00000			-
Total	19	4.91029				-

Table 7.6: Regression of coefficients for output responses (a) Cf_x (b) Nu_x.

Terms	Coefficient	P-value	Significant
(a)			
Constants	1.9262	0.000	Yes
A	-0.5462	0.000	Yes
B	0.5389	0.000	Yes
C	0.0000	1.000	No
A^2	-0.1880	0.004	Yes
B^2	-0.2236	0.001	Yes
C^2	0.0348	0.512	No
AB	-0.5135	0.000	Yes
AC	0.0000	1.000	No
BC	0.0000	1.000	No
	$R^2 = 99.17\%$		$Adj\ R^2 = 98.42\%$
(b)			
Constants	1.6117	0.000	Yes
A	0.0728	0.000	Yes
B	-0.0720	0.000	Yes
C	0.6819	0.000	Yes
A^2	0.0633	0.042	Yes
B^2	0.0667	0.033	Yes
C^2	-0.1895	0.000	Yes
AB	0.0599	0.217	No
AC	0.0209	0.218	No
BC	-0.0209		
	$R^2 = 99.59\%$		$Adj\ R^2 = 99.22\%$

7.4 Sensitivity analysis

The sensitivity of the Cf_x and Nu_x to γ, We and Pr was investigated in this work. By using Eqn. (7.10) and Eqn. (7.11) the sensitivity function of output responses (Cf_x and Nu_x) are developed in Eqs. (7.2 - 7.17).

$$\frac{\partial}{\partial A}(Cf_x) = -0.5462 - 0.376A - 0.5135B, \tag{7.12}$$

$$\frac{\partial}{\partial B}(Cf_x) = 0.5389 - 0.4472B - 0.5135A, \tag{7.13}$$

$$\frac{\partial}{\partial C}(Cf_x) = 0, \tag{7.14}$$

$$\frac{\partial}{\partial A}(Nu_x) = 0.0728 + 0.1266A + 0.0599B, \tag{7.15}$$

$$\frac{\partial}{\partial B}(Nu_x) = -0.0720 + 0.1334B + 0.0599A, \tag{7.16}$$

$$\frac{\partial}{\partial C}(Nu_x) = 0.6819 - 0.379C. \tag{7.17}$$

By using Eqns. (7.12 - 7.17) the sensitivity of various values γ, We and Pr is tested. Table 7.7 and Table 7.8 shows the sensitivity of Cf_x and Nu_x respectively. The response rises if the factor's bar chart is positive and falls if the bar chart is negative. The responses are more sensitive to the input factors as the bar chart's height increases. The sensitivity graphs are shown in Fig. 7.1 and Fig. 7.2 for Cf_x and Nu_x respectively.

Table 7.7: Sensitivity analysis of output response (Cf_x) when $A=0$.

B	C	$\partial Cf_x/\partial A$	$\partial Cf_x/\partial B$	$\partial Cf_x/\partial C$
-1	-1	-0.0327	0.9861	0
	0	-0.0327	0.9861	0
	1	-0.0327	0.9861	0
0	-1	-0.5462	0.5389	0
	0	-0.5462	0.5389	0
	1	-0.5462	0.5389	0
1	-1	-1.9597	0.0917	0
	0	-1.0597	0.0917	0
	1	-1.0597	0.0917	0

Table 7.8: Sensitivity analysis of output response (Nu_x) when $A=0$.

B	C	$\partial Nu_x/\partial A$	$\partial Nu_x/\partial B$	$\partial Nu_x/\partial C$
-1	-1	0.0129	-0.2054	1.0609
	0	0.0129	-0.2054	0.6819
	1	0.0129	-0.2054	0.3029
0	-1	-0.0728	-0.072	1.0609
	0	-0.0728	-0.072	0.6819
	1	-0.0728	-0.072	0.3029
1	-1	0.1327	0.0614	1.0609
	0	0.1327	0.0614	0.6819
	1	0.1327	0.0614	0.3029

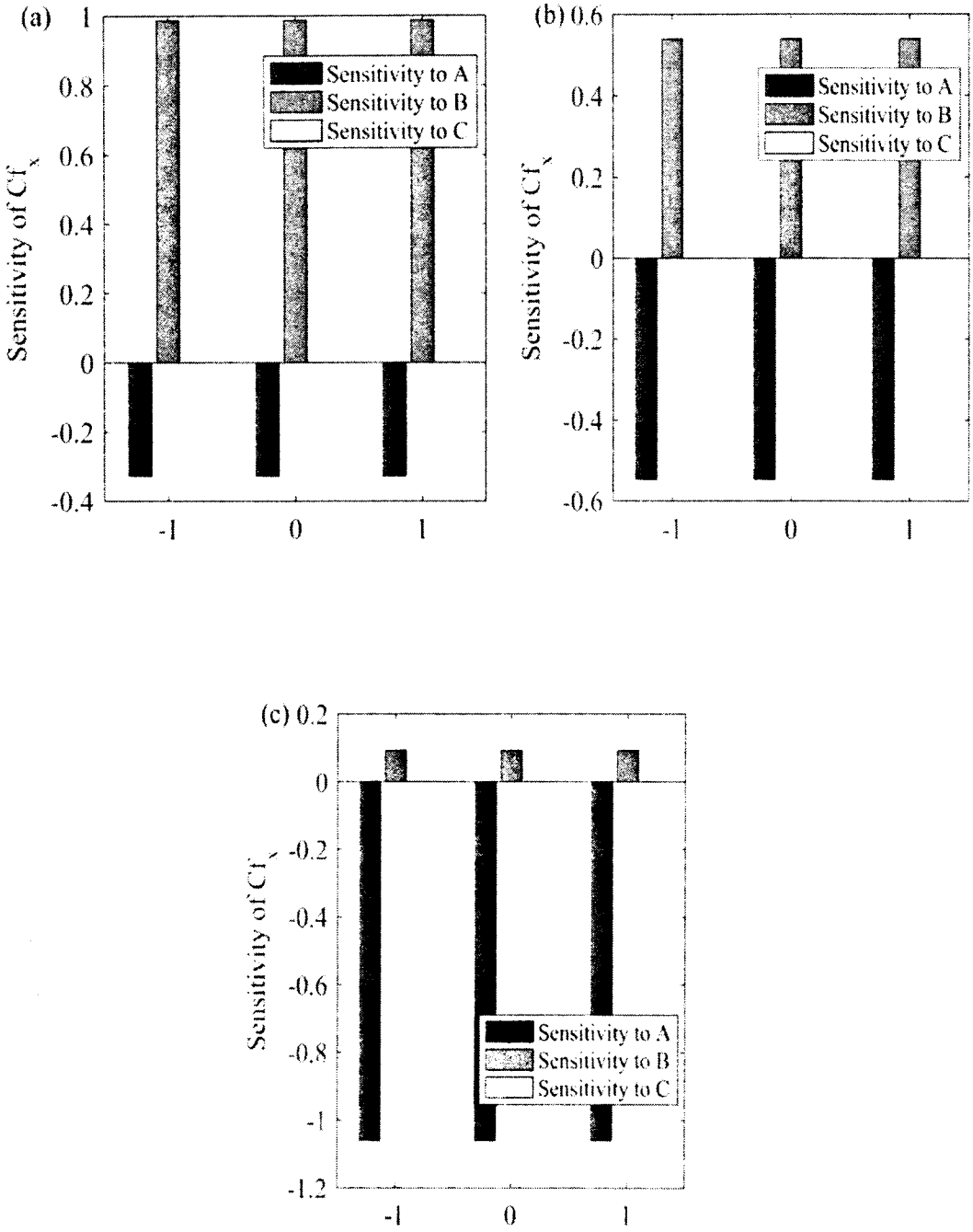

Figure 7.1: Sensitivity plots for output response (Cf_x) with $A=0$ (a) $B=-1$ (b) $B=0$ (c) $B=1$.

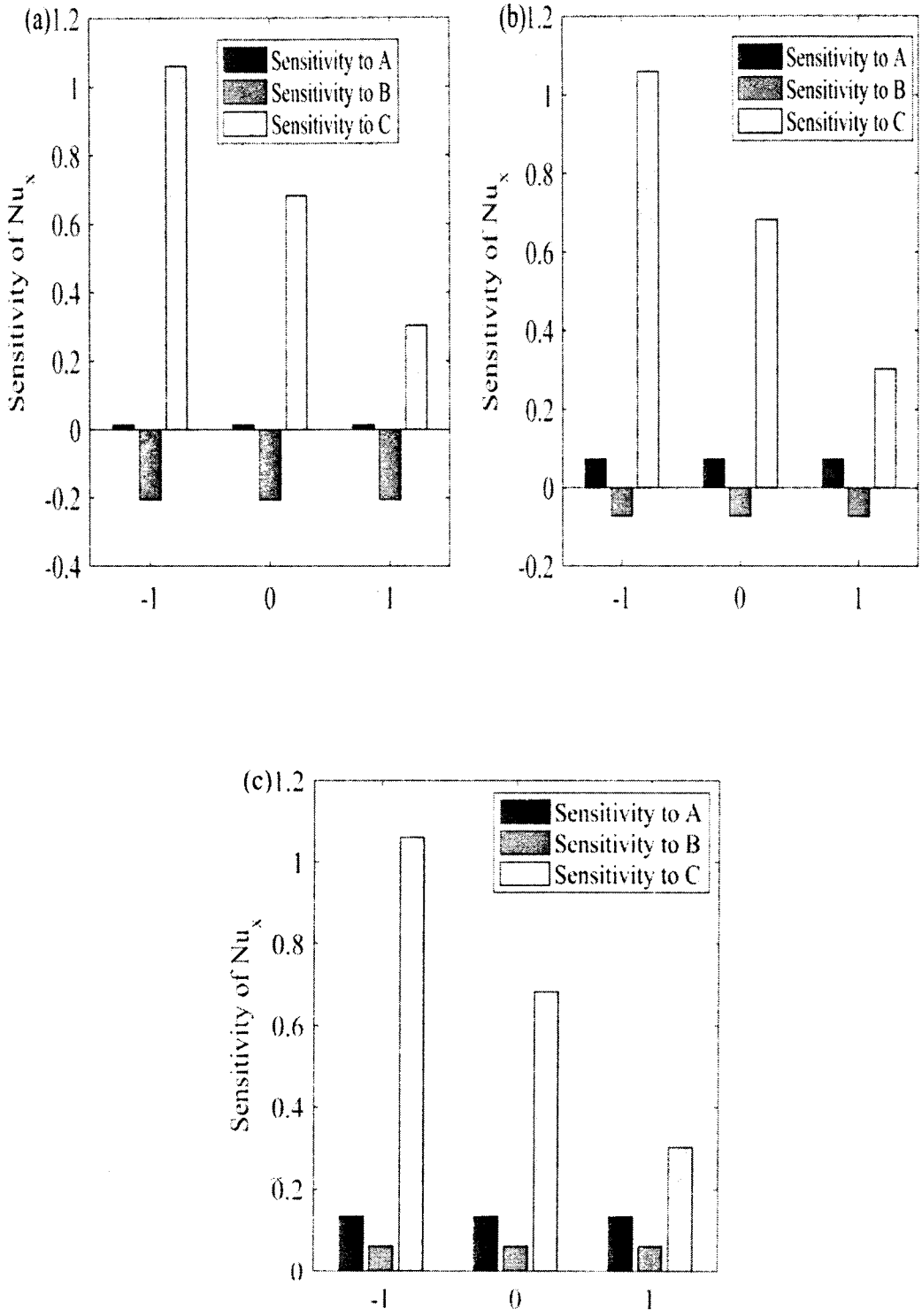

Figure 7.2: Sensitivity plots for output response (Nu_x) with $A=0$ (a) $B=-1$ (b) $B=0$ (c) $B=1$.

7.4 Discussion of the Results

This section is meant to explain the sensitivity analysis and transport performance of Carreau fluid flow with shear rate viscosity across a wedge using RSM. The numerical solutions are obtained by using Matlab's built-in package bvp4c. Then matched the results with previously published work and found correct. The major objective of this work is to perform a sensitivity analysis of output responses (Cf_x and Nu_x) for different input factors (γ We and Pr). To achieve this purpose, we constructed an expression for output responses by using RSM, which is described in Eqn. (7.10) and Eqn. (7.11). We estimated the values of responses using regression models fitted to twenty runs by using RSM which is shown in shown in Table 7.4. Table 7.5 displays the ANOVA results for Cf_x and Nu_x, as well as the related F-value and P-value. Table 7.6 displays the regression coefficients for output responses (Cf_x and Nu_x).

Fig. 7.1 displays the sensitivity plots of Cf_x for different parameters such as γ, We and Pr. As from Fig. 7.1 (a-c), it is clear that the output response Cf_x has positive sensitivity to We and negative sensitivity to γ, which means that sensitivity of Cf_x increases by increasing We and decreases by increasing the value of γ. The sensitivity plot of Pr is zero this means that there is no any effect of Pr on Cf_x. Fig. 7.2 shows the sensitivity plot of Nu_x for different input parameters γ, We and Pr. From Fig. 7.2 (a-c), it is cleared that by raising the value of and Pr the Nusselt number also rises because for both the parameters it has positive sensitivity. It is also worth mentioning that Pr number is more sensitive than other input parameters for Nu_x. It is also observed that there is a mixed behaviour of We for Nu_x (viz. Fig. 7.2 (a-c)).

The residual plots of output responses are presented in Fig. 7.3 and Fig. 7.4. The scatter plots of output responses (Cf_x and Nu_x) are shown in Fig. 7.3(a) and Fig. 7.4(a), respectively. The scatter plot depicts the relationship between the input factors and the output responses. These figures (Figs. 7.3(a) and 7.4(a)) show the strong relationship between the input factors and the output responses. The histograms in Figs. 7.3(b) and 7.4(b) have symmetrical distribution and are less skewed, indicating that the input factors and output responses have good relationships. The observation

order verses residuals of output responses (Cf_x and Nu_x) are represented in Fig. 7.3(c) and Fig. 7.4(c) respectively. The graphical representation shows that as by increasing the observation order the residuals of output responses fall. Also, the largest fluctuation can be seen for output responses, which specify the strong correlations between input parameters and output responses.

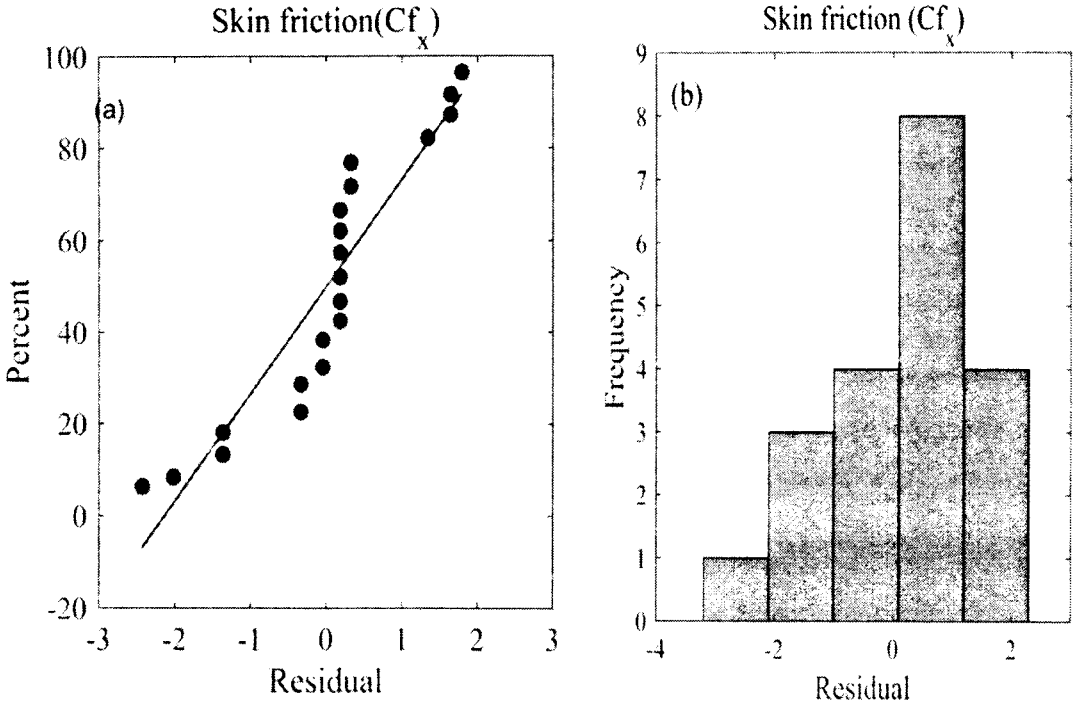

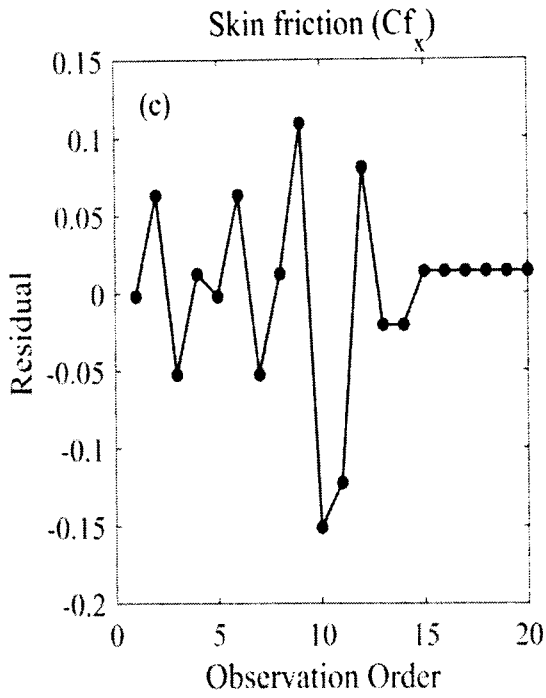

Figure 7.3: Residual plots of output response Cf_x (a) normal probability plot (b) histogram (c) residuals plot.

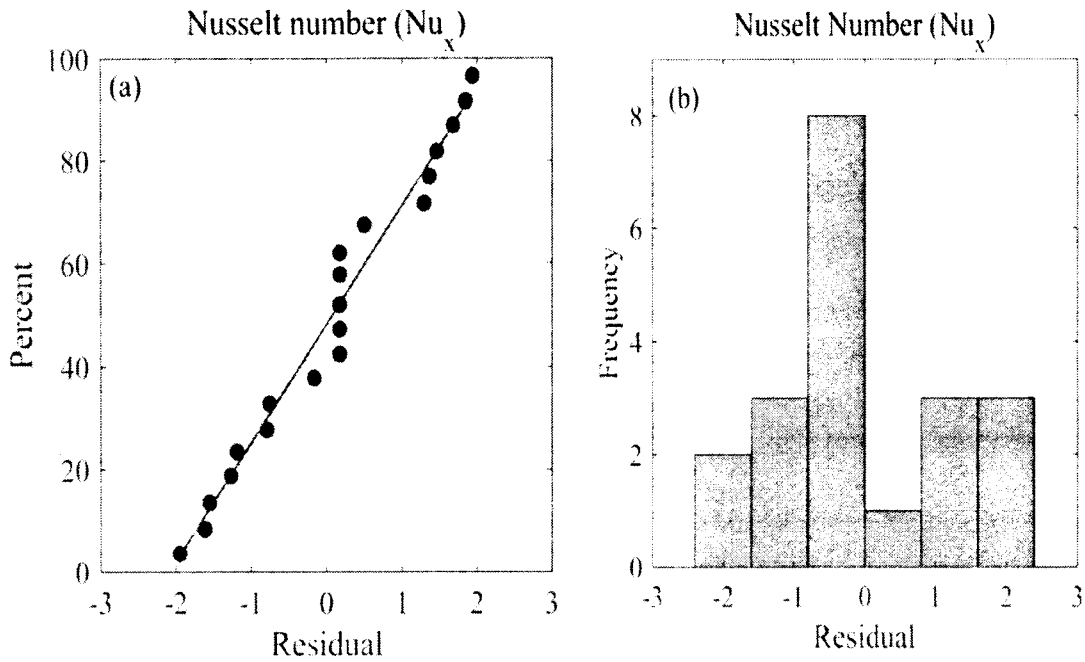

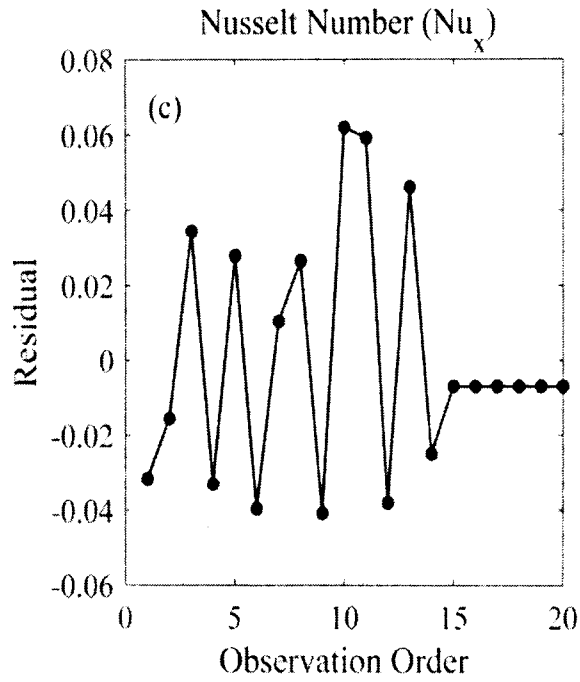

Figure 7.4: Residual plots of output response Nu_x (a) normal probability plot (b) histogram (c) residuals plot.

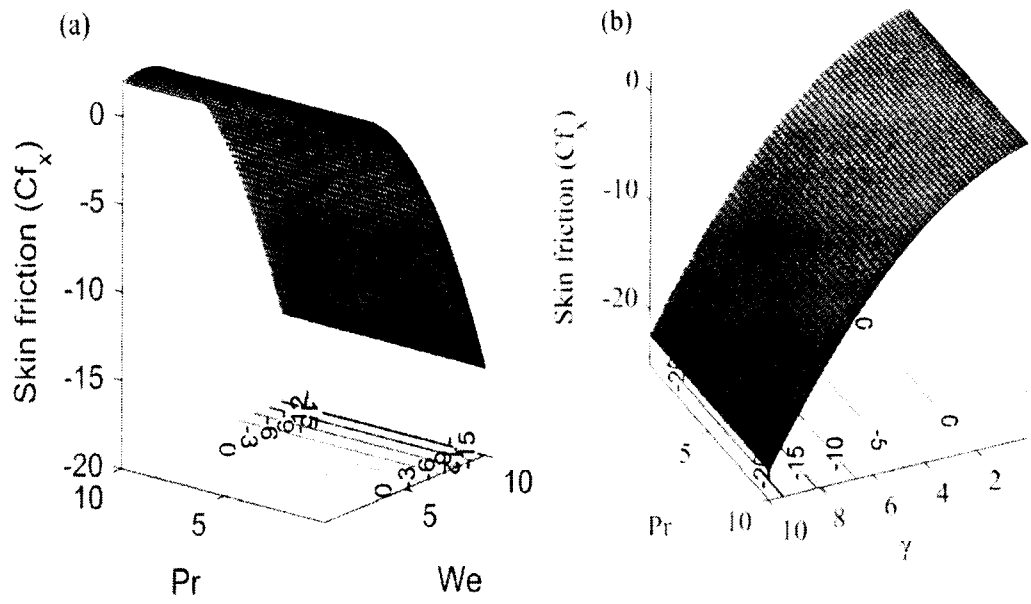

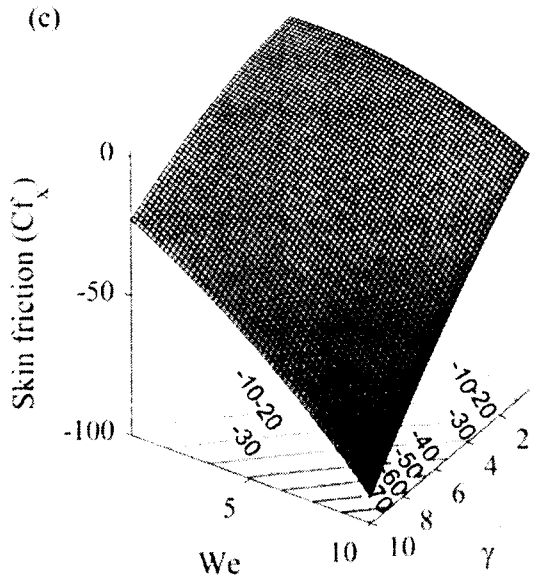

Figure 7.5: Contour plots of output response Cf_x when (a) $A=0$ (b) $B=0$ (c) $C=0$.

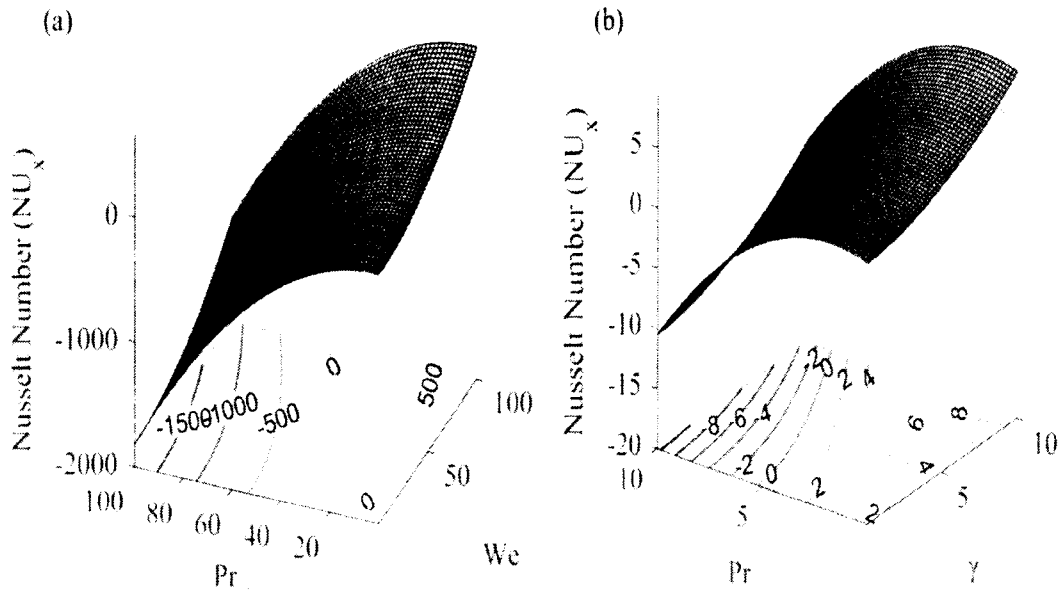

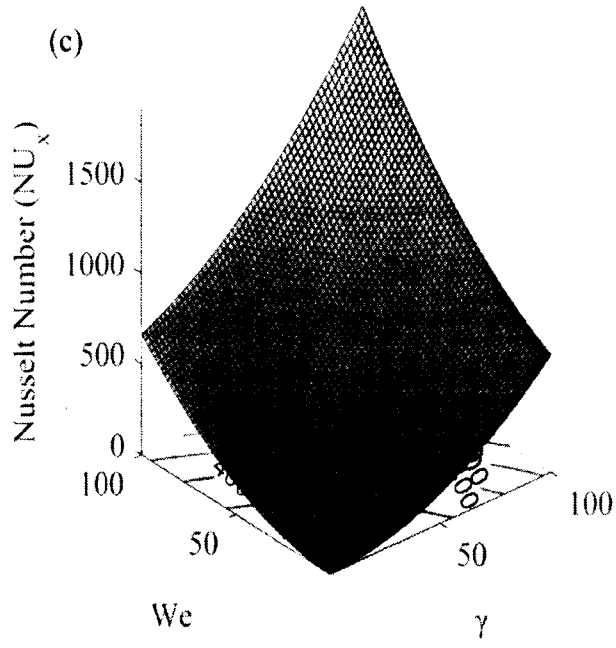

Figure 7.6: Contour of Nu_x when (a) $A=0$ (b) $B=0$ (c) $C=0$.

The contour plots of Cf_x are displayed in Fig. 7.5. According to Fig. 7.5(a) and Fig. 7.5(b), it is noted that Prandtl number has no effect on Cf_x because the contour plot shows straight line for all the values of Pr. That means Pr has no effect on Cf_x. Fig. 7.5(c) depicted the effect of We and γ on Cf_x. It is clear that Cf_x is minimum for high levels (+1) of We and γ. Cf_x decreases as increasing the value of We and γ.

Fig. 7.6 displays the contour plots of Nu_x. Fig. 7.6(a) depicted the effect of Pr and We on Nu_x .From the figure, it is clear that Nu_x enhances by decreasing the value of We and increasing the value of Pr. It is also observed that the highest value of Nu_x occurs in levels of (-1) and (+1) and lowest value occurs in levels (+1) and (-1). The same outcomes are obtained for the effects of γ and Pr on Nu_x, as shown in Fig. 7.6(b). The Nu_x increases by decreasing the value of γ and increasing the value of Pr. It was also investigated that the highest value Nu_x occurs in levels of (-1) and (+1) and lowest value occurs in levels (+1) and (-1). Fig. 7.6(c) shows the effect of γ and We on Nu_x. From the figure it can be noted that as increasing Nu_x the values of γ and We also increases. Also, it is worth mentioning that the highest value of Nu_x occurs for high levels of (+1) and lowest value occurs for low levels (-1) of γ and We.

Chapter 8

MHD-Casson Fluid Flowing over a Wedge

The aim to develop this chapter is to investigate the sensitivity of heat flux at solid liquid interface of FS flow of MHD-Casson fluid flowing over a wedge. Alongside, to develop an empirical model in terms of involving parameters. The FS flow in this case is observed under the influence of induced magnetic field. The mathematical model of the flow experiments are adopted from Dabe et al. [88] which was solved numerically by using computational software MATLAB and achieved reliable solutions- validated by comparing the numerical results with published results. A data set is extracted for wall heat flux and Sherwood number at random points, and finally by using RSM the correlation of input parameter and output responses are developed. The statistical results of ANOVA are presented in tabular form by using RSM.

8.1 Mathematical Formulation

Consider two dimensional incompressible, hydromagnetic flow over a wedge. Also, assume that the induced magnetic field applied outside the boundary layer. The governing equations are follows as [88],

$$\frac{\partial u}{\partial x}+\frac{\partial v}{\partial y}=0, \tag{8.1}$$

$$\frac{\partial H_1}{\partial x}+\frac{\partial H_2}{\partial y}=0, \tag{8.2}$$

$$u\frac{\partial u}{\partial x}+v\frac{\partial u}{\partial y}-\frac{\mu_\circ}{4\pi\rho}\left(H_1\frac{\partial H_1}{\partial x}+H_2\frac{\partial H_2}{\partial y}\right)=U_e\frac{dU_e}{dx}-\frac{\mu_\circ H_e}{4\pi\rho}\frac{\partial H_e}{\partial x}+v(1+\frac{1}{\beta}\frac{\partial^2 u}{\partial y^2}), \tag{8.3}$$

$$u\frac{\partial H_1}{\partial x}+v\frac{\partial H_1}{\partial y}-H_1\frac{\partial u}{\partial x}-H_2\frac{\partial u}{\partial y}=\mu_e\frac{\partial^2 H_1}{\partial y^2}, \tag{8.4}$$

$$u\frac{\partial T}{\partial x}+v\frac{\partial T}{\partial y}=\propto(1+\frac{16\sigma^* T_\infty^3}{3kk^*})\frac{\partial^2 T}{\partial y^2}+\frac{v}{c_p}\left(1+\frac{1}{\beta}\right)\left(\frac{\partial u}{\partial y}\right)^2+\frac{D_m k_T}{c_s c_p}(\frac{\partial^2 C}{\partial y^2}), \tag{8.5}$$

$$u\frac{\partial C}{\partial x}+v\frac{\partial C}{\partial y}=D_m\frac{\partial^2 C}{\partial y^2}+\frac{D_m k_T}{T_m}(\frac{\partial^2 T}{\partial y^2}). \tag{8.6}$$

The boundary conditions [88] are,

$$v = 0,\ u = u_w(x) = U_w x^m,\ H_1 = H_2 = 0, T = T_w,\ C = C_w,\ at\ y = 0, \tag{8.7}$$
$$u = U_e(x) = U_\infty x^m, H_1 = H_e(x) = H_\circ x^m, T = T_\infty,\ C = C_\infty,\ at\ y \to \infty.$$

The similarity transformations as follows by [88],

$$\eta = \sqrt{\frac{(m+1)U_e(x)}{2\nu x}}\, y,\ \psi = \sqrt{\frac{2\nu x U_e(x)}{(m+1)}} f(\eta),\ \varphi = H_\circ \sqrt{\frac{2\nu x x^m}{(m+1)U_\infty}} g(\eta),\ \theta = \left(\frac{T-T_\infty}{T_w-T_\infty}\right),$$
$$\emptyset = \left(\frac{C-C_\infty}{C_w-C_\infty}\right). \tag{8.8}$$

By using the similarity transformation (8.8), the simplified form of Eqn. (8.3) to Eqn. (8.6) into system of non-linear ODE is follows by [88],

$$\left(1+\frac{1}{\beta}\right) f''' + ff'' + \gamma(1-f'^2) - M[gg'' + \gamma(1-g'^2)] = 0, \tag{8.9}$$

$$\lambda g''' + fg'' - f''g = 0, \tag{8.10}$$

$$\left(1+\frac{4}{3}R_a\right)\theta'' + P_r f\theta' + P_r E\left(1+\frac{1}{\beta}\right) f''^2 + P_r D_u \phi'' = 0, \tag{8.11}$$

$$\phi'' + S_c f\phi' + S_c S_0 \phi'' = 0, \tag{8.12}$$

where $\gamma = \frac{2m}{(m+1)}$, $M = \frac{\mu H_o^2}{4\pi\rho U_\infty^2}$, $\lambda = \frac{1}{4\pi\nu\sigma}$, $E = \frac{U_e^2(x)}{c_p(T-T_\infty)}$, $P_r = \frac{\nu}{\propto}$, $R_a = \frac{4\sigma T_\infty^3}{kk^*}$,
$S_c = \frac{\nu}{D_m}$, $D_u = \frac{D_m k_T(C_w-C_\infty)}{\nu c_s c_p(T_w-T_\infty)}$, $S_o = \frac{D_m k_T(T_w-T_\infty)}{\nu T_m(C_w-C_\infty)}$.

$$f(0) = 0,\quad f'(0) = \delta,\ g(0) = 0,\ g'(0) = 0,\quad \theta(0) = 1,\ \phi(0) = 1. \tag{8.13}$$

$$f'(\infty) \to 1,\ g'(\infty) \to 1,\quad \theta(\infty) \to 0,\quad \phi(\infty) \to 0. \tag{8.14}$$

Where $\delta = \frac{U_w}{U_\infty}$.

Table 8.1: Comparision of Cf_x with [88 - 90]

γ	[88]	[89]	[90]	Present result
0.0	0.4696	-	0.4696	0.4696
0.1	0.5870	0.5870	0.5870	0.5870
0.3	0.7747	0.7747	0.7748	0.7747
0.5	0.9276	0.9276	0.9277	0.9276
1.0	1.2326	1.2325	1.2326	1.2326

8.2 Experimental Design

8.2.1 Response Surface Methodology (RSM)

By using Eqn. (2.2) the general form of correlations of output responses (Nu_x and Sh_x) can be stated in the following forms.

$$Nu_x = \alpha_0 + \alpha_1 A + \alpha_2 B + \alpha_3 C + \alpha_{11} AB + \alpha_{12} AC + \alpha_{13} BC + \alpha_{21} A^2 + \alpha_{22} B^2 + \alpha_{23} C^2, \quad (8.15)$$

$$Sh_x = \gamma_0 + \gamma_1 A + \gamma_2 B + \gamma_3 C + \gamma_{11} AB + \gamma_{12} AC + \gamma_{13} BC + \gamma_{21} A^2 + \gamma_{22} B^2 + \gamma_{23} C^2. \quad (8.16)$$

where α_i, α_{ij}, γ_i and γ_{ij} $(i = j = 1, 2, 3)$ are unknown constants. These unknown coefficients can be found by using RSM. The levels of selected input factors *Ra*, *Pr* and *Du* and their levels low (-1), central (0), and high (+1) are displayed in Table 8.2.

Table 8.2: Selected input parameters, their symbols and levels.

Type	Factor	Symbol	Levels		
			Low (-1)	Middle (0)	High (1)
Input Factors	*Ra*	*A*	0	0.5	1
	Pr	*B*	0	5	10
	Du	*C*	0	0.5	1

Table 8.3: Experimental design and measured responses.

Experiment number	Point type	Coded values			Real values			Responses	
		A	B	C	Ra	Pr	Du	Nu_x	Sh_x
1	Factorial	-1	-1	-1	0.0	0	0.0	0.1000	0.1000
2		1	-1	-1	1.0	0	0.0	0.1000	0.1000
3		-1	1	-1	0.0	10	0.0	1.6826	0.1000
4		1	1	-1	1.0	10	0.0	1.2086	0.1000
5		-1	-1	1	0.0	0	1.0	0.1000	0.7445
6		1	-1	1	1.0	0	1.0	0.1000	0.7445
7		-1	1	1	0.0	10	1.0	0.5484	0.5530
8		1	1	1	1.0	10	1.0	0.5816	0.5176
9	Axial	-1	0	0	0.0	5	0.5	0.5697	0.4079
10		1	0	0	1.0	5	0.5	1.8964	0.2600
11		0	-1	0	0.5	0	0.5	0.1000	0.5222
12		0	1	0	0.5	10	0.5	0.5397	0.4226
13		0	0	-1	0.5	5	0.0	1.0415	0.1000
14		0	0	1	0.5	5	1.0	0.6103	0.4856
15-20	Centre	0	0	0	0.5	5	0.5	0.7779	0.3040

8.2.2 Analysis of Variance (ANOVA)

The statistical software MINITAB-19 is utilized to determine the regression model values for 20 runs, and the results are displayed in Table 8.3. These results are obtained by using ANOVA and the sequential f-test. All of the statistical estimators produced using the ANOVA methodology is represented in Table 8.4 and Table 8.5.

Each of Eqn. (8.15) and Eqn. (8.16) has a unique F and P-value. The mathematical form of Eqn. (8.15) and Eqn. (8.16) may be rewritten as follows:

$$Nu_x = -0.01197 + 0.00563A + 131.186B - 0.012C - 131.207B^2 - 0.01139BC, \quad (8.17)$$

$$Sh_x = -0.03886 + 5.57056C + 0.0275B^2 - 5.5406C.^2 \quad (8.18)$$

The coefficient of determination for the models for Nu_x and Sh_x is 100%, indicating that all of the simplified models have goodness of fit which is shown in Table 5. After the determination of best fitted model for the response surface Nu_x and Sh_x, sensitivity analysis is performed , which is described in the next section.

Table 8.4: ANOVA for (a) Nu_x (b) Sh_x

Source	DF	Adj SS	Adj MS	F-Value	P-Value	
(a)						
Model	9	258169	28685	1.63617E+08	0.000	
Linear	3	172098	57366	3.27206E+08	0.000	
Square	3	86071	28690	1.63645E+08	0.000	
Interaction	3	0	0	2.06	0.169	
Error	10	0	0			
Lack-of-Fit	5	0	0	*	*	
Pure Error	5	0	0			
Total	19	258169				
(b)						
Model	9	463.516	51.502	164300.12	0.000	
Linear	3	310.312	103.437	329983.74	0.000	
Square	3	153.204	51.068	162916.62	0.000	
Interaction	3	0.000	0.000	0.000	0.000	

Error	10	0.003	0.000			
Lack-of-Fit	5	0.003	0.001	*	*	
Pure Error	5	0.000	0.000			
Total	19	463.520				

Table 8.5: Regression coefficients generated by ANOVA for output response (a) Nu_x (b) Sh_x

(a) Terms	Coefficient	P-value	Significant
Constants	-0.01197	0.025	Yes
A	0.00563	0.029	Yes
B	131.186	0.000	Yes
C	-0.01200	0.017	Yes
A^2	0.00076	0.926	No
B^2	-131.207	0.000	Yes
C^2	0.00611	0.462	No
AB	0.00158	0.743	No
AC	0.00179	0.711	No
BC	-0.01139	0.035	Yes
$R^2 = 100\%$			$Adj\ R^2 = 100\%$
(b)			
Constants	-0.03886	0.000	Yes
A	-0.00848	0.161	No
B	-0.00096	0.868	No

C	5.57056	0.000	Yes
A^2	-0.0188	0.109	No
B^2	0.0275	0.028	Yes
C^2	-5.5406	0.000	Yes
AB	-0.00011	0.987	No
AC	-0.00011	0.987	No
BC	-0.00052	0.935	No
	$R^2 = 100\%$		$Adj\ R^2 = 100\%$

8.3 Sensitivity analysis

The sensitivity of Nu_x and $Sh_x$to input parameters *Ra, Pr* and *Du* is investigated in this chapter. By using Eqn. (8.17) and Eqn. (8.18) the sensitivity function of output responses (Nu_x and Sh_x) are developed in Eqns. (8.19 – 8.24).

$$\frac{\partial}{\partial A}(Nu_x) = 0.00563, \tag{8.19}$$

$$\frac{\partial}{\partial B}(Nu_x) = 131.186 - 262.414B - 0.01139C, \tag{8.20}$$

$$\frac{\partial}{\partial C}(Nu_x) = -0.012 - 0.01139B, \tag{8.21}$$

$$\frac{\partial}{\partial A}(Sh_x) = 0, \tag{8.22}$$

$$\frac{\partial}{\partial B}(Sh_x) = 0.055B, \tag{8.23}$$

$$\frac{\partial}{\partial C}(Sh_x) = 5.57056 - 11.0812C. \tag{8.24}$$

By using Eqns. (8.19 – 8.24) the sensitivity of various values *Ra, Pr* and *Du* is tested. Table 8.6 and Table 8.7 shows the sensitivity of Nu_x and Sh_x respectively. The sensitivity graphs are shown in Fig. 8.1 and Fig. 8.2 for Nu_x and Sh_x respectively.

Table 8.6: Sensitivity analysis of output response Nu_x when $A=0$.

B	C	$\partial Nu_x/\partial A$	$\partial Nu_x/\partial B$	$\partial Nu_x/\partial C$
-1	-1	0.00563	393.61139	-0.00061
	0	0.00563	393.60000	-0.00061
	1	0.00563	393.58861	-0.00061
0	-1	0.00563	131.19739	-0.012
	0	0.00563	131.18600	-0.012
	1	0.00563	131.17461	-0.012
1	-1	0.00563	-131.21661	-0.02339
	0	0.00563	-131.22800	-0.02339
	1	0.00563	-131.23939	-0.02339

Table 8.7: Sensitivity analysis of output response Sh_x when $A=0$.

B	C	$\partial Sh_x/\partial A$	$\partial Sh_x/\partial B$	$\partial Sh_x/\partial C$
-1	-1	0	-0.055	16.65176
	0	0	-0.055	5.57065
	1	0	-0.055	-5.51064
0	-1	0	0	16.65176
	0	0	0	5.57065
	1	0	0	-5.51064
1	-1	0	0.055	16.65176
	0	0	0.055	5.57065
	1	0	0.055	-5.51064

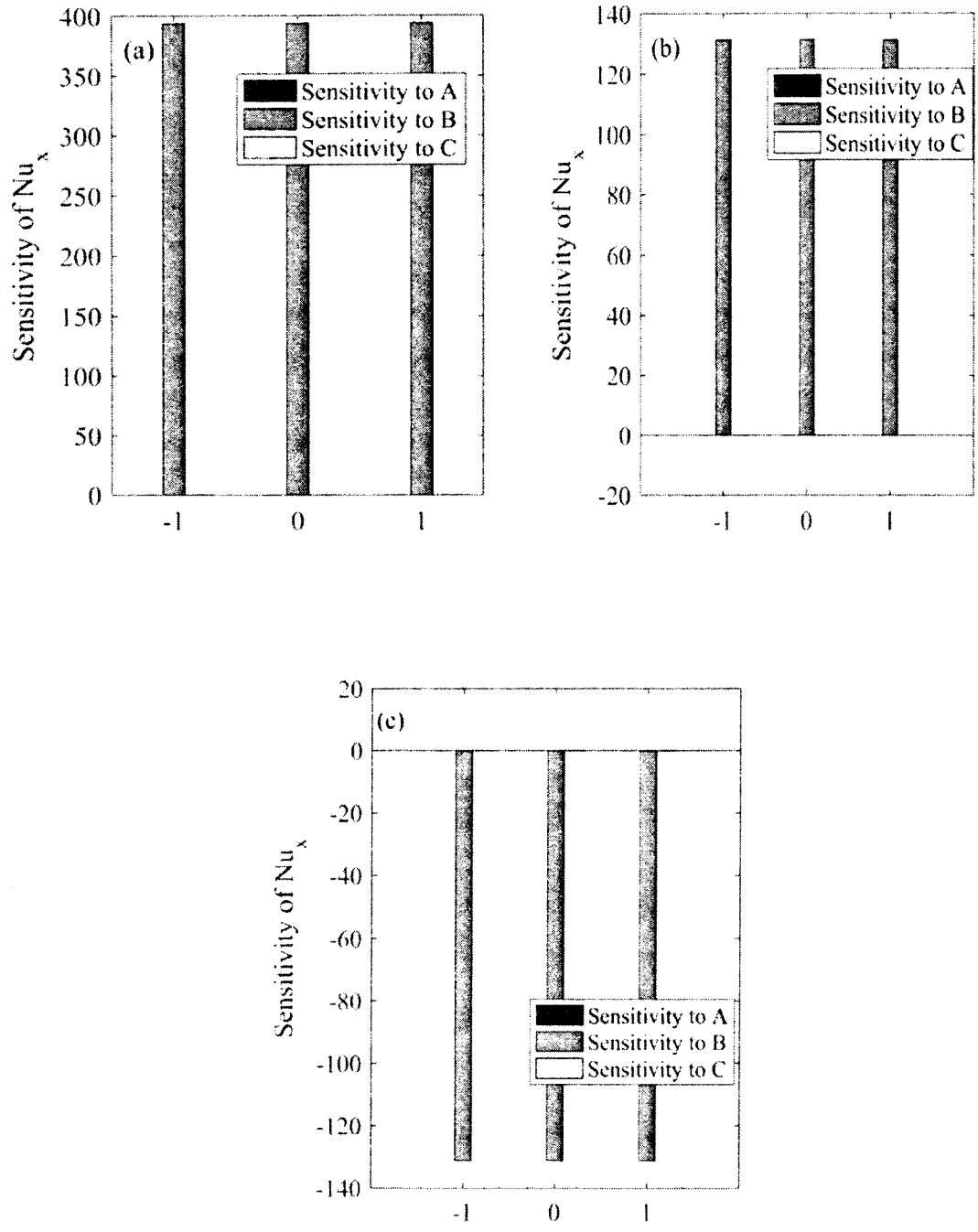

Figure 8.1: Sensitivity plots for output response (Nu_x) with $A=0$ (a) $B=-1$ (b) $B=0$ (c) $B=1$.

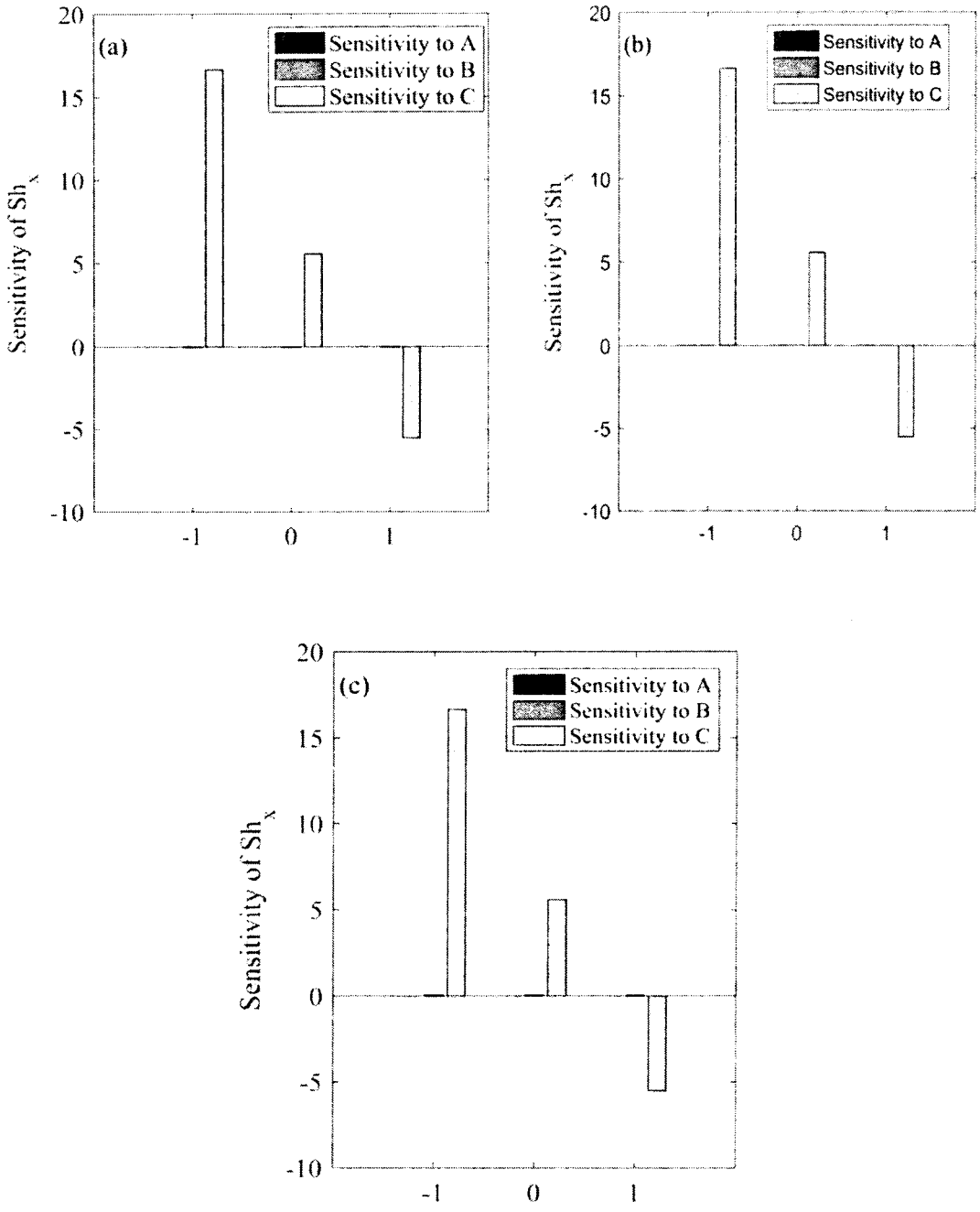

Figure 8.2: Sensitivity plots for output response (Sh_x) with $A=0$ (a) $B=-1$ (b) $B=0$ (c) $B=1$.

8.4 Discussion of the Results

This section is meant to explain the sensitivity analysis for wall heat and concentration flux of Falkner-Skan flow of Casson fluid flow with the influence of induced magnetic field. Using MATLAB's built-in package bvp4c, we

have computed a numerical solution to the problem. The results were then compared to previously published work and found to be correct. The primary goal of this chapter is to conduct sensitivity analysis of output responses (Nu_x and Sh_x) for various input factors. To accomplish this, an expression for output responses by using RSM has been generated, as shown in Eqn. (8.17) and Eqn. (8.18). The values of responses were estimated using regression models, fitted to twenty runs by using RSM which is shown in Table 8.3. Then the ANOVA table for Nu_x and Sh_x along with the associated F-value and P-values are displayed in Table 8.4.

Fig. 8.1 displays the sensitivity plots of Nu_x for different parameters such as, *Ra, Pr* and *Du*. Fig. 8.1(a) and Fig. 8.1(b) shows the positive sensitivity to input parameters *Pr* which means that by raising the value of *Pr* the value of Nu_x also rises. Also, it is worth mentioning that the effect of input parameters *Ra* and *Du* is negligible on Nu_x as the height of bar chart is very small as compare to *Pr*. Fig. 8.1(c) depicts the negative sensitivity to input parameters *Pr* and *Du* which deliberate that by increasing the value of *Pr* the Nu_x decreases. *Pr* is most sensitive as compare to other input parameters. The sensitivity plots of Sh_x is displayed in Fig. 8.2(a) to Fig. 8.2(c). From Fig. 8.2(a) to Fig. 8.2(c) it is clear that Du is most sensitive to Sh_x, also there is a mixed behaviour of *Du* on Sh_x. It is observed from figures that there is positive sensitivity of Sh_x to Du at low (-1) and middle (0) levels and negative sensitivity at high (+1) level. Also it is worth mentioning that effect of input parameters *Pr* is negligible. Sh_x is independent to input parameters *Ra* which means there is no effect of *Ra* on Sh_x.

While implementing RSM, it is important to discuss the residual errors. Fig. 8.3 and Fig. 8.4 show the residual plots of the output responses. The scatter plot demonstrates in Fig. 8.3(a) and Fig. 8.4(a) shows the strong relationship between the input factors and the output responses. The histograms in Fig. 8.3(b) and Fig. 8.4(b) are symmetrical and less skewed, indicating that the input factors and output responses have good relationships. Figures 8.3(c) and 8.4(c) shows the observation order versus residuals of output responses ($Nu_x$and Sh_x), respectively. The graphical representation shows that as the observation order is enhanced, the residuals of the output responses decrease. Output responses display the maximum fluctuation, revealing the strong correlations between input parameters and output responses.

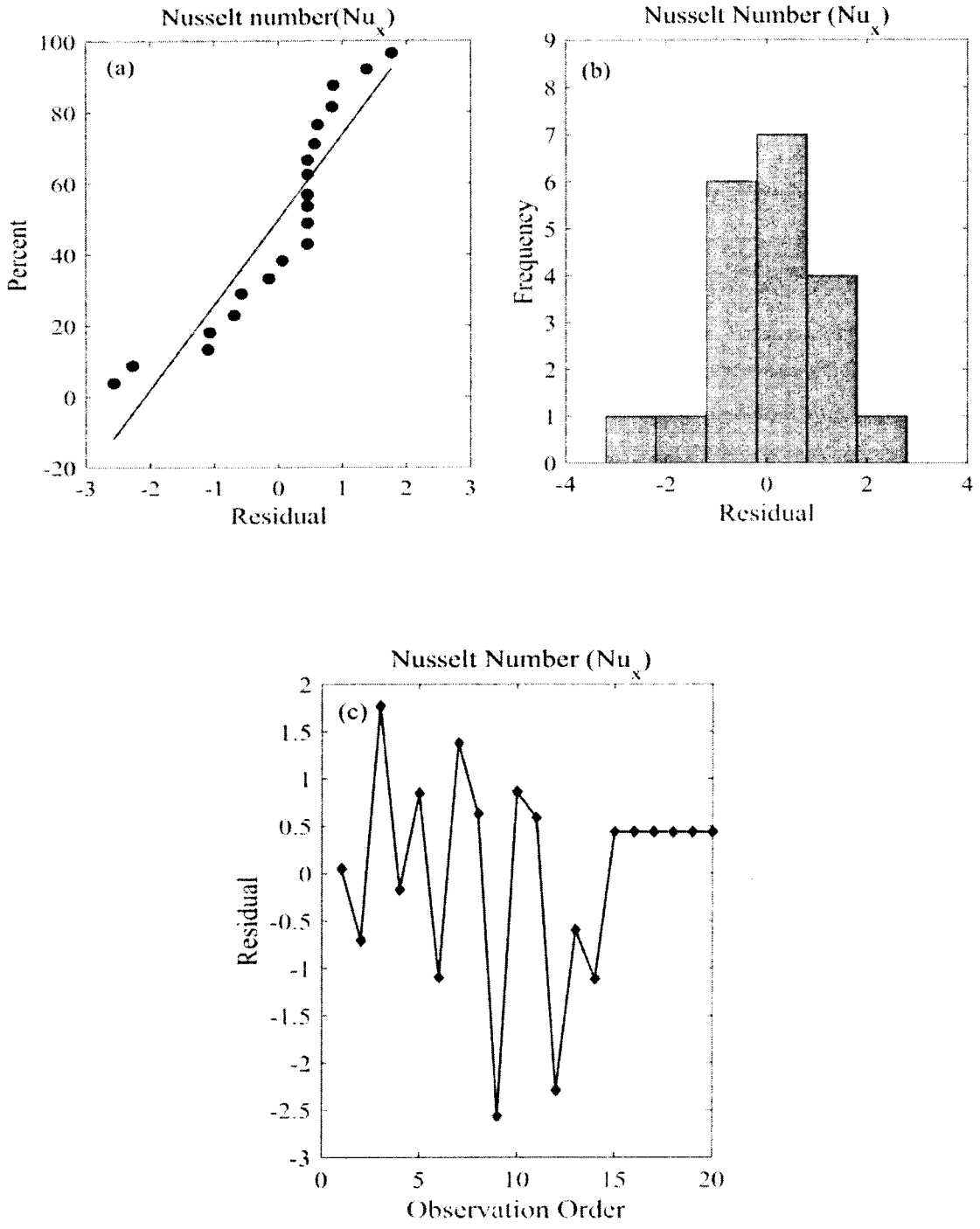

Figure 8.3: Residuals plots for Nu_x (a) normal probability plot (b) histogram (c) residual plot.

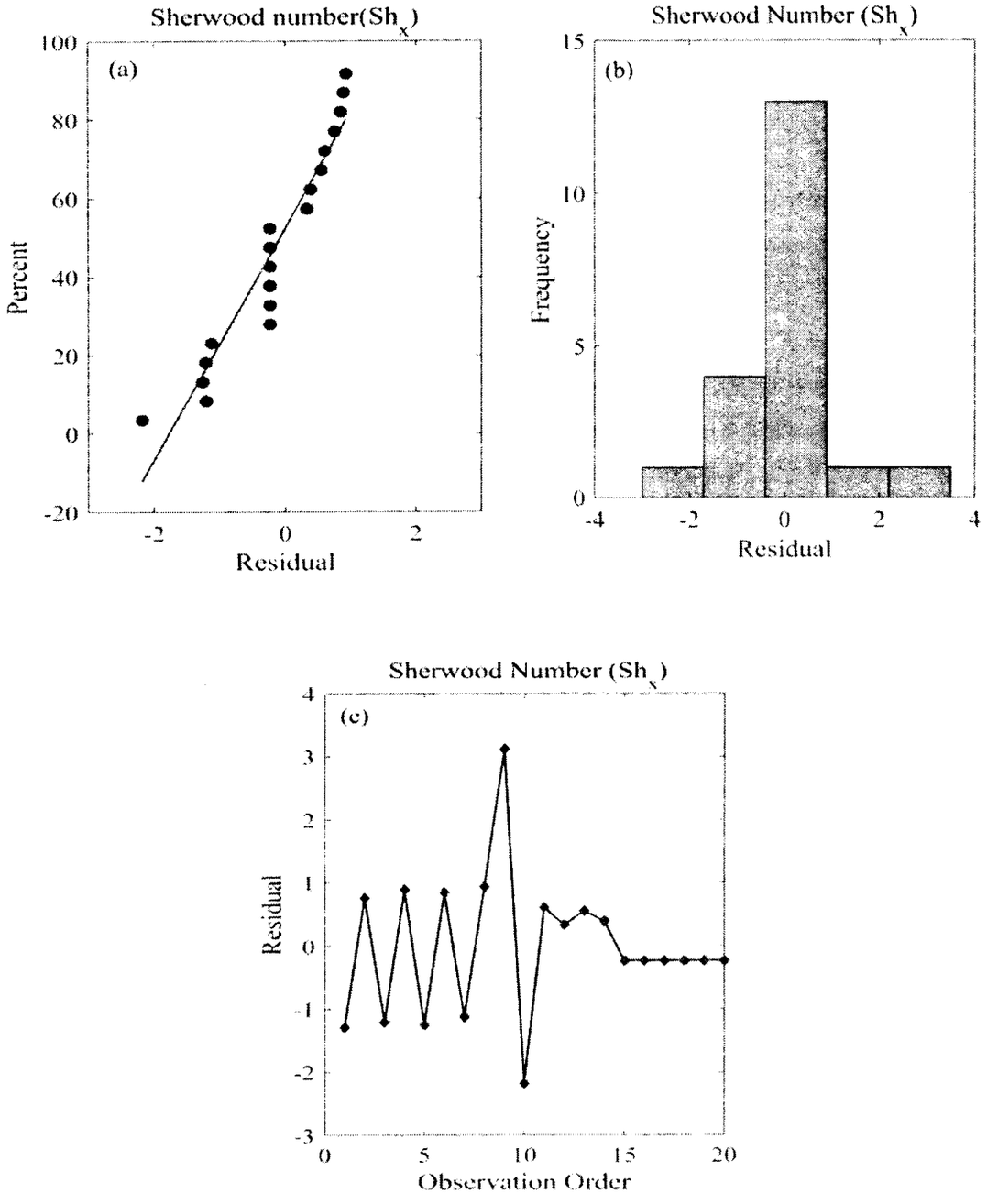

Figure 8.4: Residuals plots for Sh_x (a) normal probability plot (b) histogram (c) residual plot.

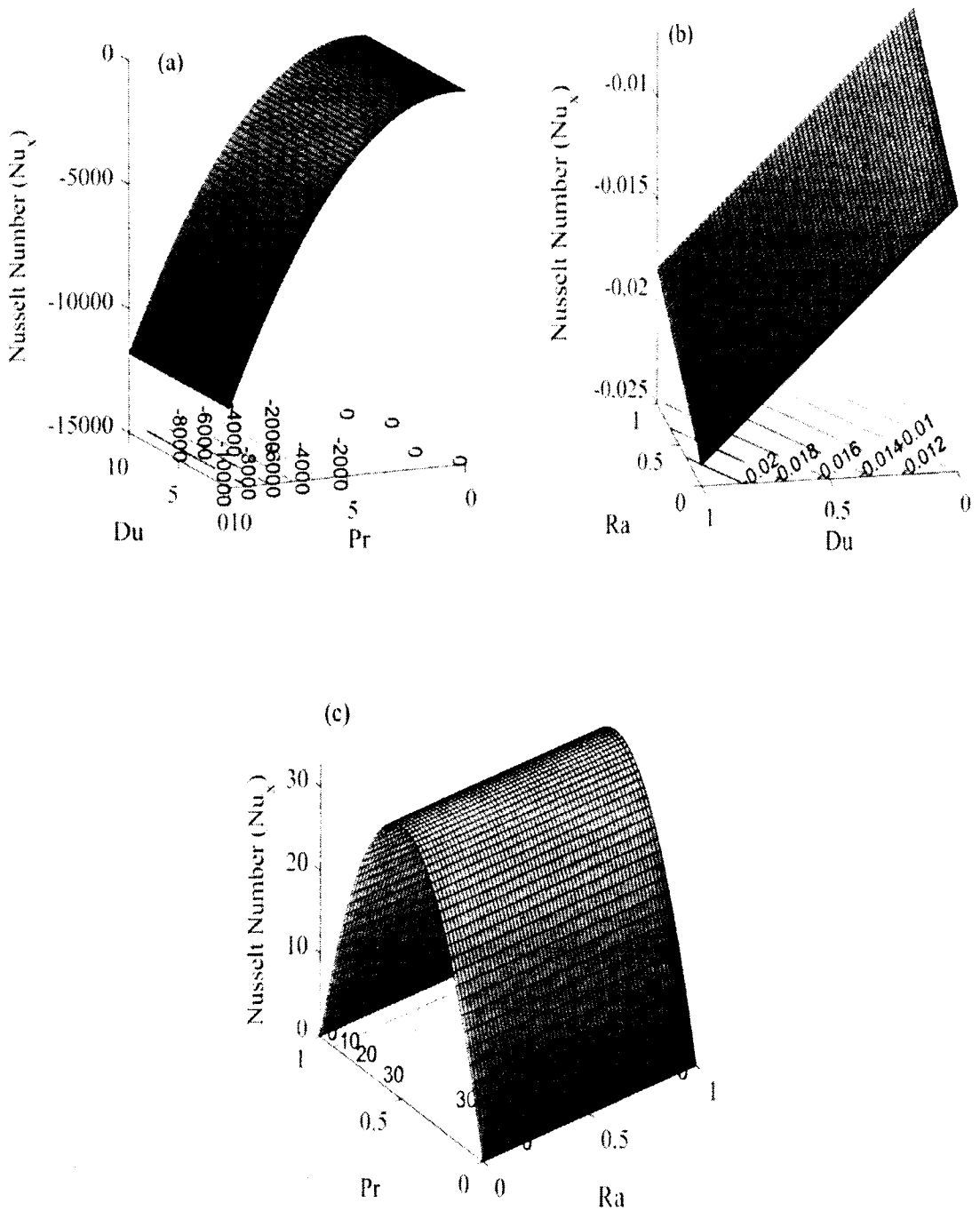

Figure 8.5: Contour plots of output response Nu_x when (a) $A=0$ (b) $B=0$

(c) $C=0$.

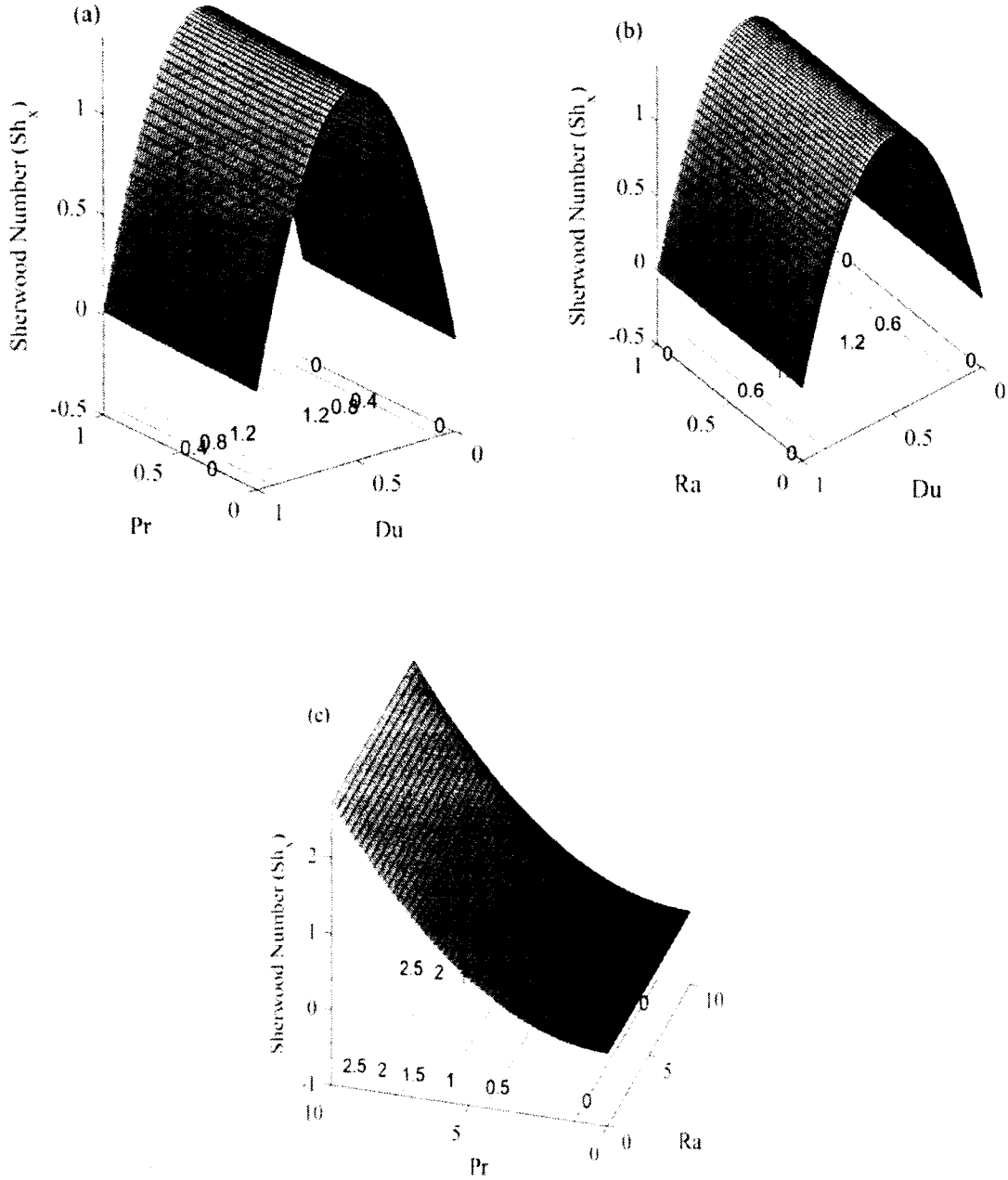

Figure 8.6: Contour plots of output response Sh_x when (a) $A=0$ (b) $B=0$

(c) $C=0$.

The effect of different input parameters on output responses are displayed in the form of surface contours plots. Fig. 8.5 and Fig. 8.6 shows surface contours plots for Nu_x and Sh_x respectively. Fig. 8.5(a) shows the surface contour plots for Nu_x when $A=0$. As it is clear from figure that Nu_x is maximum for low level (-1) of Pr and high level

(+1) of *Du*. Nu_x decreases as approaching to high level (+1) *Pr*. Fig. 8.5(b) shows the effect of *Du* and *Ra* on Nu_x. Nu_x is maximum for low level (-1) of *Du* and high level (+1) of *Ra*. From Fig. 8.5(c) it can be concluded that maximum Nu_x occurs between middle level (0) of *Pr* and high level (+1) of *Ra*. Now we will discuss the effect of input parameters on Sh_x Fig. 8.6(a) demonstrates that Sh_x is maximum between middle level (0) of *Pr* and high level (+1) of *Du*. The same result can be observed for input parameters *Du* and *Ra* which can be seen in Fig. 8.6(b). Finally the impact of *Pr* and *Ra* on Sh_x are depicted in Fig. 8.6(c). As it is clear from figure, Sh_x is maximum at high level (+1) of *Pr* and low level (-1) of *Ra*.

Chapter 9

Nanofluid Flowing over a Wedge with the Effect of Chemical Reaction and Thermal Radiation

In this chapter, the sensitivity of Brownian motion of nanoparticles in fluid and thermophoresis effects on nanofluid wedge flow is analyzed. To achieve this goal problem is modelled using basic conservation laws. The model formulated, is a set of PDEs, which was converted to set of non-linear ODEs by using similarity transformation. Then these ODEs are solved numerically by using MATLAB built in package bvp4c and compared the numerical results with [91-94] and found good results. Sensitivity analysis is performed by employing RSM to determine the relationship between the input parameters and the output responses. RSM is used to portray the statistical results of the ANOVA in tabular format. The results are discussed comprehensively with the help of tables and graphs.

9.1 Mathematical Formalism

Assuming the boundary layer two dimensional flow of an incompressible fluid flowing over a wedge with the effect of chemical reaction, thermal radiation and heat generation. Under the aforementioned assumptions the governing boundary layer equations are follows by [91],

$$\frac{\partial u}{\partial x}+\frac{\partial u}{\partial y}=0, \tag{9.1}$$

$$u\frac{\partial u}{\partial x}+v\frac{\partial u}{\partial y}=U_e\frac{\partial U_e}{\partial x}+\upsilon_f\frac{\partial^2 u}{\partial y^2}+\left(\frac{\sigma B_0^2}{\rho_f}+\frac{\upsilon_f}{K}\right)(U_e-u), \tag{9.2}$$

$$u\frac{\partial T}{\partial x}+v\frac{\partial T}{\partial y}=\alpha_f\frac{\partial^2 T}{\partial y^2}+\tau\left\{D_B\left(\frac{\partial T}{\partial y}\frac{\partial C}{\partial y}\right)+\frac{D_T}{T_\infty}\left(\frac{\partial T}{\partial y}\right)^2\right\}+\frac{Q'}{\rho C_p}(T-T_\infty)+ \tag{9.3}$$

$$\frac{\upsilon_f}{C_p}\left(\frac{\partial u}{\partial y}\right)^2+\frac{16\sigma_1 T_\infty^3}{3\rho C_p K_1}\frac{\partial^2 T}{\partial y^2},$$

$$u\frac{\partial C}{\partial x}+v\frac{\partial C}{\partial y}=D_B\frac{\partial^2 C}{\partial y^2}+\frac{D_T}{T_\infty}\frac{\partial^2 T}{\partial y^2}. \tag{9.4}$$

The boundary conditions of aforementioned flow problem are as follows,

$$u = u_w(x) = -\lambda u_e(x),\quad v = 0,\quad T = T_w, C = C_w \text{ at } y = 0,$$

$$u = u_e(x),\ T \to T_\infty\ C \to C_\infty \text{ as } y \to \infty. \tag{9.5}$$

In the above equations u and v represents the velocity components along x and y directions respectively. λ is constant and λ<0 indicates the stretching wedge, λ>0 indicates the contracting wedge and λ=0 denote fixed wedge. $U = U_\infty x^m$ represents the fluid velocity.

The similarity transformations are considered as follows,

$$\eta = y\sqrt{\frac{(m+1)U_e}{2V_f}}x^{\frac{m-1}{2}},\quad \psi(x,\eta) = \sqrt{\frac{2\upsilon_f U_e}{m+1}}x^{\frac{m+1}{2}}f(\eta),\quad f'(\eta) = \frac{u}{v},$$

$$\theta(\eta) = \frac{T-T_\infty}{T_w-T_\infty},\quad \phi(\eta) = \frac{C-C_\infty}{C_w-C_\infty}. \tag{9.6}$$

By applying the transformations (9.6), Eqns. (9.1) to (9.4) can be transformed as,

$$f''' + ff'' + \beta(1-f'^2) + \frac{1}{1+m}(M+K)[1-f'] = 0, \tag{9.7}$$

$$\frac{1+R}{Pr}\theta'' + [f\theta' + Ecf''^2 + Nb\theta'\phi' + Nt\theta'^2 + Q\theta] = 0, \tag{9.8}$$

$$\phi'' + Le(f\phi') + \frac{Nt}{Nb}\theta'' = 0. \tag{9.9}$$

The transformed boundary conditions are,

$$f = 0,\quad f' = -\lambda,\quad \theta = 1,\quad \phi = 1 \qquad at\ \eta = 0.$$

$$f' \to 1,\ \theta \to 0,\quad \phi \to 0 \qquad as\ \eta \to \infty. \tag{9.10}$$

Here,

$$M = \frac{2\sigma {B_0}^2 x^{1-m}}{\rho_f U_\infty},\ \beta = \frac{2m}{m+1},\ K = \frac{2V_f x^{1-m}}{KU_\infty},\ R = \frac{16\sigma_1 T_\infty^3}{3\rho C_p k_1 \upsilon},\ Ec = \frac{U^2}{C_p(T_w-T_\infty)},$$

$$Q = \frac{2Q'x}{\rho C_p(m+1)u_e},\ Le = \frac{\alpha_f}{D_B},\ Pr = \frac{V_f}{\alpha_f},\ Nb = \frac{\tau D_B(C_w-C_\infty)}{\upsilon_f},\ Nt = \frac{\tau D_T(T_w-T_\infty)}{\upsilon_f T_\infty}. \tag{9.11}$$

The non-dimensional form of temperature, concentration rate and velocity is as follows,

$$(Cf_x Re_x)^{\frac{1}{2}} = \frac{1}{(1-\emptyset_1)^{2.5}(1-\emptyset_2)^{2.5}}\left(\frac{m+1}{2}\right)^{\frac{1}{2}} f''(0),$$

$$\frac{Nu_x}{(Re_x)^{\frac{1}{2}}} = -\frac{k_{nf}}{k_{bf}}\left(1+\frac{4R}{3}(1+(\theta_f-1)\theta(0))^3\right)\left(\frac{m+1}{2}\right)^{\frac{1}{2}}\theta'(0)\,.$$

$$\frac{Sh_x}{(Re_x)^{\frac{1}{2}}} = -\left(\frac{m+1}{2}\right)^{\frac{1}{2}}\phi'(0). \tag{9.12}$$

The numerical results of Cf_x and Nu_x are presented in Table 9.1 and Table 9.2 respectively and compared them with [80 - 83] and found excellent agreement.

Table 9.1: Comparision table for Cf_x with [91 - 94].

m	$-f''(0)$				
	[91]	[92]	[93]	[94]	Present
0	0.4698	0.4696	0.4696	0.4696	0.4696
0.0141	0.5048	0.50461	0.5046	0.50461	0.5046
0.0435	0.5691	0.56898	0.569	0.56898	0.569
0.0909	0.6623	0.65498	0.655	0.65498	0.6549
0.2	0.8052	0.80213	0.8021	0.80213	0.8021
0.3333	0.9291	0.92765	0.9277	0.92765	0.9276
1	1.2328	*	1.2326	1.23258	1,2328

Table 9.2: Comparision table for Nu_x with [91], [92] and [94].

m	$-\theta'(0)$			
	[91]	[92]	[94]	Present
0	0.4212	0.42015	0.42016	0.4201
0.0141	0.4268	0.42578	0.42578	0.4257
0.0435	0.4363	0.43548	0.43548	0.4354
0.0909	0.4713	0.4473	0.44730	0.4713
0.2	0.4855	0.45603	0.45603	0.4560
0.3333	0.4966	0.47814	0.47814	0.4781
1	0.5196	*	*	0.5196

9.2 Experimental Design

9.2.1 Response surface methodology (RSM)

RSM requires twenty runs and nineteen degrees of freedom corresponding to three different parameters namely *Le*, *Nt* and *Nb*. The levels of these factors low (-1), central (0), and high (+1) are displayed in Table. 9.3. By using Eqn. (2.2) the general form of correlations of output responses (Nu_x and Sh_x) can be stated in the following forms.

$$Nu_x = \alpha_0 + \alpha_1 A + \alpha_2 B + \alpha_3 C + \alpha_{11} AB + \alpha_{12} AC + \alpha_{13} BC + \alpha_{21} A^2 + \alpha_{22} B^2 + \alpha_{23} C^2, \quad (9.13)$$

$$Sh_x = \gamma_0 + \gamma_1 A + \gamma_2 B + \gamma_3 C + \gamma_{11} AB + \gamma_{12} AC + \gamma_{13} BC + \gamma_{21} A^2 + \gamma_{22} B^2 + \gamma_{23} C^2. \quad (9.14)$$

where α_i, α_{ij}, γ_i and γ_{ij} $(i = j = 1, 2, 3)$ are unknown constants. These unknown coefficients can be found by using RSM. The levels of selected input factors *Ra*, *Pr* and *Du* and their levels low (-1), central (0), and high (+1) are displayed in Table 9.3.

Table 9.3 Design of input parameters, their symbol and level.

Type	Factor	Symbol	Levels		
			Low (-1)	Middle (0)	High (1)
Input Factors	*Le*	*A*	0.1	0.55	1
	Nt	*B*	0.1	0.55	1
	Nb	*C*	0.1	0.55	1

Table 9.4: Experimental design and measured responses.

Experiment number	Point type	Coded values			Real values			Responses	
		A	*B*	*C*	*Le*	*Nt*	*Nb*	Nu_x	Sh_x
1	Factorial	-1	-1	-1	0.10	0.10	0.10	0.5082	0.8501
2		1	-1	-1	1.00	0.10	0.10	0.5121	1.2171
3		-1	1	-1	0.10	1.00	0.10	0.6838	7.0921
4		1	1	-1	1.00	1.00	0.10	5.8502	43.5680
5		-1	-1	1	0.10	0.10	1.00	0.5920	0.2980
6		1	-1	1	1.00	0.10	1.00	0.5538	0.6797
7		-1	1	1	0.10	1.00	1.00	0.6654	0.9835
8		1	1	1	1.00	1.00	1.00	0.6875	1.2933
9	Axial	-1	0	0	0.10	0.55	0.55	0.5881	0.9186
10		1	0	0	1.00	0.55	0.55	0.6029	1.2604
11		0	-1	0	0.55	0.10	0.55	0.5510	0.5994
12		0	1	0	0.55	1.00	0.55	0.6763	1.7900
13		0	0	-1	0.55	0.55	0.10	0.5748	4.1099
14		0	0	1	0.55	0.55	1.00	0.6349	0.8615
15-20	Centre	0	0	0	0.55	0.55	0.55	0.6091	1.1606

9.2.2 Analysis of Variance (ANOVA)

ANOVA is a statistical methodology that provides variance to find statistically significant correlations between two or more input factors. The regression model values for twenty runs are determined using the statistical tool MINITAB-19 which is shown in Table. 9.4. These results are obtained using ANOVA and the sequential f-

test. Table 9.5 and Table 9.6 shows all of the statistical estimators produced using the ANOVA method. Eqn. (9.13) and Eqn. (9.14) each have their own *F*-value and *P*-value. Table 9.6 shows the statistically calculated coefficient of determination for the simplified models of output responses Nu_x and Sh_x. The mathematical Eqn. (9.13) and Eqn. (9.14) may be rewritten as follows:

$$Nu_x = -0.21138 + 0.15612B + 0.04480C + 0.02878AB - 0.02855AC - 0.07663BC, \quad (9.15)$$

$$Sh_x = -0.9259 + 0.1303A + 0.3165B - 0.2999C - 0.0971B^2 + 0.1371C^2 - 0.0555AB. \quad (9.16)$$

It is clear that all of the simplified models have goodness of fit because coefficient of determination for the models for Nu_x and Sh_x are 98.65% and 97.83 % respectively as given in Table 6.

Table 9.5: ANOVA for (a) Nu_x (b) Sh_x

Source	DF	Adj SS	Adj MS	*F*-Value	*P*-Value	
(a)						
Model	9	0.329649	0.036628	81.13	0.000	Significant
Linear	3	0.264765	0.088255	195.48	0.000	-
Square	3	0.004764	0.001588	3.52	0.000	-
Interaction	3	0.060121	0.020040	44.39	0.000	-
Error	10	0.004515	0.000451			
Lack-of-Fit	5	0.004515	0.000903	*	*	
Pure Error	5	0.000000	0.000000			
Total	19	0.334164				
(b)						
Model	9	2.18266	0.24252	50.16	0.000	Significant
Linear	3	2.07080	0.69027	142.76	0.000	-

Square	3	0.06050	0.02017	4.17	0.037	-
Interaction	3	0.05137	0.01712	3.54	0.056	-
Error	10	0.04835	0.00484			
Lack-of-Fit	5	0.04835	0.00967	*	*	
Pure Error	5	0.00000	0.00000			
Total	19	2.23101				

Table 9.6: Regression coefficients for (a) Nu_x (b) Sh_x

Terms	Coefficient	P-value	Significant
(a)			
Constants	-0.21138	0.000	Yes
A	0.00977	0.177	No
B	0.15612	0.000	Yes
C	0.04480	0.000	Yes
A^2	-0.0154	0.256	No
B^2	-0.0153	0.259	No
C^2	-0.0047	0.722	No
AB	0.02878	0.003	Yes
AC	-0.02855	0.003	Yes
BC	-0.07663	0.000	Yes
	$R^2 = 98.65\ \%$		$Adj\ R^2 = 97.43\ \%$
(b)			
Constants	-0.9259	0.000	Yes
A	0.1303	0.000	Yes

B	0.3165	0.000	Yes
C	-0.2999	0.000	Yes
A^2	-0.0446	0.313	No
B^2	-0.0971	0.043	Yes
C^2	0.1371	0.008	Yes
AB	-0.0555	0.048	Yes
AC	0.0432	0.109	No
BC	-0.0384	0.150	No
	$R^2 = 97.83\ \%$		$Adj\ R^2 = 95.88\ \%$

9.3 Sensitivity analysis

The sensitivity of the Nu_x and Sh_x corresponding to input parameters *Le*, *Nt* and *Nb* was investigated in this work. By using Eqn. (9.15) and Eqn. (9.16) the sensitivity function of output responses (Nu_x and Sh_x) are developed in Eqns. (9.17 – 9.22).

$$\frac{\partial}{\partial A}(Nu_x) = 0.02878B - 0.02855C, \tag{9.17}$$

$$\frac{\partial}{\partial B}(Nu_x) = 0.15612 + 0.02878A - 0.07663C, \tag{9.18}$$

$$\frac{\partial}{\partial C}(Nu_x) = 0.04480 - 0.02855A - 0.07663B, \tag{9.19}$$

$$\frac{\partial}{\partial A}(Sh_x) = 0.1303 - 0.0555B, \tag{9.20}$$

$$\frac{\partial}{\partial B}(Sh_x) = 0.3165 - 0.1942B - 0.0555A, \tag{9.21}$$

$$\frac{\partial}{\partial C}(Sh_x) = -0.2999 + 0.2742C. \tag{9.22}$$

By using Eqns. (9.17 – 9.22) the sensitivity of various values *Le*, *Nt* and *Nb* is tested. Table 9.7 and Table 9.8 shows the sensitivity of Nu_x and Sh_x respectively. The response rises if the factor's bar chart is positive and falls if the bar chart is negative. The responses are more sensitive to the input factors as the bar chart's height

increases. The sensitivity graphs are shown in Fig. 9.1 and Fig. 9.2 for Nu_x and Sh_x respectively.

Table 9.7: Sensitivity analysis of Nu_x when A=0.

B	C	$\partial Nu_x/\partial A$	$\partial Nu_x/\partial B$	$\partial Nu_x/\partial C$
-1	-1	-0.00023	0.23275	0.12143
	0	-0.02878	0.15612	0.12143
	1	-0.05733	0.07949	0.12143
0	-1	0.02855	0.23275	0.0448
	0	0	0.15612	0.0448
	1	-0.02855	0.07949	0.0448
1	-1	0.05733	0.23275	-0.03183
	0	0.02878	0.15612	-0.03183
	1	0.00023	0.07949	-0.03183

Table 9.8: Sensitivity analysis of Sh_x when $A=0$.

B	C	$\partial Sh_x/\partial A$	$\partial Sh_x/\partial B$	$\partial Sh_x/\partial C$
-1	-1	0.1858	0.5107	-0.5741
	0	0.1858	0.5107	-0.2999
	1	0.1858	0.5107	-0.0257
0	-1	0.1303	0.3165	-0.5741
	0	0.1303	0.3165	-0.2999
	1	0.1303	0.3165	-0.0257
1	-1	0.0748	0.1223	-0.5741
	0	0.0748	0.1223	-0.2999
	1	0.0748	0.1223	-0.0257

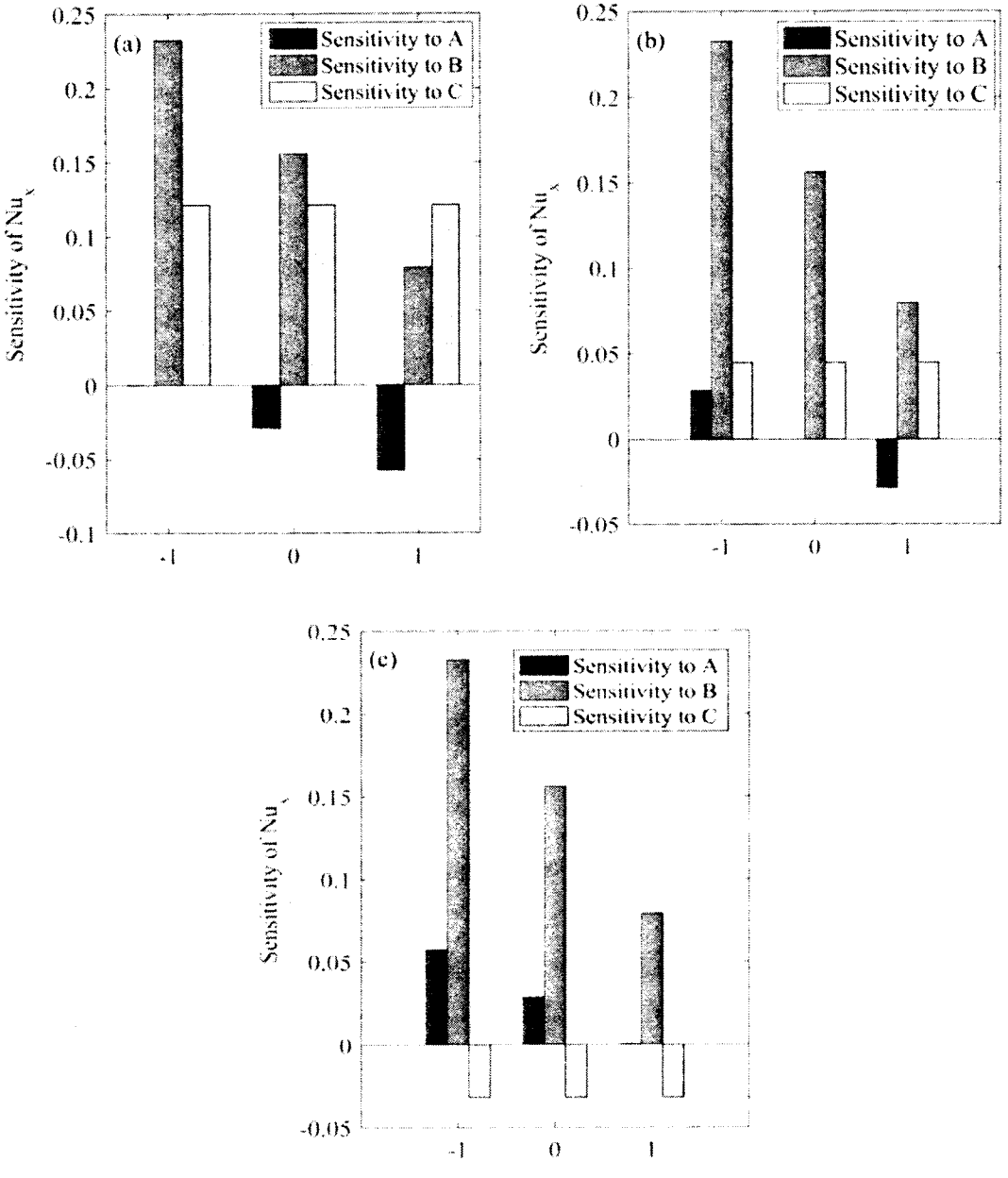

Figure 9.1: Sensitivity plots for Nu_x A=0, (a) *B=-1* (b) *B=0* (c) *B=1*.

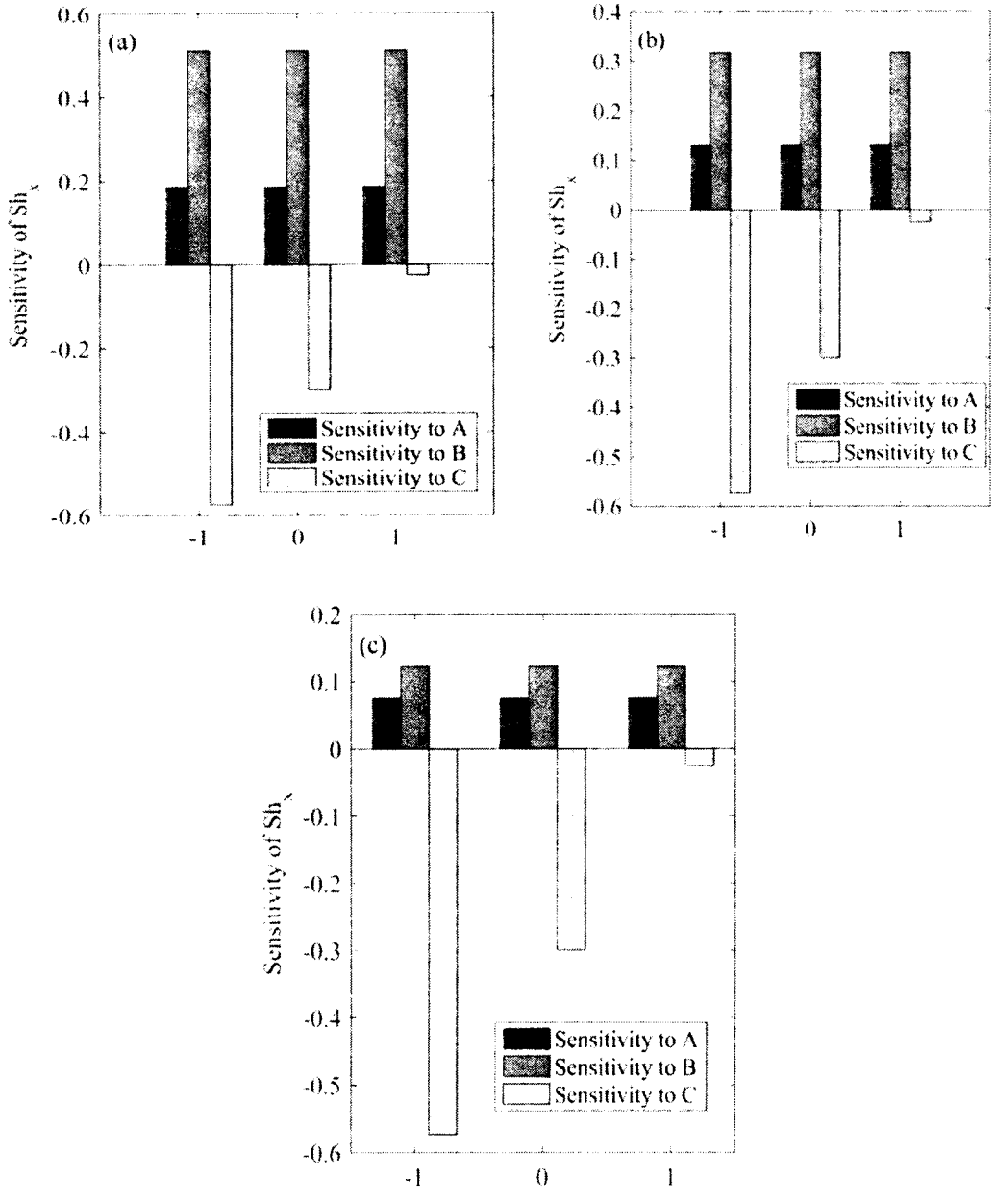

Figure 9.2: Sensitivity plots for Sh_x *A=0*, (a) *B=-1*(b) *B=0* (c) *B=1*.

9.4 Discussion of the Results

This section is meant to explain the sensitivity analysis of nanofluid flowing over a wedge with the influence of radiation by applying RSM. The numerical results of the stated problem are obtained by using Matlab's built-in package bvp4c. Then compared the results with previously published work and found correct. The main focus of this chapter is to perform sensitivity analysis of output responses (Nu_x and Sh_x) for different input factors. To achieve this purpose we constructed an expression for

output responses by using RSM which is described in Eqn. (9.15) and Eqn. (9.16). We estimated the values of responses using regression models fitted to twenty runs by using RSM which is shown in shown in Table 9.4. Table 9.5 displays the ANOVA results and related P-value of Nu_x and Sh_x. Table 9.6 displays the regression coefficients for output responses Nu_x and Sh_x.

The sensitivity plots for Nu_x and Sh_x against the input parameters *Le*, *Nt* and *Nb* are plotted in Fig. 3 and Fig. 4 respectively. These sensitivity diagrams are plotted with the help of sensitivity functions which are described in Eqns. (9.17) – (9.22). The numerical values of these sensitivity plots are also depicted in tabular form which can be seen in Table 9.7 and Table 9.8. All the sensitivity diagrams are plotted against $A=0$ and varying values of *B* and *C*. The sensitivity of Nu_x for parametric variation is illustrated in Fig. 9.1. These figures reflect that sensitivity of Nu_x for input parameters *Le* is positive for all levels. Also these figures demonstrate that *Nt* is most sensitive among other parameters as the height of bar chart is largest as compare to others. Positive sensitivity means, by increasing the value of input parameters the output also increases and vice versa for negative sensitivity. It is also clear from these figures, *Le* has little influence on Nu_x. Also there is a mixed behaviour of *Le* on Nu_x. The sensitivity of *Nb* for $B=-1$ and $B=0$ is positive and negative sensitivity for $B=+1$. Which means at high level of *Nb* there is a negative sensitivity of Nu_x. It is clear that sensitivity of Nu_x decreases as increasing the value of *Nb*.

Fig. 9.2 depicts these sensitivity plots. From Figs. 9.2(a - c) it is clear that sensitivity of Sh_x against the input parameters *Le* and *Nt* are positive for all levels and each cases. And negative sensitivity of Sh_x are observed for input parameters *Nb* for all levels and every cases. Which means that by increasing the value of *Le* and *Nt* the sensitivity of Sh_x also increases and by increasing the value of *Nb* the sensitivity of Sh_x decreases. Also it is worth mentioning that Sh_x is most sensitive to *Nb* among other input parameters.

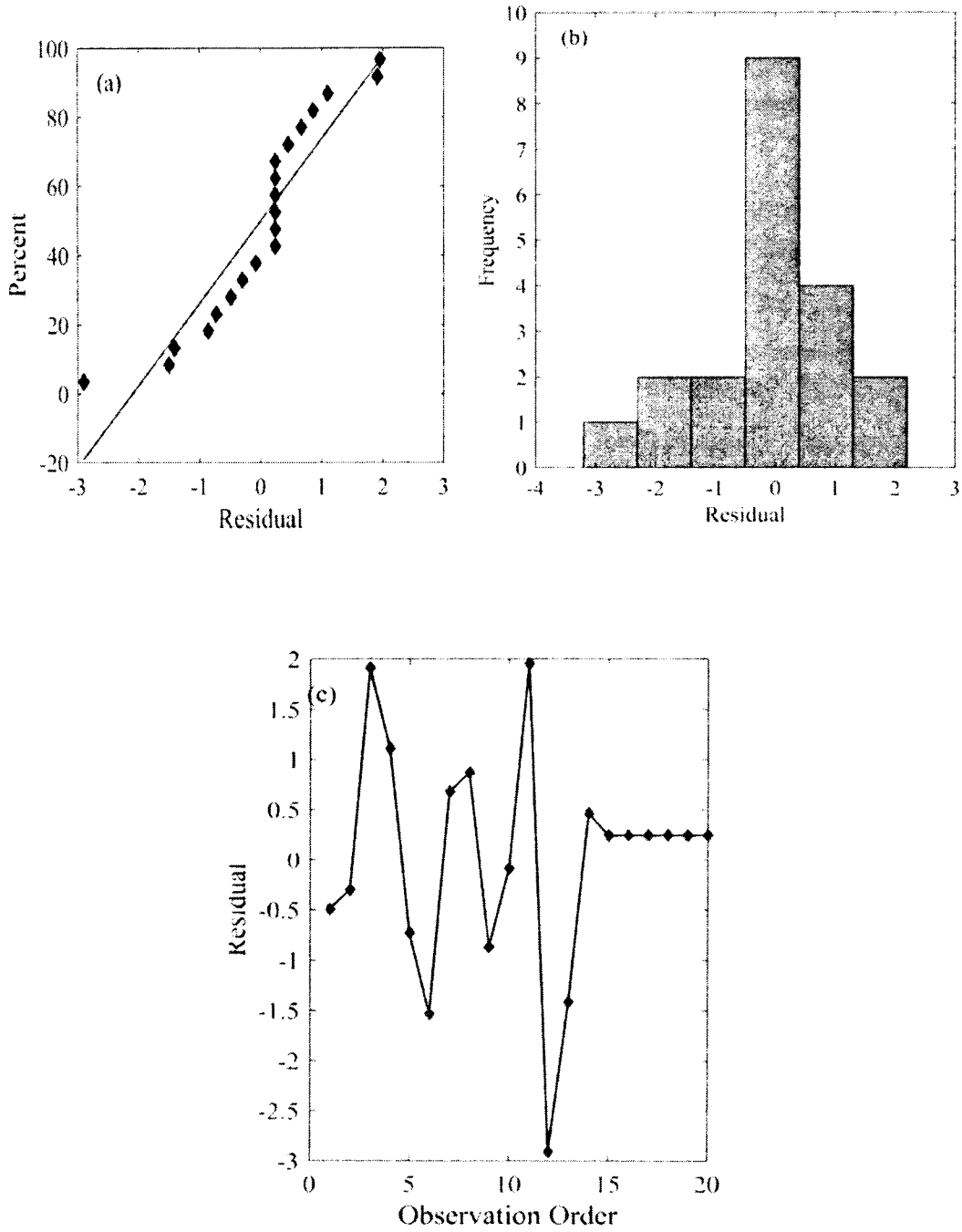

Figure 9.3: Residual plots for Nu_x (a) Normal probability plot (b) Histogram (c) Residual plot

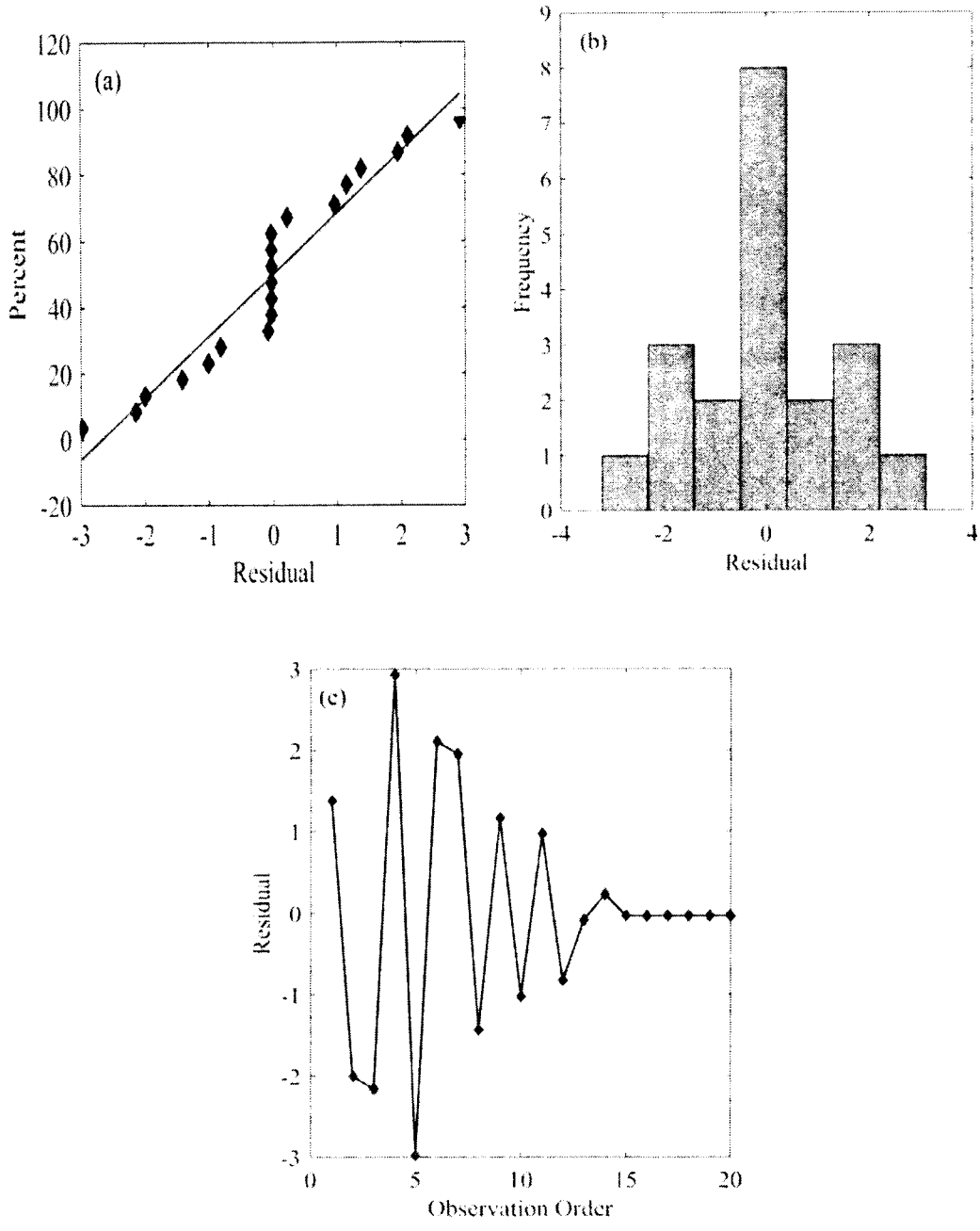

Figure 9.4: Residual plots for output responses Sh_x (a) Normal probability plot (b) Histogram (c) Residual plot.

It is essential to discuss the observation order of residuals and lack of fit while implementing RSM. The residual plots of output responses are presented in Fig. 9.3 and Fig. 9.4. The scatter plots of output responses (Nu_x and Sh_x) are shown in Fig. 9.3(a) and Fig. 9.4(a), respectively. The scatter plot depicts the relationship between the input factors and the output responses. These figures (Figs. 9.3(a) and 9.4(a))

show the strong relationship between the input factors and the output responses. The histograms in Figs. 9.3(b) and 9.4(b) have symmetrical distribution and are less skewed, specifying that the input factors and output responses have good relationships. The observation order verses residuals of output responses (Nu_x and Sh_x) are represented in Fig. 9.3(c) and Fig. 9.4(c) respectively. The graphical representation shows that as by increasing the observation order the residuals of output responses fall. Also, the largest fluctuation can be seen for output responses, which specify the strong correlations between input parameters and output responses.

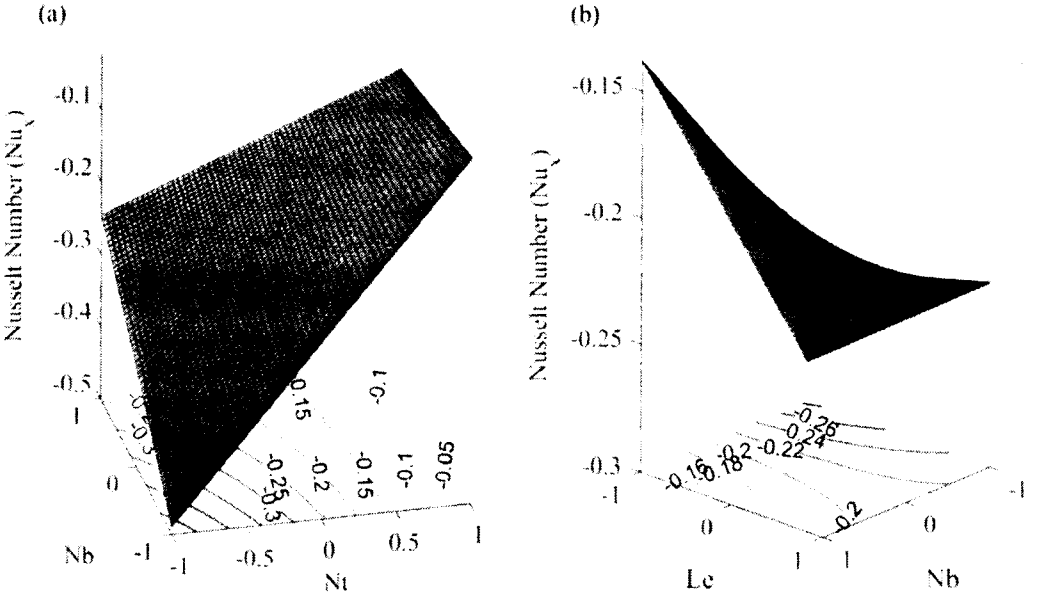

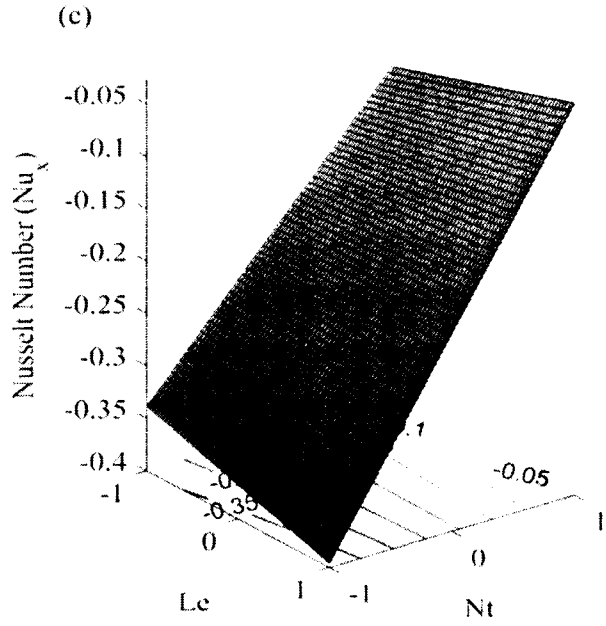

Figure 9.5: Contour plots of Nu_x (a) $A=0$ (b) $B=0$ (c) $C=0$.

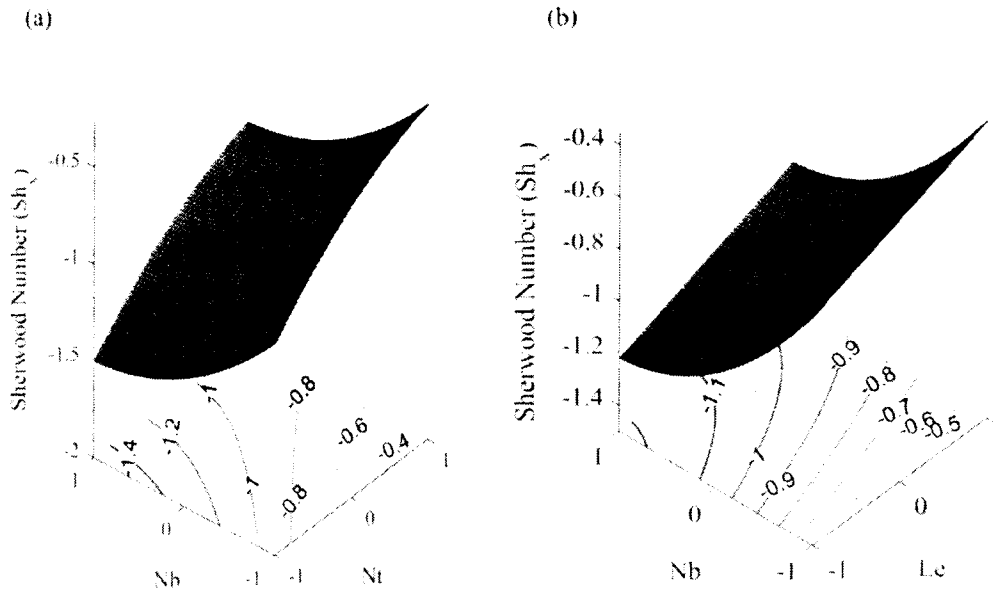

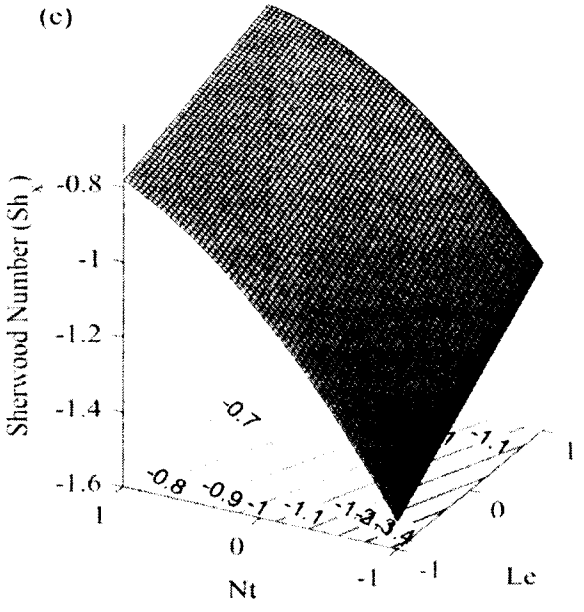

Figure 9.6: Contour plots of Sh_x (a) *A=0* (b) *B=0* (c) *C=0.*

The contour plots of Nu_x and Sh_x are displayed in Fig. 9.5 and Fig. 9.6 respectively. Fig. 9.5(a) shows the effects of *Nt* and *Nb* on Nu_x. It can be noted that maximum Nu_x occurs at the low level (-1) of *Nt* and *Nb.* Fig. 9.5(b) displays the effect of *Le* and *Nb* on Nu_x, as it is clear from figure Nu_x is maximum at low levels (-1) of input parameters *Le* and *Nb.* The effect of *Le* and *Nt* are displayed in Fig. 9.5(c). From figure it is clear that maximum Nu_x occurs at high level (+1) of *Le* and low level of *Nt.* Now we will discuss the effects of input parameters *Le, Nt* and *Nb* on Sh_x . Fig. 9.6(a) displays the effect of *Nt* and *Nb* on Sh_x . Sh_x occurs maximum at low level (-1) of *Nt* and high level (+1) of *Nb.* The same effects can be seen in Fig. 9.6(b). Sh_x is maximum at low level (-1) of *Le* and high (+1) level of *Nb.* Finally, Fig. 9.6(c) shows the effect of *Le* and *Nt* on Sh_x. From figure it is clear that maximum Sh_x occurs at low level (-1) of *Le* and *Nt.*

Chapter 10

Casson Nanofluid Flowing over a Wedge with Activation Energy

The aim of the chapter is to investigate sensitivity analysis of Falkner-Skan nanofluid flow with different input parameters on output responses. For this purpose the model of nanofluid over a wedge with activation energy is considered. The mathematical model which was considered is two-dimensional highly non-linear PDEs are transformed into set of nonlinear ODEs by using similarity transformations. The numerical technique bvp4c have been used to solve the non-linear ODEs. The numerical values are compared [95] and found excellent match. RSM is used to find the correlation between input factors and output variables. Sensitivity analysis has been carried out and the results of sensitivity are presented in graphical and tabular form.

10.1 Mathematical Formulation

Consider a steady two dimensional incompressible non-Newtonian Casson nanofluid flowing over a wedge with the effect of activation energy and chemical reaction. The governing PDEs utilizing the approximation of boundary layer with the aforementioned assumptions are follow as [95],

$$\frac{\partial u}{\partial x}+\frac{\partial v}{\partial y}=0. \tag{10.1}$$

$$u\frac{\partial u}{\partial x}+v\frac{\partial u}{\partial y}-U_e\frac{dU_e}{dx}=v\frac{\partial^2 u}{\partial y^2}-\sigma B_\circ^2(u-U_e), \tag{10.2}$$

$$u\frac{\partial T}{\partial x}+v\frac{\partial T}{\partial y}=\propto\frac{\partial^2 T}{\partial y^2}+\Lambda[D_B\frac{\partial C}{\partial y}\frac{\partial T}{\partial y}+(\frac{D_T}{T_\infty})(\frac{\partial T}{\partial y})^2. \tag{10.3}$$

$$u\frac{\partial C}{\partial x}+v\frac{\partial C}{\partial y}=D_B\frac{\partial^2 C}{\partial y^2}+\left(\frac{D_T}{T_\infty}\right)\left(\frac{\partial^2 T}{\partial y^2}\right)-k_r^2(\frac{T}{T_\infty})^{n_1}e^{-\frac{E_a}{kT}}, \tag{10.4}$$

The associated boundary conditions are followed by [95],

$$u=0, v=0, T=T_w, C=C_w, \text{at } y=0, \tag{10.5}$$

$$u \to U_e(x), T \to T_\infty, C = C_\infty \; as \; y \to \infty. \tag{10.6}$$

The similarity transformations to transformed the governing PDEs into ODEs are gives as [95],

$$\gamma = \mu_B \sqrt{\frac{2\pi_c}{p_y}}, \; k_r^2 (\frac{T}{T_\infty})^{n_1} e^{-\frac{E_a}{kT}}, \; \eta = y\sqrt{\frac{c(n+1)}{2v}} x^{\frac{n+1}{2}}, \; \Psi = \sqrt{\frac{2cv}{(n+1)}} x^{\frac{n+1}{2}} f(\eta), \tag{10.7}$$

$$\theta(\eta) = \frac{T-T_\infty}{T_w-T_\infty}, \; \phi(\eta) = \frac{C-C_\infty}{C_w-C_\infty},$$

The transformed ODEs are [95],

$$(1+\tfrac{1}{\gamma})f''' + ff'' + \beta(1-f'^2) + M^2 \frac{2}{(n+1)}(1-f') = 0, \tag{10.8}$$

$$\theta'' + Prf\theta' + PrNb\theta'\phi' + PrNt\theta'^2 = 0. \tag{10.9}$$

$$\Phi'' + Scf\phi' + \frac{Nt}{Nb}\theta'' - \beta_1 Sc(1+\delta\theta)^{n_1} exp(-\frac{E}{1+\delta\theta})\Phi = 0. \tag{10.10}$$

The transformed associated boundary conditions are follows by [95],

$$f(0) = 0, f'(0) = 0, \theta(0) = 0, \Phi(0) = 1, \tag{10.11}$$

$$f'(\infty) \to 1, \theta(\infty) \to 0, \Phi(\infty) \to 0. \tag{10.12}$$

Where

$$M^2 = \frac{\sigma B_\delta^2 x^{1-n}}{\rho c}, \; \beta = \frac{2n}{(1+n)}, \; Nb = \frac{\Lambda D_B (C_w - C_\infty)}{v}, \; Nt = \frac{\Lambda D_T (T_w - T_\infty)}{T_\infty V}, \; E = \frac{E_a}{kT_\infty},$$
$$\beta_1 = \frac{k_r^2}{cx^{n-1}}, \delta = \frac{(T_w - T_\infty)}{T_\infty}. \tag{10.13}$$

The Cf_x, Nu_x and Sh_x are,

$$C_{fx} = \frac{\tau_w}{\rho {U_e}^2}, \; Nu_x = -\frac{x m_w}{k(T_w - T_\infty)}, \; Sh_x = \frac{x m_w}{D_B(C_w - C_\infty)}. \tag{10.14}$$

Where,

$$\tau_w = \left(\mu_B + \frac{p_y}{\sqrt{2\pi}}\right)\left(\frac{\partial T}{\partial y}\right)_{y=0}, q_w = -k\left(\frac{\partial T}{\partial y}\right)_{y=0} \text{ and } \; m_w = -D_B\left(\frac{\partial C}{\partial y}\right)_{y=0}. \tag{10.15}$$

Now the local Cf_x, Nu_x and Sh_xmay be expressed as,

$$C_f Re_x^{\frac{1}{2}} = \sqrt{\frac{n+1}{2}} f''(0), \quad Sh_x Re_x^{-\frac{1}{2}} = -\sqrt{\frac{n+1}{2}}\theta'(0) \text{ and}$$

$$Nu_x Re_x^{-\frac{1}{2}} = -\sqrt{\frac{n+1}{2}}\theta'(0). \tag{10.16}$$

Where $Re_x = \frac{xU_e}{\hat{\upsilon}}$. The numerical results of Cf_x, Nu_x and Sh_x are computed with the help of computer software bvp4c and compared with [95] and found correct which is displayed in Table 10.1.

Table 10.1: Comparision of numerical results of Cf_x, Nu_x and Sh_x with [95].

γ	n	$Cf_x Re_x^{1/2}$		$Nu_x Re_x^{-1/2}$		$Sh_x Re_x^{-1/2}$	
		[95]	Present	[95]	Present	[95]	Present
0.1	0	1.2851	1.2889	0.2169	0.2112	0.2523	0.2596
	0.3	2.4554	2.4335	0.2836	0.2826	0.3031	0.3025
	0.5	3.0170	3.0041	0.3161	0.3161	0.3309	0.3306
	1	4.1081	4.1020	0.3819	0.3816	0.3901	0.3899
0.2	0	0.8644	0.8485	0.2321	0.2307	0.2595	0.2588
	0.3	1.7955	1.7942	0.3094	0.3094	0.3159	0.3159
	0.5	2.2178	2.2173	0.3448	0.3448	0.3453	0.3453
	1	3.0292	3.0292	0.4161	0.4161	0.4072	0.4072
0.4	0	0.6474	0.6467	0.2516	0.2515	0.2693	0.2692
	0.3	1.3703	1.3703	0.3345	0.3345	0.3287	0.3287
	0.5	1.6934	1.6934	0.3721	0.3721	0.3590	0.3590
	1	2.3135	2.3135	0.4478	0.4478	0.4231	0.4231
0.6	0	0.5646	0.5645	0.2627	0.2627	0.2750	0.2750
	0.3	1.1961	1.1961	0.3475	0.3475	0.3353	0.3353
	0.5	1.4782	1.4782	0.3861	0.3861	0.3661	0.3661
	1	2.0194	2.0194	0.4640	0.4640	0.4310	0.4310

10.2 Experimental Design

10.2.1 Response Surface Methodology (RSM)

For the case of full quadratic model under RSM, we can express Eqn. (2.2) for output responses Nu_x and Sh_x in the following forms:

$$Nu_x = \alpha_0 + \alpha_1 A + \alpha_2 B + \alpha_3 C + \alpha_{11} AB + \alpha_{12} AC + \alpha_{13} BC + \alpha_{21} A^2 + \alpha_{22} B^2 + \alpha_{23} C^2 , \quad (10.17)$$

$$Sh_x = \gamma_0 + \gamma_1 A + \gamma_2 B + \gamma_3 C + \gamma_{11} AB + \gamma_{12} AC + \gamma_{13} BC + \gamma_{21} A^2 + \gamma_{22} B^2 + \gamma_{23} C^2 . \quad (10.18)$$

The design table for input parameters (*Nt*, *Nb* and *Pr*) with their symbol and levels are depicted in Table 2.

Table 10.2: Design input factors and their levels.

Type	Factor	Symbol	Levels		
			Low (-1)	Middle (0)	High (1)
Input Factors	*Nt*	*A*	0.1	0.55	1
	Nb	*B*	0.1	0.55	1
	Pr	*C*	0.1	0.55	1

Table 10.3: Experimental design and measured responses.

Experiment number	Point type	Coded values			Real values			Responses	
		A	*B*	*C*	*Nt*	*Nb*	*Pr*	Nu_x	Sh_x
1	Factorial	-1	-1	-1	0.10	0.10	0.10	0.2023	0.5605
2		1	-1	-1	1.00	0.10	0.10	0.1948	0.3525
3		-1	1	-1	0.10	1.00	0.10	0.1893	0.5873
4		1	1	-1	1.00	1.00	0.10	0.1815	0.5750
5		-1	-1	1	0.10	0.10	1.00	0.4640	0.4310
6		1	-1	1	1.00	0.10	1.00	0.3316	0.1552
7		-1	1	1	0.10	1.00	1.00	0.2792	0.5807
8		1	1	1	1.00	1.00	1.00	0.1955	0.6431
9	Axial	-1	0	0	0.10	0.55	0.55	0.3295	0.5697
10		1	0	0	1.00	0.55	0.55	0.2688	0.5522
11		0	-1	0	0.55	0.10	0.55	0.3466	0.1753
12		0	1	0	0.55	1.00	0.55	0.2538	0.5813
13		0	0	-1	0.55	0.55	0.10	0.1920	0.5680
14		0	0	1	0.55	0.55	1.00	0.3046	0.5615
15-20	Centre	0	0	0	0.55	0.55	0.55	0.2974	0.5457

10.2.2 Analysis of Variance (ANOVA)

Table 10.4 displayed the ANOVA result for different input parameters and output responses. The ANOVA results for regression of coefficients are depicted in Table. 10.5. Now by using these tables Eqns. (10.17) – (10.18) may be written as,

$$Nu_x = 0.29712 - 0.02921A - 0.044B + 0.0615C - 0.0484C^2 + 0.00605AB - 0.02510AC - 0.03682BC, \quad (10.19)$$

$$Sh_x = -3.53787 - 0.01353A + 0.11128B + 0.02497A^2 - 0.05836B^2 + 0.03163C^2 + 0.04723AB + 0.04001AC + 0.04142BC. \quad (10.20)$$

Table 10.4: ANOVA for output responses (a) Nu_x (b) Sh_x

Source	DF	Adj SS	Adj MS	*F*-Value	*P*-Value	
(a)						
Model	9	0.092024	0.010225	264.21	0.000	Significant
Linear	3	0.065715	0.021905	566.03	0.000	Significant
Square	3	0.010128	0.003376	87.23	0.000	Significant
Interaction	3	0.016182	0.005394	139.38	0.000	Significant
Error	10	0.000387	0.000039			
Lack-of-Fit	5	0.000387	0.000077	*		
Pure Error	5	0.000000	0.000000			
Total	19	0.092411				
(b)						
Model	9	0.180153	0.020017	233.43	0.000	Significant
Linear	3	0.125706	0.041902	488.64	0.000	Significant
Square	3	0.010068	0.003356	39.13	0.000	Significant
Interaction	3	0.044379	0.014793	172.51	0.000	Significant
Error	10	0.000858	0.000086			
Lack-of-Fit	5	0.000858	0.000172	*	*	
Pure Error	5	0.000000	0.000000			
Total	19	0.181011				

Table 10.5: Regression coefficients for output responses (a) Nu_x (b) Sh_x

Terms	Coefficient	P-value	Significant
(a)			
Constants	0.29712	0.000	Yes
A	-0.02921	0.000	Yes
B	-0.04400	0.000	Yes
C	0.06150	0.000	Yes
A^2	0.00245	0.528	No
B^2	0.00350	0.373	No
C^2	-0.04840	0.000	Yes
AB	0.00605	0.020	Yes
AC	-0.02510	0.000	Yes
BC	-0.03682	0.000	Yes
	$R^2 = 99.58\,\%$		$Adj\ R^2 = 99.20\,\%$
(b)			
Constants	-3.53787	0.000	Yes
A	-0.01353	0.001	Yes
B	0.11128	0.000	Yes
C	-0.00216	0.478	No
A^2	0.02497	0.001	Yes
B^2	-0.05836	0.000	Yes
C^2	0.03163	0.000	Yes
AB	0.04723	0.000	Yes
AC	0.04001	0.000	Yes

BC	0.04142	0.000	Yes
	$R^2 = 99.53\,\%$		$Adj\ R^2 = 99.10\,\%$

10.3 Sensitivity analysis

Now by using Eqns. (10.19) – (10.20) the sensitivity functions for output responses Nu_x and Sh_x are calculated as follows;

$$\frac{\partial}{\partial A}(Nu_x) = -0.02921 + 0.00605B - 0.02510C, \tag{10.21}$$

$$\frac{\partial}{\partial B}(Nu_x) = -0.044 + 0.00605A - 0.03682C, \tag{10.22}$$

$$\frac{\partial}{\partial C}(Nu_x) = 0.0615 - 0.0968C - 0.0251A - 0.0368B, \tag{10.23}$$

$$\frac{\partial}{\partial A}(Sh_x) = -0.01353 + 0.04994A + 0.04723B + 0.04001C, \tag{10.24}$$

$$\frac{\partial}{\partial B}(Sh_x) = 0.11128 - 0.11672B + 0.04723A + 0.04142C, \tag{10.25}$$

$$\frac{\partial}{\partial C}(Sh_x) = 0.06326C + 0.04001A + 0.04142B. \tag{10.26}$$

The sensitivity of various input model parameters is examined using Eqns. (10.21)–(10.26). The sensitivity of Nu_x and Sh_x are shown in Table 10.6 and Table 10.7 respectively. By using Table 10.6 and Table 10.7 the sensitivity graphs for Nu_x and Sh_x is displayed in Fig. 10.1 and Fig. 10.2 respectively.

Table 10.6: Sensitivity analysis of output response Nu_x when $A=0$.

B	C	$\partial Nu_x/\partial A$	$\partial Nu_x/\partial B$	$\partial Nu_x/\partial C$
-1	-1	-0.01016	-0.00718	0.1951
	0	-0.03536	-0.04400	0.0983
	1	-0.06036	-0.08082	0.0015
0	-1	-0.00411	-0.00718	0.1583
	0	-0.02921	-0.04400	0.0615
	1	-0.05431	-0.08082	-0.0353
1	-1	0.00194	-0.00718	0.1215
	0	-0.02316	-0.04400	0.0247
	1	-0.04826	-0.08082	-0.0721

Table 10.7: Sensitivity analysis of output response Sh_x when $A=0$.

B	C	$\partial Sh_x/\partial A$	$\partial Sh_x/\partial B$	$\partial Sh_x/\partial C$
-1	-1	-0.10077	0.18658	-0.10468
	0	-0.06076	0.228	-0.04142
	1	-0.02075	0.26942	0.02184
0	-1	-0.05354	0.06986	-0.06326
	0	-0.01353	0.11128	0
	1	0.02648	0.1527	0.06326
1	-1	-0.00631	-0.04686	-0.02184
	0	0.0337	-0.00544	0.04142
	1	0.07371	0.03598	0.10468

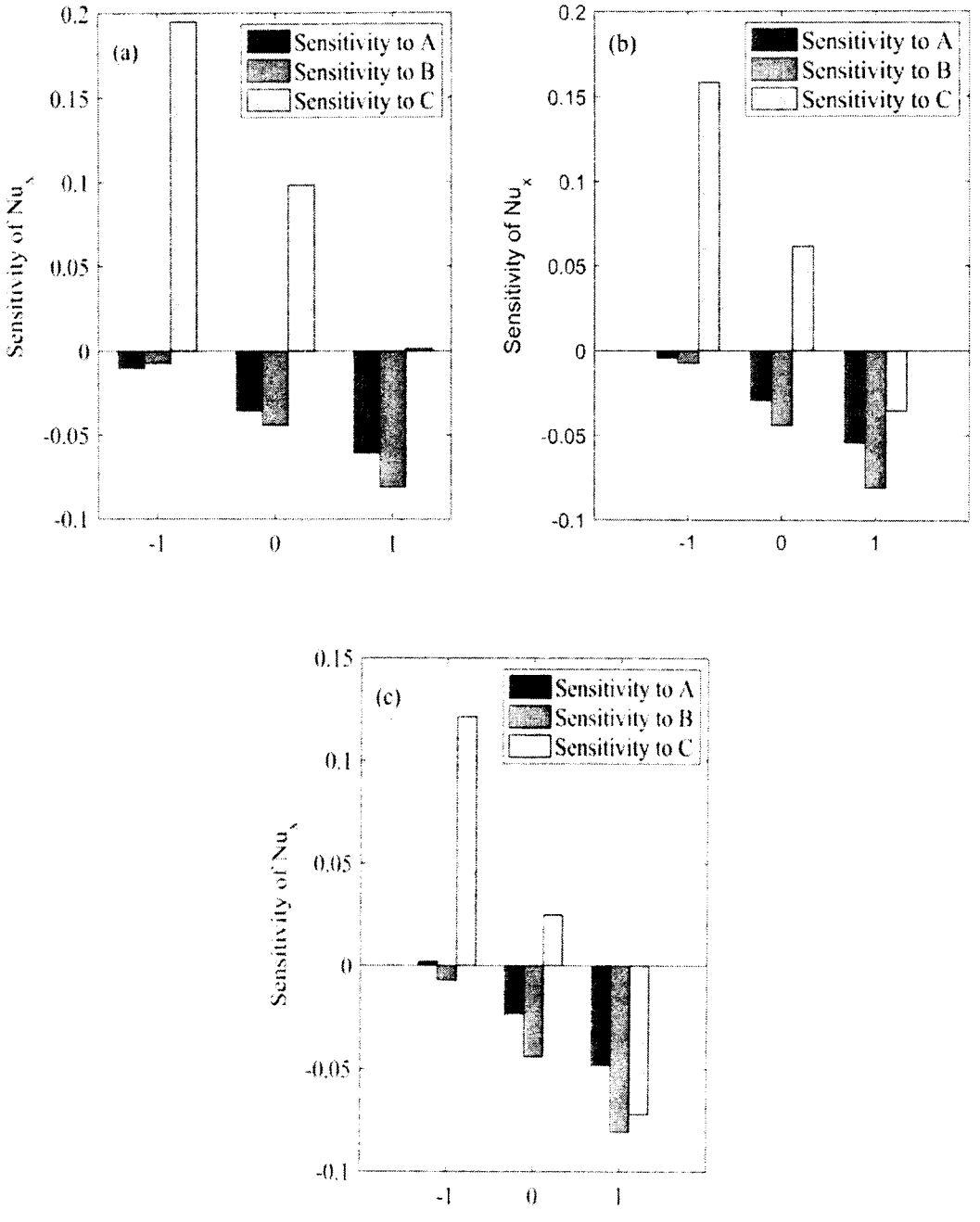

Figure 10.1: Sensitivity plots for output response Nu_x when $A=0$ (a) $B=-1$ (b) $B=0$ (c) $B=1$.

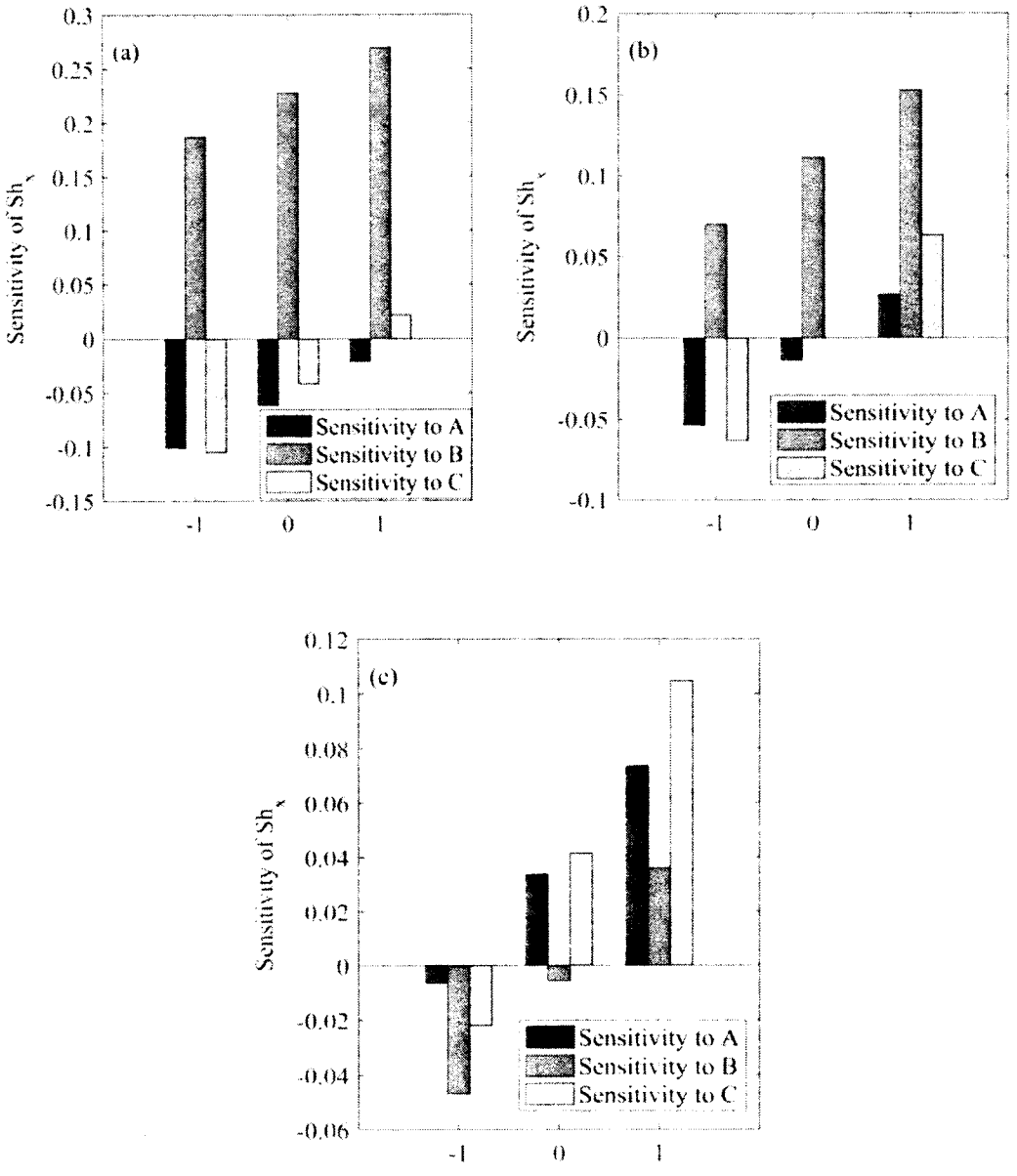

Figure 10.2: Sensitivity plots for output response Sh_x when $A=0$

(a) $B=-1$ (b) $B=0$ (c) $B=1$

10.4 Discussion of the Results

This section explains the sensitivity analysis of a nanofluid flowing over a wedge with activation-energy using RSM. The numerical solution of the problem is computed by using MATLAB's built-in package bvp4c. The results are matched to earlier published work and determined to be correct which can be observed in Table 10.1. The main goal of this research is to conduct sensitivity analysis of output responses

for various input parameters. By using RSM, The ANOVA results are obtained. The values of responses are also estimated using regression models fitted to twenty runs using RSM, as shown in Table 10.3. The ANOVA results for output responses are displayed in Table 10.4 with associated F and P-value. The regression coefficients of Nu_x and Sh_x are displayed in Table 10.5 and mentioned the significant input parameters. The input parameter whose p-value is less then 0.05 is selected as significant. By using these significant input parameters a correlation are developed in Eqn.(10.19) and Eqn. (10.20). To check the validity of RSM residuals of output responses are found and depicted in different forms of plots such as normal probability, histogram and observation order which can be seen in Fig. (10.3) and Fig. (10.4). All these plots show good relations between input parameters and output responses.

By using Eqn. (10.21) to Eqn. (10.26), Table 10.6 and Table 10.7, sensitivity bar graph are plotted for output response which is displayed in Fig. 10.1 and Fig. 10.2. The height of bar graph denotes the sensitivity of different input parameters. The responses are more sensitive to the input factors as the bar chart's height increases. The greatest height of bar chart denotes the most sensitive parameters. The bar chart in positive direction indicates positive sensitivity. Positive sensitivity means by increasing the value of input parameters the output response also increases. And the bar chart in negative direction indicates negative sensitivity, means by increasing the value of input parameter, the sensitivity of output response will decrease. The sensitivity plots of output responses (Nu_x) and (Sh_x) are depicted in Fig. 10.1 and Fig. 10.2 respectively. Fig. 10.1(a) shows the sensitivity of Nu_x for input parameters *Nt, Nb* and *Pr*. The sensitivity of Nu_x for *Nt* and *Nb* is negative for all levels. Whereas positive sensitivity is observed for *Pr* for all levels. This demonstrates that as increasing *Nt* and *Nb* the output response Nu_x decreases and by increasing the input parameters *Pr*, the output response Nu_x increases. The same results are drawn for input parameters *Nt* and *Nb* for the case $B=0$. But mixed behaviour is observed for input factor *Pr*, which is portrayed in Fig. 10.1(b). From Fig. 10.1(c) it is concluded that the sensitivity of output response Nu_x is negative to *Nb* for all levels. It is worth mentioning that, sensitivity of Nu_x to *Nt, Nb* and *Pr* are negative at high level and mixed behaviour can be observed at low and middle level. Overall the input parameter

Pr is most sensitive among others. Also it is observed that sensitivity of Nu_x to *Pr* is greatest at low levels and its sensitivity decreases as approaching to high level.

From Fig. 10.2 (a-c) it is observed that sensitivity of Sh_x to *Nt, Nb* and *Pr* have a mixed behaviour at different levels. The sensitivity of Sh_x to *Nt, Nb* and *Pr* increases at all levels for the case B=-1 which is shown in Fig. 10.2(a). From Fig. 10.2(b) it is observed that *Pr* has no effect on output response Sh_x at middle level. Also negative sensitivity is observed at lower level and positive sensitivity at higher level. The sensitivity of *Nb* increases from lower to higher level and have a mixed behaviour for input parameter *Nt* and *Pr*. Finally, the discussion on the sensitivity of Sh_x for the case *B=+1* are made, which is plotted in Fig. 10.2(c). From figure it is clear that sensitivity of Sh_x to *Nt, Nb* and *Pr* are negative at low level and positive at high level. At middle level the sensitivity of *Nt* and *Pr* is positive and *Nb* is negative. It is also noted that *Nb* is most sensitive for Sh_x in the case of *B=-1, B=0* and *Pr* is most sensitive among others for the case *B=+1*.

By using RSM it is necessary to discuss the residuals, lack of fit and observation order. The residual plots for Nu_x and Sh_x ae shown in Fig. 10.3 and Fig. 10.4 respectively. When the residuals are matched to the fitted values its shows a strong connection.

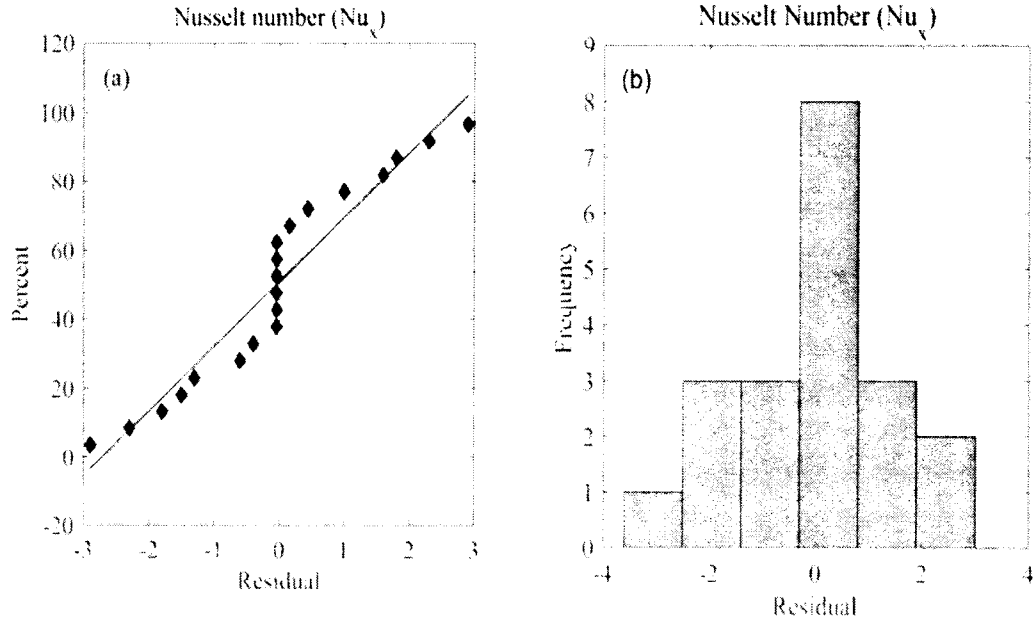

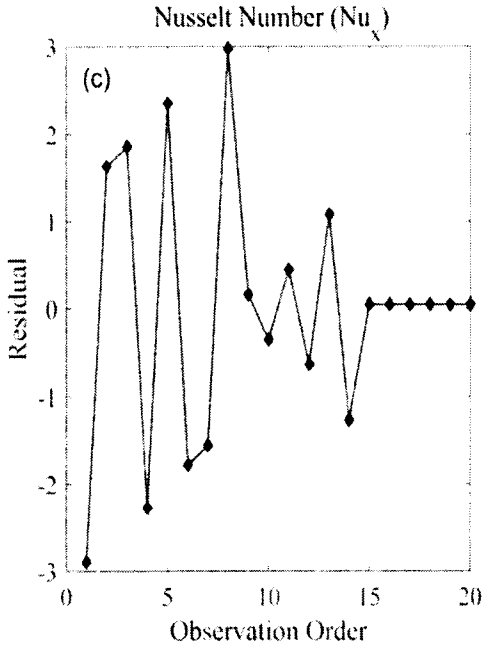

Figure 10.3: Residual plots for Nu_x (a) Normal probability plot (b) Histogram (c) Residual plot.

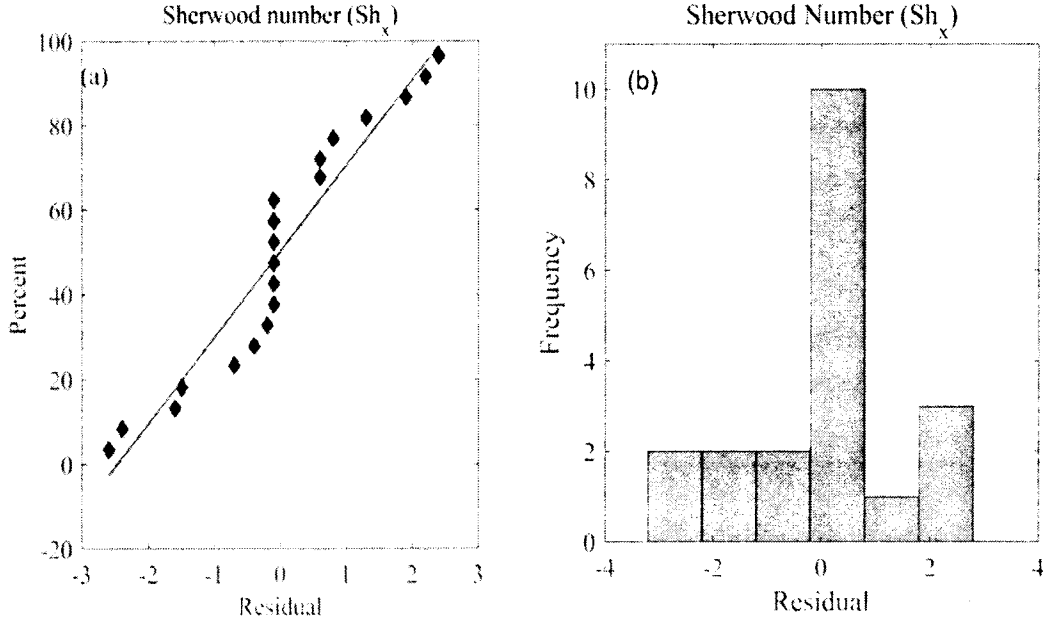

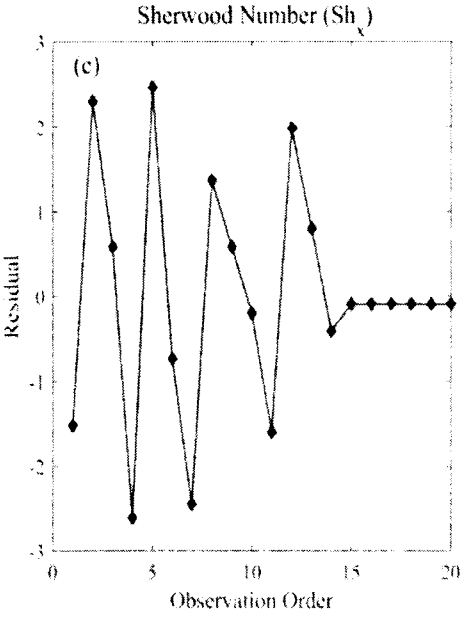

Figure 10.4: Residual plots for Sh_x (a) Normal probability plot (b) Histogram (c) Residual plot.

Fig. 10.3(a) and 10.4(a) shows the scatter plot for output responses Nu_x and Sh_x. Scatter plot shows the connection between the input variables and output responses. While interpreting the scatter plots the strength between the two variables is very important. The strongest linear relationship occurs when the slope is 1. This means that by increasing the input variables, the output responses also increases with the same rate. So Fig. 10.3(a) and 10.4(a) demonstrates the strong connection between the input parameters and output responses (Nu_x and Sh_x). The histogram in Fig. 10.3(b) and 10.4(b) has the symmetrical scattering and less skewed which demonstrates the good relationship of Nu_x and Sh_x with input selected parameters. Fig. 10.3(c) and 10.4(c) depicted the observation order verses residuals for Nu_x and Sh_x respectively. The outcomes also demonstrate that if observation order is increased, the residual of the output responses drops, demonstrating good agreement between the probabilities plots. The residuals graph shows the largest fluctuation for both Nu_x and Sh_x indicates that the model is correct.

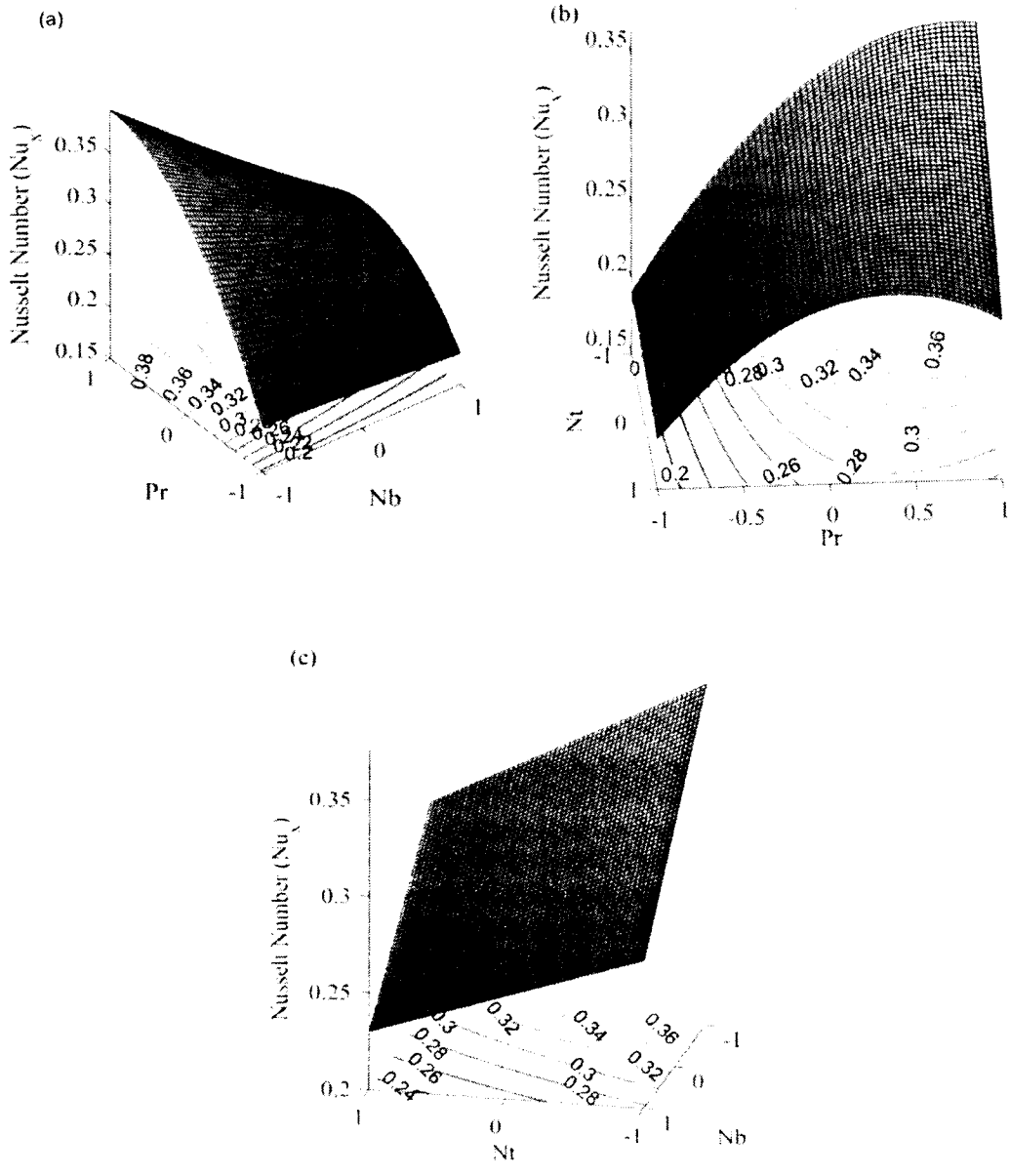

Figure 10.5: Contour plots for output response Nu_x (a) $A=0$

(b) $B=0$ (c) $C=0$.

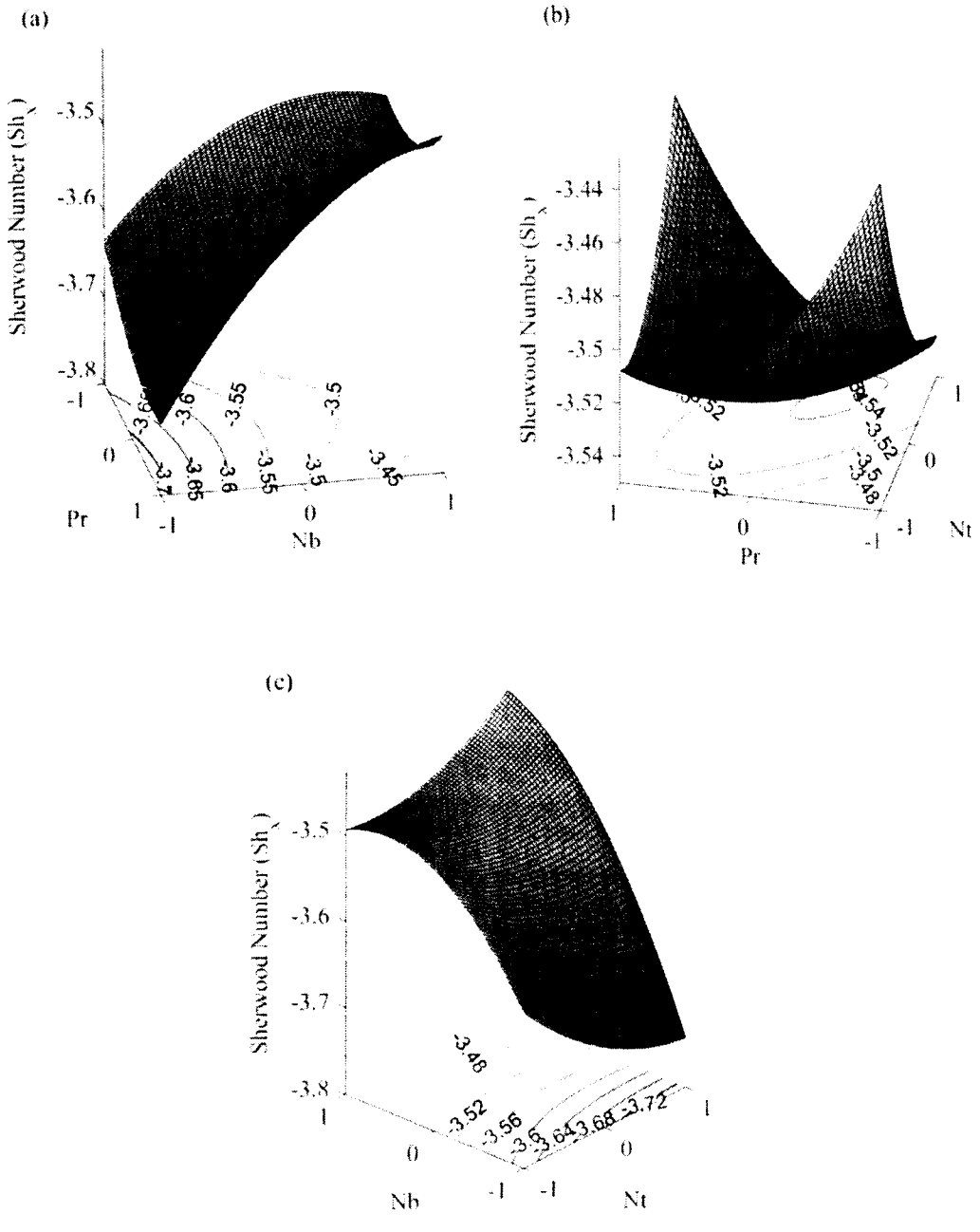

Figure 10.6: Contour plots for output response Sh_x (a) $A=0$

(b) $B=0$ (c) $C=0$.

The surface contour of the predicted responses as a function of different input parameters *Nt*, *Nb* and *Pr* are shown in Fig. 10.5 and Fig. 10.6. The effects of the input parameter *Nb* and *Pr* on output response Nu_x are depicted in Fig. 10.5(a). It is observed from figure that maximum Nu_x occurs near the low level of *Pr* and *Nb*. Also, it is noted that Nu_x decreases near the upper level for *Pr* and the region

between mid and upper level of *Nb*. The effect of input parameter *Pr* and *Nt* are displayed in Fig. 10.5(b). From the figure it is clear that the maximum Nu_x occurred at upper levels of *Pr* and *Nt*. It is also concluded that the effect of *Nt* on Nu_x at low level is negligible. The effect of *Nt* and *Nb* are displayed in Fig. 10.5(c). It can be observed from figure 10.5(c), Nu_x occurs maximum at upper level of *Nt* and low level of *Nb*. By decreasing the value of *Nt* and *Nb* the output response Nu_x increases.

The predicted output response Sh_x as a function of *Nt*, *Nb* and *Pr* are analyzed in Fig. 10.6. The effects of input parameter *Nb* and *Pr* are displayed in Fig. 10.6(a). It is noted that maximum Sh_x occurs at upper level of *Pr* and low level of *Nb*. Sh_x decreases at the middle level of both input parameters *Nb* and *Pr*. The effects of *Nt* and *Pr* on Sh_x are displayed in Fig. 10.6(b). It is indicted that Sh_x is maximum at low level and upper level of *Nt* and *Pr*. It is also observed that Sh_x occurs minimum at middle level of *Nt* and *Pr*. Finally, the effects of *Nt* and *Nb* on output response Sh_x are displayed in Fig. 10.6(c). It is investigated from figure that maximum Sh_x occurs at upper level of *Nt* and low level of *Nb*. Also it is observed that there is no effect of *Nt* at low level and *Nb* at high level on Sh_x.

Chapter 11

Gyrotactic Nanofluid with Activation Energy over a Wedge

In any natural flow, there are different factors which influence the movement of microorganism in fluid, some factors are significant while others are not. In this chapter sensitivity of movement of motile Gyrotactic Microorganism to variation in Schmidt number, Brownian motion of nanoparticle and chemical reaction parameter is studied. The formulated mathematical equations are high non-linear PDEs. These equations are transformed into non-linear ODEs by using similarity transformations. The transformed ordinary differential equations have been studied numerically by using MATLAB built in software bvp4c and compared the numerical results with [96-98] and displayed good results. The effects of different input parameters on Sh_x and Nu_x have been studied by designing an empirical models using RSM. Finally, the dependency of output variables on input factors is analyzed graphically by performing sensitivity analysis.

11.1 Mathematical Formulation

Consider a steady, incompressible two dimensional bioconvective nanofluid flow over a wedge. The gyrotactic microorganisms are added in dilute suspension of nanofluid with Arrhenius activation energy and thermal radiation. The governing equations for continuity, momentum, energy, nanoparticle concentration and density of gyrotactic microorganisms are follows by [96],

$$\frac{\partial u}{\partial x}+\frac{\partial v}{\partial y}=0 \tag{11.1}$$

$$u\frac{\partial u}{\partial x}+v\frac{\partial u}{\partial y}=\nu_f\frac{\partial^2 u}{\partial y^2}+U_e\frac{dU_e}{dx}+\frac{\nu_f}{k}(U_e-u)+\frac{1}{\rho_f}[\rho_f g\beta(1-C_\infty)(T-T_\infty)-g(\rho_p-\rho_f)(C-C_\infty)-g\gamma(\rho_m-\rho_f)(N-N_\infty)] \tag{11.2}$$

$$u\frac{\partial T}{\partial x}+v\frac{\partial T}{\partial y}=\alpha\frac{\partial^2 T}{\partial y^2}+\tau\left[D_B\frac{\partial C}{\partial y}\frac{\partial T}{\partial y}+\frac{D_T}{T_\infty}\left(\frac{\partial T}{\partial y}\right)^2\right]+\frac{v_f}{c_p}\left(\frac{\partial u}{\partial y}\right)^2-\frac{1}{\rho c_p}\frac{\partial q_r}{\partial y} \tag{11.3}$$

$$u\frac{\partial C}{\partial x}+v\frac{\partial C}{\partial y}=D_B\frac{\partial^2 C}{\partial y^2}+\frac{D_T}{T_\infty}\frac{\partial^2 T}{\partial y^2}-K_r^2\left(\frac{T}{T_\infty}\right)^n\times Exp(-\frac{E_a}{KT})(C-C_\infty) \tag{11.4}$$

$$u\frac{\partial N}{\partial x}+v\frac{\partial N}{\partial y}+\frac{bW_c}{(C_w-C_\infty)}[\frac{\partial}{\partial y}(N\frac{\partial C}{\partial y})]=D_m\frac{\partial^2 N}{\partial y^2} \tag{11.5}$$

The expression $\left(\frac{T}{T_\infty}\right)^n\times Exp\left(-\frac{E_a}{KT}\right)(C-C_\infty)$ is known as Arrhenius function. The radiation heat flux can be taken as

$$q_r=-\frac{4\sigma^*}{3k^*}\frac{\partial T^4}{\partial y}, \tag{11.6}$$

where k^* is the absorption coefficient and σ^* is known as Stefan-Boltzman constant. Eqn. (11.6) can be now written as

$$q_r=-\frac{16\sigma^* T^3}{3k^*}\frac{\partial T}{\partial y} \tag{11.7}$$

The boundary conditions for aforementioned problem are given as [85]

$$u=u_x(x),v=-v_x,T=T_w,C=C_w,N=N_w\ at\ y=0 \tag{11.8}$$

$$u=U(x),T\to T_\infty,C\to C_\infty,N\to N_\infty,as\ y\to\infty \tag{11.9}$$

The stream function ψ and similarity function η can be defined as,

$$\eta(x,y)=y\sqrt{\frac{(1+m)U_e}{2v_f x}},\psi=\sqrt{\frac{2U_e v_f x}{1+m}}f(\eta) \tag{11.10}$$

The temperature, nanoparticle concentration and density of microorganism are taken as,

$$\theta(\eta)=\frac{T-T_\infty}{T_w-T_\infty},\phi(\eta)=\frac{C-C_\infty}{C_w-C_\infty},\chi(\eta)=\frac{N-N_\infty}{N_w-N_\infty} \tag{11.11}$$

By using similarity transformation in Eqn. (11.10) and Eqn. (11.11), Eqn.(11.2) to Eqn. (11.5) are transformed into the following form;

$$f'''+ff''+\frac{2m}{1+m}(1-f')+\frac{Da^{-1}}{1+m}(1-\frac{2}{1+m})+\frac{2}{1+m}Gr(\theta-Nr\phi-Rb\chi)=0 \tag{11.12}$$

$$[1+R\{1+(\theta_w-1)\theta\}^3]\theta''+Pr[f\theta'+Ecf''^2+Nb\theta'\phi'+Nt\theta'^2]+ \tag{11.13}$$

$$3R\{1+(\theta_w-1)\theta\}^2(\theta_w-1)\theta'^2=0$$

$$\theta''+Scf\theta'+\frac{Nt}{Nb}\theta''-\frac{2}{1+m}Sckr^2\{1+n(\theta_w-1)\theta\}\times \quad (11.14)$$

$$Exp(\frac{E}{1+(\theta_w-1)\theta})\phi=0$$

$$\chi''+Lbf\chi'-Pe[\chi'\phi'+(\Omega+\chi)\phi'']=0 \quad (11.15)$$

The transformed associated boundary conditions are as follows;

$$f(0)=\frac{2}{1+m}S, f'(0)=\lambda, \theta(0)=1,\ \phi(0)=1,\ \chi(0)=1 \quad (11.16)$$

$$f'(\infty)=1,\ \theta(\infty)=0, \phi(\infty)=0, \chi(\infty)=0 \quad (11.17)$$

The local Cf_x, Nu_x, Sh_x and Nn_x are given as follows,

$$Cf_x=\frac{\tau_w}{\rho U(x)^2}, Nu_x=\frac{xq_w}{k(T_w-T_\infty)},\ Sh_x=\frac{xq_m}{D_B(C_w-C_\infty)}, Nn_x=\frac{xq_n}{D_m(N_w-N_\infty)}, \quad (11.18)$$

where,

$$\tau_w=\mu(\frac{\partial u}{\partial y})_{y=0},\quad q_w=-k\left(\frac{\partial T}{\partial y}\right)_{y=0}, q_m=-D_B\left(\frac{\partial C}{\partial y}\right)_{y=0},$$

$$q_n=-D_m(\frac{\partial N}{\partial y})_{y=0}. \quad (11.19)$$

Now substituting the values of Eqn. (19) into (18), we have,

$$Cf_x\sqrt{Re_x}=\sqrt{\frac{1+m}{2}}f''(\infty), \frac{Nu_x}{\sqrt{Re_x}}=-\sqrt{\frac{1+m}{2}}\theta'(0), \frac{Sh_x}{\sqrt{Re_x}}=-\sqrt{\frac{1+m}{2}}\phi'(0),$$

$$\frac{Nn_x}{\sqrt{Re_x}}=-\sqrt{\frac{1+m}{2}}\chi'(0) \quad (11.20)$$

Table 11.1: Comparision table for Cf_x and Nu_x

m	[96]		[97]		[98]		Present Results	
	$f''(0)$	$-\theta'(0)$	$f''(0)$	$-\theta'(0)$	$f''(0)$	$-\theta'(0)$	$f''(0)$	$-\theta'(0)$
0.0141	0.506206	0.430370	0.50461	0.42578	0.50481	0.42614	0.5046	0.4257
0.0435	0.569671	0.438611	0.56898	0.43548	0.56890	0.43544	0.5690	0.4355
0.0909	0.655147	0.448898	0.65498	0.44730	0.65493	0.44740	0.6550	0.4472
0.1429	0.732183	0.459295	0.73200	0.45694	0.73196	0.45707	0.7320	0.4569
0.2000	0.802123	0.465153	0.80213	0.46503	0.80215	0.46517	0.8021	0.4650
0.3333	0.927648	0.478188	0.92765	0.47814	0.92767	0.47841	0.9277	0.4780

11.2 Experimental Design

11.2.1 Response surface methodology (RSM)

In our present case the response variables are Sherwood number, and Density number and input parameters are *Sc, Kr* and *Nb*. The general form of correlations for output responses by Eqn. (2.2) are given as follows,

$$Sh_x = \alpha_0 + \alpha_1 A + \alpha_2 B + \alpha_3 C + \alpha_{11} AB + \alpha_{12} AC + \alpha_{13} BC + \alpha_{21} A^2 + \alpha_{22} B^2 + \alpha_{23} C^2, \quad (11.21)$$

$$Sn_x = \gamma_0 + \gamma_1 A + \gamma_2 B + \gamma_3 C + \gamma_{11} AB + \gamma_{12} AC + \gamma_{13} BC + \gamma_{21} A^2 + \gamma_{22} B^2 + \gamma_{23} C^2, \quad (11.22)$$

where $\alpha_i, \alpha_{ij}, \gamma_i$ *and* γ_{ij} are unknown constants. These unknown coefficients can be found by using RSM. RSM requires 20 runs and 19 degrees of freedom corresponding to three different parameters namely *Sc*, *Kr* and *Nb*. The levels of these factors low (-1), central (0), and high (+1) are displayed in Table 11.2. The experimental design along with coded and real values with twenty runs is displayed in Table 11.3.

Table 11.2: Design input factor and their level.

Type	Factor	Symbol	Levels		
			Low (-1)	Middle (0)	High (1)
Input Factors	*Sc*	*A*	1	2	3
	Kr	*B*	0.1	0.55	1
	Nb	*C*	0.1	0.55	1

Table 11.3: Experimental design and measured responses.

Experiment number	Point type	Coded values			Real values			Responses	
		A	*B*	*C*	*Sc*	*Kr*	*Nb*	Sh_x	Sn_x
1	Factorial	-1	-1	-1	1	0.10	0.10	0.8094	1.0992
2		1	-1	-1	3	0.10	0.10	1.8805	1.8822
3		-1	1	-1	1	1.00	0.10	1.9081	1.9055
4		1	1	-1	3	1.00	0.10	3.6013	3.1847
5		-1	-1	1	1	0.10	1.00	0.8890	1.1499
6		1	-1	1	3	0.10	1.00	1.9347	1.9192
7		-1	1	1	1	1.00	1.00	1.8891	1.8898
8		1	1	1	3	1.00	1.00	3.5800	3.1680
9	Axial	-1	0	0	1	0.55	0.55	1.2737	1.4323
10		1	0	0	3	0.55	0.55	2.5539	2.3878
11		0	-1	0	2	0.10	0.55	1.4323	1.5454
12		0	1	0	2	1.00	0.55	2.8137	2.5859

13		0	0	-1	2	0.55	0.10	1.9595	1.9428
14		0	0	1	2	0.55	1.00	1.9603	1.9409
15-20	Centre	0	0	0	2	0.55	0.55	1.9602	1.9410

11.2.2 Analysis of Variance (ANOVA)

By using statistical software MINITAB-19, ANOVA will be performed. By using RSM, ANOVA calculate the R^2, $Adj\ R^2$, F-value, and P-value. Table 11.4 displayed the ANOVA result for different input parameters and output responses.

Table 11.4: ANOVA for (a) Sh_x (b) Nu_x

Source	DF	Adj SS	Adj MS	F-Value	P-Value	
(a)						
Model	9	9.57602	1.06400	2614.26	0.000	Significant
Linear	3	9.28640	3.09547	7605.60	0.000	Significant
Square	3	0.08497	0.02832	69.59	0.000	Significant
Interaction	3	0.20464	0.06821	167.60	0.000	Significant
Error	10	0.00407	0.00041			
Lack-of-Fit	5	0.00407	0.00081	*	*	
Pure Error	5	0.00000	0.00000			
Total	19	9.58009				
(b)						
Model	9	5.38612	0.59846	2554.59	0.000	Significant
Linear	3	5.20581	1.73527	7407.24	0.000	Significant
Square	3	0.05219	0.01740	74.26	0.000	Significant
Interaction	3	0.12811	0.04270	182.28	0.000	Significant
Error	10	0.00234	0.00023			

Lack-of-Fit	5	0.00234	0.00047	*	*	
Pure Error	5	0.00000	0.0000			
Total	19	5.38836				

By using RSM, regression coefficient for output response is depicted in Table 11.5. The unknown coefficients in Eqn. (11.21) and Eqn. (11.22) will determine by using the regression Table 11.5. Hence, Eqns. (11.21) – (11.22) may be written as,

$$Sh_x = 1.96235 + 0.67811A + 0.68463B + 0.15841AB - 0.02176BC - 0.0518A^2 + 0.1574B^2, \quad (11.23)$$

$$Sn_x = 1.94256 + 0.50652A + 0.51380B + 0.12564AB - 0.01501BC - 0.03485A^2 + 0.12075B^2. \quad (11.24)$$

Table 11.5: Regression coefficients for (a) Sh_x (b) Nu_x

Terms	Coefficient	*P*-value	Significant
(a)			
Constants	1.96235	0.000	Yes
A	0.67811	0.000	Yes
B	0.68463	0.000	Yes
C	0.00943	0.170	No
A^2	-0.0518	0.002	Yes
B^2	0.1574	0.000	Yes
C^2	-0.0057	0.651	No
AB	0.15841	0.000	Yes
AC	-0.00346	0.638	No
BC	-0.02176	0.012	Yes
$R^2 = 99.96\ \%$			$Adj\ R^2 = 99.92\ \%$

(b)			
Constants	1.94256	0.000	Yes
A	0.50652	0.000	Yes
B	0.51380	0.000	Yes
C	0.00534	0.296	No
A^2	-0.03485	0.004	Yes
B^2	0.12075	0.000	Yes
C^2	-0.00305	0.748	No
AB	0.12564	0.000	Yes
AC	-0.00184	0.741	No
BC	-0.01501	0.020	Yes
	$R^2 = 99.96\,\%$		$Adj\ R^2 = 99.92\,\%$

11.3 Sensitivity analysis

To analyze the sensitivity of different input parameters on output response take the partial derivative of output response. The sensitivity functions of output responses (Sh_x and Sn_x) are developed by using Eqns. (11.23 - 11.24), Table 11.6 and Table 11.7.

$$\frac{\partial}{\partial A}(Sh_x) = 0.67811 + 0.15841B - 0.1036A, \tag{11.25}$$

$$\frac{\partial}{\partial B}(Sh_x) = 0.68463 + 0.15841A - 0.02176C + 0.3148B, \tag{11.26}$$

$$\frac{\partial}{\partial C}(Sh_x) = -0.02176B, \tag{11.27}$$

$$\frac{\partial}{\partial A}(Sn_x) = 0.50652 + 0.12564B - 0.0697A, \tag{11.28}$$

$$\frac{\partial}{\partial B}(Sn_x) = 0.5138 + 0.12564A - 0.01501C + 0.2415B, \tag{11.29}$$

$$\frac{\partial}{\partial C}(Sn_x) = -0.01501B. \tag{11.30}$$

By using Eqns. (11.25 – 11.30) the sensitivity of various values of input parameter is tested. Table 11.6 and Table 11.7 shows the sensitivity of Sh_x and Sn_x respectively. Sensitivity graphs are shown in Fig.11.1 and Fig.11.2 for Sh_x and Sn_x respectively.

Table 11.6: Sensitivity analysis Sherwood number of when $A=0$.

B	C	$\partial Sh_x/\partial A$	$\partial Sh_x/\partial B$	$\partial Sh_x/\partial C$
-1	-1	0.5197	0.39159	0.02176
	0	0.5197	0.36983	0.02176
	1	0.5197	0.34807	0.02176
0	-1	0.67811	0.70639	0
	0	0.67811	0.68463	0
	1	0.67811	0.66287	0
1	-1	0.83652	1.02119	-0.02176
	0	0.83652	0.99943	-0.02176
	1	0.83652	0.97767	-0.02176

Table 11.7: Sensitivity analysis of density number when $A=0$.

B	C	$\partial Sn_x/\partial A$	$\partial Sn_x/\partial B$	$\partial Sn_x/\partial C$
-1	-1	0.38088	0.28731	0.01501
	0	0.38088	0.2723	0.01501
	1	0.38088	0.25729	0.01501
0	-1	0.50652	0.52881	0
	0	0.50652	0.5138	0
	1	0.50652	0.49879	0
1	-1	0.63216	0.77031	-0.01501
	0	0.63216	0.7553	-0.01501
	1	0.63216	0.74029	-0.01501

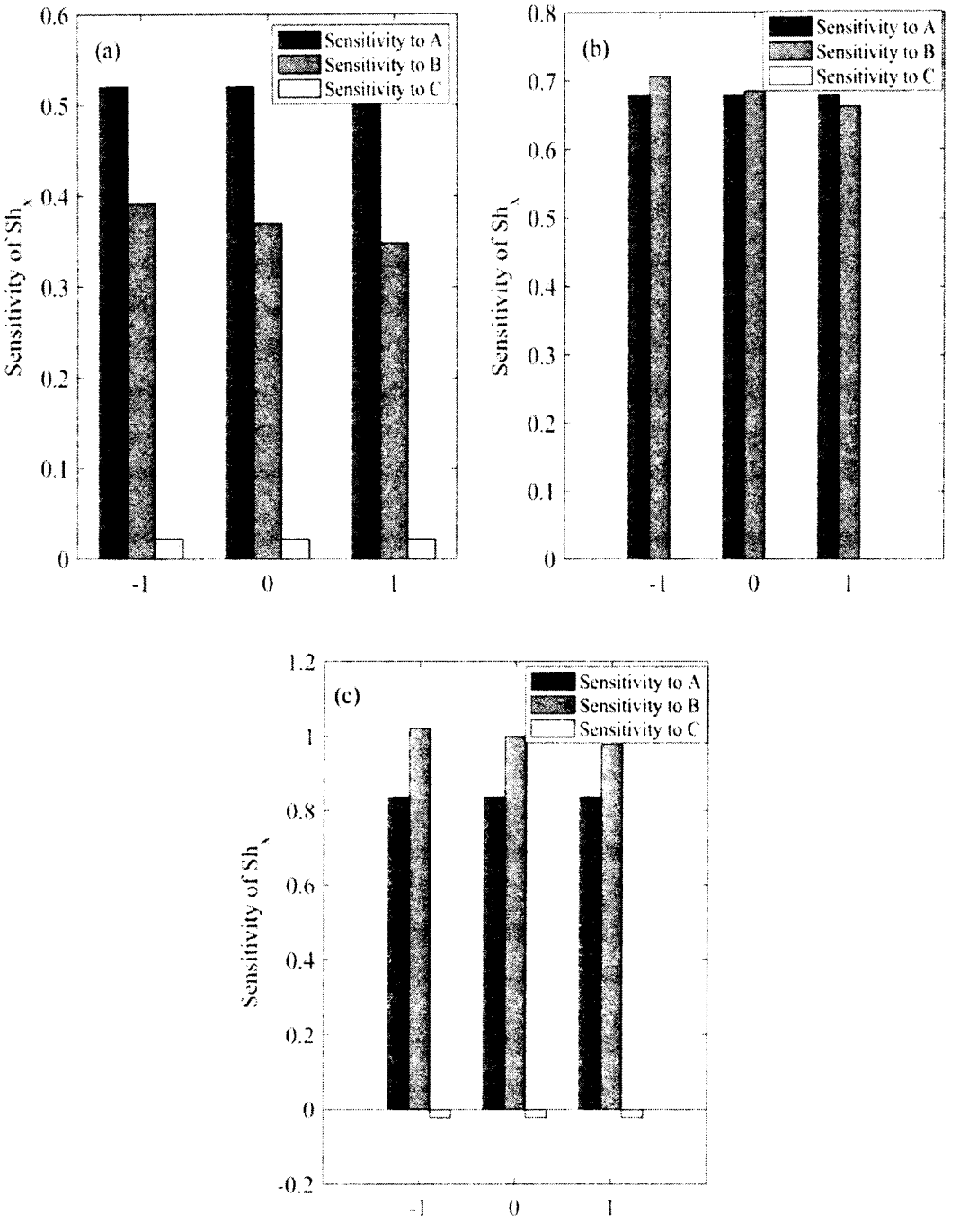

Figure 11.1: Sensitivity plots for output responses Sh_x when $A=0$

(a) $B= -1$ (b) $B=0$ (c) $B=1$.

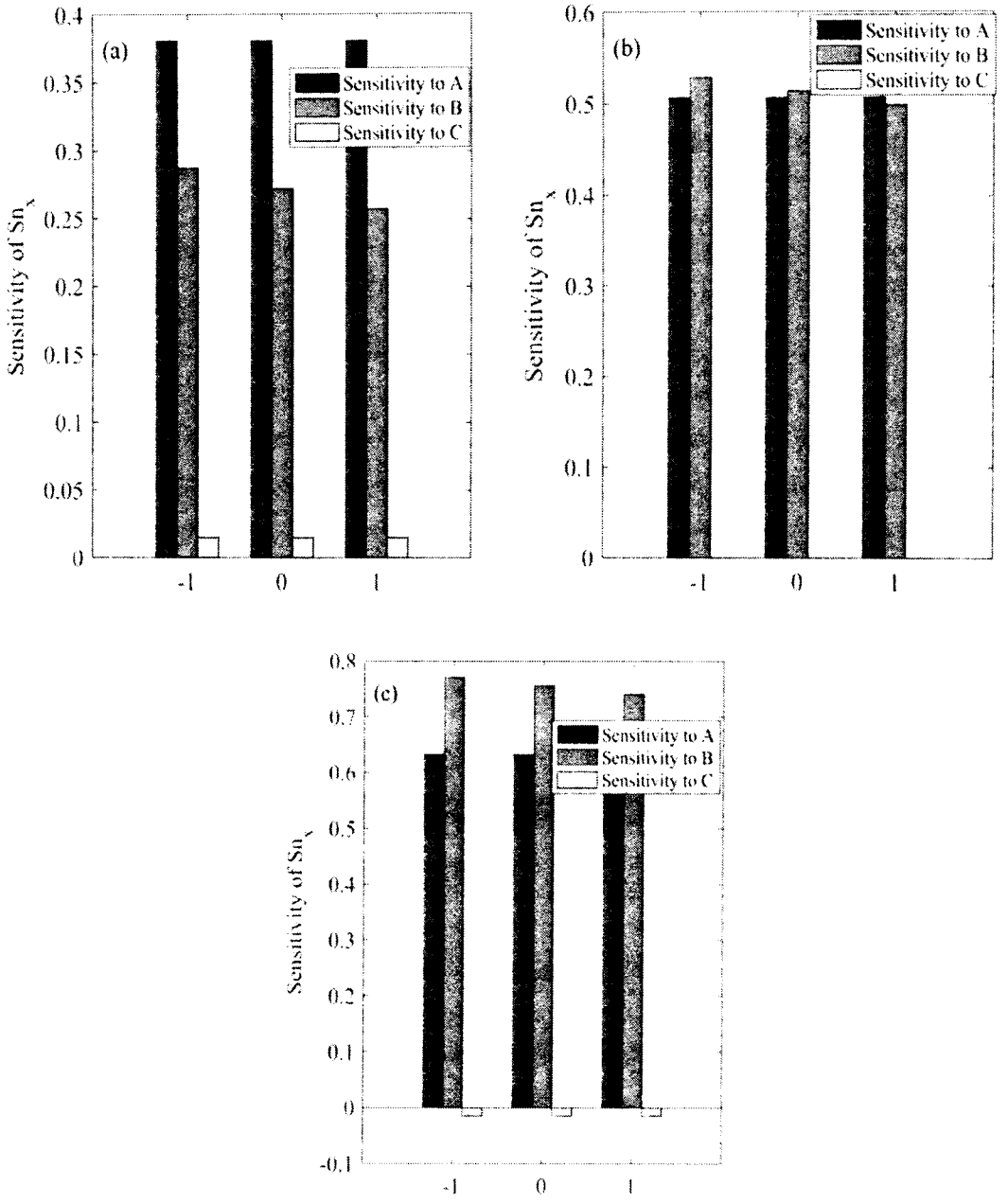

Figure 11.2: Sensitivity plots for Sn_x when $A=0$ (a) $B=-1$ (b) $B=1$ (c) $B=1$.

11. 4 Discussion of the Results

In this section the sensitivity analysis and empirical development of Gyrotactic flow of a nanofluid with activation energy over a wedge is discussed. To perform sensitivity analysis of output responses, a numerical data is need. So, we have computed a numerical solution of non-linear ODEs in Eqns. (11.12 – 11.16) along with associated boundary conditions. These numerical results are compared with already existing work and found correct. By using RSM a correlation is developed in

terms of input parameters and output response which is described in Eqns. (11.23 – 11.24). By using these equations sensitivity analysis is performed and graphical results are displayed in Fig. 11.1 and Fig. 11.2.

The sensitivity of input parameters *Sc*, *Kr* and *Nb* against output responses Sh_x and Sn_x are plotted in Fig.4 and Fig. 5. The bar graph denotes the sensitivity of input parameters. As the height of bar graph increases the sensitivity of input factors is high. The sensitivities of Sh_x for parametric variation is illustrated in Fig. 11.1. From Fig. 11.1(a-c) it is clear that sensitivity of Sh_x for input parameters *Sc* and *Kr* are positive for all levels and each case. This means that by raising the input factors *Sc* and *Kr* the output responses Sh_x also increases for all cases and levels. The effect of sensitivity of *Nb* is positive in first case but negative in last case but it has no effect of *Nb* on Sh_x in case of $A=0$, $B=0$ which can be observed in Fig. 11.1(a-c). Also it is clear that Sc is most sensitive as compare to *Kr* and *Nb* in case of $A=0$ and $B=-1$ which is depicted in Fig. 11.1(a). And Kr is most sensitive among other parameters for the case $A=0$, $B=0$ and $A=0$, $B=+1$, which can be seen in Fig. 11.1(b) and Fig. 11.1(c) respectively.

The sensitivity of output response Sn_x for parametric variation is plotted in Fig. 11.2. From Fig. 11.2(a-c) it is clear that sensitivity of Sn_x for input parameters *Sc* and *Kr* are positive for all levels and each case. The effect of sensitivity of *Nb* is positive in first case but negative in last case but it has no effect of *Nb* on Sh_x in case of $A=0$, $B=0$ which can be observed in Fig. 11.2(a-c). Also it is clear that *Sc* is most sensitive as compare to *Kr* and *Nb* in case of $A=0$ and $B=-1$ which is depicted in Fig. 11.2(a). And *Kr* is most sensitive among other parameters for the case $A=0$, $B=-1$ and $A=0$, $B=+1$, which can be seen in Fig. 11.2(b) and Fig. 11.2(c) respectively.

Fig. 11.3 and Fig. 11.4 illustrate the residual plots for the $Sh_x$and Sn_x respectively. When the residuals are compared to the fitted values, a strong relationship is revealed. Fig. 11.3(a) and 11.4(a) shows the scatter plot for output responses Sh_x and Sn_x. Scatter plot shows the connection between the input variables and output responses. Fig. 11.3(a) and 11.4(a) demonstrates the strong connection between the input variables and output responses (Nu_x and Sh_x). The histogram in Fig. 11.3(b) and 11.4(b) has the symmetrical scattering and less skewed which demonstrates the good relationship of Nu_x and Sh_x with input parameters. Fig. 11.3(c) and 11.4(c) depicted

the observation order verses residuals for Nu_x and Sh_x respectively. The outcomes also demonstrate that if observation order is increased, the residual of the output responses drops, demonstrating good agreement between the probabilities plots. The residuals graph shows the largest fluctuation for both Nu_x and Sh_x indicates that the model is correct.

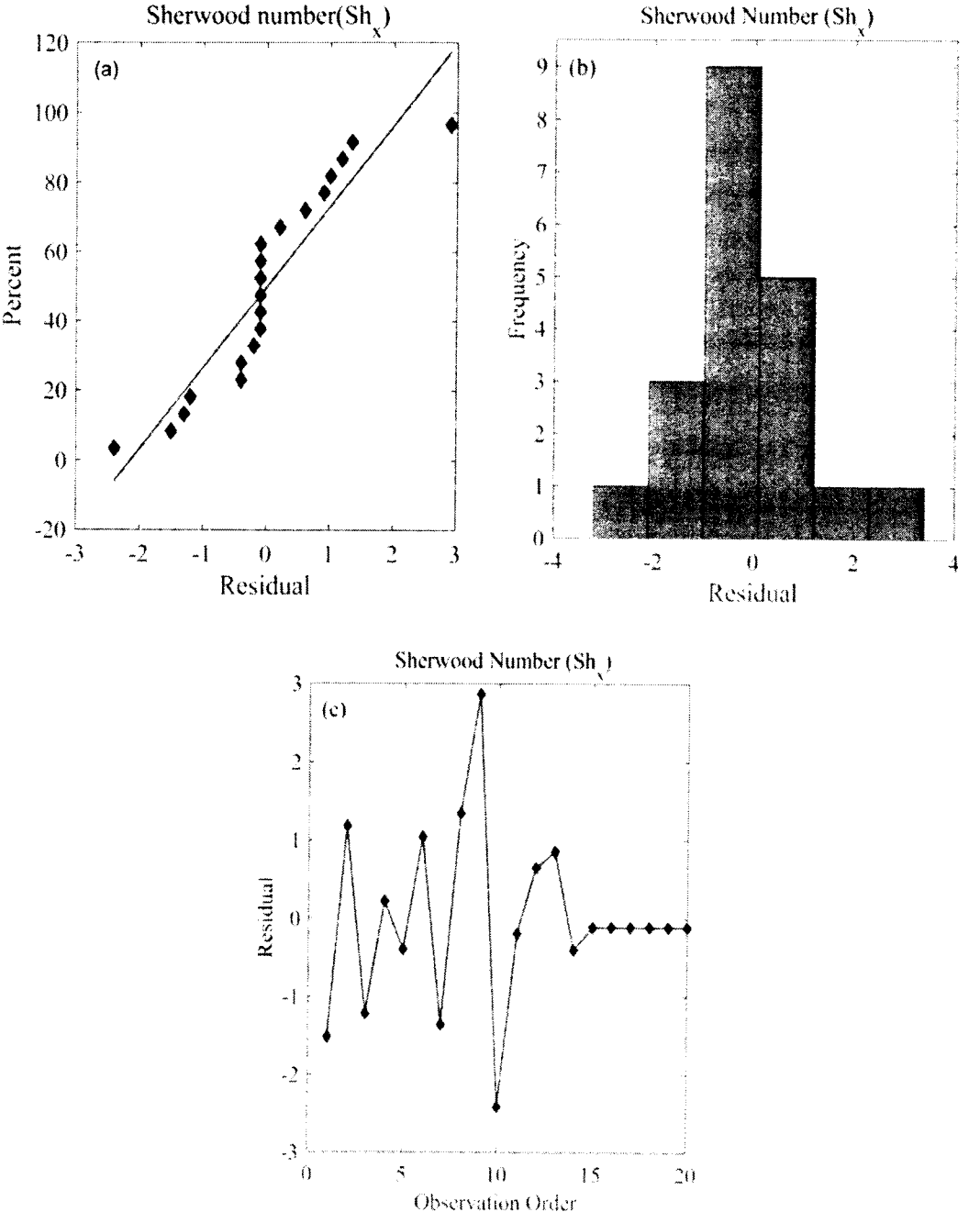

Figure 11.3: Residual plots for output responses Sh_x (a) Normal probability (b) Histogram (c) Residual plot.

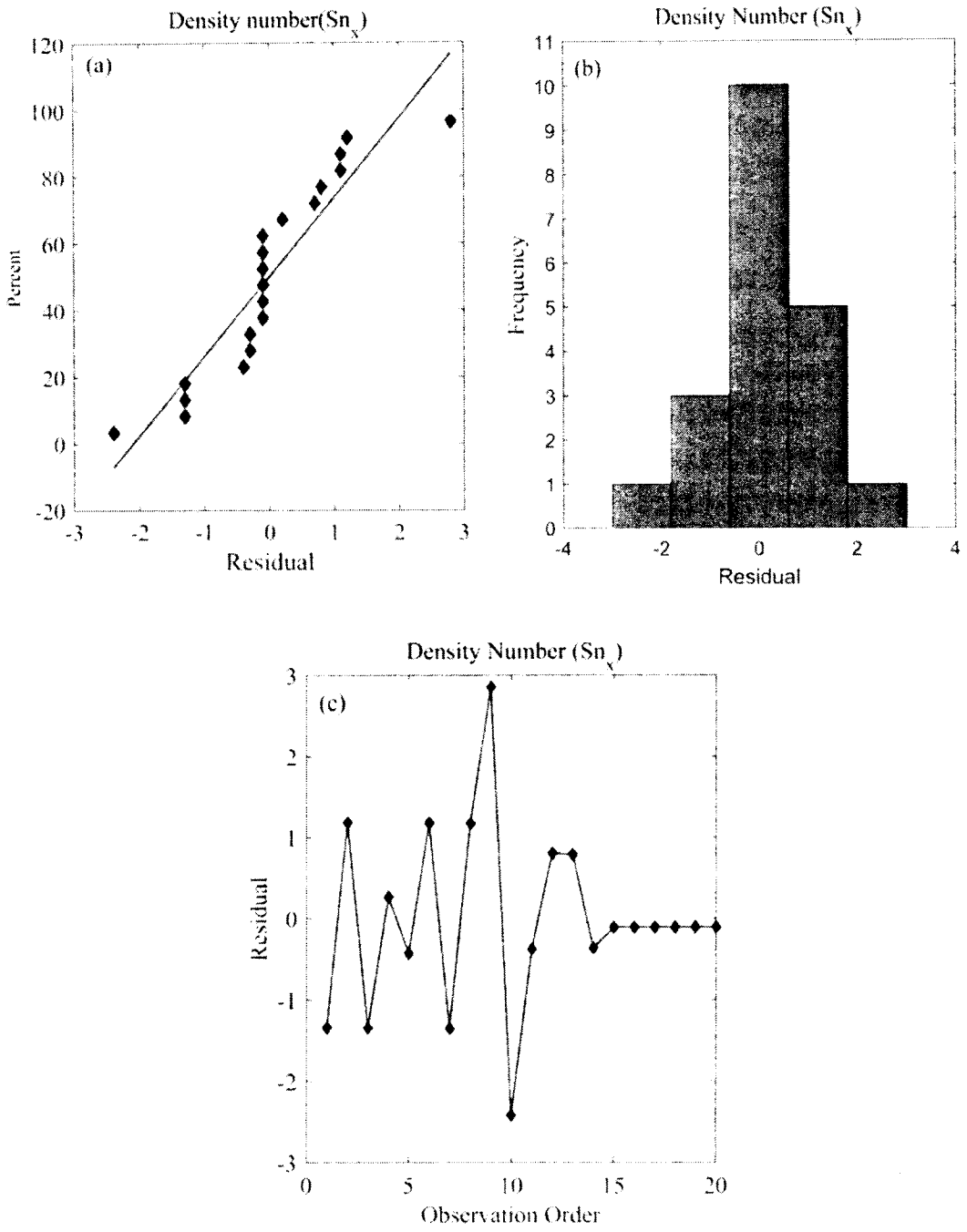

Figure 11.4: Residual plots for Sn_x (a) Normal probability (b) Histogram (c) Residual plot.

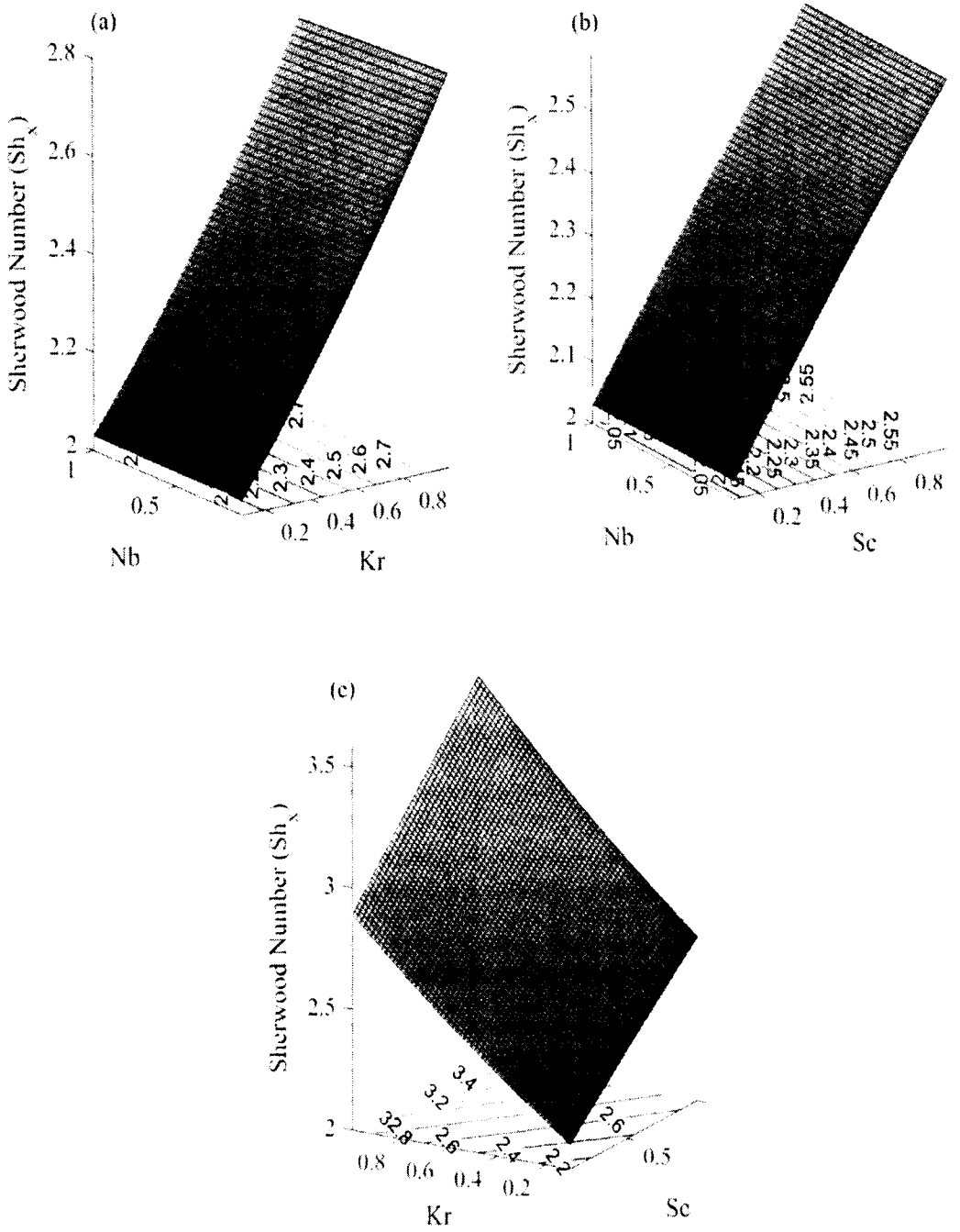

Figure 11.5: Contour plots for output responses Sh_x when

(a) $A=0$ (b) $B=0$ (c) $C=0$.

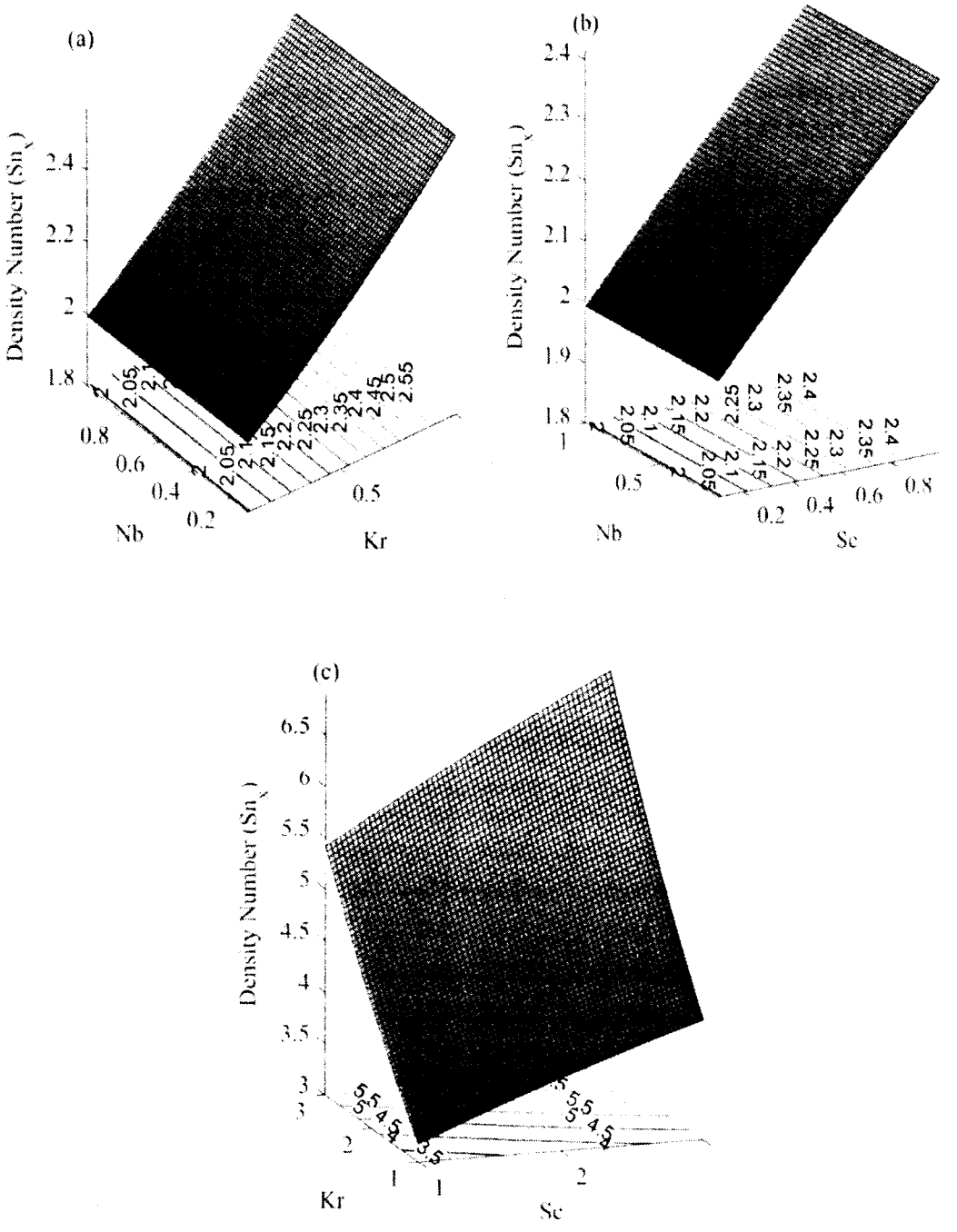

Figure 11.6: Contour plots for output responses Sn_x when (a) $A=0$ (b) $B=0$ (c) $C=0$.

The contour plots of output responses (Sh_x and Sn_x) against the input parameters (*Sc*, *Kr* and *Nb*) are plotted in Fig. 11.5 and Fig. 11.6. Fig. 11.5(a) shows the interaction of input parameters *Kr* and *Nb* on output response Sh_x. This figure demonstrates that minimum Sh_x occurs at lower level of *Kr* and higher level of *Nb*. Since the surface has symmetrical shape towards the input parameters *Kr* and *Nb*, so both the input

parameters have equally affected on output response Sh_x. The same results can be drawn for the input parameters *Sc* and *Nb* which can be seen in Fig. 11.5(b). Again both the input factors have equally affected on Sh_x. It is also observed that, Sh_x occurs minimum at lower level of *Sc* and higher level of *Nb*. The effect of *Sc* and *Kr* are demonstrated in Fig. 11.5(c). It is concluded that maximum Sh_x follows at high level of *Sc* and *Kr* and by increasing the *Sc* and *Kr* the Sh_x also increases. The results for output response Sn_x, depicted in Fig. 11.6(a-c) is same as the results concluded from Fig. 11.5(a-c) respectively.

Chapter 12

Viscous Fluids Flowing over a Wedge with Heat Transfer

In this chapter the sensitivity analysis of viscous flow over a wedge with thermal effect is studied numerically and statistically. The PDEs are transformed into non-linear ODEs by using similarity transformations, and these transformed ODEs are solved with the help of MATLAB's built-in code bvp4c. The numerical outcomes are compared with [99-102] and were found to be correct. Then, using RSM a correlation between the independent parameters and dependent output responses are developed. Sensitivity analysis is performed and the results are shown using tables and graphs.

12.1 Mathematical Formulation

Consider a steady, two dimensional, laminar boundary layer viscous flows flowing over a wedge with heat transfer. The governing boundary layer equations for continuity, momentum and energy equation for aforementioned assumptions are follows as [99],

$$\frac{\partial u}{\partial x}+\frac{\partial v}{\partial y}=0, \tag{12.1}$$

$$u\frac{\partial u}{\partial x}+v\frac{\partial u}{\partial y}=U_e\frac{dU_e}{dx}+\frac{1}{\rho}\frac{\partial}{\partial y}\left(\mu\frac{\partial u}{\partial y}\right), \tag{12.2}$$

$$u\frac{\partial T}{\partial x}+v\frac{\partial T}{\partial y}=\kappa\frac{\partial^2 T}{\partial y^2}. \tag{12.3}$$

The corresponding boundary conditions for the problem is given by

$$u=0, v=0, T=T_w \ at \ y=0, \tag{12.4}$$

$$u=U_e(x)=x^m, T=T_\infty \ as \ y\to\infty \tag{12.5}$$

The stream function are given as

$$u=\frac{\partial \psi}{\partial y} \text{ and } v=-\frac{\partial \psi}{\partial x}. \tag{12.6}$$

The similarity transformation are followed by [99],

$$\eta = y\sqrt{\frac{m+1}{2v}}x^{\frac{m-1}{2}}, \psi = \sqrt{\frac{2v}{m+1}}x^{\frac{m+1}{2}}f(\eta), \tag{12.7}$$

$$\theta = \frac{T-T_\infty}{T_w-T_\infty}. \tag{12.8}$$

By using the similarity transformation in Eqn. (12.7) and (12.8), the Eqn. (12.2) to Eqn. (12.4) may be written as,

$$f''' + ff'' + \frac{2m}{m+1}(1-f'^2)=0, \tag{12.9}$$

$$\frac{1}{Pr}\theta'' + f\theta' = 0. \tag{12.10}$$

Where $Pr = {}^{\nu}/_{\kappa}$ and the boundary conditions in Eqn. (4) and Eqn. (5) becomes,

$$f'(\eta) = 0, f(\eta) = 0, \theta = 1 \; at \; \eta \to \infty, \tag{12.11}$$

$$f'(\eta) = 1, \theta = 0 \; at \; \eta \to \infty. \tag{12.12}$$

The comparison table for numerical values of Cf_x and Nu_x obtained by bvp4c with existing work are showed in Table 12.1 and Table 12.2 respectively.

Table 12.1: Comparison table for Cf_x for various values of m.

m	[99]	[100]	Present results
-0.05	0.2135	0.2138	0.2135
0	0.3320	0.3322	0.3321
0.33	0.7574	0.7575	0.7543
1	1.2325	1.2327	1.2326

Table 12.2: Comparison table for Nu_x for various values of Pr.

Pr	[101]	[102]	Present results
0.01	0.0515	0.0515	0.0515
1	0.3320	0.3320	0.3321
10	0.7281	0.7281	0.7281
100	1.5718	1.5718	1.5718
1000	3.3871	3.3870	3.3871
10000	7.274	7.2974	7.2975

12.2 Experimental Design

12.2.1 Response Surface Methodology

In this chapter, the experimentation parameters are Falkner–Skan exponent (m) and the Prandtl number (Pr). Table 12.3 shows these factors and their values of low (-1), central (0), and high (+1). RSM requires thirteen runs and twelve degrees of freedom corresponding to two different parameters. In this study, the experimentation parameters are Falkner–Skan exponent (m) and the Prandtl number (Pr). The experimental design for these input parameters and output responses are displayed in Table 12.4. The correlations of Cf_x and Nu_x can be stated in the following general manner in terms of input parameters.

$$Cf_x = \alpha_0 + \alpha_1 A + \alpha_2 B + \alpha_{12} AB + \alpha_{11} A^2 + \alpha_{22} B^2 , \tag{12.13}$$

$$Nu_x = \gamma_0 + \gamma_1 A + \gamma_2 B + \gamma_{12} AB + \gamma_{11} A^2 + \gamma_{22} B^2 , \tag{12.14}$$

where α_i ,α_{ij}, γ_i and γ_{ij} are unknown coefficients that need to be found using RSM.

Table 12.3: Symbols and levels of input factors.

Type	Factor	Symbol	Levels		
			-1	0	+1
Input Factors	m	A	0	0.5	1
	Pr	B	0	5000	10000

Table 12.4: Experimental design with coded and real values.

Experiment number	Point type	Coded values		Real values		Responses	
		A	B	m	Pr	Cf_x	Nu_x
1	Factorial	-1	-1	0.0	0.0	0.3321	0.1250
2		1	-1	1.0	0.0	1.2326	0.1250
3		-1	1	0.0	10000.0	0.3321	7.2975
4		1	1	1.0	10000.0	1.2326	22.8706
5	Axial	-1	0	0.0	5000.0	0.3321	5.7920
6		1	0	1.0	5000.0	1.2326	18.1356
7		0	-1	0.5	0.0	0.8997	0.1250
8		0	1	0.5	10000.0	0.8997	16.9349
9-13	Centre	0	0	0.5	5000.0	0.8997	13.4285

12.2.2 Analysis of Variance (ANOVA)

To get the optimal polynomial correlations for the responses (Cf_x and Nu_x), multiple regressions are utilised. ANOVA is used to assess the regression model's fit with thirteen runs which is displayed in Table 12.4. Table 12.5 and Table 12.6 displays all of the statistical estimators generated using the ANOVA method. Each of the Eqn.(12.13) and Eqn. (12.14) has its own F-value and P-value. The variance of the data is calculated using the F-value. If the F-value is greater the 1 then we will consider the input data is accurate. Table 12.6 shows the statistical estimated

regression coefficients for the simplified models of Cf_x and Nu_x. The ANOVA shows the results of $R^2 = 100\%$ and $Adj\ R^2 = 100\%$ for Cf_x and $R^2 = 98.73\%$ and $Adj\ R^2 = 97.82\ \%$ for Nu_x. These Results show the best correlation between input parameters and output responses

Table 12.5: ANOVA for (a) Cf_x (b) Nu_x.

Source	DF	Adj SS	Adj MS	*F*-Value	*P*-Value	
(a)						
Model	5	1.26084	0.25217	*	*	Significant
Linear	2	1.21635	0.60818	*	*	-
Square	2	0.04449	0.02225	*	*	-
Interaction	1	0.00000	0.00000	*	*	
Error	7	0.00000	0.00000	*	*	
Lack-of-Fit	3	0.00000	0.00000	*	*	Significant
Pure Error	4	0.00000	0.00000	*	*	-
Total	12	1.26084				-
(b)						
Model	5	642.378	128.467	108.82	0.000	Significant
Linear	2	493.808	246.904	209.12	0.000	-
Square	2	87.840	43.970	37.24	0.000	-
Interaction	1	60.630	60.630	51.35	0.000	-
Error	7	8.265	1.181			-
Lack-of-Fit	3	8.265	2.755	*	*	Significant
Pure Error	4	0.000	0.000			-
Total	12	650.643				-

Table 12.6: ANOVA Regression coefficients of responses for (a) Cf_x (b) Nu_x.

Terms	Coefficient	*P*-value	Significant
(a)			
Constants	0.8997	0	Yes
A	0.4502	0	Yes
B	0.0000	0	Yes
A^2	-0.1174	0	Yes
B^2	0.0000	0	Yes
AB	0.0000	0	Yes
	$R^2 = 100.00\%$		$Adj\ R^2 = 100.00\%$
(b)			
Constants	13.354	0.000	Yes
A	4.653	0.000	Yes
B	7.788	0.000	Yes
A^2	-1.204	0.108	No
B^2	-4.638	0.000	Yes
AB	3.893	0.000	Yes
	$R^2 = 98.73\%$		$Adj\ R^2 = 97.82\%$

12.3 Sensitivity Analysis

The sensitivity of the $Cf_x$and Nu_x to m and Pr has investigated in this chapter. The regression coefficients for Cf_x and Nu_x are shown in Table 12.6. By using Table 12.6, mathematical Eqns. (12.13 and 12.14) may be rewritten as follows,

$$Cf_x = 0.8997 + 0.4502A - 0.1174A^2, \qquad (12.15)$$

$$Nu_x = 13.354 + 4.653A + 7.788B + 3.893AB - 4.638B^2 . \quad (12.16)$$

The sensitivity functions developed below can be used to calculate the rising or falling trend of the responses with regard to the input parameters A and B.

$$\frac{\partial}{\partial A}(Cf_x) = 0.4502 - 0.2348\,A \quad (12.17)$$

$$\frac{\partial}{\partial B}(Cf_x) = 0, \quad (12.18)$$

$$\frac{\partial}{\partial A}(Nu_x) = 4.653+3.893\,B, \quad (12.19)$$

$$\frac{\partial}{\partial B}(Nu_x) = 7.788+3.893\,A - 9.276\,B. \quad (12.20)$$

The sensitivity of various values of m and Pr is tested. Table 12.7 shows the sensitivity of the output responses Cf_x and Nu_x to changes in m and Pr. The response variables increase as by increasing the bar chart in positive direction and vice versa. As the height of the bar chart rises, the reaction becomes more sensitive to the variable. The sensitivity plots are depicted in Fig. 12.1.

Table 12.7: Sensitivity analysis of Cf_x and Nu_x.

A	B	$\partial Cf_x/\partial A$	$\partial Cf_x/\partial B$	$\partial Nu_x/\partial A$	$\partial Nu_x/\partial B$
-1	-1	0.685	0	0.76	13.171
	0	0.685	0	4.653	3.895
	1	0.685	0	8.546	-5.381
0	-1	0.4502	0	0.76	17.064
	0	0.4502	0	4.653	7.788
	1	0.4502	0	8.546	-1.488
1	-1	0.2154	0	0.76	20.975
	0	0.2154	0	4.653	11.681
	1	0.2154	0	8.546	20.957

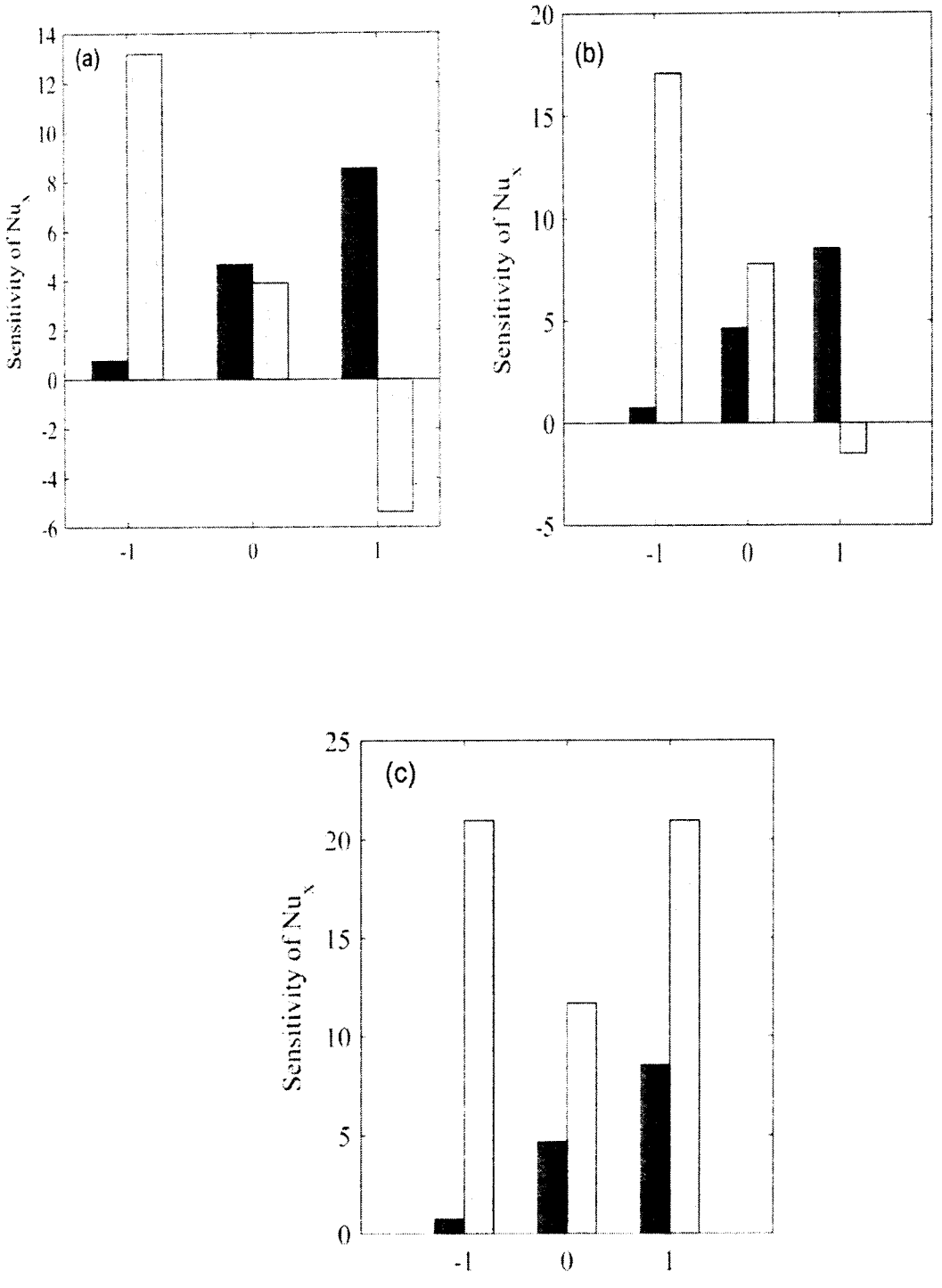

Fig. 12.1: Sensitivity plots for Nu_x

12.4 Discussion of the Results

This section is intended for discussion of the results obtained for sensitivity analysis and empirical development of viscous flow via a wedge using RSM. Matlab's built-in software bvp4c are used to compute a numerical solution of the problem. The results of Cf_x and Nu_x were then compared to previously published work and showed good agreement, as shown in Tables 12.1 and 12.2. The primary focus of this research is to perform sensitivity analysis of $Cf_x$and Nu_x for the parameters m and Pr. To accomplish this goal, we created expressions for Cf_x and Nu_x and used RSM to construct the equations of output responses which are described in Eqns. (12.15 and 12.16).

To perform sensitivity analysis, empirical relationships between output variables and input factors must be developed. Empirical development is an effective method for determining correlations between output/response variables and input factors. It is important in numerous experimental investigations to create empirical models for nanomaterial viscosity and thermal conductivity ratios. By using RSM we have calculated the values of responses using regression models fitted to thirteen runs which is shown in Table 12.4. Table 12.5 shows the ANOVA table for both Cf_x and Nu_x along with the corresponding F-value and P-value. The regression coefficients for Cf_x and Nu_x are shown in Table 12.6. The P-value is used to determine which terms are preserved and which are ignored. A P-value of less than 0.05 is required for empirical development subsequently, it will be ignored.

Fig. 12.1 displayed the sensitivity plots of Nu_x for different parameters such as m and Pr. Fig. 12.1(a) to Fig. 12.1(c) displays the positive sensitivity of $Nu_x$to m and mixed behaviour to Pr. Which means that the sensitivity of Nu_x increases as by increasing m and the sensitivity of Nu_x decreases as by increasing m at its high level (viz Fig.12.1 (a-b)). It is also worth mentioning that Pr is more sensitive to Nu_xthan m. From Table 12.7 it is clear that Sensitivity of Cf_x only depends upon m as the partial derivative to Pr is zero throughout the column. Which means that Cf_x is independent to Pr.

The residual plots for Nusselt number are shown in Fig. 12.2. When the residuals are matched to the fitted values its shows a strong connection. Fig. 12.2(a) shows the scatter plot of Nu_x. The figure demonstrates the strong connection between the input

variables and output responses. The histogram in Fig. 12.2(b) has the symmetrical scattering and less skewed which demonstrates the good relationship of Nu_x with input parameters. Fig. 12.2(c) depicted the observation order verses residuals. The outcomes also demonstrate that if observation order is increased, the residual of the Nu_xdrops. These residual plots show good relationship between input parameters and output responses, and also demonstrate good fit of empirical model.

It is important to note that normal plot of effects of Cf_x is not presented because the normal error for effects is zero. So the histogram of residual verses frequency could not also draw because error is zero for Cf_x. It is also noted that the mean square error is equal to zero which means the degrees of freedom for error is zero so therefore no graph of residual for Cf_xwill formed. The results are displayed in Table 12.5(a) and Table 12.6(a).

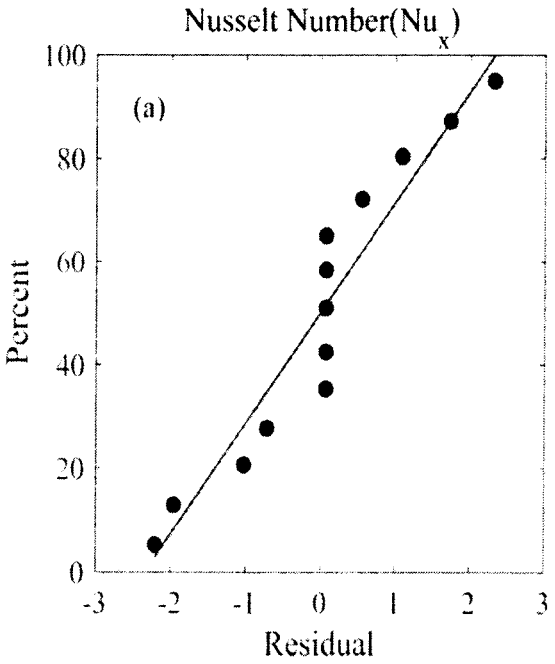

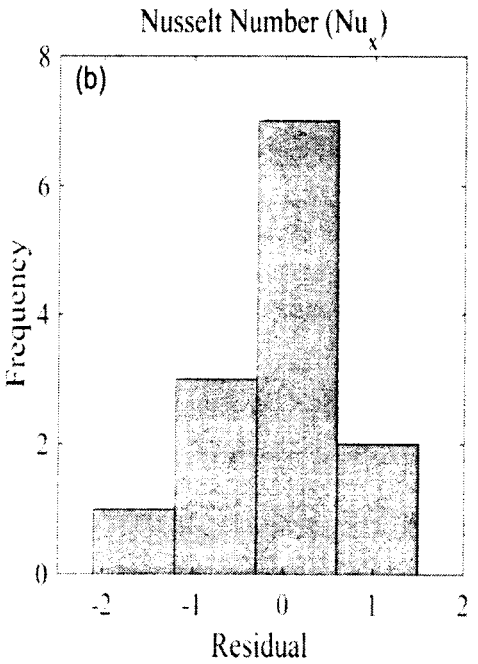

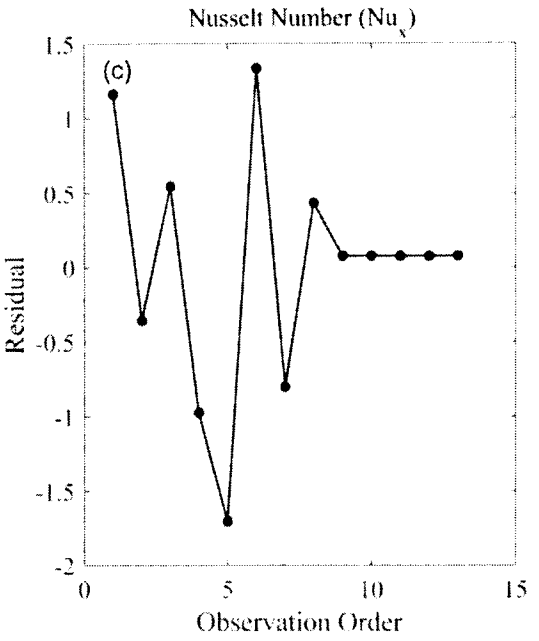

Fig. 12.2: (a) Normal probability plot (b) histogram (c) residuals for Nu_x.

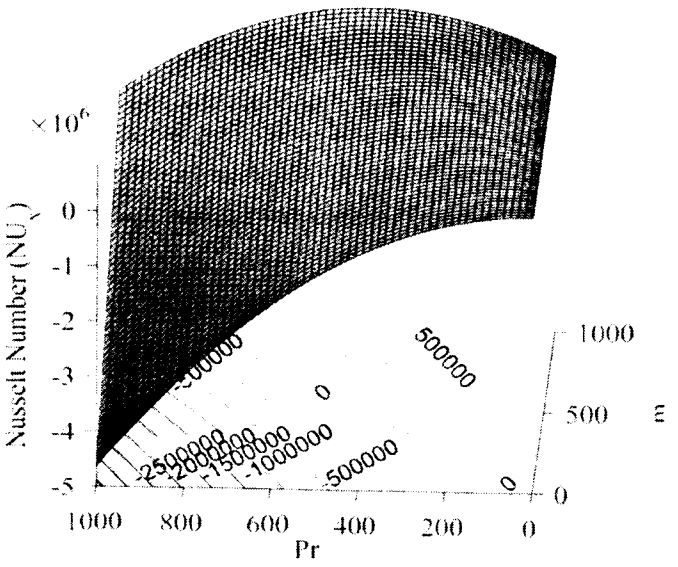

Fig. 12.3: Contour plot for Nu_x.

The contour plots of Nu_x is displayed in Fig. 5. From the figure it is noted that maximum Nu_x arises near low and middle level of *Pr*. And the effect of *m* on Nu_x is negligible.

Chapter 13

Conclusion and Future Work

This chapter summarizes the main findings of each chapter and the future work.

13.1 Conclusion

The aim of this thesis is to accomplish sensitivity analysis of fluid flow over a wedge. To perform sensitivity analysis we first transformed the Partial Differential Equation (PDEs) into a set of non-linear ODEs by using a suitable similarity transformation. The transformed Odes are then solved with the help of MATLAB's built in software bvp4c and compared the obtained numerical results with existing work and found excellent agreement. The numerical values are then used to calculate the data to correlate the input variables and output responses. By using a statistical software MINITAB-19 ANOVA tables are generated in each chapter and developed the correlations between input parameters and output responses. Also, the residual plots are represented in each chapter to show the validity of correlated functions. Finally, sensitivity analysis is performed and results are shown using tables and graphs.

As the first chapter is some basic definitions related to current work, literature review, research motivation and objectives. Chapter 2 comprises methodology, experimental technique, RSM, ANOVA, Sensitivity analysis and geometry of the problem. Chapter 3 and onward, the main published and submitted work is discussed. The conclusion of chapter 3 and onward is summarized as follows;

13.1.1 Conclusion of chapter 3

In chapter 3 the sensitivity analysis of viscous incompressible fluid flow through a wedge surface has been investigated. The governing nonlinear PDE are converted into local non-similarity boundary layer equations using suitable similarity transformations. After that, the solution is derived by combining the perturbation approach with the MATLAB's built-in code bvp4c. The values of Cf_x and Nu_x are computed for various parametric values using a numerical approach on nonlinear ODEs. The solution is then compared by the existing values which show excellent agreement. The numerical findings are then subjected to a sensitivity analysis to

determine the output responses dependency on the various controlling factors. The outcomes are as follows:

- R^2 and $Adj\,R^2$ have large values, indicating that the independent input parameters and output responses are perfectly correlated.
- The highest residuals among all responses are observed to be in the proximity of 0.25 and 0.075 for the Cf_x and Nu_x respectively.
- As ξ value is increased, the sensitivity of Cf_x increases.
- The sensitivity of the Cf_x decreases by increasing ε.
- There is no influence of thermal conductivity radiations on Cf_x.
- By increasing the values of the ξ, Cf_x becomes more sensitive to γ.
- The sensitivity of the Nu_x rises as the controlling parameter, namely the ξ increases, but it decreases for γ.
- For all levels of γ, there is no influence on the sensitivity of the ε.
- For three distinct ξ values and all γ levels, Nu_x is more sensitive to the ε.
- From the 3D plots it is found that, minimum Cf_x occurs for the low level of ξ and high level for ε.
- Minimum Cf_x occurs for lower level of ξ and higher level of γ whereas maximum value is achieved for high level of ξ and low level of γ.
- Cf_x is minimum for higher level of both ε and γ however Cf_x is maximum near lower level of ε and high level of γ.
- The Nu_x decreases near the higher level of γ for $A=0$.
- Finally it is concluded that maximum Nu_x occurs for higher level of ξ and lower level of γ and minimum Nu_x occurs near lower level of ξ and higher level of γ.

13.1.2 Conclusion of chapter 4

The sensitivity analysis and empirical development of transport performance quantities of flow of tangent hyperbolic nanofluid over a wedge has been investigated numerically and statistically. Using appropriate similarity transformations, the governing PDEs are converted into systems of non-linear ODEs. The numerical findings are then obtained by using Matlab built in routine bvp4c. Then perform

sensitivity analysis for the output responses Cf_x, Nu_x and Sh_x by using the numerical values for different input parameters. The outcomes are gives as follows:

- The high value of R^2 and $Adj\ R^2$ shows the strong correlation between input and output variables.
- Cf_x is more sensitive to *We* when compared to *Nt* and *Nb*.
- Fig. 2 leads to the conclusion that sharp changes in Nu_x occurs with the variation in *Nt*. Therefore Nu_x is most sensitive to *Nt*.
- Sh_x is most sensitive to *Nb*. Moreover, the sensitivity function for Sh_x against *Nb* changes sign which implies by intermediate value theorem that Sh_x will have a critical value against *Nb*.

Then we have developed empirical relations for response variables Cf_x, Nu_x and Sh_x from numerical data of input and response variables using Response Surface Methodology (RSM).

- From level surfaces of Cf_x against variation of *Nt* and *Nb* it can be concluded that optimum value occurs at low levels of *Nt* and *Nb*.
- The level surface of Cf_x for $B = 0$ one can see that maximum value of Cf_x occurs near high levels of *We* and *Nb*.
- Fig. 4.7 (c) shows that level surface of Cf_x for $C = 0$ *Nb* has its minimum value for low level of *We* and *Nt*.
- Fig. 4.8(a)-(c) represent the level surfaces for Nu_x at $A = 0, B = 0$ and $C = 0$ respectively. It is observed that Nu_x is maximum for low levels of *Nt* and *Nb*.
- Nu_x is maximum for lower levels both *We* and *Nb*.
- Nu_x is maximum at lower level of *Nt* and higher level of *We*.
- The level surface for Sh_x at $A = 0$ shows that it achieves maximum value at high levels of *Nt* and *Nb*.

13.1.3 Conclusion of chapter 5

The numerical and sensitivity analysis of flow of non-Newtonian Casson fluid past a wedge by using RSM has been investigated. The non-linear ODEs with boundary conditions are solved by using MATLAB built in routine bvp4c. The acquired results are then compared with existing work and excellent agreement is formed. Then by

using the numerical results sensitivity analysis is performed by using RSM. The outcomes are as follows:

- The large values of R^2 and $Adj\ R^2$ shows the strong correlation between independent input parameters and output responses.
- The sensitivity of Cf_x increases as by increasing Falkner-Skan exponent (m) and decreases by increasing Casson fluid parameter β.
- The sensitivity of Cf_x is increases by increasing the parameters β and m.
- Nu_x is most sensitive to Pr.
- The sensitivity of Cf_x is not effected by Pr.
- For the case $A = 0$ and $B = 1$ by increasing the parameter β the Cf_x also increases and by increasing the parameter m the Cf_x decreases.
- Maximum Cf_x occurs near high level of both β and m.
- Nu_x is minimum for low levels of m and Pr.
- Fig. 5.6(b) displays that Nu_x is minimum for high levels both β and Pr.
- From Fig.5.6(c) we infer that Nu_x is minimum at low level of m and β

13.1.4 Conclusion of chapter 6

The sensitivity analysis and empirical development of magneto-Carreau fluid across a wedge by using RSM is investigated in this chapter. To accomplish this aim the non-linear ODEs [82] are adopted and solve these non-linear ODEs by using MATLAB built in package bvp4c. To check the validity of our numerical results we have compared these numerical values with already existing work [82- 86] and found correct. By using RSM we have find the correlation model for output responses Cf_x and Sh_x. The ANOVA tables and regression of coefficients are generated by using statistical software MINITAB-19. Also, to check the validity of correlated models residuals are plotted in graphical form and found a strong correlation between input parameters and output responses (Cf_x and Sh_x). Finally, sensitivity analysis is performed and showed the results in graphical form and concluded the important results as,

- Cf_x is positive sensitivity to Ha and β and negative sensitivity to We.
- Cf_x is most sensitive to We.

- γ is most sensitive to Sh_x at low and middle level and Sc is most sensitive for high level.
- Cf_x is maximum for upper level of Ha and β.
- Cf_x occurs maximum at lower level of We and upper level of β.
- Cf_x occurs maximum at lower level of We and upper level of Ha.
- Sh_x occurs maximum at a upper level of Sc and γ.
- Sh_x occurs maximum at a upper level of Ha and γ.
- Sh_x occurs maximum at upper level of Ha and Sc.

13.1.5 Conclusion of chapter 7

The sensitivity analysis of the empirical development of Carreau fluid with shear rate viscosity across a wedge by using RSM has been investigated numerically. To obtain this objective, first of all the numerical values of Cf_x and Nu_x are obtained by using Matlab software bvp4c and compared these numerical values by [87] and displayed good results. RSM is applied to define the correlation between input factors and output responses by using statistical software MINITAB-19. Then, using ANOVA regression of coefficients and residuals errors are calculated. These hybrid numerical and statistical values are utilized to perform sensitivity analysis of different independent input parameters on dependent output responses. The important results are as follows:

- The ANOVA shows higher values of R^2 and $Adj\ R^2$ for Cf_x and Nu_x which shoes a strong correlation between input factors and output responses.
- The straight line of normal probability plots of Cf_x and Nu_x proved that data is normal.
- Sensitivity of Cf_x increases as by increasing We.
- Sensitivity of Cf_x decreases as by increasing the value of γ.
- We is most sensitive for Cf_x.
- Nu_x increases by increasing the value of γ and Pr.
- Pr is most sensitive for Nu_x.
- Cf_x is minimum for high levels (+1) of We and γ.
- Nu_x is maximum at lower level of Pr and higher level of We and minimum at higher level of Pr and lower level of We .

- Nu_x is maximum at lower level of γ and higher level of Pr and minimum at higher level of γ and lower level of Pr.
- Nu_x is maximum for higher levels and minimum for lower levels of γ and We.

13.1.6 Conclusion of chapter 8

The sensitivity analysis for wall heat and concentration flux of Falkner-Skan Casson fluid flow has been investigated in this chapter. To obtain this objective first of all the numerical values of Nu_x and Sh_x are calculated by using Matlab software bvp4c and compared these numerical values by [88-90] and displays good results. The model for the correlation between input parameters and output responses are developed by using RSM. Then using ANOVA, regression of coefficients and residuals errors are calculated. These hybrid numerical and statistical values are utilized to perform sensitivity analysis of different independent input parameters on dependent output responses. The important results are as follows:

- The ANOVA shows higher values of R^2 and $Adj\ R^2$ for Nu_x and Sh_x which shows a strong correlation between input factors and output responses.
- The straight line of normal probability plots of Nu_x and Sh_x proved that data is normal.
- The effect of input parameters Ra and Du is negligible on Nu_x.
- Pr is most sensitive among other input parameters for Nu_x.
- Du is most sensitive to Sh_x.
- Sh_x is independent to input parameters Ra.
- Nu_x is maximum for lower level (-1) of Pr and higher level (+1) of Du.
- Nu_x is maximum for lower level (-1) of Du and higher level (+1) of Ra.
- Maximum Nu_x occurs between middle level (0) of Pr and higher level (+1) of Ra.
- Sh_x is maximum between middle level (0) of Pr and higher level (+1) of Du.
- Sh_x is maximum at higher level (+1) of Pr and lower level (-1) of Ra.

13.1.7 Conclusion of chapter 9

The sensitivity analysis of MHD Casson nano fluid flowing over a wedge with the influence of radiation by using RSM has been investigated numerically and statistically. To obtain this objective first of all we have intended the numerical values of Nu_x and Sh_x by using Matlab built in software bvp4c and matched these numerical values by [91 - 94] and displayed good results. Then, by using RSM we have made a correlation between input parameters and output responses/variables. Regression of coefficients and residual errors is also calculated with the help of ANOVA. These numerical and statistical values are employed to perform sensitivity analysis of different independent input parameters on dependent output responses. The conclusions of the detail analysis are as follows;

- The higher values of R^2 and $Adj\ R^2$ for Nu_x and Sh_x displays a strong correlation between input factors and output variables.
- The residual plots of Nu_x and Sh_x also proved that data is normal and there is a good relationship between input parameters and output responses.
- Nu_x is most sensitive to *Nt* as compare to *Le* and *Nb*.
- Sh_x is most sensitive to *Nb* as compare to *Le* and *Nt*.
- maximum Nu_x occurs at the lower levels (-1) of *Nt* and *Nb*.
- Nu_x is maximum at lower levels (-1) of input parameters *Le* and *Nb*.
- Nu_x is maximum at higher level (+1) of *Le* and lower level of *Nt*.
- Sh_x occurs maximum at lower level (-1) of *Nt* and higher level (+1) of *Nb*.
- Sh_x is maximum at low level (-1) of *Le* and high level (+1) of *Nb*.
- maximum Sh_x occurs at low level (-1) of *Le* and *Nt*.

13.1.8 Conclusion of chapter 10

In this pioneering work the sensitivity analysis of nanofluid flowing over a wedge with activation energy by using RSM has been inspected numerically as well as statistically. To obtain this objective first of all the numerical values of Nu_x and Sh_x are calculated by using Matlab software bvp4c and compared these numerical values by [95] and displayed good results which are depicted in Table 10.1 By using statistical software MINITAB-19 RSM is applied to find the correlation between input parameters and output responses/variables. Then using ANOVA regression of

coefficients and residuals errors are calculated to check the validity of correlated models. The residuals plots for Nu_x and Sh_x shows a good correlation between input parameters and output responses which can be seen in Fig.10.3 and Fig.10.4 respectively. These hybrid numerical and statistical values are used to perform sensitivity analysis. The conclusions of this pioneering work are as follows

- The high values of R^2 and $Adj\, R^2$ for output responses (Nu_x and Sh_x) depicts the strong correlation between input factors and output responses.
- The residual plots of output responses proved the good relationship between input factors and output responses.
- *Pr* is most sensitive input parameter for output response Nu_x.
- *Nb* is most sensitive input parameter for $\mathrm{Sh_x}$ in the case $B = -1, B = 0$ and *Pr* is most sensitive among others for the case $B=+1$.
- Nu_x occurs maximum near the lower level of *Pr* and *Nb*.
- Nu_x occurs maximum at upper levels of *Pr* and *Nt* also the effect of *Nt* on Nu_x at low level is negligible.
- Nu_x occurs maximum at upper level of *Nt* and lower level of *Nb*.
- Sh_x occurs maximum at upper level of *Pr* and lower level of *Nb*.
- Sh_x is maximum at lower level and upper level of *Nt* and *Pr* and minimum at middle level of *Nt* and *Pr*.
- Sh_x occurs maximum at upper level of *Nt* and lower level of *Nb*.

13.1.9 Conclusion of chapter 11

Analysis of sensitivity and empirical modelling of Gyrotactic nanofluid flow over a wedge has been investigated numerically and statistically. To accomplish this goal the numerical values of Sh_x and Sn_x are computed by using Matlab and compared these numerical values by [96-98] and displayed good results. Then, by using RSM we have designed a model between input factors and output responses which are described in Eqns. (11.23 – 11.24). To check the validity of designed models, residual errors are calculated and their graphical results are displayed in Fig. 11.3 and Fig. 11.4. These graphical results show good relationships between input factors and output responses. These numerical and statistical values are utilized to perform sensitivity analysis and the important results are as follows:

- The high values of R^2 and $Adj\,R^2$ for output responses (Nu_x and Sh_x) depicts the strong correlation between input factors and output responses.
- The straight line of normal probability plots, symmetry of histograms and less skewed of verses order of output responses (Sh_x and $Sn_{x)}$ proved that data is normal.
- *Sc* is most sensitive as compare to *Kr* and *Nb* in case of *A=0* and *B=-1*.
- *Kr* is most sensitive among other parameters for middle and upper case *B*.
- *Sc* is most sensitive as compare to *Kr* and *Nb* in case of *A=0* and *B=-1*.
- *Kr* is most sensitive among other parameters for lower and upper case of *A=0*.
- Sh_x occurs minimum at lower level of *Kr* and higher level of *Nb*.
- Sh_x occurs minimum at lower level of *Sc* and higher level of *Nb*. Sh_x occurs maximum at higher level of *Sc* and *Kr*.
- Sn_x occurs minimum at lower level of *Kr* and higher level of *Nb*.
- Sn_x occurs minimum at lower level of *Sc* and higher level of *Nb*.
- Sn_x maximum occurs at higher level of *Sc* and *Kr*.

13.1.10 Conclusion of chapter 12

The flow of empirical development of viscous fluid past a wedge by using RSM has been investigated numerically. The numerical values of Cf_x and Nu_x are calculated by using Matlab software bvp4c and then compared by [99 - 102] and shows good results. These numerical values are utilized to perform sensitivity analysis of different independent input parameters on dependent output responses. The important results are as follows:

- The higher values of both R^2 and $Adj\,R^2$ shows that the input factors and output responses are completely correlated.
- The normal probability plots of both Cf_x and Nu_x are along the straight line which proved that data is normal.
- The standard error for effects for Cf_x is zero.
- Mean square error / degrees of freedom for error for Cf_x is zero.
- Cf_x is independent to *Pr*. So the sensitivity of Cf_x only depends on *m*.
- *Pr* is more sensitive to Nu_x.
- Nu_x occurs maximum near the middle level of *Pr*.

- Effect of m on Nu_x is negligible.

13.2 Future works with applicability

Sensitivity analysis is the study of how different sources of uncertainty in an input can be identified and separated and assigned to the output of a mathematical model or system (whether it be numerical or not). Uncertainty analysis is a similar technique that places more emphasis on the quantification and propagation of uncertainty; ideally, uncertainty and sensitivity analysis should be carried out simultaneously. A wide range of reasons may arise from the process of recalculating results under different hypotheses to assess the influence of a variable in a sensitivity investigation, including:

- testing the system's or model's ability to produce reliable results in uncertain conditions.
- A more comprehensive understanding of how input and output variables interact in a system or model.
- Reducing uncertainty by identifying model inputs that significantly influence output uncertainty.
- A primary sensitivity test, which focuses on the sensitive parameters, might facilitate the calibration step in models with many parameters that need to be calibrated.

References

[1] Falkner, V. M., & Skan, S. W. (1931). Solutions of the boundary-layer equations. *The London, Edinburgh, and Dublin Philosophical Magazine and Journal of Science*, 12(80), 865-896.

[2] Hartree, D. R. (1937). On an equation occurring in Falkner and Skan's approximate treatment of the equations of the boundary layer. *In Mathematical Proceedings of the Cambridge Philosophical Society*, 33(2), 223-239.

[3] Lin, H. T., & Lin, L. K. (1987). Similarity solutions for laminar forced convection heat transfer from wedges to fluids of any Prandtl number. *International journal of heat and mass transfer*, 30(6), 1111-1118.

[4] Watanabe, T., & Pop, I. (1993). Magnetohydrodynamic free convection flow over a wedge in the presence of a transverse magnetic field. *International communications in heat and mass transfer*, 20(6), 871-881.

[5] Garg, V. K., & Rajagopal, K. R. (1991). Flow of a non-Newtonian fluid past a wedge. Acta Mechanica, 88(1), 113-123.

[6] Ishak, A., Nazar, R., & Pop, I. (2007). Falkner-Skan equation for flow past a moving wedge with suction or injection. *Journal of Applied Mathematics and Computing*, 25(1), 67-83.

[7] Riley, N., & Weidman, P. D. (1989). Multiple solutions of the Falkner–Skan equation for flow past a stretching boundary. *SIAM Journal on Applied Mathematics*, 49(5), 1350-1358.

[8] Liao, S. J. (1999). A uniformly valid analytic solution of two-dimensional viscous flow over a semi-infinite flat plate. *Journal of Fluid Mechanics*, 385, 101-128.

[9] Abbasbandy, S., & Hayat, T. (2009). Solution of the MHD Falkner-Skan flow by Homotopy Analysis Method. *Communications in Nonlinear Science and Numerical Simulation*, 14(9-10), 3591-3598.

[10] Liu, C. S., & Chang, J. R. (2008). The Lie-group shooting method for multiple-solutions of Falkner–Skan equation under suction–injection

conditions. *International Journal of Non-Linear Mechanics*, 43(9), 844-851.

[11] Fang, T., & Zhang, J. (2008). An exact analytical solution of the Falkner-Skan equation with mass transfer and wall stretching. *International Journal of Non-Linear Mechanics*, 43(9), 1000-1006.

[12] Pal, D., & Mondal, H. (2009). Influence of temperature-dependent viscosity and thermal radiation on MHD forced convection over a non-isothermal wedge. *Applied Mathematics and Computation*, 212(1), 194-208.

[13] Harris, S. D., Ingham, D. B., & Pop, I. (2002). Unsteady heat transfer in impulsive Falkner–Skan flows: constant wall temperature case. *European Journal of Mechanics-B/Fluids*, 21(4), 447-468.

[14] Harris, S. D., Ingham, D. B., & Pop, I. (2009). Impulsive Falkner-Skan flow with constant wall heat flux: revisited. *International Journal of Numerical Methods for Heat & Fluid Flow*. 19(8), 1007-1037.

[16] Schlichting, H., & Gersten, K. (2000). Fundamentals of boundary-layer theory, *Springer, Berlin, Heidelberg*, 29-49.

[17] Leal, L. G. (2007). Advanced transport phenomena: fluid mechanics and convective transport processes (Vol. 7). Cambridge University Press.

[18] Kafoussias, N. G., & Nanousis, N. D. (1997). Magnetohydrodynamic laminar boundary-layer flow over a wedge with suction or injection. *Canadian Journal of Physics*, 75(10), 733-745.

[19] Yacob, N. A., Ishak, A., & Pop, I. (2011). Falkner–Skan problem for a static or moving wedge in nanofluids. *International Journal of Thermal Sciences*, 50(2), 133-139.

[20] Riley, N., & Weidman, P. D. (1989). Multiple solutions of the Falkner–Skan equation for flow past a stretching boundary. *SIAM Journal on Applied Mathematics*, 49(5), 1350-1358.

[21] Ishak, A., Nazar, R., & Pop, I. (2007). Falkner-Skan equation for flow past a moving wedge with suction or injection. *Journal of Applied Mathematics and Computing*, 25(1), 67-83.

[22] Sakiadis, B. C. (1961). Boundary-layer behavior on continuous solid surfaces: I. Boundary-layer equations for two-dimensional and axisymmetric flow. *AIChE Journal*, 7(1), 26-28.

[23] Yacob, N. A., Ishak, A., & Pop, I. (2011). Falkner–Skan problem for a static or moving wedge in nanofluids. *International Journal of Thermal Sciences*, 50(2), 133-139.

[24] Asaithambi, A. (1998). A finite-difference method for the Falkner-Skan equation. *Applied Mathematics and Computation*, 92(2-3), 135-141.

[25] Kumari, M., Takhar, H. S., & Nath, G. (2001). Mixed convection flow over a vertical wedge embedded in a highly porous medium. *Heat and Mass Transfer*, 37(2), 139-146.

[26] Yang, H. T., & Chien, L. C. (1975). Analytic Solutions of the Falkner–Skan Equation when β=-1 and γ=0. *SIAM Journal on Applied Mathematics*, 29(3), 558-569.

[27] Fang, T., & Zhang, J. (2008). An exact analytical solution of the Falkner-Skan equation with mass transfer and wall stretching. *International Journal of Non-Linear Mechanics*, 43(9), 1000-1006.

[28] Das, K., Sharma, R. P., & Duari, P. R. (2017). Hydromagnetic rarefied fluid flow over a wedge in the presence of surface slip and thermal radiation. *International Journal of Applied Mechanics and Engineering*, 22(4), 827-837.

[29] Garg, V. K. (1992). Non-Newtonian flow over a wedge with suction. *International journal for numerical methods in fluids*, 15(1), 37-49.

[30] Chamkha, A. J., Mujtaba, M., Quadri, A., & Issa, C. (2003). Thermal radiation effects on MHD forced convection flow adjacent to a non-isothermal wedge in the presence of a heat source or sink. *Heat and Mass Transfer*, 39(4), 305-312.

[31] Kim, K. H., & Eraslan, A. H. (1969). Flow of a non-Newtonian fluid past wedges with wall mass injection. *Journal of Hydronautics*, 3(1), 57-59.

[32] Hsu, C. H., Chen, C. S., & Teng, J. T. (1997). Temperature and flow fields for the flow of a second grade fluid past a wedge. *International journal of non-linear mechanics*, 32(5), 933-946.

[33] Massoudi, M. (2001). Local non-similarity solutions for the flow of a non-Newtonian fluid over a wedge. *International Journal of Non-Linear Mechanics*, 36(6), 961-976.

[34] Watanabe, T. (1990). Thermal boundary layers over a wedge with uniform suction or injection in forced flow. *Acta Mechanica*, 83(3), 119-126.

[35] Watanabe, T., & Pop, I. (1993). Magnetohydrodynamic free convection flow over a wedge in the presence of a transverse magnetic field. *International communications in heat and mass transfer*, 20(6), 871-881.

[36] Kumari, M., Takhar, H. S., & Nath, G. (2001). Mixed convection flow over a vertical wedge embedded in a highly porous medium. *Heat and Mass Transfer*, 37(2), 139-146.

[37] Hossain, M. A., Munir, M. S., & Rees, D. A. S. (2000). Flow of viscous incompressible fluid with temperature dependent viscosity and thermal conductivity past a permeable wedge with uniform surface heat flux. *International journal of thermal sciences*, 39(6), 635-644.

[38] Pantokratoras, A. (2006). The Falkner–Skan flow with constant wall temperature and variable viscosity. *International Journal of Thermal Sciences*, 45(4), 378-389.

[39] Pal, D., & Mondal, H. (2009). Influence of temperature-dependent viscosity and thermal radiation on MHD forced convection over a non-isothermal wedge. *Applied Mathematics and Computation*, 212(1), 194-208.

[40] Kandasamy R, Muhaimin, H., I., & Ruhaila. (2008). Thermophoresis and chemical reaction effects on non-Darcy mixed convective heat and mass transfer past a porous wedge with variable viscosity in the presence of suction or injection. *Nuclear Eng Design*. 238, 2699–2705.

[41] Riley, N., & Weidman, P. D. (1989). Multiple solutions of the Falkner-Skan

equation with suction or injection. *J Appl Math Comput*, 25, 67-83.

[42] Ishak, A., Nazar, R., & Pop, I. (2006). Moving wedge and flat plate in a micropolar fluid. *International journal of engineering science*, 44(18-19), 1225-1236.

[43] Ishak, A., Nazar, R., & Pop, I. (2007). Falkner-Skan equation for flow past a moving wedge with suction or injection. Journal of Applied Mathematics and Computing, 25(1), 67-83.

[44] Kandasamy, R., Muhaimin, I., & Rosmila, A. K., (2014). The performance evaluation of unsteady MHD non-Darcy nanofluid flow over a porous wedge due to renewable (solar) energy, *Journal of Renewable Energy*, 64, 1–9.

[45] Chan, S. Q., Aman, F., & Mansur, S. (2018). Sensitivity analysis on thermal conductivity characteristics of a water-based bionanofluid flow past a wedge surface. *Mathematical Problems in Engineering*,

[46] Darbari, B., Rashidi, S., & Abolfazli Esfahani, J. (2016). Sensitivity analysis of entropy generation in nanofluid flow inside a channel by response surface methodology. Entropy, 18(2), 52.

[47] Rashidi, S., Bovand, M., Esfahani, J. A. (2015). Heat transfer enhancement and pressure drop penalty in porous solar heat exchangers: A sensitivity analysis. *Energy Convers. Manag.* 103, 726–738.

[48] Rashidi, S. Bovand, M., & Esfahani, J.A. (2015). Structural optimization of nanofluid flow around an equilateral triangular obstacle. *Energy*, 88, 385–398.

[49] Rashidi, S., Bovand, M., Esfahani, J.A., & Ahmadi, G. (2016). Discrete particle model for convective Al2O3 -water nanofluid around a triangular obstacle. *Appl. Therm. Eng.*

[50] Vahedi, S. M., Pordanjani, A. H., Raisi, A., & Chamkha, A. J. (2019). Sensitivity analysis and optimization of MHD forced convection of a Cu-water nanofluid flow past a wedge. *The European Physical Journal Plus*, 134(3), 1-21.

[51] Shafiq, A., Sindhu, T. N., & Khalique, C. M. (2020). Numerical investigation and sensitivity analysis on bioconvective tangent hyperbolic nanofluid flow towards stretching surface by response surface methodology. *Alexandria Engineering Journal,* 59(6), 4533-4548.

[52] Darbari, B., Rashidi, S., & Abolfazli Esfahani, J. (2016). Sensitivity analysis of entropy generation in nanofluid flow inside a channel by response surface methodology. Entropy, 18 (2), 52-67.

[53] Shirvan, K. M., Mamourian, M., Mirzakhanlari, S., & Ellahi, R. (2016). Two phase simulation and sensitivity analysis of effective parameters on combined heat transfer and pressure drop in a solar heat exchanger filled with nanofluid by RSM. Journal of Molecular Liquids, 220 (2016), 888-901.

[54] Vahedi, S. M., Pordanjani, A. H., Raisi, A., & Chamkha, A. J. (2019). Sensitivity analysis and optimization of MHD forced convection of a Cu-water nanofluid flow past a wedge. The European Physical Journal Plus, 134 (3), 1-21.

[55] Abdelmalek, Z., Mahanthesh, B., Basir, M. F. M., Imtiaz, M., Mackolil, J., Khan, N. S., & Tlili, I. (2020). Mixed radiated magneto Casson fluid flow with Arrhenius activation energy and Newtonian heating effects: Flow and sensitivity analysis. Alexandria Engineering Journal, 59(5), 3991-4011.

[56] Hussain, D., Asghar, Z., Zeeshan, A., & Alsulami, H. (2022). Analysis of sensitivity of thermal conductivity and variable viscosity on wall heat flux in flow of viscous fluid over a porous wedge. International Communications in Heat and Mass Transfer, ***135***, 106104.

[57] Mehmood, T., Ramzan, M., Howari, F., Kadry, S., & Chu, Y. M. (2021). Application of response surface methodology on the nanofluid flow over a rotating disk with autocatalytic chemical reaction and entropy generation optimization. Scientific Reports, 11(1), 1-18.

[58] Shafiq, A., Sindhu, T. N., & Khalique, C. M. (2020). Numerical investigation and sensitivity analysis on bio convective tangent hyperbolic nanofluid flow towards stretching surface by response surface methodology. Alexandria

Engineering Journal, 59 (6), 4533-4548.

[59] Mackolil, J., & Mahanthesh, B. (2021). Optimization of heat transfer in the thermal Marangoni convective flow of a hybrid nanomaterial with sensitivity analysis. Applied Mathematics and Mechanics, 1-12.

[60] Shirvan, K. M., Ellahi, R., Mirzakhanlari, S., & Mamourian, M. (2016). Enhancement of heat transfer and heat exchanger effectiveness in a double pipe heat exchanger filled with porous media: Numerical simulation and sensitivity analysis of turbulent fluid flow. Applied Thermal Engineering, 109, 761-774.

[60] Pordanjani, A. H., Vahedi, S. M., Aghakhani, S., Afrand, M., Öztop, H. F., & Abu-Hamdeh, N. (2019). Effect of magnetic field on mixed convection and entropy generation of hybrid nanofluid in an inclined enclosure: sensitivity analysis and optimization. The European Physical Journal Plus, 134 (8), 1-20.

[61] Bode, H. W. Network analysis and feedback amplifier design. (1945).

[62] Hemmat, E, M., Alidoust, S., Mohammadnejad A, E., Kamyab, M. H., & Toghraie, D. (2022). Experimental Study of Rheological Behaviour of MWCNT-Al2O3/SAE50 Hybrid Nanofluid to Provide the Best Nano-lubrication Conditions. *Nanoscale Research Letters*, 17(1), 1-13,

[63] Esfe, M. H., Arani, A. A. A., & Esfandeh, S. (2018). Improving engine oil lubrication in light-duty vehicles by using of dispersing MWCNT and ZnO nanoparticles in 5W50 as viscosity index improvers. *Applied Thermal Engineering*, 143, 493-506,

[64] Abdulrahman, A. (2021). Modelling and optimization of dynamic viscosity of copper nanoparticles dispersed in gear oil using response surface methodology. *Materials Today*, 42, 771-775.

[65] Kole, M., & Dey, T. K. (2011). Role of interfacial layer and clustering on the effective thermal conductivity of CuO–gear oil nanofluids. *Experimental thermal and fluid science*, 35(7), 1490-1495,

[66] Box, G.E.P., & Wilson, K.B. (1951). On the experimental attainment of optimum conditions. *Journal of the Royal Statistical Society: Series B*, 13(1),

1–45.

[67] Joardar, H. Das, N.S. & Sutradhar, G. (2011). An experimental study of effect of process parameters in turning of LM6/SiC P metal matrix composite and its prediction using response surface methodology. *International Journal of Engineering, Science and Technology*, 3(8), 132–141.

[68] Gürel, A. E., Ağbulut, Ü. & Biçen, Y. (2020). Assessment of machine learning, time series, response surface methodology and empirical models in prediction of global solar radiation. *Journal of Cleaner Production*, 277, 122353,

[69] Acherjee, B., Kuar, A. S., Mitra, S. & Misra, D. (2015). Empirical modelling and multi-response optimization of laser transmission welding of polycarbonate to ABS. *Lasers in manufacturing and materials processing*, 2, 103-123.

[70] Montgomery, D. C. (1996). Design and Analysis of Experiments, 3rd ed., *John Wiley*, New York.

[71] Khuri, A.I. (2006). Response Surface Methodology and Related Topics, World Scientific, New Jersey.

[72] Bode, H. W. Network analysis and feedback amplifier design. (1945).

[73] Hemmat, E, M., Alidoust, S., Mohammadnejad A, E., Kamyab, M. H., & Toghraie, D. Experimental Study of Rheological Behaviour of MWCNT-Al2O3/SAE50 Hybrid Nanofluid to Provide the Best Nano-lubrication Conditions. *Nanoscale Research Letters*, vol. 17, no. 1, 1-13, (2022).

[74] Esfe, M. H., Arani, A. A. A., & Esfandeh, S. Improving engine oil lubrication in light-duty vehicles by using of dispersing MWCNT and ZnO nanoparticles in 5W50 as viscosity index improvers. *Applied Thermal Engineering*, vol. 143, 493-506, (2018).

[75] Abdulrahman, A. Modelling and optimization of dynamic viscosity of copper nanoparticles dispersed in gear oil using response surface methodology. *Materials Today*: Proceedings, 42, 771-775, (2021).

[76] Kole, M., & Dey, T. K. Role of interfacial layer and clustering on the effective thermal conductivity of CuO–gear oil nanofluids. *Experimental thermal and fluid science*, 35(7), 1490-1495, (2011).

[77] Mahdy, A., & Chamkha, A., J., (2018). *Int. J. Numer. Methods Heat Fluid Flow*. 11 2567-2580

[78] Mukhopadhyay, S., Mondal, I. C. & Chamkha, A. J. (2013). Casson fluid flow and heat transfer past a symmetric wedge. *Heat Transfer-Asian Research*, 42(8), 665-675.

[79] Chamkha, A. J., Mujtaba, M., Quadri, A. & Issa, C. (2003). Thermal radiation effects on MHD forced convection flow adjacent to a non-isothermal wedge in the presence of a heat source or sink. *Heat and Mass Transfer*, 39(4), 305-312.

[80] Pal, D., & Mondal, H. (2009). Influence of temperature-dependent viscosity and thermal radiation on MHD forced convection over a non-isothermal wedge. *Applied Mathematics and Computation*, 212(1), 194-208.

[81] Lin, H. T. & Lin, L. K. (1987). Similarity solutions for laminar forced convection heat transfer from wedges to fluids of any Prandtl number. *International journal of heat and mass transfer*, 30(6), 1111-1118.

[82] Khan, M. (2018). Effects of multiple slip on flow of magneto-Carreau fluid along wedge with chemically reactive species. *Neural Computing and Applications*, 30(7), 2191-2203.

[83] Khan, M. S., Karim, I., Islam, M. S. & Wahiduzzaman, M. (2014). MHD boundary layer radiative, heat generating and chemical reacting flow past a wedge moving in a nanofluid. *Nano Convergence*, 1:20.

[84] Yih. K. A. (1998). Uniform suction (blowing) effect on forced convection about a wedge: uniform heat flux. *Acta Mech.* 128(3), 173–181.

[85] White. F. M. (1991). Viscous fluid flow, 2nd edition. *McGraw-Hill, New York*

[86] Watanabe. T. (1990). Thermal boundary layer over a wedge with uniform

suction or injection in forced flow. *Acta Mech.* 83, 119–126.

[87] Khan, M. & Sardar, H. (2018). On steady two-dimensional Carreau fluid flow over a wedge in the presence of infinite shear rate viscosity. *Results in physics*, 8, 516-523,

[88] El-Dabe, N. T., Ghaly, A. Y., Rizkallah, R. R., Ewis, K. M., & Al-Bareda, A. S. (2015). Numerical solution of MHD boundary layer flow of non-Newtonian Casson fluid on a moving wedge with heat and mass transfer and induced magnetic field. *Journal of Applied Mathematics and physics*, 3(06), 649.

[89] Rajagopal, K., R., Gupta, A.S., & Nath, T., Y. (1983). A Note on the Falkner-Skan Flows of a Non-Newtonian Fluid. *International Journal of Non-Linear Mechanics,* 18, 313-320.

[90] Ishak, A., Nazar, R., & Pop, I. (2009). MHD Boundary Layer Flow past a Moving Wedge. Magnetohydrodynamics, 45, 3-10.

[91] Amar, N., & Kishan, N. (2021). The influence of radiation on MHD boundary layer flow past a nano fluid wedge embedded in porous media. *Partial Differential Equations in Applied Mathematics*, 4, 100082.

[92] Watanabe, T. (1990). Thermal boundary layer over a wedge with uniform suction and injection in forced flow. *Acta Mech.* 83(3–4) 119–126.

[93] Ullah, I. Khan, I., & Shafie, S. (2016). Hydromagnetic Falkner-Skan flow of Casson fluid past a moving wedge with heat transfer. *Alex Eng J.* 55(3), 2139–2148.

[94] Ibrahim, W., & Tulu, A., (2019). Magnetohydrodynamic (MHD) boundary layer flow past a wedge with heat transfer and viscous effects of nanofluid embedded in porous media. *Math Problem Eng.* 4507852.

[95] Zaib, A., Rashidi, M. M., Chamkha, A. J., & Bhattacharyya, K. (2017). Numerical solution of second law analysis for MHD Casson nanofluid past a wedge with activation energy and binary chemical reaction. *International Journal of Numerical Methods for Heat & Fluid Flow.*

[96] Mondal, K. S., & Pal, D. (2022). Gyrotactic mixed bioconvection flow of a nanofluid over a stretching wedge embedded in a porous media in the presence of binary chemical reaction and activation energy. *International Journal of Ambient Energy*, 43(1), 3443-3453,

[97] Kasmani, M., Sivasankaran, R. S., Bhuvaneswari, M., & Hussein, A. K. (2017). Analytical and Numerical Study on Convection of Nanofluid Past A Moving Wedge with Soret and Dufour Effects. *International Journal of Numerical Methods for Heat and Fluid Flow* 27 (10), 2333–2354,

[98] Ganapathirao, Ravindran, M., R., & Pop. I. (2013). Non-uniform Slot Suction (Injection) on an Unsteady Mixed Convection Flow Over a Wedge with Chemical Reaction and Heat Generation or Absorption. *International Journal of Heat and Mass Transfer*, 67, 1054–1061.

[99] Cebeci, T., & Bradshaw, P. (1984). Physical and Computational Aspects of Convective Heat Transfer, New York, Springer-*Verlag*, 1st ed., p. 385.

[100] Chamkha, A. J., Mujtaba, M., Quadri, A., & Issa, C. (2003). Thermal radiation effects on MHD forced convection flow adjacent to a non-isothermal wedge in the presence of a heat source or sink. *Heat and Mass Transfer*, 39(4), 305-312.

[101] Lin, H. T., & Lin, L. K. (1987). Similarity solutions for laminar forced convection heat transfer from wedges to fluids of any Prandtl number. *International journal of heat and mass transfer*, 30(6), 1111-1118.

[102] Pal, D., & Mondal, H. (2009). Influence of temperature-dependent viscosity and thermal radiation on MHD forced convection over a non-isothermal wedge. *Applied Mathematics and Computation*, 212(1), 194-208.